Population Health Sciences Institute
Newcastle University

Population Variations In Ankle Complex Structure Using Machine-Learning 3D-MRI Statistical Shape Modelling And Implications For Osteoarthritis: The Newcastle Thousand Families Study Cohort

Mohammed Esa

In Partial Fulfilment of the Requirements

for the Degree of

Doctor of Philosophy

May 2023

Abstract

Background: Osteoarthritis (OA) is the most common joint condition. Although risk factors are well-recognised, the underlying pathogenesis is not fully understood. OA may be linked to biomechanics and force distribution during activities, with the ankle playing a crucial role in absorbing and transferring lower-limb forces. The ankle is structurally complex and understudied. Further understanding of ankle morphology could lead to better prevention of, and treatments for OA. This study aims to reconstruct Three-dimensional Statistical Shape Models (3D-SSM) from ankle MRIs, identify key ankle morphological features and explore their inter-relation to OA in the Newcastle Thousand Families birth cohort.

Methods: Prospectively collected data from 206 cohort participants aged 62 was used: 3D-SSM were built using ankle MRI images to quantify morphological features (bone shape/area, and joint space widths (JSW)) of ankle bones and joints. Sex differences, presence/absence of knee/hip OA, and associations between quantified morphological features and other clinical variables (body anthropometry, bone mineral density (BMD), and self-reported questionnaire data) were analysed.

Results: This study found significant sex differences in ankle morphology, with females having smaller JSW, bone area, and thinner bone shapes. Knee OA showed a pes-plan foot bone shape while the hip OA had pes-cavus. Positive associations were found between ankle JSW and BMD. Subtalar posterior JSW showed a positive association with knee JSW. Several ankle JSWs showed a positive association with hip JSW in males only. Participants with hip/knee OA have smaller ankle JSWs compared to others.

Conclusions: This is the first study using novel machine-learning techniques simplifying morphological complexity to examine ankle structure and its association with OA, using a population birth cohort. Results showed significant associations between ankle morphology and OA. This indicates ankle morphology may have direct effects on knee and hip OA through gait and mechanical force distribution. However, further studies are needed to confirm this hypothesis, which could be tested in subsequent reviews of this cohort.

Acknowledgements

I cannot help but feel an immense sense of gratitude for the people who supported me along the way as I sit here, having finished my PhD thesis and getting ready for submission. My supervisors, Mark Pearce, and Fraser Birrell, who helped me with advice, mentorship, and encouragement throughout my studies, have my sincere gratitude. They were crucial to my development as a researcher and assisted me in achieving my academic objectives.

I would also like to thank my collaborators, especially Mike Bowes, the Senior Director of Imorphics Clinical Applications, who generously shared his knowledge, technology, and resources with me. Working and learning from one of the top experts in machine learning applications and statistical shape modelling was a privilege, and I am grateful for this opportunity.

I am deeply indebted to my wife, Wejdan Al Hamid, and my son, Saad Esa, for their unwavering love, kindness, and compassion. They were my pillar of support, especially during the most challenging times in this journey, and kept me motivated to continue. I would also like to thank my parents for their constant support and encouragement, without which I would not have achieved this milestone.

Finally, I want to thank my sponsors King Faisal Medical City in Saudi Arabia for their kind support in allowing me to continue my education at Newcastle University. This accomplishment would not have been possible without their support and help. I am humbled and appreciative of everyone's support and encouragement throughout my academic journey. Working and learning from such exceptional people was a privilege. I will always be appreciative of their unwavering support, which served as the centrepiece of my achievement.

Table of Contents

List of figures

List of tables

List of abbreviations

3D: Three-Dimensional

AAM: Active Appearance Models

AP: Anteroposterior

ATFL: The Anterior Talofibular Ligament

BMD: Bone Mineral Density

BLOKS: The Boston Leeds Osteoarthritis Knee Score

BML: Bone Marrow Lesions

CT: Computed Tomography

DMOAD: Disease-Modifying Osteoarthritis Drug

DXA: Dual-Energy X-Ray Absorptiometry

FDA: The Food And Drug Administration

GBD: The Global Burden Of Disease

HKA: The Hip-Knee-Ankle Angle

ICC: Intraclass Correlation Coefficient

JSN: Joint Space Narrowing

JSW: Joint Space Widths

K&L: Kellgren-Lawrence

KOSS: The Knee Osteoarthritis Scoring System

MPTA: Medial Proximal Tibial Angle

MOAKS: The MRI Osteoarthritis Knee Score

MRI: Magnetic Resonance Imaging

NICE: National Institute For Health And Care Excellence

NSAIDS: Non-Steroidal Anti-Inflammatory Drugs

NTFS: Newcastle Thousand Families Study

OARSI: The Osteoarthritis Research Society International

OA: Osteoarthritis

OR: Odds Ratio

PCA: Principal Component Analysis

PC: Principal Component

RA: Rheumatoid Arthritis

RMSE: Root Mean Square Error

ROM: Range Of Motion

SD: Stander Deviation

SRM: Standardised Response Mean

SSM: Statistical Shape Models

TKR: Total Knee Replacement

WBCT: Weight-Bearing Computed Tomography

WHO: The World Health Organisation

WOMAC: Western Ontario And Mcmaster Universities Osteoarthritis Index

WORMS: The Whole Organ Magnetic Resonance Imaging Score

Chapter 1: Introduction

1.1 Background

Osteoarthritis (OA) is a prevalent degenerative joint condition that affects millions of people worldwide, causing pain, disability, and reduced quality of life (1). OA is exemplified by the progressive deterioration of the cartilage and other structures in and around the joint, leading to pain and decreased mobility (2). OA is increasingly thought of as a disease of 'tear, flare and repair' (3). Although it can affect other joints like the hands and feet, it is most clinically important in weight-bearing joints for instance the hips and knees (4). Even though the specific cause of OA is still not completely understood, it is believed to be the result of a combination of factors including ageing, joint injury, genetics, obesity, and biomechanical factors (4).

The prevalence of OA varies by geographical region and demographic variables, but older adults and women are at higher risk of developing the disease (5). According to the National Institute for Health and Care Excellence (NICE), OA affects an estimated 8.75 million people over the age of 45 years in the UK (6). As the population ages and the prevalence of obesity continues to rise, this number is anticipated to increase (6). In addition, OA is the most common form of arthritis in the UK, accounting for over half of all cases (7). It is estimated that, by 2030, over 15 million people in the UK will be living with OA (8). OA is a significant burden on healthcare systems, causing significant pain and disability and leading to decreased quality of life. The increasing prevalence of OA is likely to increase the burden on healthcare systems globally in the future, with an estimated 78 million cases expected by 2040 in the United States alone (9).

The clinical assessment of OA includes two main methods. The first is a structural assessment which mainly uses imaging modalities to evaluate the structure of the joint (10). Conventional radiography is the gold standard imaging modality used for the diagnosis and monitoring of OA (11). Radiographs show a visual representation of the joint and can detect signs of OA such as joint space narrowing (JSN), osteophytes, and subchondral sclerosis (11). There are several radiographic grading systems used for the assessment of OA. The most widely used is the

Kellgren-Lawrence (K&L) grading system for the evaluation of the severity of OA, scoring from 0 to 4 based on osteophyte formation, JSN, and other radiographic findings (12, 13). For hip OA, a modification of the K&L grading system was introduced by Croft, Cooper (14). Known as Croft's grading system, it classifies the condition in five grades based on radiographic features, with each grade indicating various levels of severity. In addition, joint space width (JSW) is another measure and is the single standard criterion used by the USA Food and Drug Administration (FDA) in clinical trials assessing potential disease-modifying OA drugs (15). The use of JSW as a gold standard helps in the assessment of the progression of OA in different populations over time (15).

Secondly, functional assessments are also used in the evaluation and management of OA, in both in the clinic and research (10). They include physical performance and blood tests, joint fluid analysis, and self-report questionnaires (16). One commonly used functional assessment tool for OA is the Western Ontario and McMaster Universities Osteoarthritis Index (WOMAC) questionnaire (17). It consists of 24 questions evaluating pain, stiffness, and physical function in daily activities such as walking (17). These assessments help healthcare professionals to determine an individual's functional abilities and limitations and can guide treatment plans, track progress, and identify areas for improvement in the management of OA symptoms (18).

While there is no known curative treatment for OA, there are numerous approaches that seek to control its symptoms, such as reducing pain, improving joint function, and potentially slowing the progression of the disease (19). Non-surgical means such as physical therapy, weight management, and education are often the first line of treatment (20). The addition of non-steroidal anti-inflammatory drugs (NSAIDs) can help to reduce pain and inflammation. Physical therapy can help to improve joint mobility and reduce pain, while weight management can help to reduce the load on affected joints (20). Nevertheless, in more severe cases, joint replacement surgery may be necessary (19).

Risk factors for OA involve increasing age, obesity, joint injury, genetics, and biomechanical factors (21). Older individuals are at higher risk of developing OA due to age-related changes in the joints (18). Obesity increases the risk of OA as a result of the increased load on weight-bearing joints and biochemical effects such as the release of CRP from visceral fat (22).

In addition, joint trauma such as from sports injuries can also increase the risk of OA later in life (23).

Genetic factors may also play a role, and individuals with a family history of OA are at higher risk compared to others (24). Another important factor that plays a significant role in the progression of OA is related to joint biomechanics. For example, repetitive stress placed on joints may lead to an increase in the mechanical forces applied to the joints, leading to local inflammation and gradual cartilage loss, which further promotes the development of OA alongside other risk factors (25).

The foot and ankle play a crucial part in transforming the mechanical force throughout the lower limb (26, 27). During the gait cycle, mechanical force travels from the ankle complex region to the hip through the bones and joints of the lower limb, including the ankle, knee, and hip joints (28). This transfer of force is crucial for normal human locomotion and for everyday activities such as walking, running, and jumping (29). The bones and joints in the lower limb act as mechanical levers, allowing the force to be transmitted from the ankle up the limb and ultimately to the hip (30). Given the critical role that the foot and ankle play in the reception, absorption, and distribution of forces during the gait cycle, alterations in foot and ankle characteristics such as morphological variations in the bones forming the ankle region, variations in the alignment of the bones, and static foot posture can increase the stress on other joints of the lower limb, potentially influencing OA onset and progression (31).

Lower limb joints with structural or symptomatic OA can initiate similar symptoms in other kinematically connected joints (4). Despite this, the majority of research in this area has concentrated mostly on how the knee and hip interact, with little focus on the ankle joint. A few studies have aimed to explore associations between ankle symptoms such as pain and other lower limb OA functional and symptomatic features. For example, Gross, Niu (32) found no link between ankle complex alignment and hip pain, while Paterson, Hinman (33) found ankle pain worsened knee OA symptoms represented by worsening scores on WOMAC subscales. A subsequent study by Paterson, Kasza (34) reported a correlation between ankle/foot symptoms and knee pain, but no such association with worsening radiographic

knee OA. Most recently, Perry, Segal (35) found a significant link between baseline ankle pain and frequent knee pain at follow-up.

Other studies focus on the evaluation of the association between foot posture, ankle complex alignment, lower limb alignment, and knee and hip OA. Results from various studies have shown a significant association between foot posture and OA in the knee and hip. For instance, Reilly, Barker (36), Reilly, Barker (37) and Abourazzak, Kadi (38) found relationships between pronated foot posture and knee OA, and supinated foot posture and hip OA. Additionally, Gross, Felson (39) established a relationship between pronated foot posture and knee pain, cartilage damage, and OA symptoms. Recently, Zhang, Nie (40) found a higher risk of both radiographic and functional knee OA symptoms in participants with a pronated foot type. Furthermore, a recent systematic review and meta-analysis published by Almeheyawi, Bricca (31) concluded that pronated foot posture was present in people with knee OA, yet the relationship between OA and other foot and ankle characteristics was uncertain due to the heterogeneity of studies and the need for further studies using more common measurements was recommended.

Several studies have investigated the relationship between OA in both the hip/knee and the incidence of ankle OA. Some studies have shown that the severity of valgus and varus deformities in the knee joint can significantly impact the alignment of the lower limb and change the hip-knee-ankle angle, affecting the ankle (41-43). Also, a 3-year follow-up study by Kraus, Worrell (44), which used nuclear medicine bone scans to evaluate ankle joint abnormalities in 159 subjects with radiographic knee OA, found a significant correlation between ankle bone scan abnormality and a decrease in knee JSW. In addition, a high prevalence of ankle OA has been found in patients with hip and knee OA, with reported prevalence levels of 29% Tallroth, Harilainen (45) 37% Xie, Jiang (43) and 24% (46). These findings indicate a structural association between the lower limb joints, where abnormality in one joint may affect others.

These investigations have focused primarily on the correlation between OA in both the hip and knee joints and various aspects of the ankle and foot such as pain, alignment, the incidence of OA and several functional characteristics, indicating an association possibly

driven by biomechanics and force distribution factors between the ankle and foot and OA in other joints of the lower limb, but the specific relationship remains to be further explored.

Despite significant findings from the studies mentioned above, they all share limitations in terms of representativeness and generalisability. Most studies used convenience sampling methods which may not accurately reflect the larger population, and only included participants exhibiting advanced stages of OA. Additionally, these studies did not directly examine the morphological aspects of the ankle joint complex and its interrelation with hip and knee OA. Instead, they primarily focused on using methods such as measurements of lower limb alignment and foot posture and functional classification systems of the lower limb joints.

Recent studies by Almeheyawi, Bricca (31) and Perry, Segal (35) highlighted the importance of assessing the structural association between ankle complex morphology and both the hip and knee joints in their recommendations. One possible reason for the failure to investigate such an association is that the ankle is a complex anatomical region composed of several interconnecting bones (26). Previous studies aimed at understanding the structure of the ankle joint have primarily relied on two-dimensional (2D) measures from standard radiographs, but these methods may not accurately represent the complex three-dimensional (3D) morphology of the ankle joint (47, 48). As a result, the use of 2D radiographs to evaluate such an association may not be effective, leading researchers to focus on other methods for the measurement of the characteristics of the foot and ankle in order to investigate their association with features of OA in other lower limb joints (49).

Rapid technological developments in the last decade have given insights into 3D joint morphology (50). For example, magnetic resonance imaging (MRI) has the capability to evaluate joints so as to visualise all of the aspects of their anatomy and morphology in 3D without the need for ionising radiation. Another advantage of MRI is the ability to apply novel image analysis applications such as statistical shape modelling (SSM). This is a novel approach in medical imaging that applies statistical techniques to model the variability in shape of a population of anatomical structures (51). In comparison to conventional radiography, SSM offers several advantages. Firstly, it can incorporate large amounts of data for the creation of

a more accurate representation of the structure of interest, resulting in improved diagnostic accuracy. Secondly, it provides a more accurate representations of the 3D structure of a part of the anatomy, allowing for detailed automatic quantifications of important measurements compared to conventional radiography. Thirdly, it has the ability to account for variations in patient anatomy, allowing for a more personalised analysis. Finally, it can account for changes in shape that occur over time, permitting the monitoring of disease progression and the response to treatment (51).

Recently in research into OA, SSM has been applied to musculoskeletal imaging with a focus on the hip and knee joints (50, 52-54). By modelling the variability in shape of the bones and cartilage in these joints, SSM provides a more comprehensive understanding of the joint structure and can be used to identify subtle changes that may indicate the development of OA (54). The advantages of SSM in OA imaging include improved diagnostic accuracy, a reduction in observer variability, and the ability to quantify disease progression over time (51). While SSM has proven to be a valuable tool in the imaging of knee and hip joints, its application in the imaging of the ankle joint complex is still limited (47). One of the main challenges in using SSM to explore the morphology of the ankle complex is the limited availability of imaging data sets. Since the initial clinical evaluation of the ankle is usually achieved by standard radiography, the use of 3D cross-sectional imaging such as computed tomography (CT) or MRI which is needed to construct 3D SSM is not typically used (47).

Recent studies have attempted to use SSM on CT images of the ankle complex region to provide a clearer understanding of the complexity of the morphology of the ankle (47, 55-57). These studies aimed to either validate the method or explore differences in morphology between the sexes. Despite these efforts, the sample sizes used in these studies were limited, with the largest including only 66 participants (57). Furthermore, these studies did not examine the relationship between morphological variations in the ankle complex and OA in the hip and knee.

The Newcastle Thousand Family Study (NTFS) (58), which is discussed in more detail later in chapter 5, offers a valuable opportunity to explore the morphology of the ankle joint in a larger and more representative sample. This birth cohort study has undergone several follow-

ups, the most recent of which took place at age 62 where a musculoskeletal examination was conducted. Radiographic and functional assessments of OA were performed on both the hip and knee joints, and MRI images were collected of the ankle complex region as well as other clinical variables such as bone mineral density (BMD) and body anthropometry. The availability of such rich data from the NTFS presents a unique opportunity to study morphological variations in the ankle complex region in a population using 3D MRI SSM and to examine its interrelation with OA in other lower limb joints.

1.2 Aims and objectives.

This study aimed to use MRI data to construct 3D SSM of the ankle complex region, in order to simplify our understanding of the anatomical complexity of the area and quantify important morphological features. These models can provide baseline morphological data for a cohort of participants and could be used in future follow-up studies.

The first objective is to summarise the key morphological features of the ankle joint complex, such as JSW, bone shape, and bone area, from the 3D SSMs constructed using MRI data obtained from the study population.

The second objective was to identify any associations between morphological variations in the ankle and demographic factors such as sex, body anthropometry and regional BMD measurements. This information provides insights into any sex-related morphological variations within the population studied as well as the relationship between regional BMD and ankle morphology.

The final objective was to examine the interrelation between the key morphological features quantified using the 3D MRI SSMs and the radiographic features of both hip and knee OA, such as K&L scores and JSW, and functional features including pain and WOMAC scores. This analysis will provide insights into the relationship between ankle morphology and joints that are susceptible to OA and share the same kinematic chain. Although cross-sectional and limited to the establishment of associations rather than causality between ankle morphological variables quantified from 3D SSM and OA, this study represents a crucial first step towards the design of a more valuable longitudinal cohort study.

1.3 Hypotheses:

Hypothesis 1: 3D MRI statistical shape models help to simplify the evaluation of morphological variations in the anatomically complex region of the ankle by quantifying key morphological features such as bone shape, bone area, and JSW in individuals participating in the NTFS cohort at the age of 62.

Hypothesis 2: Clinical variables such as sex and body anthropometry significantly affect key morphological features of the ankle complex as quantified by 3D SSM.

Hypothesis 3: An association exists between the morphological features of the ankle complex region quantified such as JSW as identified by 3D MRI SSM and regional bone density measurements.

Hypothesis 4: Key morphological features such as bone shape and JSW of the ankle complex region quantified by 3D MRI SSM are associated with radiographic and functional variables of both knee and hip OA.

1.4 COVID-19 impact statement

The COVID-19 pandemic has had a major impact on early-career researchers, including myself. I encountered difficulties in conducting primary data collection for my PhD programme at National Health Service (NHS) facilities, specifically the Royal Victoria Infirmary in Newcastle upon Tyne, UK, due to the restrictions imposed by COVID-19. The process of obtaining the required research passport and ethical approval was finally received in September 2020 having been delayed for over 8 months after I had submitted the research passport in January 2020 before the pandemic outbreak. Despite gaining the required approval, access to NHS facilities was still not granted for several months due to lockdowns and restrictions on non-essential work and research activities, causing a total delay of 10 months.

The UK government's announcement of lockdowns and later restrictions imposed by institutions such as Newcastle University were the reasons for the disruption in accessing the necessary facilities for my PhD research. Additionally, even outside of lockdown, access to specific NHS facilities was limited due to reductions in the numbers of researchers allowed in order to comply with social distancing rules. To support my family's well-being, I temporarily returned to Saudi Arabia during the first lockdown, which included a 14-day hotel quarantine

and curfew regimen. This further impacted my mental and physical health and limited my time for non-facility-based work such as writing this thesis.

The second and third national lockdowns in November-December 2020 and January-March 2021 also resulted in limited access to NHS facilities and affected my collaboration with the Imorphics company in Manchester, since domestic travel was not allowed, and I did not have full access to the technology necessary for image analysis. After the completion of data collection, I needed to make changes to the research objectives which were necessary to alter the PhD track, which required more time to adjust previously written chapters. However, I have compensated for this lost time by putting more effort into completing my studies with the help and support of my supervisors and collaborators.

The COVID-19 pandemic has presented challenges to me personally including disruptions to my family life, and also to my research, but it has also provided the opportunity to develop and refine several personal skills, such as adaptability, critical thinking, problem-solving, online collaboration, and time management. The changing circumstances of the pandemic have required me to be resourceful and self-sufficient, and I have learned to find new ways to conduct my research and balance my work with personal responsibilities. Many PhD students were not able to continue their studies during this difficult time. I am very grateful and consider myself lucky to have been able to complete my research and submit my thesis regardless of all of the obstacles that I and many other students have faced.

1.5 Thesis outline

The thesis outline serves as a roadmap for the reader, giving a comprehensive overview of the entire thesis, including the content and structure of each chapter. Below is a breakdown of each chapter in this thesis:

Chapter 1: Introduction. This chapter introduces the study and includes a short background section followed by the research hypotheses and the aims and objectives of the study. Finally, a COVID-19 impact statement is also included.

Chapter 2: Osteoarthritis. This first part of the literature review focuses on the definition, prevalence, and incidence of OA. It also offers a review of all the risk factors associated with

the disease. This chapter helps in understanding the background of OA and the factors that contribute to its development.

Chapter 3: Anatomy and biomechanics of the ankle joint complex. The second part of the literature review focuses on the anatomy of the ankle joint complex, including of the bones and joints, followed by a discussion of the biomechanics of the ankle. The specific anatomical terminologies used in this thesis are also defined.

Chapter 4: Role of imaging in OA. The final part of the literature review explores the use of various diagnostic imaging modalities such as MRI, X-ray, and DXA. It introduces statistical shape modelling and reviews previous work conducted on the knee and ankle joint, thus providing a comprehensive understanding of the diagnostic tools used in the study and the significance of their role in the evaluation of OA.

Chapter 5: Methods. This chapter introduces the main source of data used in this study, which is the NTFS cohort. It also illustrates how data were collected and the methods used in SSM construction. This chapter provides a detailed understanding of the study design, data collection methods used, and statistical analysis applied in the research.

Chapter 6: Bone shape results. This chapter presents the results relating to morphological variations in the shape of the ankle bone and bone area in the population and their association with other relevant variables.

Chapter 7 Joint space width results. This chapter reports the results from the ankle JSW analysis in which the association with other variables is explored, and a detailed explanation of the findings is provided.

Chapter 8 Discussion. This chapter considers the results presented in the two previous chapters, compares them to similar findings found in the literature, and links the outcomes to the aims and objectives of this research. The scientific contributions of the research are also discussed, along with the limitations of the study and recommendations for future research. The research conclusions are also presented.

Chapter 2 Osteoarthritis

2.1 Summary

The chapter showed that OA is a prevalent disease mostly affecting older people and is described as a disease that affects the structure of the joint. In the UK, more than 8 million people are diagnosed with OA, which places a significant burden on healthcare systems, and causes pain, disability, and reduced quality of life. In recent years, researchers have focused on explorations of several aspects of the disease so as to better understand the risk factors involved and to introduce new management and prevention methods. One area of recent interest has been modifiable risk factors, and particularly biomechanical factors. While progressive OA is biochemically mediated, it is also mechanically driven. Therefore, the modification of biomechanical risk factors could potentially reduce the disease's progression. The ankle complex region can affect the biomechanics of the lower limb, but it has as yet received limited attention, with few studies exploring the relationships between ankle morphology, symptoms, and function and the knee and hip joints. An understanding of the relationship between the ankle complex region and other joints that share the same kinematic chain could shed light on the biomechanical effects of ankle structure that may influence the development and progression of knee and hip OA.

2.2 Historical context of OA

According to Scally and Womack (59), a consideration of the historical context of any disease is important if its nature is to be understood. Therefore, an exploration of the history of OA can extend our perspective on the disease by looking at past and present controversies. This section highlights how OA has historically been conceptualised and what has changed in our understanding in recent times.

'Rheumatic gout' (now known as gout) has been identified as the first joint disease to be characterised. It was initially recognised in 2640 BC by the Egyptians, and Hippocrates, who was an early Greek physician known as the father of medicine, referred to it in the fifth century BC as 'the un-walkable disease' (60). The word 'gout' was derived from the Latin word *gutta*, which means a drop of a substance. The use of this term is based on a belief from the middle

ages to which pain and swelling in the joint were explained in terms of a drop of phlegm under specific circumstances (60).

Based on many historical sources, it was assumed in the past that all forms of chronic arthritis emerged from gout (60). This was the case until 1782, and in particular when William Heberden distinguished between rheumatic gout and rheumatism, also known as arthritis (61). He also discovered bony growths on the fingers, which are now named after him as Heberden's nodes (61). In 1800, French student Augustin-Jacob of Landre-Beauvais defined a new disorder in the joint that was different from rheumatic gout and conventional rheumatism. This clarification resulted in the designation known as Rheumatoid Arthritis (RA) which was introduced in 1859 by Alfred Baring Garrod, based on the Augustin-Jacob theory (62).

In the mid-1850s the first description of OA was presented by Richard von Volkmann after consideration of the condition from a pathological and anatomic viewpoint. This resulted in it being differentiated from gout and RA (2). In 1890 the disease was named osteoarthritis by Sir Archibald Edward Garrod and it has been known as such until the present time (2).

Radiography played an important role in confirming the previous distinctions between the different forms of arthritis, and it remains a mainstay in the diagnosis of OA today (2). In 1895, radiographs were first introduced by Wilhelm Konrad Röntgen. The invention motivated many scientists, such as Goldthwaite and others, to explore arthritis in more depth. This resulted in the first radiographic differentiation between RA and OA from an exploration of new bone formation identified in the radiographs of different patients (61). In 1952, the x-ray was used by Kellgren and Moore to explore the difference between primary OA and secondary OA, following the theory of Heberden's nodes (61). Furthermore, in 1957 Kellgren and Lawrence used radiographic images to strengthen diagnostic methods for OA by presenting a classification scheme that is still accepted nowadays as the current gold standard for the diagnosis of OA (12).

Figure 2-1 below briefly explains the history of OA. It is clear that the condition has been subject to research for the past 200 years, yet it remains a disease that is not fully understood and which affects many people around the world. In addition, it is apparent that the use of

diagnostic imaging modalities has in the past enhanced many aspects of OA diagnosis and that they still play a vital role in clinical assessment and epidemiological studies. These issues are considered in more detail in chapter 4.

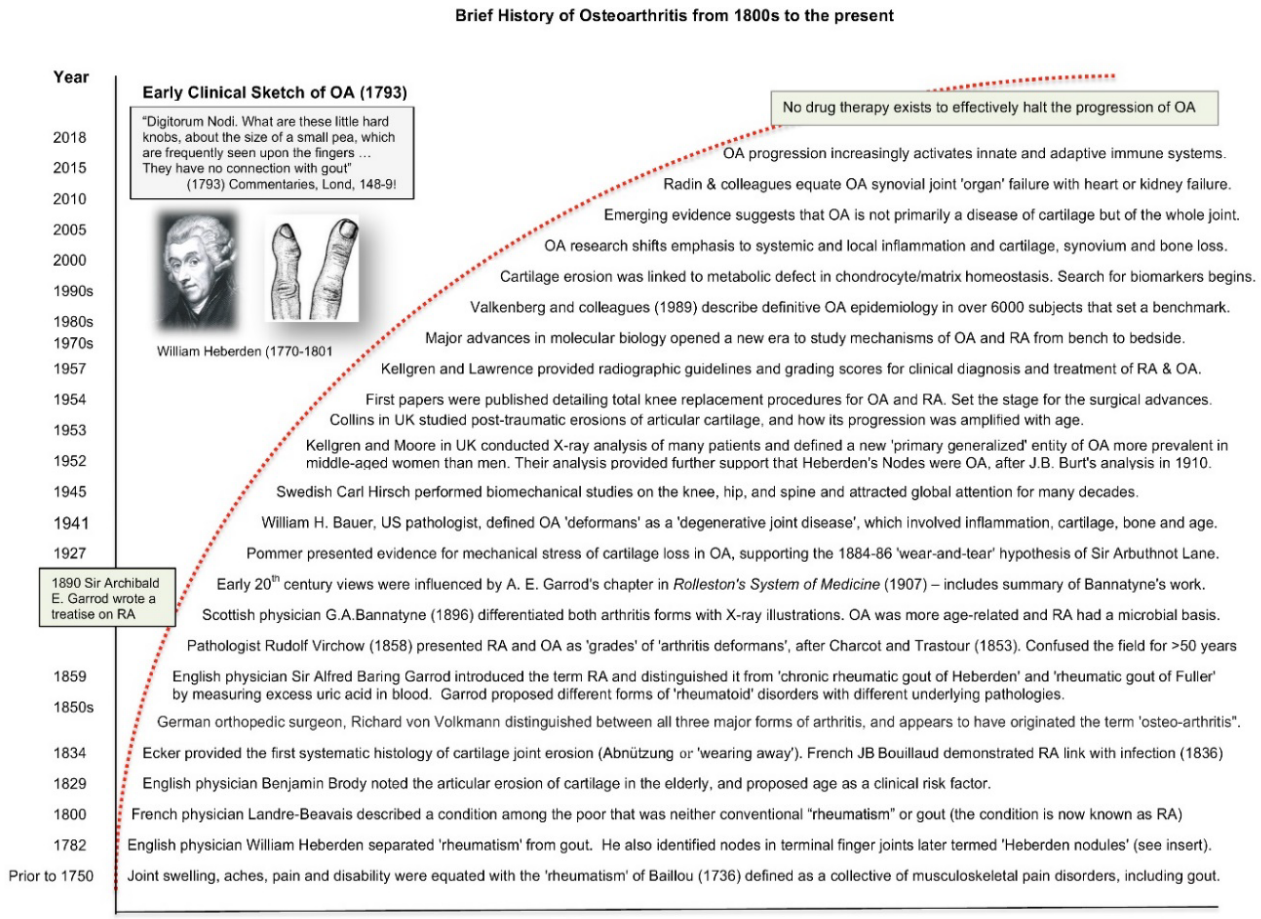

Figure 2-1. Brief history explaining the chain of knowledge about osteoarthritis from the 1800s to the present time adapted from; (2). Permission for use available via ELSEVIER LICENCE: #4666700040335.

2.3 Definition of OA

In the past, many researchers and clinicians have deliberated over the correct definition of OA. However, various scientific organisations have their definitions that differ from one another, but have the same general meaning. For example, the American Rheumatism Association defined OA as follows:

> *"A heterogeneous group of conditions that lead to joint symptoms and signs which are associated with defective integrity of cartilage, in addition to the related changes in the underlying bone and at the joint margin" (63).*

Additionally, the Osteoarthritis Research Society International (OARSI) has defined OA by conducting a review with the aim to create a consistent description of OA that can serve as a building block for researchers in the field. This has resulted in the following comprehensive definition:

> *"Osteoarthritis is a disorder that can affect any moveable joint of the body, for example knees, hips and shoulders. It can show itself as a breakdown of tissues and abnormal changes to cell structures of joints which can be initiated by injury.' AND 'Osteoarthritis first shows itself as a change to the biological processes within a joint, followed by abnormal changes to the joint itself (such as the breakdown of cartilage, bone reshaping, bony lumps, joint inflammation, loss of joint function). This can result in pain, stiffness and loss of movement"* (64).

2.4 Pathogenesis of OA

The pathogenesis of a disease is defined as the chain of events that generates and develops the biological mechanism underlying the disease (65). For many years, researchers have been studying the pathogenesis of OA and, initially, it was thought of as a disease that affects articular cartilage causing 'wear and tear' changes. This resulted in it being labelled as a degenerative joint disease (66). However, clear recent evidence indicates that episodic joint inflammation and OA are now increasingly being thought of as diseases of 'tear, flare and repair' (3). The term 'tear' refers to damage to supporting structures such as ligaments and tendons leading to joint instability and promoting early OA. The term 'flare' refers to the episodic inflammation process that occurs in and around the joint, and the term 'repair' reflects the joint's innate capacity to self-repair. This evidence shows that it is not simply a 'wear and tear' disease that affects the cartilage only; in fact, many morphological changes occur in other structures in and around the joint (3). Figure 2-2. Morphological differences between a healthy knee and a severely osteoarthritic knee, such as meniscal tears, subchondral bone remodelling, changes in the synovium, the development of bone marrow lesions and the formation of osteophytes caused by biomechanical stresses and cellular changes (65).

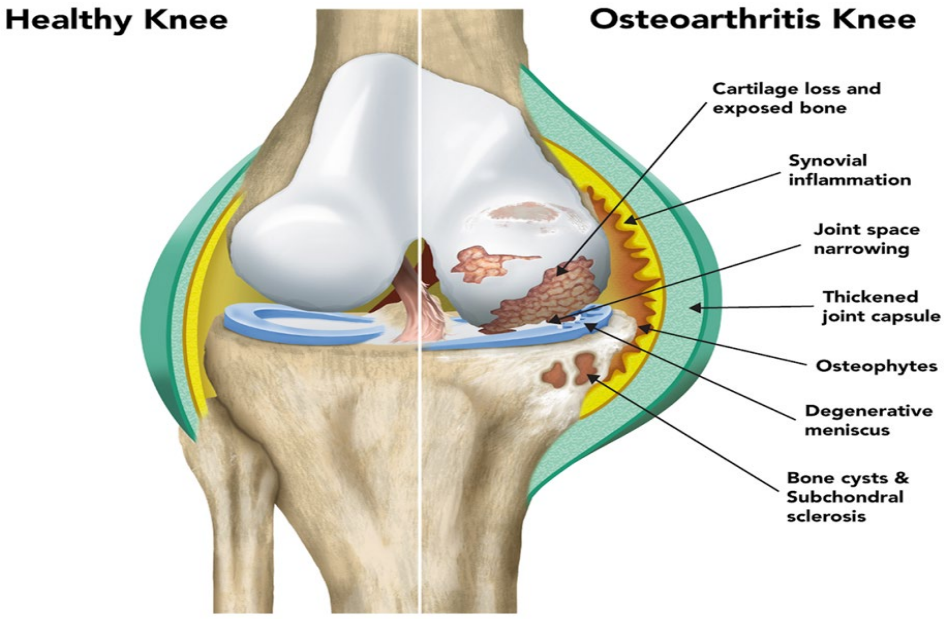

Figure 2-2. Morphological differences between a healthy knee and a severely osteoarthritic knee available via licence: Attribution 4.0 International CC BY 4.0).

As a result, the pathogenesis of OA is much more complex than was previously assumed. It is a whole-joint disease causing structural alterations in the joint affected (67). Inflammatory, mechanical and metabolic factors are all part of the complex pathogenesis of OA and such factors lead to structural damage in the joint (67). Finally, the disease is not a degenerative or so-called 'wear and tear' joint disease, but is an active disease of dynamic alteration that occurs due to the inequity between damage and repair to joint tissues (18); thus, it would more accurately be described as 'tear, flare and repair'.

2.5 Diagnosis of OA

2.5.1 Clinical assessment

In order to clinically diagnose OA, a full clinical assessment needs to be performed (10). This starts by exploring the patient's history, focusing on specific symptoms of the disease, like use-related pain and absent or short-lived morning stiffness (10). This will help to discriminate between different types of arthritis (10). Afterwards, a physical examination aims to elicit joint signs, including muscle wasting, crepitus, cool effusion and reduced range of movement (68). Some physicians may also use clinical classification criteria and specific scoring systems such as the Western Ontario and McMaster Arthritis Index test (WOMAC) to help assess impact (69). Medical imaging plays an important role in the diagnosis of OA, which is explored in more

detail in chapter 4. The following section reviews the signs and symptoms associated with OA, taking a general overview of the physical examination, and gives an overview of the clinical criteria and scoring systems used.

2.5.2 Signs and symptoms:

Patients suffering from OA usually develop symptoms that increase over time (70). These symptoms may differ in severity from one patient to another, and can start in one joint and develop to include other joints (70). As with any disease, OA has various signs and symptoms, which are defined in Table 2-1. If a patient presents at a clinic with these signs, this increases the possibility of being diagnosed with OA (71). The following section briefly reviews the most important signs and symptoms of OA.

Table 2-1. Signs and symptoms of OA adapted from (71)

Signs and symptoms of OA	
Symptoms	**Signs**
Pain	Limitation of motion
Stiffness	Tenderness
Swelling of the joint	Crepitus
Weakness	Altered gait
Instability and Grating sensation	Bony swelling
Deformity	Effusion

2.5.3 Pain

Pain is known to be one of the first predominant symptoms of OA and it is usually the main reason for OA patients to visit their doctor (71). The severity of the pain varies in weight-bearing joints compared to other joints, and it is usually described by the patients as an in-joint ache (70). Furthermore, the pain felt in weight-bearing joints such as the knee is worse when walking or standing and is relieved by resting (72). Some reports suggest that the origin of the pain in the joint may be represented by anatomical changes in the joint itself (73). For example, knee OA patients who suffer from lateral compartment OA define the origin of the pain as being localised in the lateral part of the knee.

However, others argue that the origin of the pain in the joint does not necessarily represent anatomical changes (72). They rely on the fact that several anatomical parts in the joint do not have any nerves (pain receptors). For example, undamaged cartilage, meniscus and synovial cavity in the knee do not have any nerves in them; therefore, any anatomical changes in these sites will not present pain that can be directly linked to that change (74).

2.5.4 Stiffness

Localised joint stiffness is a common symptom of OA. The stiffness is reported to occur in the early morning or after a long period of inactivity and it lasts for several minutes and is reduced by the motion of the joint (69). However, more severe, and prolonged stiffness is also known to be a symptom of different types of arthritis such as RA and it can be used to distinguish between one type and another depending on its duration. It is not, therefore, specifically linked with OA alone (69).

2.5.5 Limitation of motion

In the early stages of OA progression, patients complain of having difficulties in joint motion alongside pain (10). Such limitations gradually start to affect the quality of life and result in several limitations that make basic daily activities hard to achieve. In patients suffering from hip and knee OA, this may include walking and climbing stairs (10). Limitations in hand motion and loss of grip strength are noted in patients suffering from hand OA (75). Therefore, such limitations are noted as clear clinical signs of OA in the affected joint.

2.5.6 Physical examination

Physical examination is an important part of clinical assessment. It aims to lead to a diagnosis of OA or to rule it out, and the outcomes of the physical examination can help in establishing the stage of the disease in some cases (16). The examination will include a general inspection of the joint, palpation to look for joint deformity, the presence of inflammation or swelling, and a general gait assessment to examine the motion of the joint (16). The nature of the examination may vary depending on the joint affected, since each joint may present different characteristics in the physical examination (69).

2.5.7 Clinical criteria and scoring systems

The use of clinical criteria is an important part of a diagnosis of OA and will remain a vital factor until an improved diagnostic method that can integrate all aspects of the clinical assessment, including clinical findings, laboratory tests and radiological procedures, is established (10). One of the most widely used classification systems for the diagnosis of OA was developed by the American College of Rheumatology for the diagnosis of knee, hip and hand OA (63). The classification criteria for the knee are summarised in table 2-2 below. It is clear that the highest sensitivity and specificity are achieved by following the classification for clinical and radiographic criteria, with 91% sensitivity and 86% specificity (63).

Table 2-2. Criteria for the American College of Rheumatology classification of osteoarthritis of the knee adapted from (63).

Criteria for classification of osteoarthritis of the knee (American College of Rheumatology)		
Clinical and laboratory	**Clinical and radiographic**	**Clinical**
Knee pain + at least 5 of the following: • Age >50 years • Stiffness <30 minutes • Crepitus • Bony tenderness • Bony enlargement • No palpable warmth • ESR <40 mm/hour • RF <1:40 • SF OA	Knee pain + at least 1 of the following: • Age >50 years • Stiffness <30 minutes • Crepitus • Plus, the presence of osteophytes	Knee pain + at least 3 of the following: • Age >50 years • Stiffness <30 minutes • Crepitus • Bony tenderness • Bony enlargement • No palpable warmth
92% sensitive, 75% specificity	91% sensitive, 86% specificity	95% sensitive, 69% specificity

2.6 Epidemiology of OA

2.6.1 Prevalence and incidence

The estimation and determination of the incidence and prevalence of OA is difficult, since they both vary depending on the definition and criteria used (76). For example, using radiographic criteria gives different incidence and prevalence rates compared to symptomatic criteria (68). The radiographic prevalence of hand OA as determined from the Osteoarthritis Initiative data was 41% compared to 12.4% symptomatic prevalence (77). Similarly, the Johnston County

Osteoarthritis Project's data on knee OA also revealed a 28% radiological prevalence compared to a 16% symptomatic incidence (78). A possible explanation for such variation is the fact that not all symptomatic criteria such as pain correlate with radiographic criteria (68). Despite that, several studies around the world have focused on estimations of both the prevalence and incidence of OA.

In a study led by Lawrence, Felson (79), which focused on defining the prevalence of OA from 2003 to 2005 based on all the published analyses of national surveys in the United States, it was shown that the prevalence of OA increases with age. More than 26.9 million Americans over the age of 25 years had some kind of OA. Furthermore, their study found that the prevalence of radiographic OA differs depending on the joint affected. For the knee joint, 37.4% of adults above the age of 60 years exhibited radiographic evidence of OA. Also, in the hand joints, around 27.2% of adults showed radiographic signs of OA, and the percentage increased to 80% in adults who were 65 years old. It was further shown that the prevalence of symptomatic OA is lower than that from radiographic criteria, where the symptomatic prevalence of hand OA was 6.8% of all adults and 16.7% for the knee joint.

The ankle joint has the lowest OA prevalence compared to that for other lower limb joints (80). For example, UK data from 2017 reported a prevalence of ankle OA of 0.3% (81). That could be due to the fact that ankle OA is categorised as secondary OA usually following a specific injury (82). However, several studies have reported a much higher prevalence of ankle OA in individuals diagnosed with knee OA. Tallroth, Harilainen (45) reported that 28.8% of participants with knee OA also had ankle OA, Xie, Jiang (43) found a 36.8% prevalence of ankle OA in their study population and, most recently Kikuchi, Kanamori (46) reported a 24% prevalence of ankle OA in their sample which contained knee OA participants, indicating a possible structural association between the two joints.

A considerable literature has been published regarding the incidence of OA (83-86). For example, Oliveria, Felson (84) examined the incidence rates of hand, hip and knee OA using data from 696 participants who were members of the Fallon Community Health Plan in Massachusetts, USA. Participants were defined using radiographic and clinical symptoms of OA obtained from a multispecialty group practice, and the study results showed that the

standardised incidence rates were 240 per 100,000 person-years for knee OA, 88 per 100,000 person-years for hip OA, and 100 per 100,000 person-years reported for hand OA.

Furthermore, a more recent study conducted by (86) analysed data from a random sample of both primary and secondary health records from British Colombia, Canada (n=640,000 participants) during the period between 1991 to 2009 to calculate incidence rates of OA. The total crude incidence rates were 14.6 and 16.3 per 1000 person-years for men and women, respectively, with approximate annual increases of 2.5-3.3% per year. The variations between studies in estimates of incidence rates for OA may differ due to variations in the criteria used and the numbers of participants included in each study. However, a majority of reports agree that both sex and age have significant associations with rates of OA incidence (76).

2.6.2 Burden of OA

2.6.2.1 Disability

The Global Burden of Disease (GBD) study led by the World Health Organisation aims to document diseases such as OA that disable, injure and kill people around the world (87). In the 1990 GBD study, OA was ranked 15th in a list comparing the diseases that were most likely to cause disability. However, in a more recent GBD study conducted in 2010, OA was ranked 11th (88). Additionally, OA burden ranked 10th in America, 6th in Asia, 13th in Western European countries and 7th in Eastern Europe (88). This demonstrates that OA is currently one of the leading global causes of disability.

Disability from OA is well documented in the literature (89, 90). OA limits activity in persons diagnosed with the disease, which restricts their participation in various daily life activities (91). For example, in a health disability survey conducted in France, OA was the main cause of disability. The authors reported that 22% of the participants had difficulty walking, 19% struggled to carry out objectives and 13% experienced difficulties dressing (92). Also, in the Third National Health and Nutrition Examination Survey in the USA, 80% of participants with OA had movement limitations, of them 11% required personal assistance, and 25% could not easily perform regular daily activities (93).

2.6.2.2 Comorbidity and mortality

Mortality has not been one of the major areas of research in the OA population (94). Many epidemiological studies focus more on disability and the economic burden of this disease. However, some studies have partially focused on investigating the co-morbidity associated with OA and the mortality ratio (95). A large population study led by Nüesch, Dieppe (96) involved men and women with confirmed radiographic evidence of lower limb OA, which aimed to evaluate the disease and causes of mortality in the OA population. The standardised mortality ratio was 1.55 (95%CI 1.41-1.70), which was similar to those for both cardiovascular diseases at 1.71 (95%CI 1.49-1.98) and dementia at 1.99 (95%CI 1.22-3.25). Additionally, increased walking disability was reported to increase the risk of death ($p<0.001$). The authors concluded that the increase in mortality attributable to cardiovascular disease in the OA population could be attributed to their lack of physical activity and the fact that patients with severe OA-related disabilities are at a greater risk of mortality than other OA patients (96).

In a more recent propensity score-matched analysis, Hawker, Croxford (97) confirmed the results from the previous study. The population in this study consisted of patients with clinical and radiographic symptoms of lower limb OA. The authors established that the majority of the causes of mortality were associated with the limitations on physical activity among OA patients and that the risk factor of cardiovascular disease death increases in patients who specifically have a severe walking disability (97).

However, data from two Dutch cohort studies that included patients with both upper and lower limb symptoms of OA have been analysed, and no mortality risk increase in the OA population was found (98). The results of these studies conflict with those of the two previously cited studies but was arguably underpowered and with a potential healthy cohort effect.

2.6.2.3 Health care costs

Reports show that more than 13 million clinical visits were made by patients complaining of OA symptoms in France in 2002 (99). The cost of such visits exceeded 1.4 billion Euros (including 570 million for medication and 820 million for in-patient treatment), which is 1.7% of the total cost of the health care system in France (99). In addition, OA was the second most expensive overall of all medical diseases treated in American hospitals in 2013, accounting for 4.3% ($18.4 billion) of the total cost of hospitalisation ($415 billion) (100). In the UK around £1 billion at 2010 prices is thought to have been spent on OA-related medical expenses (101).

In the United States, the total cost of hip and knee replacement surgeries increased nearly threefold in under 10 years. In 1997, the cost was approximately 7.9 billion dollars and by 2004 this had increased to 22.6 billion dollars (102). Since the ageing population in the world is increasing and rates of replacement surgery are also increasing, the economic situation is predicted to worsen in the future (100, 103).

2.7 Risk factors for OA

Many factors can increase the risk of developing OA during the lifetime, and these are categorised in two groups. The first is non-modifiable risk factors which include age, sex, and bone density. The second group are modifiable risk factors such as obesity and biomechanical risk factors such as the abnormal loading of the joint and joint malalignment (19). Some of these risk factors are explored in the following sections.

2.7.1 Age

Osteoarthritis is known to be an age-related disorder, since age is classified as one of the main risk factors for the disease (18). Research has shown that 30-50% of people over the age of 65 have already developed radiographic OA in at least one joint(104). This illustrates the fact that the prevalence of OA increases in ageing populations (79). Prieto-Alhambra, Judge (85) conducted a large study to estimate the incidence of OA relative to age and sex in different joints. The study included data for over 3 million people aged 40 years or more who had been diagnosed with OA for 4 years extracted from an electronic database of medical records representing a Spanish population. The results showed that the incidence rates of OA in the hand, hip and knee are higher in females and increase substantially with age for both sexes, reaching a peak near the age of 75 years. Figure 2-3 shows OA incidence per 1000 person-

years: 16-17 for the knee, 6 for the hip, and 4-5 for the hand. Additionally, a recent study by Cui, Li (105) aimed to estimate the global prevalence and incidence of knee OA by conducting a random-effects meta-analysis. It was found that, in participants aged over 15 years, the knee OA prevalence was 16% while for those over the age of 40 years it was 23%. The association between age and OA is well-established in epidemiological studies, and the results mentioned above, and others have confirmed that age is a significant risk factor for the development and progression of OA.

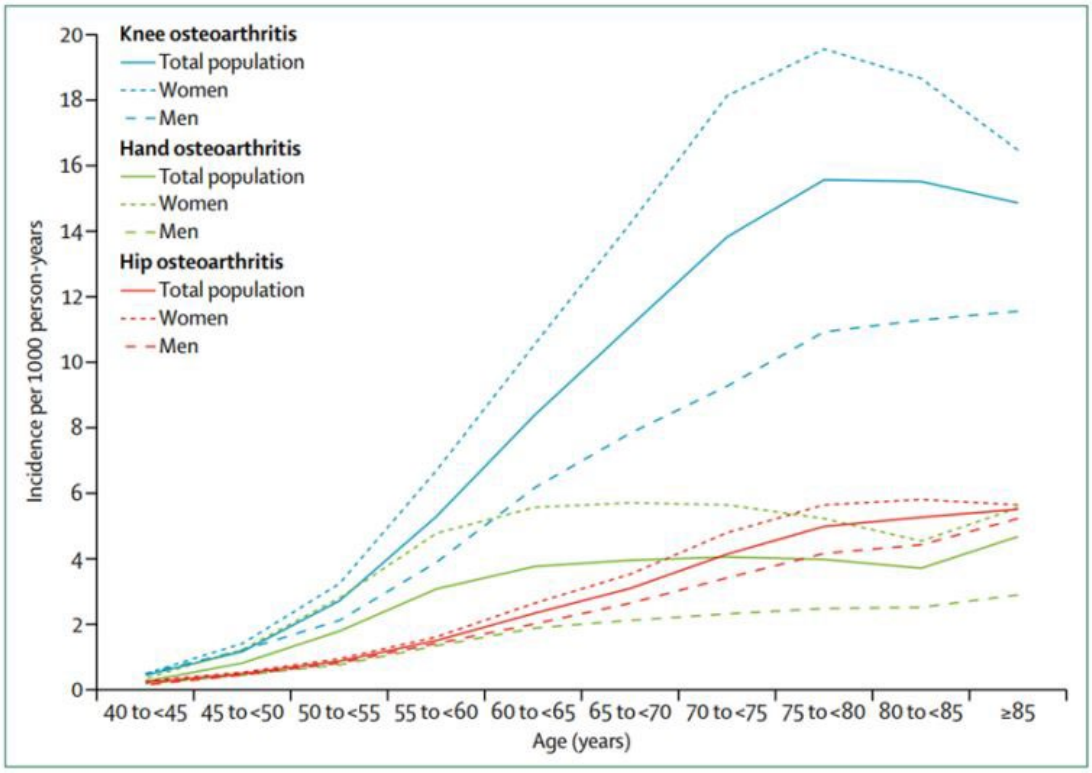

Figure 2-3. Incidence of hand, hip, and knee OA in relation to sex and age, showing that incidence increases with age reaching a peak around 75 years and females have a higher incidence of OA in all joints compared to males adapted from (85).

The conceptual framework established by Ling and Ju (106) offers a possible explanation of the relationship between ageing and the development of OA. It is based on the theory that, in general, ageing results in the weakening of the bones, muscles, ligaments, and tendons constituting the musculoskeletal system. This in turn increases the risk of OA, but does not cause it alone. Such weaknesses produce changes both within the joint and outside of it; for example, due to the occurrence of changes in the cells and matrix within the joint and the development of sarcopenia outside the joint. Such changes increase the probability of OA in

the joint in conjunction with other risk factors (see Figure 2-4 below), but it is not the main cause. This is because OA incidence has a multifactorial nature and not all older people develop OA (23).

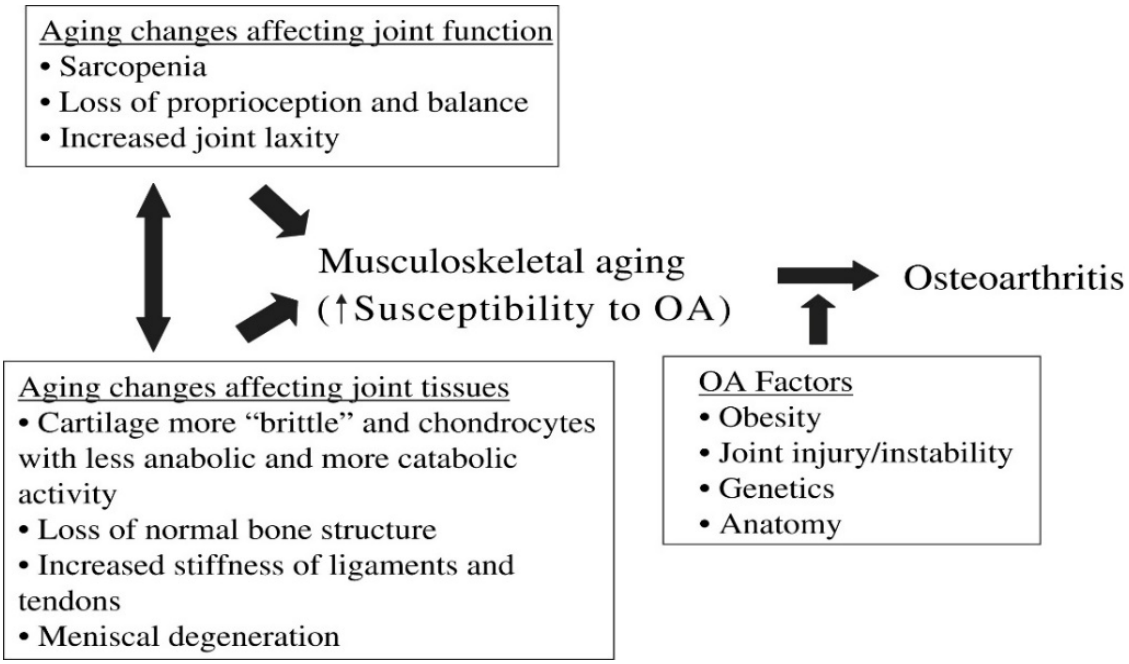

Figure 2-4. Framework for ageing and the development of OA adapted from(23); permission to use available via ELSEVIER LICENCE: #4666700903053.

2.7.2 Sex

Several studies have reported that females tend to have higher ratios of prevalence and incidence of OA compared to males (81, 85, 105, 107). In a meta-analysis conducted by Srikanth (107), which focused on the correlation between sex and the prevalence of OA, it was reported that females have more severe, and a higher prevalence of OA compared to males. For example, in knee OA the results showed that the risk of the outcome in males compared to females was significantly lower for males with (pooled RR 0.63, 95% CI 0.53–0.75). Also, the results showed that females are more often affected by knee, foot, and hand OA. Furthermore, following menopause, females present more severe radiographic knee OA symptoms. Additionally, the results of a random-effects meta-analysis which included 88 studies with more than 10 million participants showed that female were at much greater risk than males. In particular, females had a 1.39 times higher incidence than men (95% CI, 1.24-1.56) and a 1.69 times higher prevalence than males (1.59-1.80) (105).

Recent data from a sizable primary care database that is representative of the UK was used to estimate both the prevalence and incidence of OA (81). The study focused on the period from 1997 to 2017 and included data from more than 1.5 million participants. The results showed that the incidence of any OA in females was higher than in males at 8.1 compared to 5.5 per 1000 person-years respectively. Similarly, the prevalence ratio of any OA type was also higher in females at 12.8% compared to 8.6% for males.

Such data showing females to have a higher prevalence and incidence of OA compared to males could be attributed to a combination of several factors that have been studied and that show differences between sexes, including differences in joint size and alignment (108, 109), bone strength (110), pregnancy (111), hormonal status (107), and neuromuscular factors (112).

2.7.3 Obesity

Obesity is defined as having a body mass index (BMI) greater than 30 kg/m^2 (113). Many studies have considered obesity to be a substantial risk factor for the development of OA in specific weight-bearing joints such as the hip and knee (114, 115). For instance, Coggon, Reading (114) carried out population-based case-control research using data from three different health areas in England. The study sample consisted of 525 participants aged 45 and older who were on the surgical waiting list for knee replacement. Another 525 participants matched for age and sex were recruited to serve as a control group. The results showed that, when the BMI was below 20, the odds ratio for having OA was 0.1 (95% CI 0.0-0.5), whereas if the BMI was above 36 it increased to 13.6 (95% CI 5.1-36.2).

Likewise, a dose-response association between the possibility of knee OA and obesity was established in a meta-analysis which concluded that every increase of 5 units in a participant's BMI was accompanied by a 35% increase in the risk of knee OA (22). A Swedish population study reported that people with BMIs in the highest quartile were substantially more likely to develop knee OA than those in the lowest quartile. With a relative risk estimate of 8.1 (95% CI, 5.3 to 12.4) (116). Another study focused on weight loss and its association with the risk of developing knee OA, reporting the risk decreased by half for each 5kg body weight loss (117).

A recent systematic review and meta-analysis of the results of 23 studies conducted by Solanki, Hussain (118) investigated the relationship between weight increase and the clinical characteristics and structural development of knee OA and rates of total knee replacement (TKR). It was concluded that an increase in weight is linked to elevated clinical and structural knee OA and TKR. The authors recommended that methods for the prevention weight gain should be considered in order to slow progression and improve the management of such diseases.

The previously mentioned studies show that obesity is an important risk factor for OA, and the World Health Organisation also consider that it is becoming a global issue (119). Therefore, further research is needed to develop new prevention methods to minimise any increases in the incidence rate of OA in the future.

2.7.4 Bone density

A crucial indicator of bone health and strength is bone density, which is also known as bone mineral density (BMD) (120). It reflects the volume of bone that contains a certain quantity of mineral content. Low BMD values are associated with a higher risk of fractures, especially in older individuals and people with various medical problems (120). The most common method for the determination of bone density is dual-energy X-ray absorptiometry (DXA) (121). This is a type of diagnostic imaging technique that uses low-dose X-rays to evaluate BMD in several parts of the body (122). Owing to its precision, repeatability, and minimal exposure to radiation, this approach is extensively used (122).

There has been much discussion in the literature on the association between OA and BMD. The majority of studies have focussed on the hand, spine, hip, and knee joints with none assessing the association with the ankle or foot joints (123). However, the results of such studies have been controversial. Several have shown a link between higher BMD and an increased incidence of radiographic hip and knee OA, concluding it to be a risk factor for OA (110, 124-126). In contrast, other studies found no such association (127-130). Such conflicting findings could be attributed to differences between studies regarding the outcome measures used, the characteristics of participants included, or the health status of the joints considered.

For instance, studies which used the K&L as a measure of radiographic incidence show a significant association with higher BMD measurements (126), whereas those that used both K&L and joint space narrowing (JSN) as measures of radiographic occurrence found no association with JSN measurements (130, 131). This could be attributed to the K&L grading incorporating osteophytes (132), which are known to have a significant association with BMD as explained in terms of the mechanisms of bone remodelling (123).

Therefore, the relationship between OA and BMD seems to be complex and may differ depending on the specific joint studied and several other factors that may confound the association, such as age, sex, and BMI (123). Further research such as studying other joints and using new methods is essential to help developing our understanding of the complex relationship between OA and BMD.

2.7.5 Biomechanics

As previously mentioned, one of the characteristics of OA is the progressive loss of articular cartilage within a joint (66). Even though the precise aetiology of OA is yet to be determined, several studies have indicated that biomechanical factors can increase the probability of both onset and progression of OA (133). Biomechanical factors are physical variables increasing the mechanical load and stress on joints, which might eventually lead to articular cartilage damage (25). Such altered loading that potentially has a negative effect on cartilage structure as well as function has been recognised for many years (134). Many factors can result in alterations in the mechanical load in lower limb joints, including joint injury, obesity, high-impact sports, and malalignment (135). These factors are discussed in this section.

Several studies report that, when an individual experiences a joint injury, their risk of developing OA increases significantly (136-139). For example, a study conducted by Gelber, Hochberg (138) explored the risk of developing knee OA with a history of knee and hip injury in 1321 younger adults who were followed up for 36 years. The results showed that, for the 141 participants who had reported injured joints, the relative risk of developing knee and hip OA increased by 5.17 (95%CI, 3.07-8.71) and 3.50 (95%CI, 0.84-14.69) respectively. A recent systematic review by Poulsen, Goncalves (139) reported that, compared to those with intact knee joints, individuals with an isolated anterior cruciate ligament injury afterwards had 4.2

times higher odds of developing knee OA, while those who suffered an isolated meniscus injury had 6.3 times higher odds of developing knee OA.

A possible explanation for this association is that injuries to the joints can result in increased inflammation, instability, and altered joint alignment (140, 141). Over time this can result in alterations in joint mechanics, leading to abnormal loading patterns on the joint and then to articular cartilage damage (141).

As seen in the studies mentioned in section 2.7.3, obesity is a well-established risk factor for OA. However, in terms of biomechanical risk factors, obesity has been shown to affect both the gait cycle and the joints, possibly resulting in increasing joint stress (142-144). Messier, Legault (145) studied the effect of loss of weight on the amount of mechanical load applied to the knee joint in 316 obese participants diagnosed with knee OA, for whom knee joint forces and moments were calculated using 3D gait analysis over 18 months. The results revealed that the loss of 10% of body weight is associated with lower knee joint forces and moments, with possible beneficial alterations in the mechanical pathway of OA. A systematic review concluded that obese people walk at a slower speed, with shorter and wider steps and longer stance duration than normal-weight people at a self-selected speed (146). However, although such biomechanical changes may affect the load-bearing regions of articular cartilage, their potential involvement as risk factors for OA remains unclear (144).

Various studies have highlighted a correlation between repetitive joint use and an increased risk of OA (147-149). The risk of developing knee OA is twice as high for individuals who work in jobs that depend on repetitive specific physical performance such as squatting and kneeling, particularly if they are obese, compared to those who do not engage in such physical activity as part of their work (147). Similarly, prolonged standing and lifting have been linked to hip OA (150). Such a concept of a negative effect of repetitive joint use associated with occupation could also be linked to any physical activity (151).

While exercising and engaging in sports activities are considered to be beneficial for joint health, overloading the joint and especially sports injuries may cause harm (152). Some studies have reported an increased risk of OA associated with repetitive, intensive, and high-impact sports like tennis, squash, and various team sports (153, 154). The prevalence of knee

and ankle OA in former professional footballers was explored in a systematic review by Kuijt, Inklaar (155) and it was concluded that the prevalence of OA in that group was higher compared to the general population.

Another systematic review explored the relationship between hip OA and participation in professional high-impact sports (156). The results showed that such athletes had an increased risk of developing hip OA compared to others (156). Such evidence indicates an increased risk of OA associated with occupations that require physical activity and long-term participation in high impact activities. However, more research is needed to determine if the association between joint injury and OA is solely related to increased mechanical loads on joints, or if the presence and severity of injury also play a role.

Alignment relates to the relative positioning and orientation of bones and joints in the body (157). Improper alignment, also known as malalignment, can cause higher stress on joints which may lead to the onset and progression of OA (158). The frontal plane alignment in the knee is known to be a strong predictor of knee OA progression (159). A recent Chinese longitudinal study by Wang, Liu (160) reported that both varus and valgus knee malalignment were associated with the increased prevalence of both medial and lateral knee OA respectively, with values of OR 6.1 (95% CI: 4.4-8.6) and 5.0 (95% CI: 2.4-10.5) respectively. In addition, altered knee loading during walking had been previously noted in a participant with varus knee alignment. Meanwhile, a meta-analysis conducted by Van Tunen, Dell'Isola (161) showed a higher adduction moment during walking in participants with medial knee OA (OR = 3.0; 95% CI 1.9-4.9) compared to others.

Only limited evidence of biomechanical risk factors associated with the characteristics of gait in hip OA participants has been published (162). Tateuchi, Koyama (163) conducted a detailed analysis of the gait cycle in hip OA participants aiming to understand biomechanical risk factors related to hip OA progression. They concluded that increased cumulative hip loading during daily activities is significantly associated with hip OA progression over 12 months (OR = 1.34; 95% CI 1.06-1.70; P = 0.0130).

The structure and function of the ankle joint complex can also alter the biomechanics of the lower limb. The foot and ankle play a crucial role in transmitting mechanical force throughout

the lower limb (26). The mechanical force travels from the ankle complex region during the gait cycle to the hip through the bones and lower limb joints, including the ankle, knee, and hip (28, 164). This transfer of force is crucial for normal human locomotion and for everyday activities such as walking, running, and jumping (29). The lower limb bones and joints act as mechanical lever systems, allowing force generated at the ankle to be transmitted up the limb and ultimately to the hip (30). The foot and ankle thus play a critical role in the reception, absorption, and transfer of forces during the gait cycle. Any alterations in foot and ankle characteristics, such as variations in the morphology or alignment of the bones in the ankle region or static foot posture can increase the mechanical loading on other joints of the lower limb, thereby influencing OA progression (31).

Many studies have explored the association between the hip and knee joints, focusing on OA-related factors such as biomechanical, structural, functional, and symptomatic variables. However, less attention has been given to the association between the ankle and the hip and knee joints, and this may be because ankle OA has a much lower prevalence than that of the knee and hip, as discussed in section 2.6.1. Despite such paucity of research, some studies have considered the functional and symptomatic connections between the ankle and the other joints. Gross, Niu (32) found no association between rear-foot varus alignment and reported hip pain, whereas Paterson, Hinman (33) concluded that participants with ankle pain reported a 39% worse score on all WOMAC subscales indicating worsening symptomatic OA in the knee joint. A subsequent study Paterson, Kasza (34) found that reported ankle and foot symptoms were associated with worsening knee pain, but no such association with radiographic knee JSW was noted. Most recently, Perry, Segal (35) showed a significant association between baseline ankle pain and frequent knee pain at follow-up.

These investigations focused primarily on correlations between various aspects of the ankle and foot, such as pain and functional characteristics, and OA in both the hip and knee joints indicating an association between ankle and foot symptoms and OA, but any specific relationship involved remains to be further explored. Nevertheless, the structural association between the ankle, hip, and knee remains relatively unexplored. In fact, Perry, Segal (35)

highlighted the importance of an assessment of the structural association between the complex morphology of the ankle and the hip and knee joints.

In addition, other research has evaluated the alignment of the ankle complex and lower limb as well as foot posture in participants with knee and hip OA. The results of various studies using different methods have shown a significant association between a pronated foot posture and knee OA and between supinated foot posture and hip OA. Reilly, Barker (36), Reilly, Barker (37) showed that participants with knee OA had a pronated foot posture, while those with hip OA had a supinated foot posture, and Abourazzak, Kadi (38) found a significant correlation between foot pronation and knee OA in a Moroccan population. Furthermore, Gross, Felson (39) concluded that knee pain and damage to the medial knee cartilage are significantly associated with a pronated foot posture. Most recently, Zhang, Nie (40) found that participants with pronated feet had an increased risk of more severe knee OA symptoms and cartilage damage based on K-L grade, pain score, and loss of function. Additionally, a recent systematic review and meta-analysis by Almeheyawi, Bricca (31) concluded that pronated foot posture was present in people with knee OA, but the relationship between other foot and ankle characteristics and knee OA is not yet established due to heterogeneity between the limited number of studies. The authors recommended the need for a more common measurements methods when exploring the association between knee OA and foot and ankle characteristics.

The structural relationship between the hip, knee, and ankle joints has also been investigated in a number of studies. In a 3-year follow-up study, Kraus, Worrell (44) used nuclear medicine bone scans to evaluate ankle joint abnormalities in 159 participants with radiographic knee OA. The finding of a hazard ratio of 1.41 (95%CI 1.14-1.73; $p<0.001$), demonstrated a significant relationship between ankle bone scan abnormality and lower knee JSW. Additionally, Xie, Jiang (43) reviewed 96 full-leg radiographic images of participants with end-stage knee OA to explore the association between knee malalignment and the development of radiographic ankle OA. Knee malalignment was evaluated by two radiographic measures, the hip-knee-ankle angle (HKA) and medial proximal tibial angle (MPTA), and the results indicated a structural association between knee malignment and the development of ankle

OA with odds ratios of 0.72 (p=0.0009) for the HKA and 1.13 (P=0.0169) for the MPTA. Other studies have reported the same conclusion, suggesting that the severity of valgus and varus deformity in the knee joint could have a significant impact on the alignment of the lower limb, thus changing HKA alignment and affecting the ankle(41-43).

While more research is needed, the evidence available from the above-mentioned studies suggests that OA may be linked to biomechanics and force distribution during activity, with the structures of both the ankle and foot playing crucial roles in absorbing and transferring lower-limb forces. However, these studies share similar limitations such that the representativeness and generalisability of their findings are limited. The majority used convenience sampling methods which select participants depending on their availability and willingness to participate or focused more on participants at the end stages of OA and not exploring such associations with participants at earlier stages of the disease. Resulting in limiting the generalisability of the findings to the larger population.

In addition, none of the studies directly considered the morphology of the ankle and its interrelation with hip and knee OA. Instead, they focused on the use of measurement methods such as for lower limb alignment and foot posture and structural and functional classification systems for the lower limb joints. That could be due to the fact that the ankle is a complex anatomical region composed of several interconnecting bones limiting the ability of assessing its morphology, such complexity is discussed further in chapter 3. Therefore, further research is needed to overcome these limitations and explore the structural and functional association between OA in the hip and knee joint and morphological variations of the ankle region. New methods capable of simplifying ankle complexity are needed- these might include 3D-SSM.

Chapter 3 The ankle joint complex

3.1 Summary

The ankle complex is a vital part of the human body, contributing significantly to mobility, stability, and load distribution in the lower extremities. The region consists of bones, joints, muscles, and ligaments that all work together to offer the stability and flexibility required for everyday activities (26). It is essential to understand the complex anatomy and biomechanics of a vital weight-bearing joint such as the ankle complex as a key part of the lower kinetic chain contributing significantly to human locomotion(27).

The four bones that make up the ankle complex are the distal tibia, distal fibula, calcaneus, and talus. The distal tibia and fibula are two of the lower leg bones. Both bones connect with the talus which rests on top of the calcaneus. Another important bone is the navicular bone, which serves as a bridge between the tarsal bones and the bones that form the ankle. All of these bones connect with each other, formulating several joints. The talonavicular, subtalar, and tibiotalar joints are the three primary joints in the ankle complex region. These joints are stabilised by several ligaments which attach to the bones, preventing excessive movement and injury (26, 165).

This chapter gives a thorough description of the bones, joints, and ligaments of the ankle complex region. Additionally, the biomechanics of the ankle joints are also explored. Together this will provide a comprehensive understanding of the ankle's complex anatomy and function, highlighting the significant contribution that it provides to the stability and mobility of the lower limb.

3.2 Anatomy of the ankle complex

3.2.1 Bony anatomy

3.2.1.1 Distal tibia and fibula bones

Two bones—the tibia and fibula—make up the main load-bearing structure of the lower leg. Of the two, the tibia is the larger bone. The majority of the body's weight is supported by it, and it connects two of the most important joints of the lower limb: the knee and ankle joints. Both the tibia and fibula connect to the ankle via their distal parts. The morphology of the bone of the distal tibia and fibula plays a crucial role in the formation and function of the main ankle joint. For instance, the articular surface of the distal tibial bone, which is known as the

tibial plafond, is concave and wide in the sagittal plane whereas, in the transverse plane, the surface is slightly convex. Such differences in the surface permit a smooth articulation with the talus dome and allow the smoother functioning of the main ankle joint. Additionally, the distal end of the tibia has an inferior projection known as the medial malleolus that articulates with the talus bone through the medial articular surface (166, 167).

The distal fibula bone is irregular in shape and known as the lateral malleolus. It articulates with the lateral surface of the talus and is connected to the tibia by the interosseus ligament. These three structures, the tibial plafond, medial malleolus, and lateral malleolus, form the ankle mortise and are held in place by strong ligaments making up the ankle syndesmosis (26, 168). Figures 3-1 and 3-2 show anatomical illustrations of both distal bones.

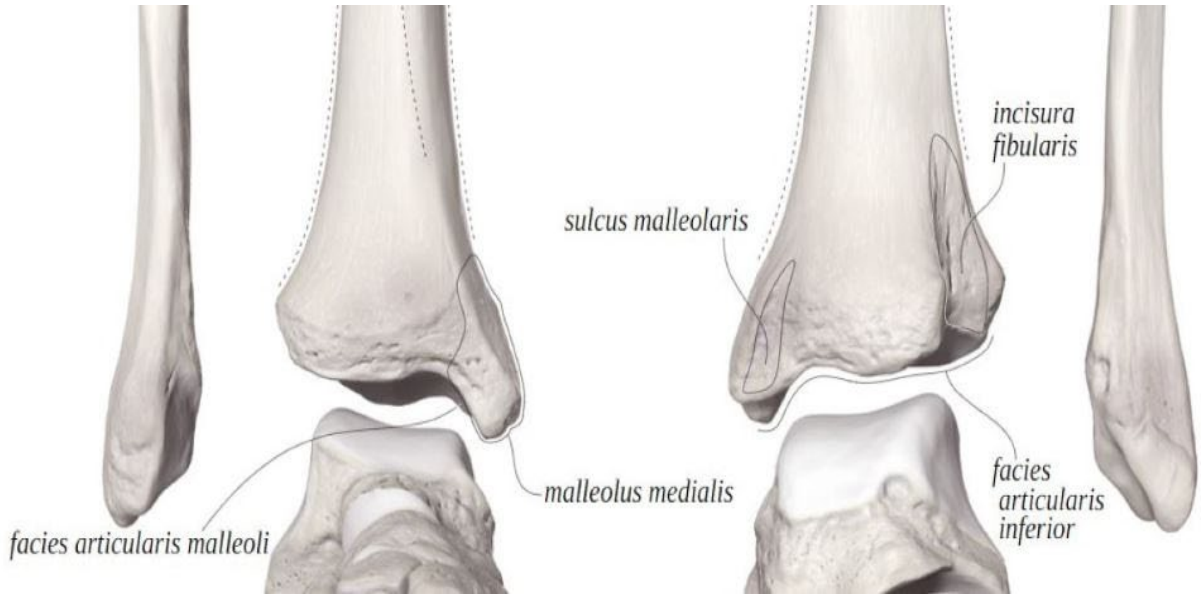

Figure 3-1. Anterior and posterior views of the distal tibia and fibula bones adapted with permission from (169).

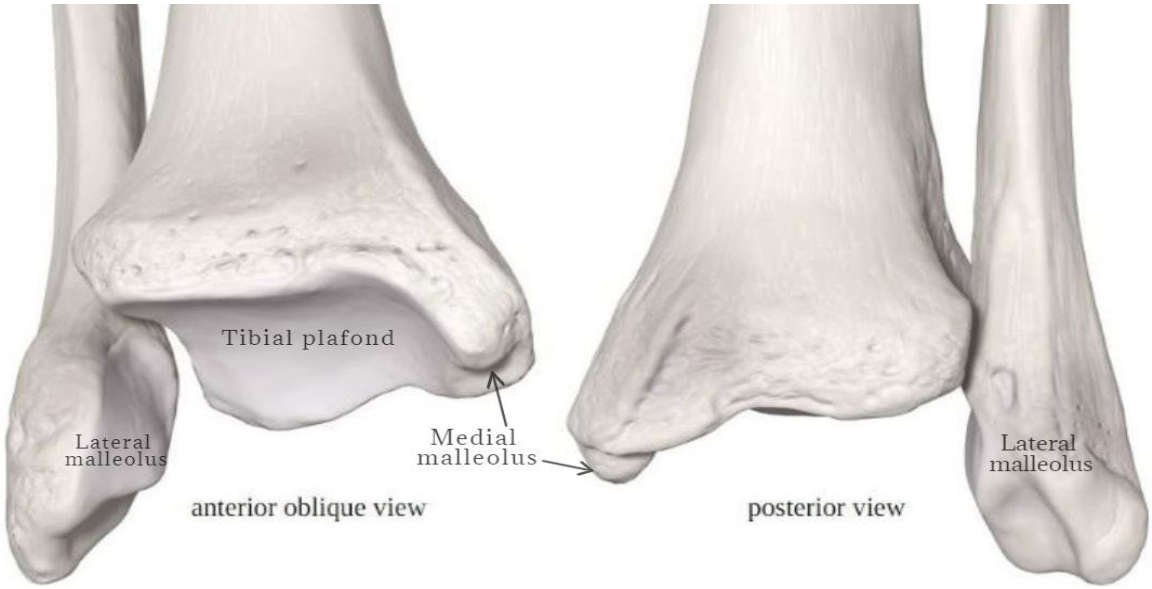

Figure 3-2. Anterior oblique and posterior views of the distal tibia and fibula bones showing the articulation surfaces adapted with permission from (169).

3.2.1.2 Talus bone

The talus bone also plays an important role in weight-bearing and is an essential component of the foot and ankle's overall structure and stability. It is located between the distal tibia and fibula bones of the lower leg and above the calcaneus as shown in figure 3-3 below. The talus is known to be an irregular bone that has a roughly cubic shape and is the second largest bone in the ankle complex region. Three main parts form the structure of the talus: the body, neck, and head (170, 171).

The body of the talus account for the majority of its size, consisting of the talar dome (the trochlear – the smooth rounded superior surface of the talus), plus the medial, lateral, and posterior surfaces. The talus body also has three processes, the lateral, medial, and posterior, which function as the locations where ligaments attach to the bone (172, 173).

The neck of the talus serves as a bridge connecting the head of the talus to the body. The inferior part of the neck on the posteromedial side forms the narrow tarsal canal. The head of the talus is found in the anterior part of the bone. It contains three articular surfaces. The largest of these is the anterior surface which articulates with the navicular bone and forms the talonavicular joint. The other two are found in the inferior part of the head where the

anterior facet articulates with the calcaneus and the medial with the sustentaculum tali (170, 173). Figure 3-3 provides a detailed illustration of the anatomy of the talus bone.

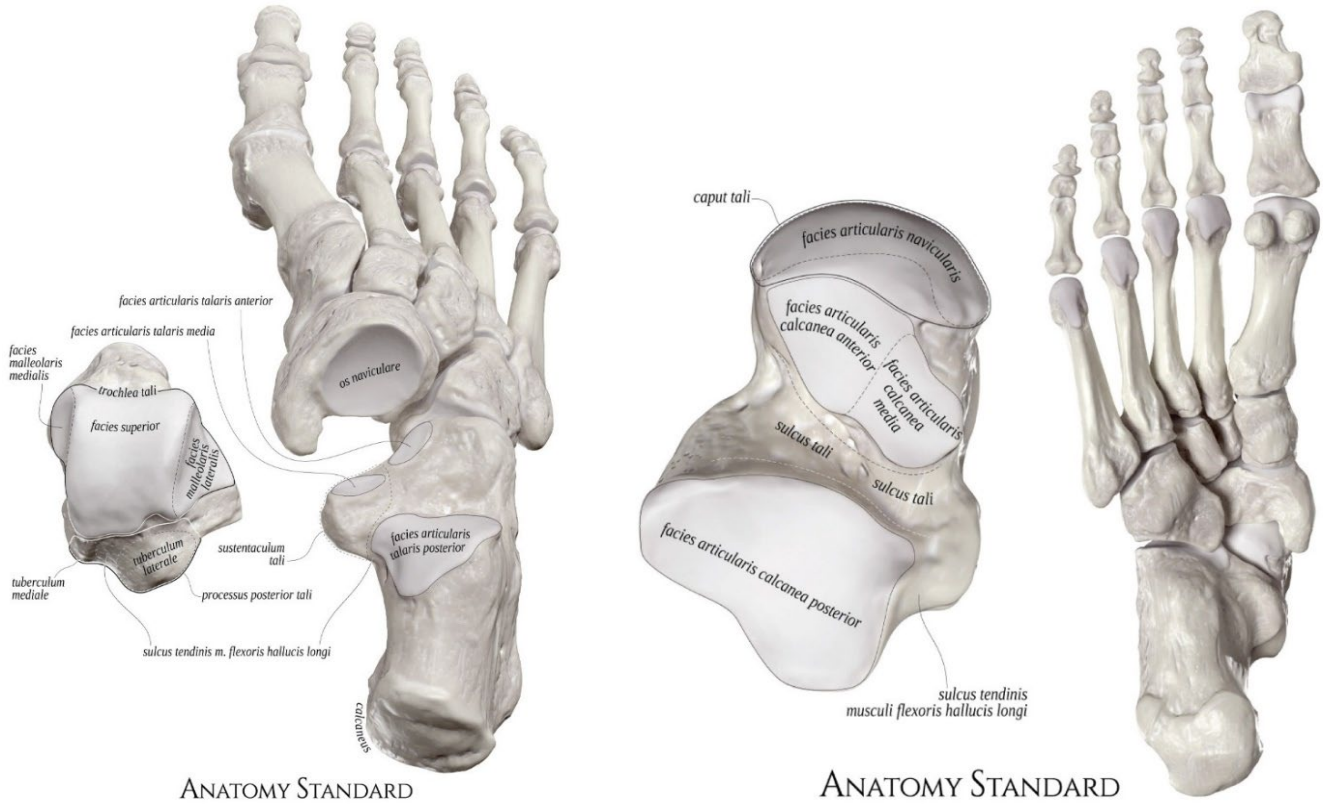

Figure 3-3. Images of the talus bone anatomy. On the left superior and the right inferior view of the talus bone from a right foot with both bone and articulation features illustrated adapted with permission from (169).

3.2.1.3 Calcaneus bone

The calcaneus bone is also known as the heel bone and is the largest in the ankle complex region. It is located at the back of the foot and under the talus bone, and functions to support the weight of the body and absorb shock during walking and other weight-bearing activities. The calcaneus is also an irregular bone presenting approximately a cuboid shape. It has six surfaces: posterior**,** superior, medial, lateral, inferior, and anterior. Each surface has structural characteristics that help its unique function (171, 174).

The anterior surface of the calcaneus is flat and connects with the midfoot bones via the cuboid bone. Both the medial and lateral surfaces of the calcaneus are flat, with some bony projections above the flat surface. For example, the peroneal tubercle on the lateral side gives attachment to tendons such as the fibularis brevis and muscles such as the longus muscles. The medial surface has a bony projection from the upper part of the medial side, which is

known as the sustentaculum tali. That articulates with the medial articulation surface of the talus head and forms part of the subtalar joint (174, 175).

The posterior surface of the calcaneus is circular with a convex structure, and is divided into three facets: superior, medial, and inferior. The superior facet is separated from the medial by the retrocalcaneal bursa. The medial facet is the area where the Achilles tendon connects to the calcaneus bone. The inferior facet has a rounded surface that bends more inferiorly and forms the calcaneal tuberosity, which has two processes: medial and lateral. Both add support to the calcaneus and form an attachment point for the plantar ligament (175, 176).

The superior surface of the calcaneus contains three articulation surfaces: anterior, medial, and posterior facets. The posterior facet is larger than the anterior, and both surfaces articulate with the talus to form the subtalar joint. Moreover, there is a deep groove known as the calcaneal sulcus between the posterior and anterior facets which, combined with the opposing talar sulcus, shapes the tarsal sinus. The large space forming the tarsal sinus hosts several ligaments and other neurovascular structures (175, 177). Figure 3-4 shows an anatomical illustration of the calcaneus bone.

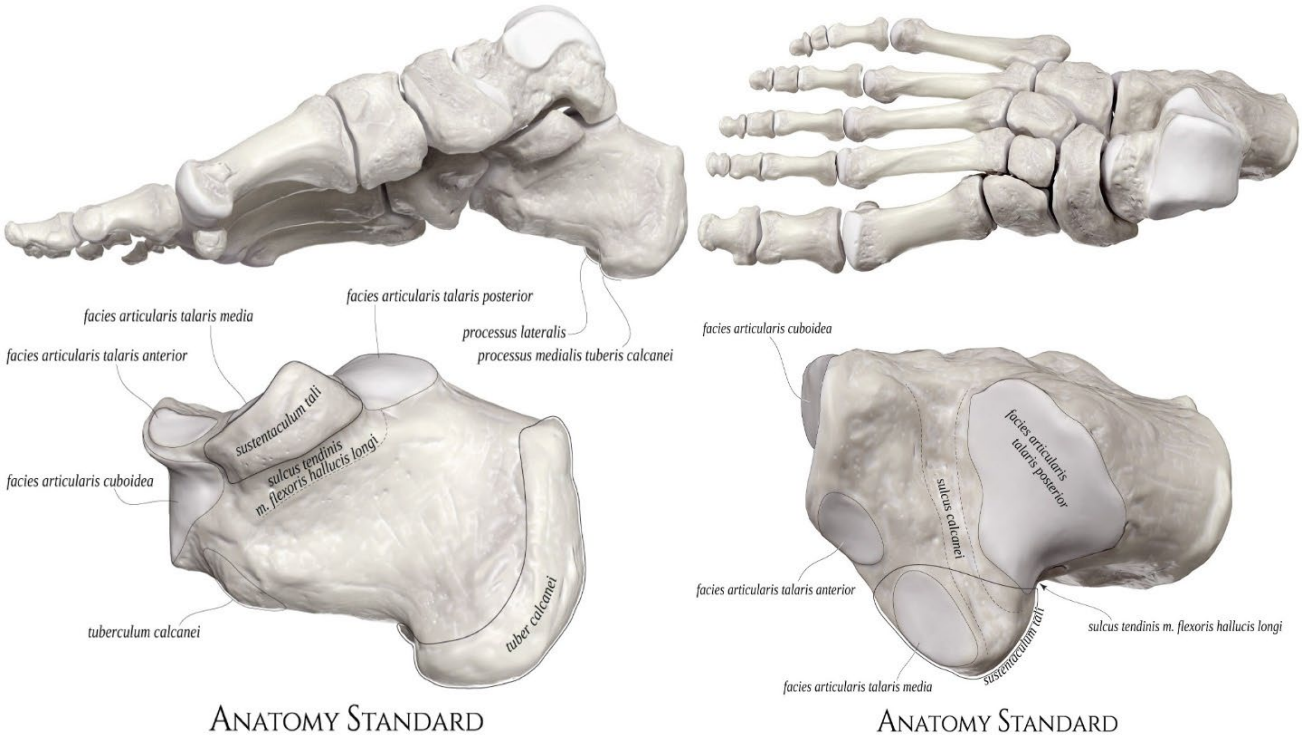

Figure 3-4. Illustration of the anatomy of the calcaneus bone. On the left is a medial view and on the right is a superior view of the calcaneus bone from a right foot; both bone and articulation features are illustrated adapted with permission from (169).

3.2.1.4 Navicular bone

The navicular bone is wedge-shaped, articulating with five tarsal bones in the foot and forming the syndesmotic joints. These bones include the talus, cuboid, and three cuneiform bones located in the midfoot. It performs as a bridge linking the forefoot bones with the ankle. The navicular has a plantar, medially located apex and a circular base at its dorsolateral end. Also, it has two ends (medial and lateral) and four sides (anterior, posterior, dorsal, and plantar) (171, 178, 179).

The navicular bone's anterior portion resembles the shape of a kidney with three articular surfaces articulating with the medial, intermediate, and lateral cuneiform bones, converging at the plantar surface to produce the foot's transverse tarsal arch. The posterior portion is concave and surrounded by articular cartilage, connecting to the talus head to form a tri-planar ball-and-socket joint known as the talonavicular joint. The dorsal and plantar parts provide attachment for a variety of capsule-ligamentous structures (171, 179, 180).

The navicular tuberosity is an osseous prominence located on the medial side of the navicular bone, where the plantar and medial navicular ligaments and the posterior tibial tendon connect. The lateral end divides into superior and inferior segments, providing articulation to the cuboid bone and serving as a point of attachment for the medial component of the lateral calcaneonavicular ligament (179). Figure 3-5 provides an anatomical illustration of the navicular bone.

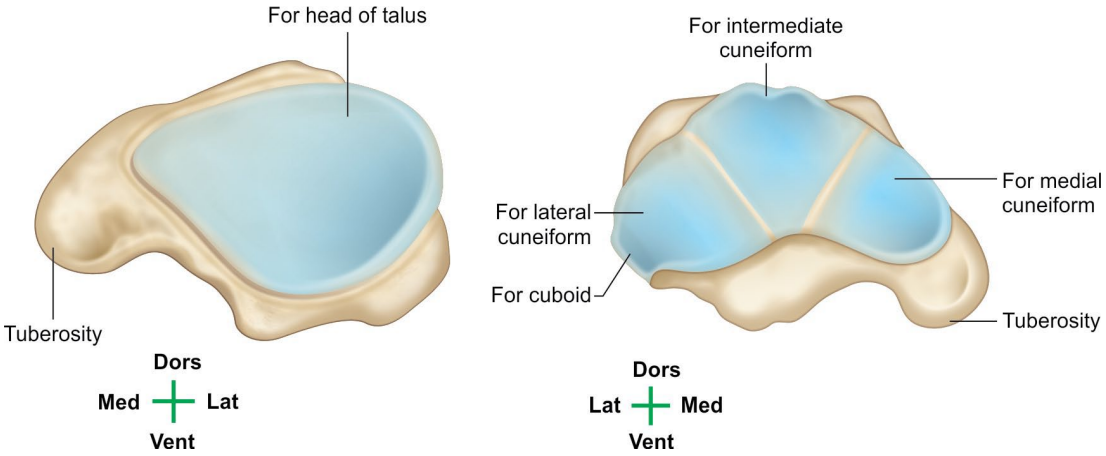

Figure 3-5. Illustration of the anatomy of the navicular bone. On the right is the posterior view showing the articulation surface with the head of the talus. The left shows the anterior view and the articulation surfaces with the cuneiform bones adapted from (171).

3.2.2 Anatomy of joints in the ankle complex

There are two major joints in the ankle region: the tibiotalar (talocrural) joint, or 'true ankle joint,' which connects the talus bone with both the distal parts of the tibia and fibula bones, and the subtalar joint, or 'talocalcaneal joint' which connects the talus and calcaneus bones. In addition, the area has a third joint frequently known as the talonavicular joint which connects the navicular bone in the foot to the ankle region. Each joint may have several articulation surfaces that connect with different parts of the corresponding bone to form other joints. The anatomy and function of each of the three joints are described in more detail in the following sections (26, 178).

3.2.2.1 The tibiotalar joint.

The tibiotalar joint, also known as the ankle joint, is a crucial hinge joint connecting the lower limb with the foot. It is particularly important in weight-bearing and locomotion, because it allows for dorsiflexion and plantarflexion which involve pointing the foot upward and

downward respectively, as well as some degree of inversion and eversion which involve turning the foot inward or outward (29, 181).

The tibiotalar joint consists of three bones, namely the tibia, fibula, and talus, which are connected by three articulation surfaces. The inside surface of the joint connects the tibia and the trochlear surface of the talus bone to form the tibial plafond joint. This articulation surface is the largest articulation in the tibiotalar joint. The medial articulation surface connects the lower end of the tibia bone, known as the medial malleolus, and the medial trochlear surface of the talus bone, forming the medial malleolus joint. Similarly, the lateral articulation surfaces include the lower end of the fibula bone, known as the lateral malleolus, and the lateral trochlear surface of the talus bone, forming the talofibular joint as seen in figures 3-1 and 3-6 (26, 166, 168).

To provide stability and support to the joint, ligaments play a crucial role in connecting the bones that form the tibiotalar joint. Ligaments are tough, fibrous bands of connective tissue that attach bone to bone and help prevent excessive movements that can cause injury. Several types of ligaments support the tibiotalar joint. The anterior talofibular ligament (ATFL) connects the anterior portion of the talus bone to the lateral malleolus of the fibula bone and is one of the most commonly injured ligaments in the ankle, particularly during inversion injuries where the ankle rolls inward causing the ligament to stretch or tear (182).

3.2.2.2 The subtalar joint

The subtalar joint is also referred to as the talocalcaneal joint and is a synovial joint located in the ankle between the talus and calcaneus bones. This joint is classified as a plane or gliding joint, allowing for back-and-forth and side-to-side movements between the two bones. It is one of the two major joints in the ankle complex and is responsible for approximately 60-70% of the inversion and eversion movements of the ankle (183, 184).

The subtalar joint is composed of three facets: the posterior, middle, and anterior facets. The largest of the three is the posterior facet located on the superior side of the calcaneus bone. It is convex in shape and articulates with the concave-shaped posterior facet of the talus bone found on the posterior aspect of the talar body. The middle facet is smaller than the posterior facet and is located on the middle aspect of the calcaneus bone to serve as the articulation

surface of the sustentaculum tali. It articulates with the medial sustentacular facet found in the inferior part of the talar head. Lastly, the anterior facet is the smallest of the three facets and is located on the anterior aspect of the calcaneus bone to articulate with the anterior facet found on the inferior part of the talar head, as shown in figures 3-4 and 3-6. Such articulations are supported by several strong ligaments, including the calcaneofibular, talocalcaneal interosseous, and cervical ligaments. These further stabilise the subtalar joint and help in preventing excessive bone movement (182, 184, 185).

The primary function of the subtalar joint is to absorb and transmit the forces generated during weight-bearing activities. Additionally, it serves as a vital link between the ankle and lower limb, transmitting load from the ankle to the tibia or vice versa. It plays a crucial role in maintaining the balance and stability of the foot and ankle in response to rapid changes in direction. Therefore, it must be able to move as required to fulfil these demands while being stable enough to bear the weight placed on it (183, 184).

The three movements that the subtalar joint can perform are inversion, eversion, and a combination of abduction and adduction. Inversion refers to the movement of the foot towards the midline of the body, while eversion is the opposite movement of the foot away from the midline. Abduction and adduction are also defined as external and internal rotations, which are movements where the foot is either turned away or towards the midline of the body respectively (183, 186).

3.2.2.3 The talonavicular joint

The talonavicular joint is a fundamental synovial joint placed in the midfoot region connecting the talus bone, located in the ankle, to the navicular bone in the midfoot. It is a crucial joint in the facilitation of weight-bearing and movement in the foot. The joint is classified as a ball-and-socket joint, with the talus bone's convex surface fitting into the navicular bone's concave surface. Supporting the joint are ligaments, including the plantar calcaneonavicular ligament, which links the heel bone to the navicular bone, and the talonavicular ligament which joins the talus bone to the navicular bone (171, 187).

The primary function of the talonavicular joint is to facilitate weight-bearing and movement in the foot. As a ball-and-socket joint, it enables a wide range of movements, including the

inversion and eversion of the foot as well as dorsiflexion and plantarflexion. These movements are essential in maintaining balance and stability during weight-bearing activities (188).

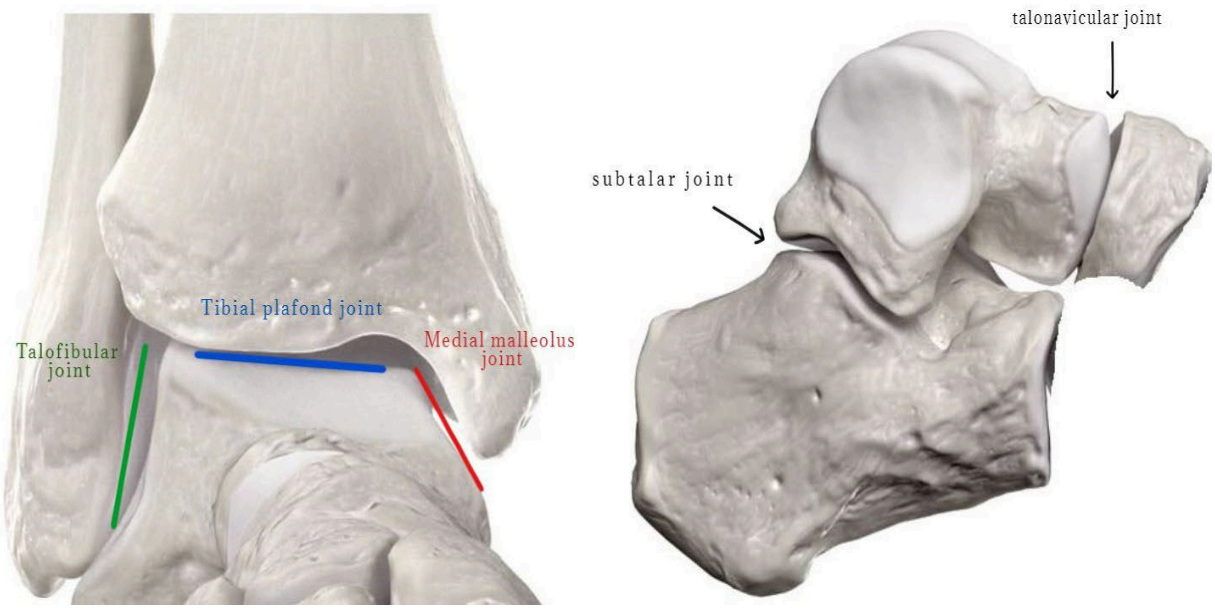

Figure 3-6. Anatomical locations of the joints forming the ankle complex region. (adapted with permission from (169).

3.3 Biomechanics of the Ankle

The ankle complex region is a highly specialised anatomical part that plays a critical role in human locomotion. Ankle biomechanics refers to the study of the movement and function of the ankle complex region. Both kinematics, which deals with motion, and kinetics, which deals with forces, torques, and power, are important quantitative branches of biomechanics (189).

3.3.1 Ankle complex motion

The ankle joint complex undergoes several movements that occur in different planes. These include dorsiflexion (bringing the foot upwards towards the tibia), plantarflexion (pointing the foot downward away from the tibia), inversion (tilting the sole inward towards the midline), and eversion (tilting the sole of the foot outward away from the midline (26, 190). The tibiotalar and subtalar joints work together to enable the motion of the ankle complex. Both the muscles and tendons that surround the joints forming the ankle complex region play important roles in supporting and controlling such movements (181).

Body axes and planes are generally used as means to help in describing the complex motion of the ankle region. The three body planes (sagittal, transverse, and frontal planes) are used to describe the foot and ankle region (26, 181). The sagittal plane separates the foot and ankle into left and right sides. Both plantarflexion and dorsiflexion take place in the sagittal plane. The transverse plane separates the foot and ankle into upper and lower parts. Abduction and adduction occur in the transverse plane. Finally, the frontal plane separates the foot and ankle into front and back parts and the motions associated with this plane are inversion and eversion. Figure 3-7 shows an illustration of these planes and motions of the foot and ankle (26, 29).

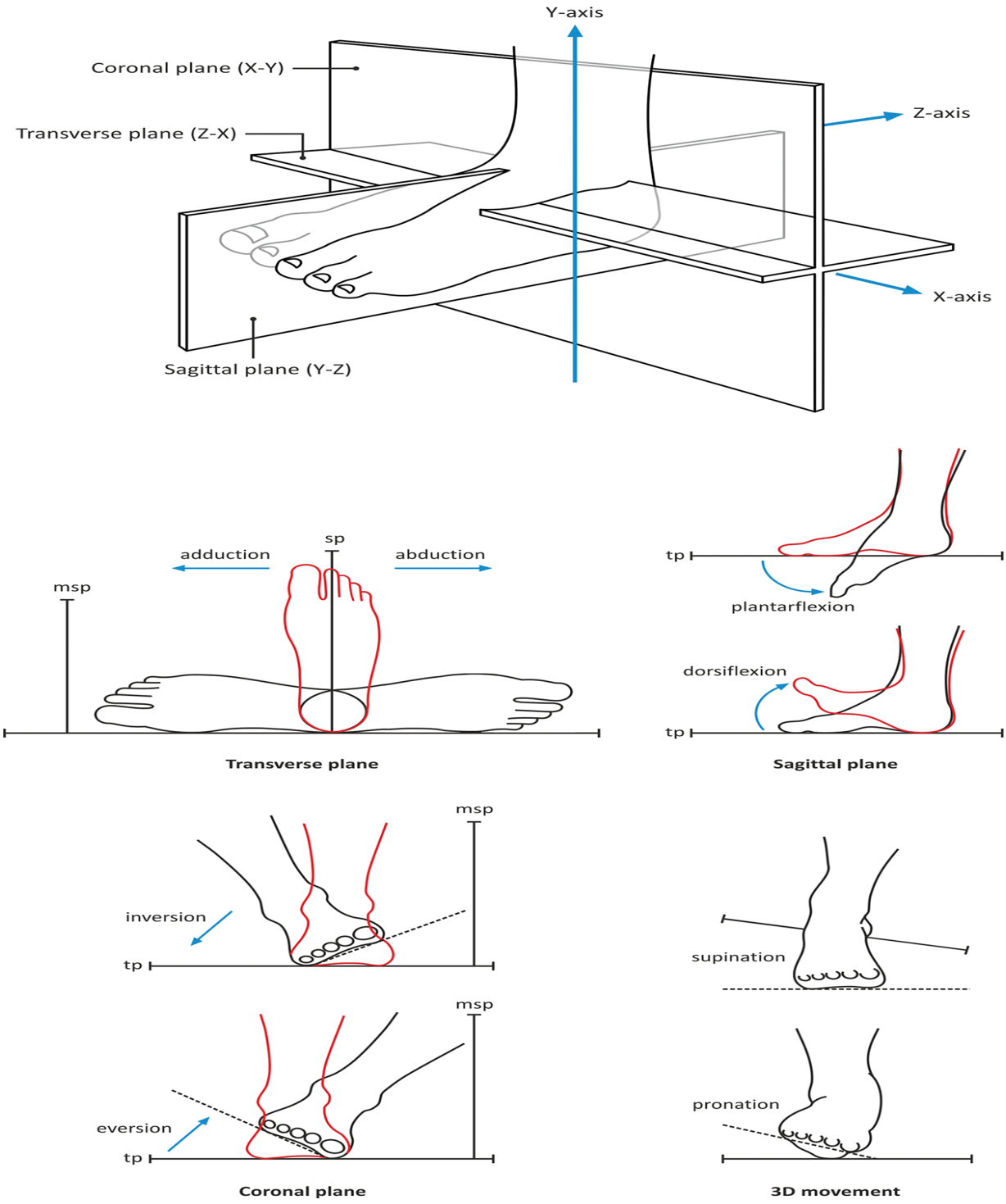

Figure 3-7. Illustrations of the body planes and axes used to describe the motion of the foot and ankle adapted from (29).

The combination of these movements across the subtalar and tibiotalar joints leads to the creation of 3D motions known as supination and pronation (184). These terms describe the orientation of the plantar surface of the foot. During supination, the plantar surface of the foot faces medially, the calcaneus inverts, the talus abducts and dorsiflexes (190).

Conversely, during pronation, the plantar surface of the foot faces laterally, the calcaneus bone everts, the talus bone adducts and plantarflexes. Figure 3-8 illustrates the posterior part of the right foot during the supination and pronation motions (190).

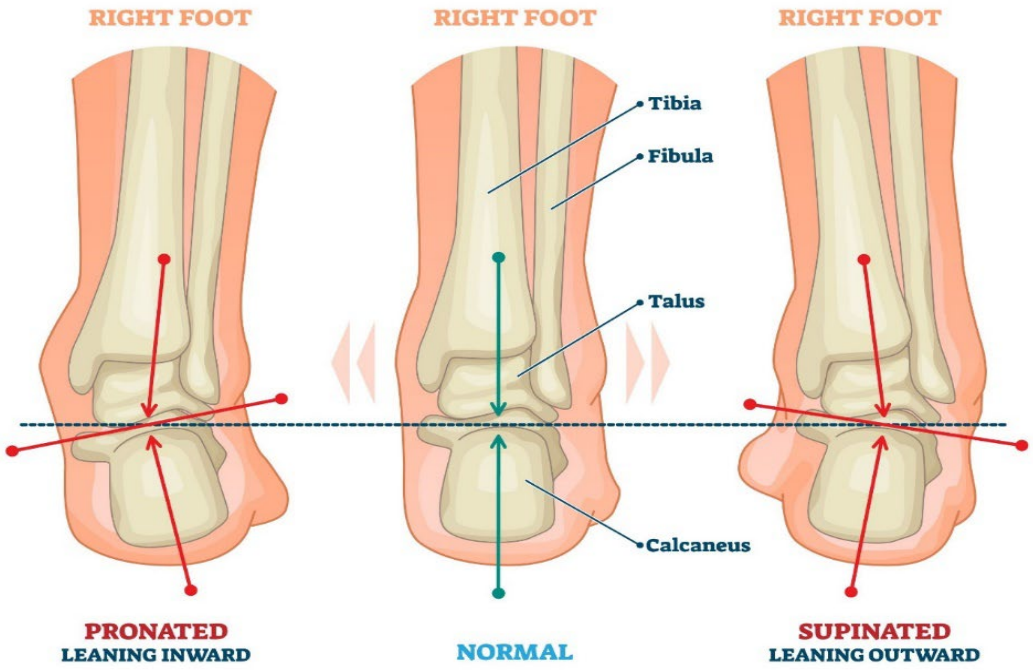

Figure 3-8. Illustration of a normal, pronated, and supinated ankle adapted from Shutterstock.com using Standard License number 382157865).

3.3.2 Range Of Motion

The range of motion (ROM) of the joints forming the ankle complex region refers to the degree to which the joint can move in different directions (191). The maintenance of normal ROM is essential for various activities such as walking, running, jumping, and balance control (29).

Dorsiflexion and plantarflexion motions have traditionally been seen as exclusively occurring at the tibiotalar joint, while inversion-eversion motion has traditionally been regarded as occurring only at the subtalar joint. The attribution of all of these movements to joints has recently been disproved, and while the majority of plantar/dorsiflexion is still thought to occur at the tibiotalar joint, a few degrees of the movement are also now accounted for at the subtalar joint. Similarly, the subtalar joint is still believed to produce the majority of inversion and eversion motions, with the tibiotalar joint contributing for some proportion (181). This shows that the motions created in the ankle complex region are now understood to be

combined motions, meaning that if one joint moves the other joint will move accordingly to some extent (29).

The normal ROMs for dorsiflexion and plantarflexion have been reported to range from 10°-20° and 40°-55° respectively (192). Additionally, for both inversion and eversion, the normal ROM is 5-10° (193). Several factors affect ankle ROM, leading to variations between individuals. These factors include sex, age, level of physical activity, and morphological variations associated with the bones and joints of the ankle (194, 195). Many studies have reported that women tend to have a greater ankle joint ROM compared to men due to differences mainly associated with joint anatomy and ligamentous laxity (191, 192, 195, 196). Also, ankle joint ROM tends to decrease with age due to the natural ageing process, leading to a loss of joint flexibility and elasticity (192, 195, 197, 198).

Various factors can constrain ankle ROM, including anatomical abnormalities, joint stiffness, and injuries (199, 200). Impaired ROM in any of the four ankle joint movements can trigger compensatory mechanisms that can cause abnormal gait patterns (29). These patterns can adversely affect other lower limb joints, consequently raising the risk of injury (201). Therefore, it is necessary to address any limitations in ankle joint ROM as early as possible in order to avoid the potential risks associated with abnormal gait and modified joint mechanics in the lower limb (202).

3.3.3 The role of the ankle in the gait cycle

The gait cycle is a term used to describe the sequence of movements that occur during walking, from the first point at which the foot contacts the ground to the subsequent point at which the same foot makes contact again. It can also be defined in terms of the time which elapses during each step. The stance and swing phases are the two main segments of this cycle. The foot contacts the ground during the stance phase, accounting for 62% of the gait cycle, and the leg bears the body's weight. During the swing phase, which accounts for the remaining 28% of the gait cycle, the foot is off the ground and the leg swings forward in preparation for the following step (203, 204).

During the stance and swing phases, the ankle, knee, and hip joints move together. For instance, during the stance phase, the ankle firstly plantarflexes, then dorsiflexes, and finally

plantarflexes again; likewise, both the knee and hip during this phase flex, extend and then flex again. In the swing phase, the ankle dorsiflexes, the knee flexes, and the hip flexes to bring the leg forward. The movements of these three joints are interdependent and work together to maintain stability, balance, and efficient energy transfer during the gait. Any disruption in the sequence or timing of these movements can result in gait abnormalities (204, 205).

The ankle joint complex plays a critical role in gait. For instance, during the stance phase, the ankle joint complex is responsible for absorbing shock and providing stability as the foot contacts the ground. To do that, the ankle complex region undergoes both pronation and supination movements. Whereas during the heel strike, the ankle joint complex pronates. Such a motion allows the foot to adapt to the ground and absorb shock. At the end of the stance phase, the body moves forward, and the ankle joint complex supinates. As a result of this motion, the foot becomes more rigid and provides a stable platform for propulsion (29, 181, 206).

The ankle joint complex transfers the force from the ground up the lower leg and into the knee joint as the foot contacts the ground. For coordinated movement, the mechanical connection between the ankle joint complex and the knee and hip joints is crucial. Therefore, disturbance factors such as injury or morphological variations in the ankle complex region may interrupt the mechanics of movement and the patterns of load transfer between the lower limb joints. This could increase the load on other joints such as the knee and hip, causing structural damage to the joints (205-208). Figure 3-9 shows an illustration of the human gait cycle with joint movements during each phase.

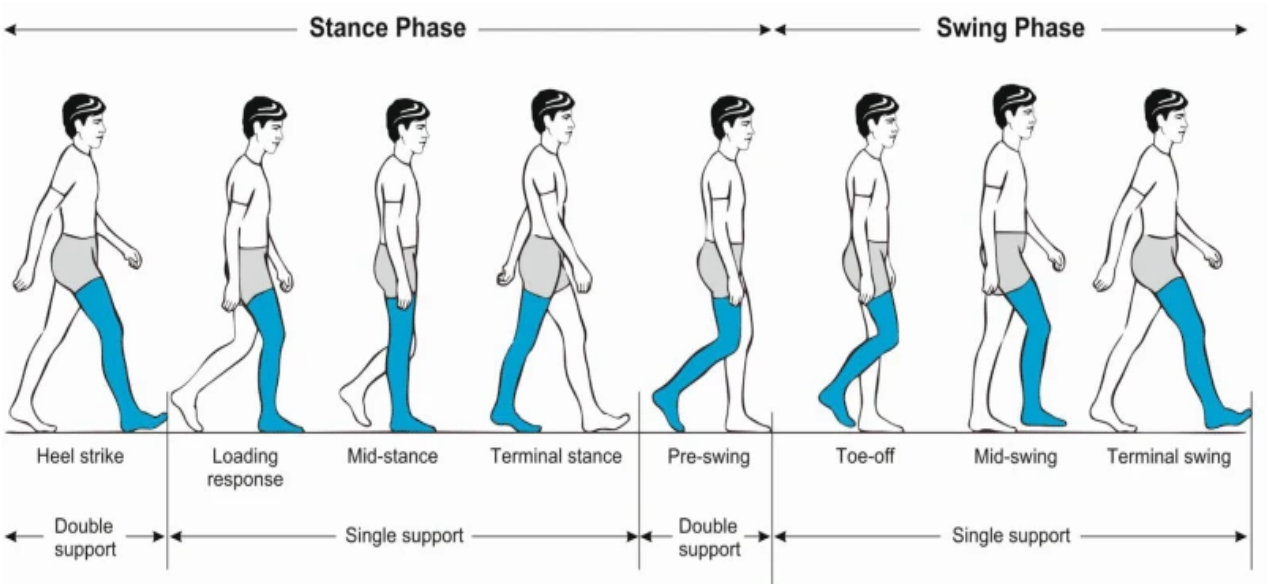

Figure 3-9. Illustration of the phases of the gait cycle adapted from (208).

3.4 Morphological variations in the ankle complex

Morphology in biology is the study of the shape, structure, and appearance of anatomical organs and their components (209). This includes an organ's exterior properties such as its size, shape, colour, and texture. The examination of variations in bone morphology is crucial because it sheds light on differences in bone patterns and structure among various groups and how these differences affect clinical conditions including joint problems, bone fractures, and diseases like osteoporosis and OA (210-212). Also, knowledge of morphological variations in the bones could help in understanding the biomechanical properties of the skeletal system, such as variations in gait patterns between different individuals (206, 213).

Variations in the population in bone morphology are thought to be caused by interactions between genetic and environmental factors (214, 215). Genetic factors determine the fundamental shape and size of bones, as well as their growth and development (216). However, environmental factors such as nutrition, physical activity, and hormonal exposure also play a significant role in bone morphological variations (214, 217). Additionally, accidents, injuries, and disease can also cause morphological variations in bones. Injuries to bones may lead to deformities or irregularities in bone structure, while specific diseases or medical conditions may impair bone development and growth (215).

The ankle complex bones, including the talus, calcaneus, distal tibia and fibula, are subject to morphological variations that can impact the normal functioning of the foot and ankle (26). Understanding these variations is crucial since it can help provide specialised treatment choices and reveal how different groups are more likely to develop particular diseases(218). Various methods are used to assess the morphology of the ankle complex, including observational anatomical measurements and classifications derived from cadaveric specimens (219). Furthermore, another method uses imaging modalities to explore ankle morphology (55). Several cadaveric and radiographic studies have aimed to assess the morphology of bones in the ankle complex region, where more attention was given to both the talus and calcaneus as they are the biggest ankle bones and have important functional properties. These studies are reviewed in this section.

Many studies have explored calcaneus morphology and reported several types of variation concerning its shape and size, which may differ between sexes and age groups and according to ethnicity. One of these variations concerns the articular surfaces of the subtalar joint. Gupta, Gupta (220) were among the first researchers to investigate morphological variations in the calcaneus facets of the subtalar joint. They analysed 401 calcanei from cadavers representing an Indian population, observing, and classifying the variations in four types. The main variations were noted in the presence and shape of the medial and anterior facets, where all calcanei had a clearly defined posterior facet. Type 1, which has one facet that combines both the medial and anterior facets, was found in 67% of the cases, whereas type 2 which has two separate facets, one anterior and the other medial, was found in 26% of the cases. Types 3 and 4 were less common, being found in only 5% and 2% of cases, respectively. Type 3 has only the posterior and medial facets, with no anterior facet present, whereas in type 4 all three facets are connected continuously.

Since then, many researchers have aimed to describe variations in different populations. Ukoha, Obazie (221) explored variations in the articular facets from 220 calcanei taken from dry cadavers in a Nigerian population. Their results showed that type 1 was most common, representing 59.6% of the cases studied. A similar study was conducted by Uygur, Atamaz (222) on 221 dry calcanei from cadavers representing a Turkish population. They reported five

types of calcanei depending on the morphology of the articular surface, with type 2 being the most common representing 58% where the anterior and medial facets were connected. Most recently, Badalahu, Qin (223) used 3D reconstructed CT images to assess the types of calcaneus articular surface in 328 participants representing a Chinese population. They found variations in the surfaces which allowed the calcaneus to be classified into 5 types, with type 1 (where the anterior and medial facets are connected, as shown in figure 3-10) being the most common representing 49% of the cases.

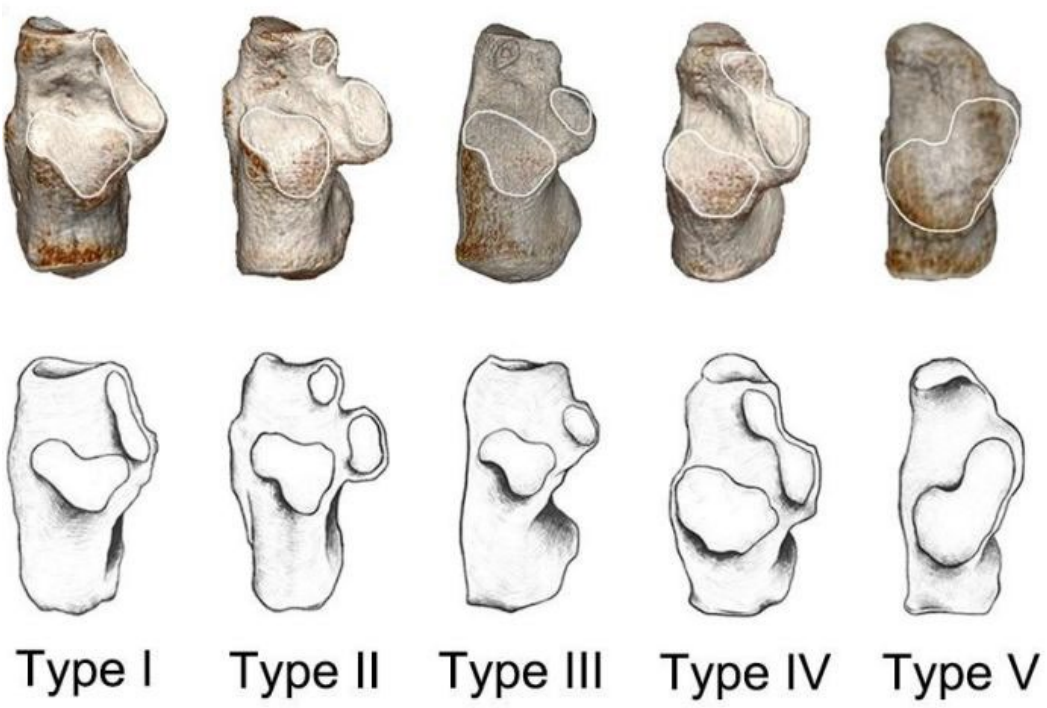

Figure 3-10. The five types of calcaneus bones with differences in the morphology of the articular surfaces forming the subtalar joint adapted from (224).

As well as morphological variations in the calcaneus articular surfaces, other variations regarding the size of the calcaneus have been reported. A study conducted by Kim, Lim (225) evaluated the normal measurements of the calcaneus bone obtained from 42 Korean cadavers, focussing on the bone's length, width, and height as well as Böhler's and Gissane's angles, which are common angular measurements used to assess the degree of calcaneus fracture (see figure 3-8 below). Their results showed that the mean (± SD) length was 74±3.0mm and the width 43±4.0mm, while the mean height was 42.5±3.0mm. The mean

angles for Gissane's and Böhler's angles were 114.4°±8.2° and 32.3°±5.0° respectively. Furthermore, Amuti, Muuthuri (226) reported measurements of 64 calcanei from cadavers representing the adult Kenyan population. Both left and right calcaneus measurements were assessed but not the angles. They reported no statistical differences in measurements between the two sides. Their results showed that the mean ± SD measurements for the right calcaneus were length 69±10mm, height 36±6mm, and width 49±8.19mm. From a Turkish population, İlhan, TETİKER (227) used 65 cadaveric calcanei to assess predefined measurements similar to the ones reported in the previous studies. They reported the measurements of the right calcaneus where the means ± SDs were length 76±5.7mm, width 43±3.7mm, height 44±4.7mm and Böhler's angle 30°±5.2°.

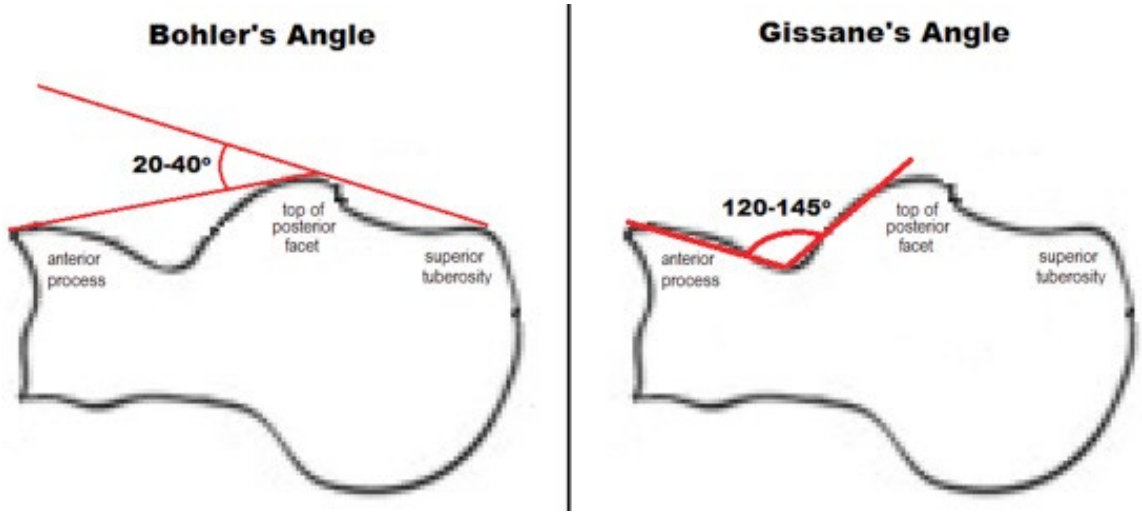

Figure 3-11. Illustration of the lines used to determine Böhler's and Gissane's angles. On the left is Böhler's angle formed by the connection of a line inserted from the top of the calcaneus anterior process to the tip of the posterior articular surface and a line from the tip of the superior tuberosity until it connects with the other line, with normal values ranging from (20-40°). On the right is the Gissane angle formed by the connection of a line from the tarsal sinus to the top of the anterior process and another from the top of the posterior facet to the tarsal sinus, the normal range of which varies from 120-145 ° (adapted from (228).

Other methods used to measure the morphological variations related to the size of the calcaneus include diagnostic imaging data from living participants. Several studies have explored sex-related morphological variations using radiographic measurements of the calcaneus (229-231). For instance, in the study by Uzuner, Geneci (231), lateral radiographic images of the ankle from 143 patients who had been referred to the radiology department (77 females and 66 males) and were felt to have a 'normal' calcaneus were used to quantify morphological measurements and to explore variations between sexes. Participants were also

categorised in subgroups depending on age. Significant differences between sexes in each age group were noted in all measurements. For example, in participants born between 1971-1985, the mean ± SD length and width of the calcaneus for males were 88±6mm and 49±4mm, and for females 75.5±7mm and 41±5mm, respectively. The authors concluded that significant differences in the calcaneus morphological measurements exist between sexes and that the calcaneus bone may play an important role in the determination of sex.

Other studies used CT post-processing techniques to reconstruct 3D objects of the calcaneus so as to quantify the morphological measurements. To overcome limitations associated with 2D radiography, a study by Qiang, Chen (232) used 179 normal CT images of the ankle (96 females and 83 males). The 3D surfaces were then used to quantify morphological measurements such as length, the height of the posterior facet of the calcaneus and Gissane's and Böhler's angles which were then used to explore morphological variations by sex in the population studied. The results showed that all measurements had excellent reproducibility and reliability, with significant differences found between the sexes ($p < 0.01$). The measurements were larger in males compared to females after adjustment for height. The main length and height of the posterior facet and Gissane's and Böhler's angles for males (mean ± SD) were 80.0 ± 3.4mm, 28.6 ± 2.9mm, 128°±6.4°and 40°±2.6° respectively. The corresponding findings for females were 69.2 ± 1.9mm, 22.4 ± 1.8mm, 123.5°±5.4°and 30.7°±3.2° respectively.

The talus bone also exhibits various morphological variations in shape and size, including those related to the articulation facets forming the subtalar joint, similar to the calcaneus. These variations have been observed among individuals of the same ethnic background as well as among those of different ethnicities. Garg, Babuta (233) conducted a study that aimed to classify the morphological variations of the talus articular facets based on 300 dry adult talus bones obtained from Indian cadavers. They identified five types of talus bone based on the presence and shape of the facets where type 2 was the most common type noted in 43.7% of the cases. All types contained a posterior facet, but the main variation was associated with the number and shape of both the anterior and medial facets on the talar head. Specifically, Type 1 exhibited a single connected facet on the head of the talus, Type 2 contained a single

facet divided by a ridge, Type 3 had two facets (anterior and medial) on the talar head, Type 4 featured two facets divided by a groove, and Type 5 contained a single facet that connected all three facets, as shown in figure 3-9 below.

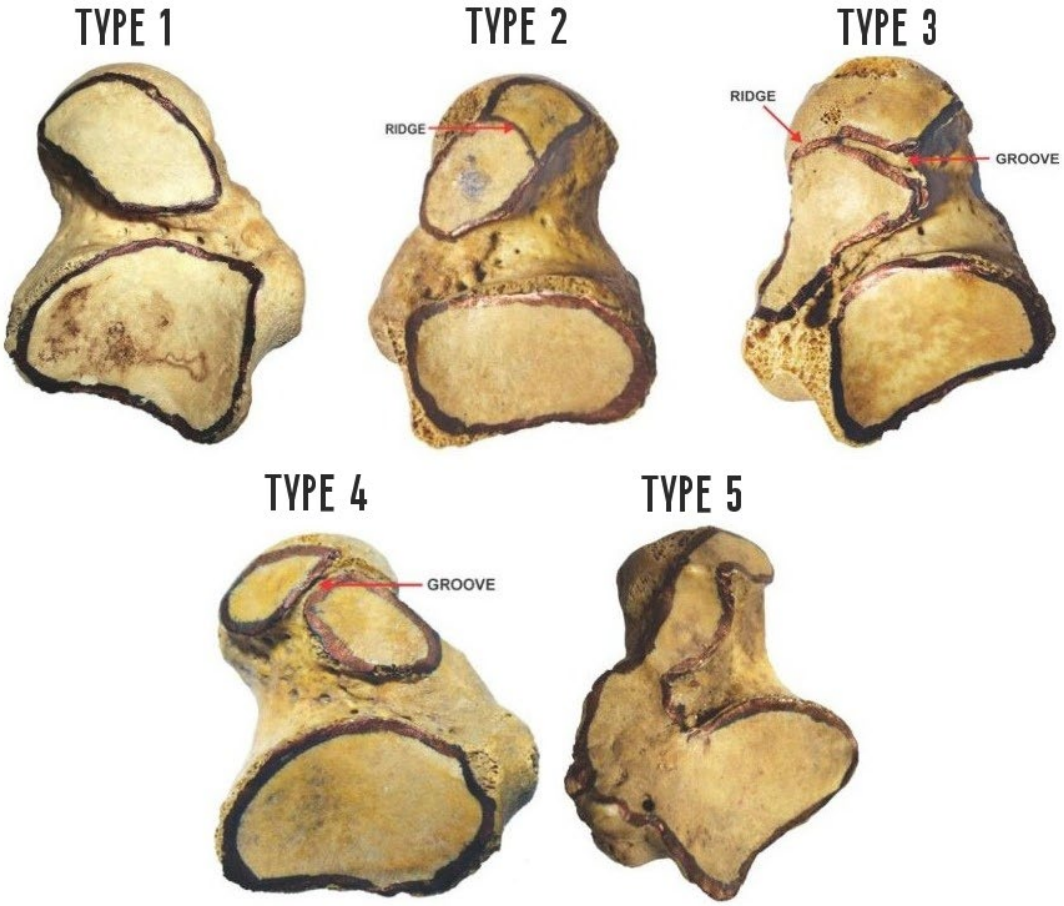

Figure 3-12. Morphological variations in talus bones showing photographic images of five types of talus classified according to the inferior articulation surfaces taken from bones of cadavers (adapted from (233)

Similarly, Lee, Jung (234) explored morphological variations in the talus articular facets on 76 tali obtained from cadavers representing a Korean population. The talus bone was classified as in a similar way as in the previous study. However, only 4 types were noted in the Korean population, and type 5 which shows all three facets to be connected was not observed. The most common type was type 2, representing 32% of cases. Furthermore, in a Thai Population, Phunchago, Uabundit (235) also explored the variations in articular facets from 367 tali obtained from cadavers. The study classified the talus into 5 types similar to those shown in figure 3-9. The most common was found to be type 2, representing 34.7% of cases.

In addition to variations associated with the articular facets of the subtalar joint as presented in the above studies, other morphological variations associated with bone size have been reported. Using 84 tali from Indian cadavers, Namburu, Kaavya (236) assessed the length, width and height of the talus bone using a digital calliper. The results for the right talus showed the mean ± SD length to be 5.4 ± 0.2cm, width 3.8 ± 0.3cm and height 2.5 ± 0.2cm. No sex-related variations were reported since the bones were from cadavers of unknown sex. In a recent study, similar measurements were quantified from 100 tali obtained from cadavers in a Bengal population (237). The mean ± SD length of the talus was reported as 53±3.7mm, the height 31±4.1mm and the width 38.6±3mm. Also, Kasar, Fazlıoğulları (238) explored the morphological measurements of 50 talus bones from Turkish cadavers of unknown sex and age. They reported mean ± SD talus length to be 55.5±4.4mm, height 31.7±3.3mm, and width 41.5±3.6mm.

Other studies have used imaging data from healthy adults to explore morphological variations in talus size. For example, Siegler, Toy (239) used CT scans from 26 healthy adults with an age range between 18-35 years. The CT images were then processed to present a 3D surface rendering of each talus bone. This surface was then used to quantify various morphological dimensions. The results showed the length from the anterior to the posterior part of the talus (mean ± SD) to be 65.1±6.6mm, medial to lateral width 48.4±7.2mm, and height 41.7±5.7mm. The width of the talus dome was also investigated, which was on average 24.8±2.8m. A method then proposed for the evaluation of the 3D morphological features of the talus bone using CT images. According to the authors, such methods could help in improving the designs of the components used in ankle replacement surgery.

More recently Han, Liu (240) applied a method similar to that of Siegler, Toy (239) to reconstruct 3D surfaces from CT images of 150 healthy Chinese adults, quantifying morphological variations in talus bone size and assessing differences between sexes. The results revealed significant differences between males and females in the length, height, and width of the talus, as well as in measurements of talar dome width. However, no adjustments were made for body anthropometry, and therefore it was not possible to determine whether or not the differences between sexes were due to variations in body size. Additionally, side-

to-side differences in morphological measurements were explored, but no significant differences were found.

In general, the studies reviewed in this section reveal considerable morphological variations in the ankle complex region, particularly in the talus and calcaneus bones. Such variations are noted in studies of samples from the same ethnic background as well as among those of different ethnicities. Also, variations associated with age and sex are noted, indicating that morphological variation in the ankle complex region may vary depending on many factors. These variations in the shape and size of these bones may have implications for the stability and function of the ankle joint. Also, they may have an effect on other joints within the lower limb such as the hip and knee joints. In the studies reviewed, variations in the methods and samples used were noted. While some studies used cadaveric specimens to investigate morphological variation, others employed radiography and CT imaging data derived from living participants.

Each method has its advantages and disadvantages. Cadaveric studies provide a more realistic representation of bone morphology and allow for direct manipulation and measurements. However, sample sizes are usually limited, and the specimens may not accurately represent a general population. Imaging studies, on the other hand, may have larger sample size and less invasive data collection methods. However, they may be limited to convenience sampling and suffer from inaccurate representations of the true morphology of the bones. For example, although radiography is widely used as the preferred method for the diagnosis of foot and ankle pathologies, there are limitations associated with its accuracy and reliability when measuring the morphological features of 3D objects such as the bones of the ankle complex region (47, 241, 242). These limitations include radiographic distortion which can expand or compress the imaged object, potentially resulting in inaccurate measurements (243). In addition, the overlapping of bones in the ankle region can obscure the true structure of the imaged object, such as with the talus bone, leading to further measurement error (244). Finally, variations in patient positioning during imaging can also have an impact on the appearance of the object and, therefore, the accuracy of the measurements obtained (48).

The use of 3D CT images instead of 2D radiography can be better for the evaluation of the shape of 3D structures like bones in the ankle region. This is because 3D-reconstructed CT images may overcome some of the limitations of 2D radiography, resulting in more reliable morphological measurements. However, the main limitation of the use of CT is associated with the radiation doses participants are exposed to(49). This can limit the possibility of studying a sample representing a true population and promotes convenience sampling methods such as searching a hospital database to extract CT images from previously requested scans to include in a study. These sampling methods are used in the aforementioned studies and have many limitations that can hinder the generalisability of the results to a larger population. Also, the use of widely available 3D image rendering techniques to represent the 3D surface of a bone may lack the ability to capture the true shape of the studied 3D object. Recent advances in machine learning and medical imaging processing have improved methods to explore morphological bone variations using a more robust method known as statistical shape modelling. In the next chapter, the use of this method to analyse musculoskeletal medical imaging and its utility for morphological assessment are discussed further.

Chapter 4 The Role of Imaging in OA

4.1 Summary

In this chapter, the role of medical imaging modalities in association with OA is reviewed, with a particular focus on the imaging modalities that was used as sources of data in this thesis: x-rays and MRI. The historical context of radiography, protocols of joint imaging, the radiographic features of OA alongside, the advantages and disadvantages of x-rays were described. It was revealed that conventional radiography remains the widely accepted gold standard for the diagnosis and grading of OA, with radiographic features playing a crucial role that helps to confirm and assess the severity of OA. The reliability of conventional radiography has been demonstrated in both clinical practice and research studies. Therefore, in this thesis, conventional radiography is used to classify OA severity in the knee and hip joints, based on its reliability, accuracy, and widespread.

Likewise, the role of MRI in OA is explored, with details provided of the methods of analysis applied and its benefit and limitations. MRI has the advantage of providing assessments and visualisations of all anatomical and morphological aspects of a joint in 3D without the use of ionising radiation. Also, it allows the application of novel machine learning techniques such as SSM that can quantitatively and rapidly assess the morphological features of joints in a population in a reliable manner. Furthermore, the application of SSM was explored in reviews of studies that have used the method in relation to the knee and ankle joints, revealing its potential advantages in knee OA research. Additionally, it was highlighted that the exploration of morphological aspects of the anatomically complex ankle joint using SSM is an area of research with limited published studies so far but showing promising results and good reliability. Thus, the use of SSM in this study is justified since it aims to investigate ankle morphology in the NTFS population while overcoming the limitations identified in previous published studies. This research also represents a novel approach which could be used to assess the interrelation between morphological variations in the ankle complex region and OA in the knee and hip joints.

4.2 Radiography

4.2.1 The history of radiography

Although radiographs are colloquially referred to as 'x-rays,' the noun radiography more properly applies to the ionising radiation itself that enables the visualization of the internal structure of the human body. To create an image, a machine emits a beam of ionising radiation towards a specific part of the patient's body. The radiation is then absorbed at different levels depending on the structure and density of the part examined. As the radiation passes through the patient's body, it is captured by a specific detection instrument or film located behind the patient's body (245).

On the 8th of November 1895, the first Nobel prize winner in Physics, Professor Conrad Wilhelm Röntgen (Figure 4-1) discovered the x-ray (246), and he called this novel phenomenon 'X radiation'. A key technology that facilitated the discovery was introduced in 1858 when the cathode ray tube was invented by Julius Plücker, a German mathematician (246). The cathode ray tube was also one of the main tools that led to the discovery of electrons. Nonetheless, it is currently a vital part of x-ray tubes and, without it, x-rays could not be produced (247).

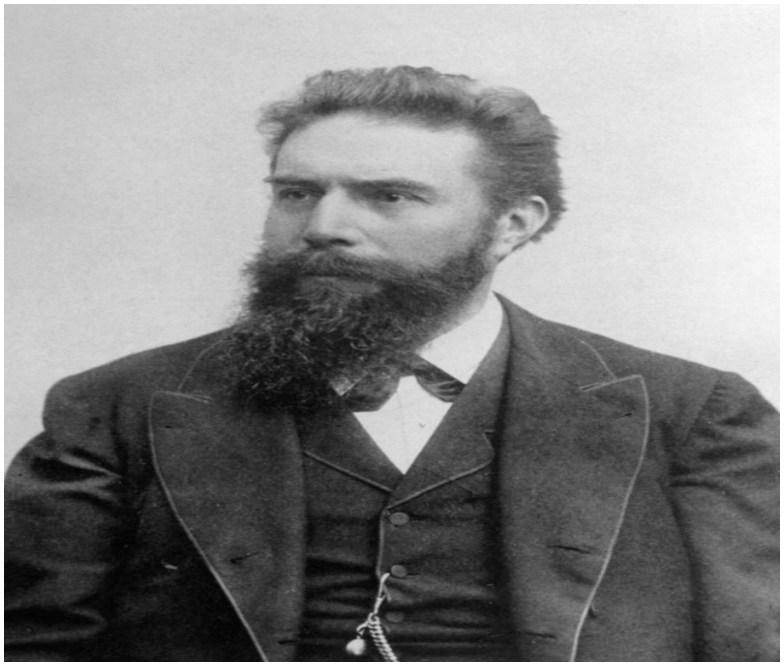

Figure 4-1. Professor Conrad Wilhelm Röntgen adapted from (248).

Many experiments using cathode ray tubes were conducted by physicists throughout the nineteenth century. For instance, Philipp Lenard and his teacher, Heinrich Hertz, were among the physicists that devoted their efforts to exploring the cathode ray tube (249). In 1894, Hertz instructed Lender to insert thin metal windows into the discharge tube which is a part of the cathode tube. They noticed that some types of rays escaped the tube and caused fluorescence over a distance of 2cm. Based on their findings, they concluded that these rays were indeed cathode rays (249).

However, Lender's experiment led Röntgen to question the type of rays that were produced. His theory relied on his suspicion that such rays were not cathode rays, and therefore he investigated them further (250). The first main experiment that Röntgen conducted involved the hermetic sealing of a cathode tube by using black cardboard covers. Following that, he connected a large induction coil to the sealed tube and then closed all the curtains in the room to make it dark and started to pass an electric current through the tube (251). During that process, it was by sheer luck that there was a small platinum-cyanide screen located approximately one metre away from the tube, and this lit up in a very strange way while the whole room was dark, as reported by Röntgen himself (251).

Moreover, he realized that some objects were lying in front of the tube but did not disrupt the path of the rays. He repeated the experiment and placed other objects in front of the tube and the rays penetrated them too (251). That was when he realised that the rays that were first produced by Lender were not cathode rays, since those rays were known to be unable to penetrate thick tubes (251). Also, the distance involved was much greater than the known distance travelled by cathode rays (251). At that moment in the afternoon of the 8th of November 1895, he became convinced that the rays were unique in their characteristics and did not correspond in any way to existing Cathode rays (250). He, therefore, devoted his time to investigating the phenomenon aiming to gain convincing clarification that would allow him to present his discovery (250).

However, that caused him to spend much more time in his laboratory which was located in the basement of his house (Figure 4-2). His absence was noticed by his wife Bertha Röntgen. She realized that he was distracted and busy all the time. (249). She asked him about the

reason for this. Röntgen then took her to his lab and revealed his discovery to her. Bertha Röntgen is reportedly the first person to whom this phenomenon was explained (249). She was then the first person to have her hand exposed to such rays when Röntgen conducted his first-ever experiment on a human body. (246). The aim was to see if the rays could penetrate the human body, since they had passed through several other objects earlier. He exposed his wife's hand to the rays for approximately 20 minutes and thus obtained the first x-ray image of a human body part (246).

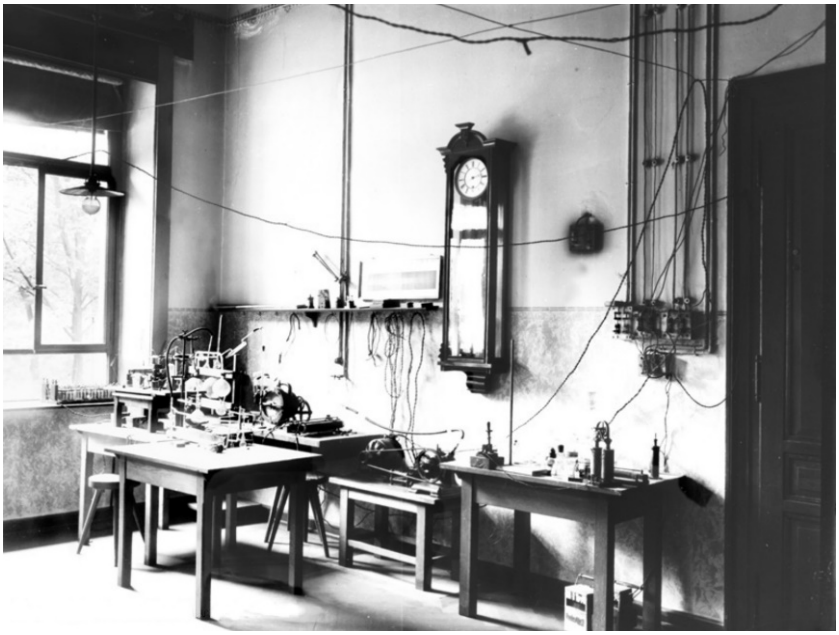

Figure 4-2. Professor Conrad Wilhelm Röntgen's laboratory adapted from (248).

After seeing the image of her hand, Bertha Röntgen stated that *"I have seen my death,"* which was a well-known popular reaction to such an amazing feeling (see Figure 4-3) (252). This information was reported in Bertha Röntgen's letter dated March 1896 to Mrs L. R. Grauel, who was Prof. Röntgen's cousin, which confirmed many theories and also the date of this first discovery. This letter was later preserved in the Museum of the American Journal of Roentgenology (252).

Figure 4-3. Bertha Röntgen and the first x-ray image of her hand adapted from (248).

Six weeks after his first experiment on his wife and before presenting his work to other scholars, Röntgen wanted to give the rays a name, and he chose to call them X-rays. The letter X in science is typically used to represent something unknown, and he did not know what type of rays were they; hence, the designation X-rays (246). Only six weeks after his discovery, Röntgen submitted his first preliminary report on 'A New Kind of Rays' in December 1895 to the administration of the Wurzburg Physical-Medical Society (251). Soon after the publication, the news travelled fast. Many newspapers and journals reported the discovery, not least due to the fact that Röntgen presented a radiograph of his wife's hand in his report (249). Such a remarkable picture was the reason for the widespread news of the discovery emanating from a small laboratory in a little-known town in Germany. His lecture attracted the attention of the media and the press. Röntgen became famous overnight. He was reported to have been invited to several formal occasions to take pictures of the hands of important personalities (249).

4.2.2 Medical use and development

John McIntyre is known to be the first to investigate the application of x-rays in a medical context (253) and he had published more than 18 articles by the end of 1896. Many of his experiments took place in his laboratory in Glasgow. In July 1896, he demonstrated the ability of x-rays to detect kidney stones (253). This is known to be the first use of x-rays for diagnostic purposes. McIntyre highlighted the importance of such rays in diagnostic medical procedures by saying that *"So long as individuals of the human race continue to professionally inject bullets into one another, it is well to be provided with easy means for inspecting the position of the injected lead, and to that extent aiding the skilled operators whose business and joy it is to extract it" (253).* Just three months after the discovery of x-rays, McIntyre asked for permission from the President of the Glasgow Royal Infirmary to open an x-ray laboratory in the basement of the hospital (253). In March 1896, permission was granted, and the department was established. It is recognised as the first-ever Radiology Department to provide radiological diagnostic services for patients (253).

At that time, people were fascinated by such a technology that brought countless knowledge to mankind and helped in ascertaining the human anatomy as well as improving surgery and the diagnosis of diseases using radiology that were until then unknown(254). However, the potential harmfulness of such rays was not investigated properly, although that was understandable since nothing suggested that such rays could be hazardous. At that time, conducting an x-ray of a hand would take around 11 minutes, during which time the skin was exposed to a huge amount of radiation which was approximately 50 times more than the dose of an exposure nowadays(254).

Many scientists and physicists who worked closely with x-rays at that time reported burns and hair loss, but they could not directly link it to the x-rays (255). On the other hand, some prominent physicists strongly denied that such effects were caused by x-rays. They proposed that x-rays were comparable to light, but unseen, unfelt, and undetectable (255). Such a phenomenon, according to so-called common sense, should not cause any harm. However, in February 1896, a child who had been shot in the head was taken to Professor John Daniel's laboratory. The aim was to perform a skull x-ray to locate the bullet, and such a procedure had

not previously been performed (255). So, Prof. Daniel volunteered in an experiment to have his skull imaged before examining the child's skull using an x-ray, and the procedure took almost one hour. Two weeks after that experiment, Prof Daniel reported hair loss and burns in the same area of the skull that was exposed to radiation (255). This event was the first-ever reported event that directly linked the cause of burns and hair loss to x-rays. This was because the affected area was reported to be 5 cm in diameter, which was the same area that was exposed to the radiation (252).

This represented a warning of the potential threat caused by radiation. However, no action was taken until 1915 when the British Roentgen Society introduced recommendations that aimed to protect a person from radiation (256). In 1920, film badges were used by radiation workers to personally monitor their radiation exposure. Also, many scientists focused on developing x-ray machines that decreased the duration of exposure to doses of radiation (256). The development of x-ray machines since has resulted in the minimisation of the time needed to accomplish an x-ray of a hand from 11 minutes down to a couple of seconds. This reduction in the amount of exposure to radiation made the use of such a technology safer for patients (256).

The understanding of the possible hazards linked to radiation exposure grew along with the use of radiography(257). It has been increasingly evident over time that exposure to high radiation levels can have negative effects on health, including a higher risk of developing cancer and other disorders(258, 259). As a result, more sophisticated radiation detection and protection technology has been developed, and strict norms and regulations have been put in place for the use of radiography in medical settings(260).

4.2.3 Radiography and OA

Over the last century there has been significant evolution in the monitoring and diagnosis of osteoarthritic joints through the use of radiography (11). Although new imaging techniques employing various modalities are rapidly developing, the use of radiography remains the gold standard for the evaluation and diagnosis of OA in joints (261, 262). This is due to several factors such as its reliability and validity, wide availability, ease of use, and being the least expensive of all contemporary diagnostic imaging modalities (245, 261, 262).

4.2.3.1 Imaging of the knee

The protocols for the radiographic imaging of the knee have been extensively researched so as to identify the most reliable protocols for use in both research and clinical evaluation (261, 263-265). Regarding clinical assessment, the most effective protocol involves taking anteroposterior (AP) and lateral views of an upright weight-bearing leg with the knee in a position of full extension (266).

However, this protocol is not advised for application for research purposes such as in longitudinal studies that aim to assess disease progression (261). This is due to reported variabilities in the images associated with anatomical variations such as in the degree of knee extension or rotation (267). Also, there may be variation associated with the alignment of the x-ray beam with the imaged object and the distance between the knee and the image receptor as well as between the knee and the x-ray beam itself, which could cause radiographic magnification (263). Such variations can result in unreliable assessments and comparisons of OA radiographic features between study participants or between images of the same participant taken over time (267).

To address this issue, many standardised radiographic protocols have been introduced that focus on imaging the knee in a semi-flexed position rather than at full extension (261). These include, but are not limited to, the metatarsophalangeal (MTP) protocol proposed by Buckland-Wright, Wolfe (268) which depends on the flexion of the knees by 7° as shown in figure 4-4, and the fixed-flexion protocol developed by Hunter, Zhang (269) which depends on the external rotation of the foot by 10° and the tilting of the x-ray source also by 10°, as seen in figure 4-5. The utilisation of such standardised radiographic protocols when imaging the

knee joint for research purposes has the advantage of minimising the variability between images associated with anatomical positioning, alignment, and radiographic magnification, resulting in the production of comparable images which lead to more reliable measurements (261, 270, 271).

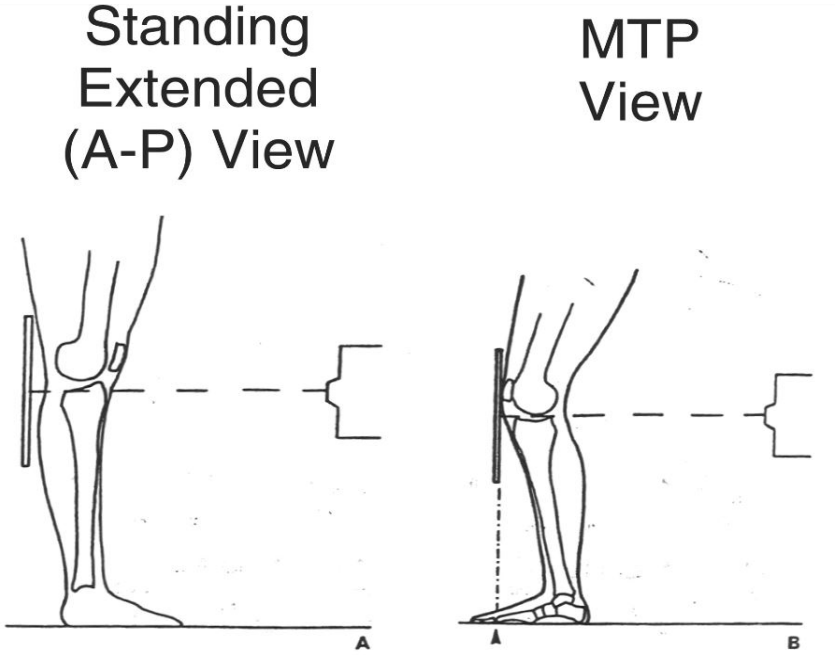

Figure 4-4. Diagram showing the differences in the positioning of the knee joint using different protocols: A) using the standard AP extended view; B) the posteroanterior MTP view adapted from (265).

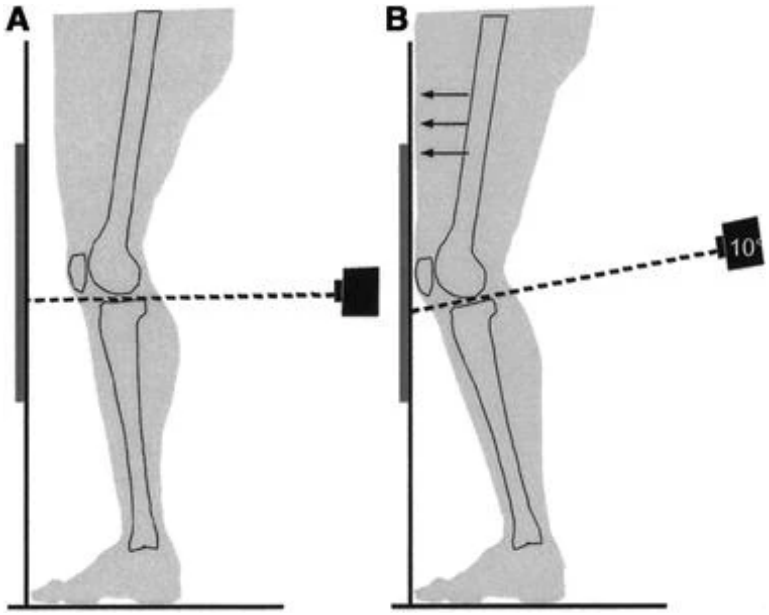

Figure 4-5. Diagram showing differences in the positioning of the knee joint using the extended and fixed-flexion protocols: A) standard PA extended view; B) fixed-flexion PA view with the x-ray tube tilted by 10° adapted from (264).

4.2.3.2 Imaging of the hip

Using radiography in the assessment of hip OA is inexpensive, widely accessible, and simple to obtain, and its interpretation is less challenging than that of other cross-sectional imaging modalities (262, 272). However, owing to its nature as a projection method, the limitations associated with radiography such as positional variability or overlapping of the surrounding anatomical structures may mean that hip joint abnormalities remain undetected (273, 274).

Moreover, morphological distortion and radiographic magnification might interfere with quantitative measurements such as the assessment of JSW (274). Therefore, the use of specific protocols for image acquisition for both clinical and research purposes, that are designed to minimise the previously stated limitation will result in ensuring the reliability of methods used to assess the hip OA radiographic features (272, 274).

The Osteoarthritis Research Society International (OARSI) has published an expert opinion to provide recommendations regarding the protocol for hip imaging (275), which involves taking two views: the first an AP pelvic view, where the hip must be internally rotated; and the second is a cross-table lateral pelvic view where the hip should be flexed and externally rotated. In

both views, the markers of the calcar femoris, larger and lesser trochanters, and other bones should be visible (275).

Furthermore, in both views, the OARSI recommended that the excessive external and internal rotation of the hip should be avoided. Additionally, the use of digital detection systems with minimal dosage exposure and a focus-to-film distance of nearly 100 cm should be applied in the protocol. Concerning the position of the patient, both standing weight-bearing and supine radiographs can offer precise measurements of JSW, while standing radiographs may provide a more accurate calculation of cartilage thickness (275).

However, imaging in a supine position is preferred in obese patients, because imaging them in a standing position might introduce hindrance to the visualisation of the hip joint due to a pannus stomach (274). However, in research settings it is important that consistency should be maintained by using the same positioning technique for all participants so as to avoid variability in measurements when the subject shifts from one position to another (274). Applying such protocols and recommendations will result in good-quality images that will allow the precise classification of the disease and measurement of JSW (275).

The use of pelvic images obtained from DXA scans in research settings to assess and grade hip OA has also been considered. For example, Yoshida et al (276) aimed to grade hip OA using DXA images and to compare these with radiographs of the same participants. The results showed that DXA images showed similar scores for inter-observer repeatability when compared to images obtained from conventional radiography. Additionally, studies by Birrell, Ottewell (277) and Yoshida, Barr (278) established that the assessment of hip OA using DXA images is a valid method that produces reliable results. Also, it may be argued that the use of such a modality is more ethically acceptable in research that aims to assess both OA and osteoporosis owing to, lower exposure to radiation among participants since a single image allows the grading of hip OA and assessment of BMD.

4.2.3.3 Imaging of the ankle

As mentioned in chapter 2, ankle OA has the lowest prevalence when compared to that for other joints and is relatively uncommon (279). Therefore, the manner of acquisition of radiographic images of the ankle complex region is similar for all suspected ankle pathologies (244). In clinical practice, the common protocol for ankle radiography includes three views: AP, lateral and mortise views (280).

The AP view is taken with the patient in a standing weight-bearing position or while supine with the legs fully extended. To achieve the ideal positioning, the leg is rotated until the foot's long axis is vertical and the foot is dorsiflexed until the plantar surface is parallel to the image receptor (281). When obtaining the AP projection X-ray, the patient is positioned either in a supine or seated position, and the foot is lifted upward until the sole is at a right angle to the image receptor. Additionally, the limb is rotated to align the foot's long axis with a vertical position. A cushion or other object is used to keep the foot in a dorsiflexed position for optimal immobilisation, and the application of these method is useful in order to obtain a clear image of the ankle for diagnostic purposes (282).

To quantitively assess the JSW of the main ankle joint, the mortise view is necessary since it allows a clear identification of this joint (283). The AP mortise view is taken using positioning methods similar to those used for the standard AP view mentioned above with minor modifications (281). In the AP mortice view, the entire lower limb is rotated internally so that the line of the inter-malleolar is perpendicular to the image receptor. The recommended degree of internal rotation necessary to achieve this view varies from author to author and from person to person (282, 284). As a result, the achievement of the correct positioning should rely on palpation techniques and anatomical presentation. The distal tibia, fibula, and talus, as well as the overlaying soft tissues, should be included in both the AP and AP mortise radiographs, as seen in figure 4-6 (282).

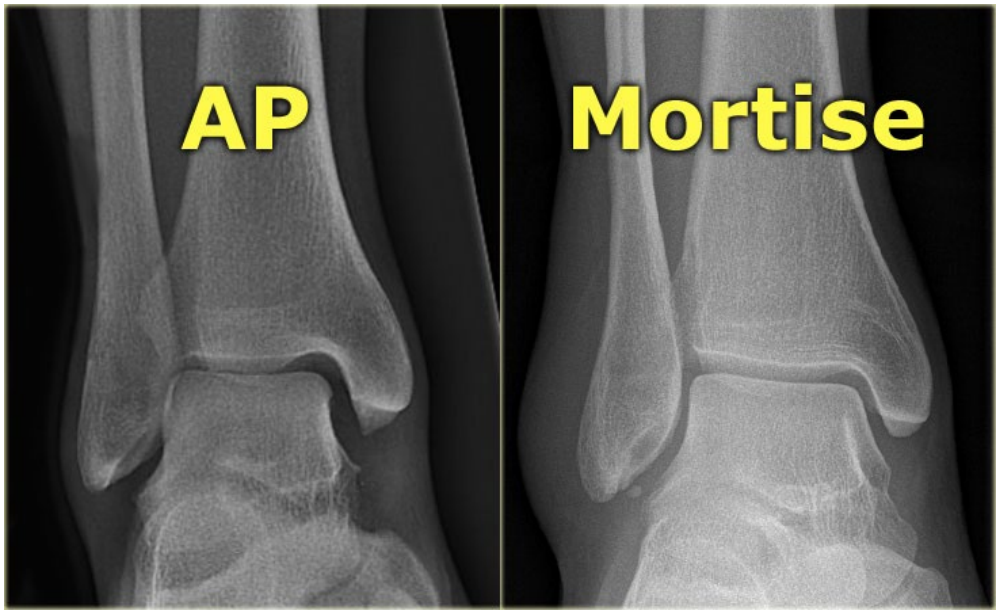

Figure 4-6. X-ray images of the ankle using different acquisition methods. On the left is an AP view and on the right a mortise view adapted from (285).

For the lateral ankle view, the supine position and standing upright are both acceptable. To achieve such a projection, the following are required: the external rotation of the foot until the medial and lateral malleoli overlap and are parallel to the image receptor, while the foot maintains a position of dorsiflexion. The lateral view should include the talus, the distal parts of the tibia and fibula, the navicular, the calcaneus and the base of the fifth metatarsal as well as the surrounding soft tissues, as seen in figure 4-7 (281, 282).

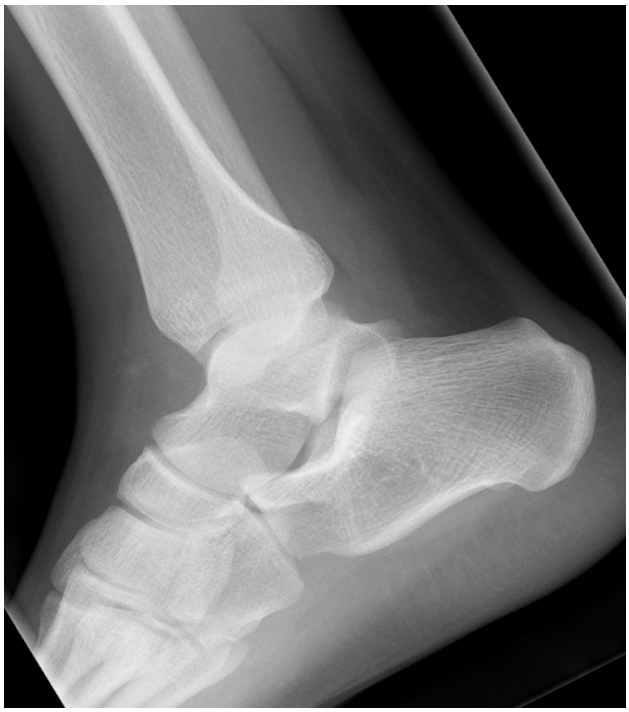

Figure 4-7. Lateral x-ray image of the ankle adapted from (285).

4.2.4 OA radiographic features

OA, as with many other diseases, has radiographic features the presence of which lead to a clearer diagnosis and can also help to determine the severity of the disease. These radiographic features are narrowing of the joint space width (JSW), subchondral sclerosis, and osteophytes, and subchondral cysts (286).

The JSW is defined as the space between the two subchondral bones in each joint (65). In a normal joint, this space consists of hyaline cartilage covering the ends of the two bones. When the cartilage in this space degrades, the joint space will become narrower in direct relation to the amount of cartilage lost from each of the two opposing surfaces (65). The quantitative assessment of JSW plays an important role in OA assessment both clinically and in research settings (261). For instance, narrowing of the JSW is known to be one of the key indicators of the structural progression of OA (274). Also, joint replacement surgery is indicated when JSW is lost (287).

However, the direct visualisation of cartilage is not possible using radiography because, as an x-ray beam travels through the body, tissues absorb it to different degrees depending upon their density and structure (288). More of the x-rays are absorbed by bones compared to soft tissues like cartilage because bones are denser and contain calcium (288). Cartilage has a far lower density than bone and absorbs x-rays to a far lower extent, appearing on a radiograph merely as an unclear shadow which is difficult to visualise (272).

However, the joint space narrowing (JSN) can be estimated indirectly by focusing on the distance between the bones, as long as positioning is consistent and efforts are made to exclude other tissues being interposed, as seen in figure 4-8 (286). A systematic review conducted by Reichmann, Maillefert (289) included 56 papers that assessed both the responsiveness to change and the reliability of radiographic JSW. The authors concluded that JSW quantified from radiographic images for participants with OA shows good reliability and moderate responsiveness.

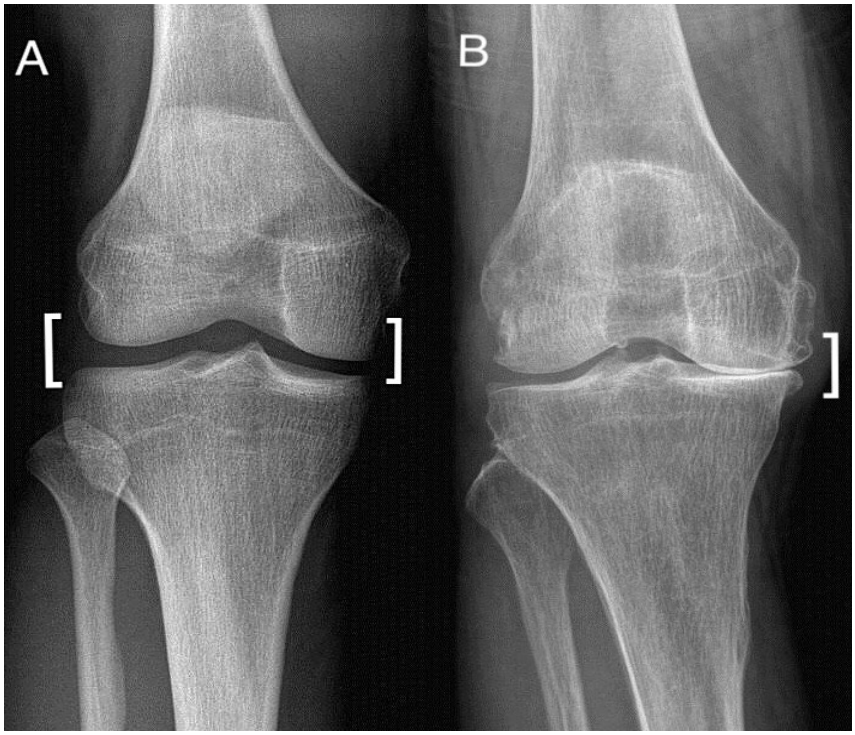

Figure 4-8. Knee x-ray images showing the difference between normal and narrowed JSW: A) radiograph for a knee joint with a normal joint space width; B) radiograph for a knee joint with clear joint space narrowing adapted from(286); permission to use available via Elsevier License: #4665930277892).

The appearance of osteophytes is another radiographic feature of OA (286). Osteophytes, also known as bone spurs, are defined as spurs that appear on bones, which usually grow from precursor cells in the periosteum in a joint that has started to lose cartilage, as seen in figure 4-9 (65). Osteophytes develop slowly and are linked with OA. They are a sign used to discriminate between OA and other forms of arthritis (65). Furthermore, they can appear in any joint with varying severity and can be used as a staging indicator (286).

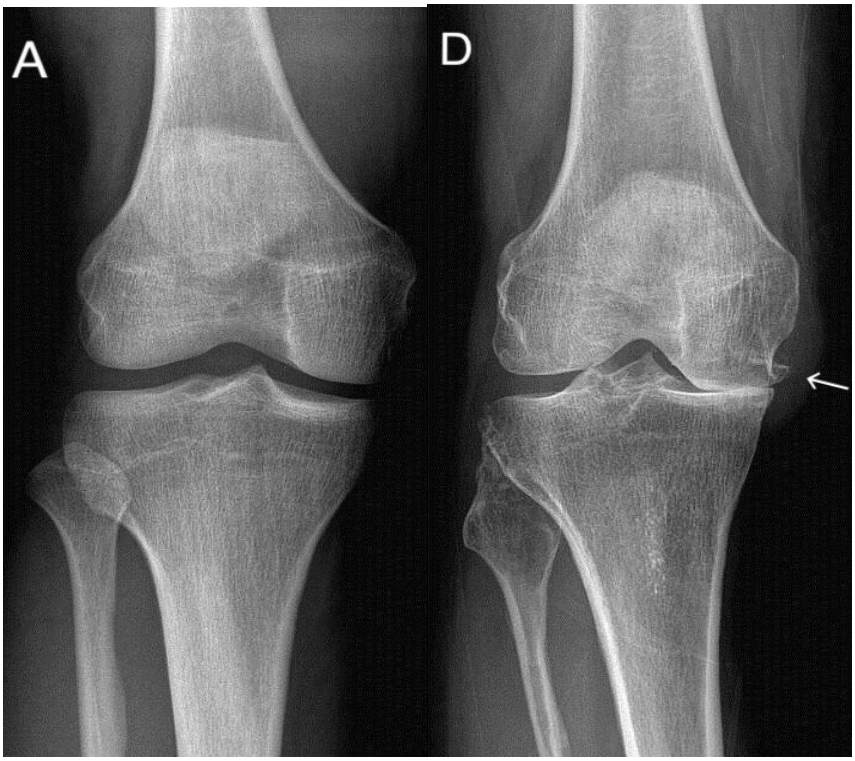

Figure 4-9. X-ray images presenting the difference between a normal knee and one with the appearance of osteophytes: A) radiograph of a normal knee with no osteophytes; D) radiograph of a knee with the appearance of osteophytes in the medial femoral (highlighted by an arrow) adapted from (286); permission to use available via ELSEVIER LICENSE: #4665930277892).

Another key radiographic feature of OA is the development of subchondral sclerosis (286). This appears in the form of areas of increased density in the subchondral bone (65); see the white lines in Figure 4-10). It reflects new bone formation in the affected joint and is a sign of the progression of OA (65).

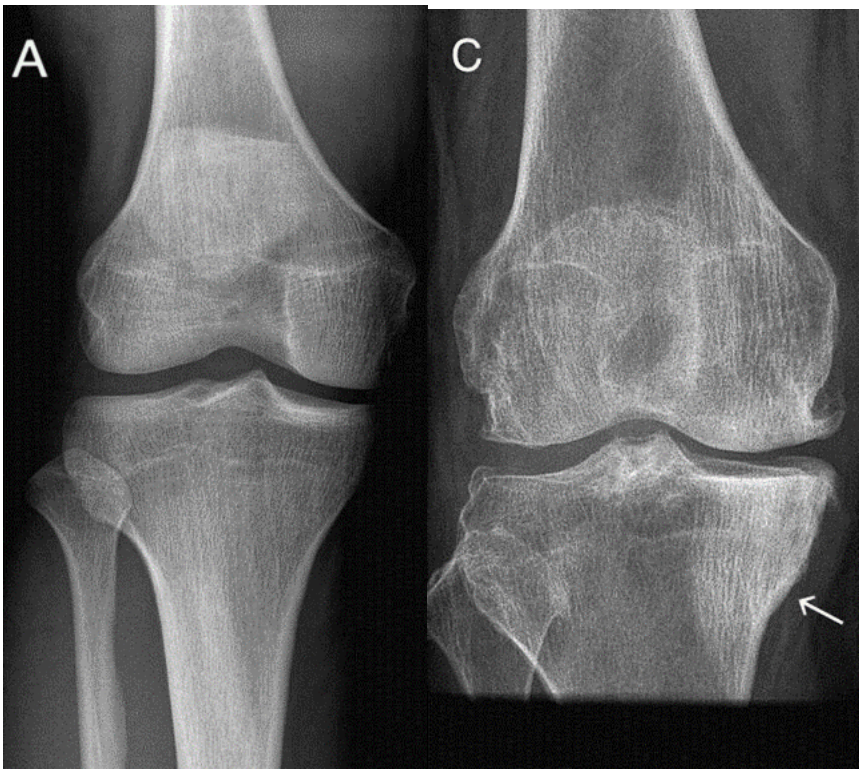

Figure 4-10. Differences between a normal knee x-ray and the appearance of subchondral sclerosis: A) radiograph of a normal knee with no subchondral sclerosis; C) radiograph of knee with the appearance of subchondral sclerosis in the medial tribal (highlighted by an arrow) (adapted from (286); permission to use available via Elsevier License: #466593027789).

4.2.4.1 Radiographic grading systems

The most widely used grading system for OA using radiographic features is the Kellgren and Lawrence (K&L) system (12, 274). This semi-quantitative assessment scale was designed in 1957 and chiefly rests on the presence of the radiographic features mentioned previously to grade the severity of OA in an affected joint. It employs a scale from 0, which is normal, to 4 which is severe as shown in table 4-1 and figure 4-11 (13). It is mainly applied in order to determine the severity of knee OA and can also be used to grade OA in other joints such as the hip and ankle joint. However, it is not as commonly accepted or validated for those joints as it is for the knee (290). Moreover, other grading schemes could be preferable in determining the extent of OA in other joints, as discussed below.

Table 4-1. Illustration of the features of the Kellgren-Lawrence grading system for OA adapted from (13)

Grade	Radiographic features
0	Normal: no radiological findings of osteoarthritis
I	Doubtful: narrowing of joint space and possible osteophytes lipping
II	Definite: osteophytes and possible narrowing of joint space
III	Moderate: multiple osteophytes, definite narrowing of joint space, small pseudocystic areas with sclerotic walls and possible deformity of bone contour
IV	Severe: large osteophytes, marked narrowing of joint space, severe sclerosis, and definite deformity of bone contour

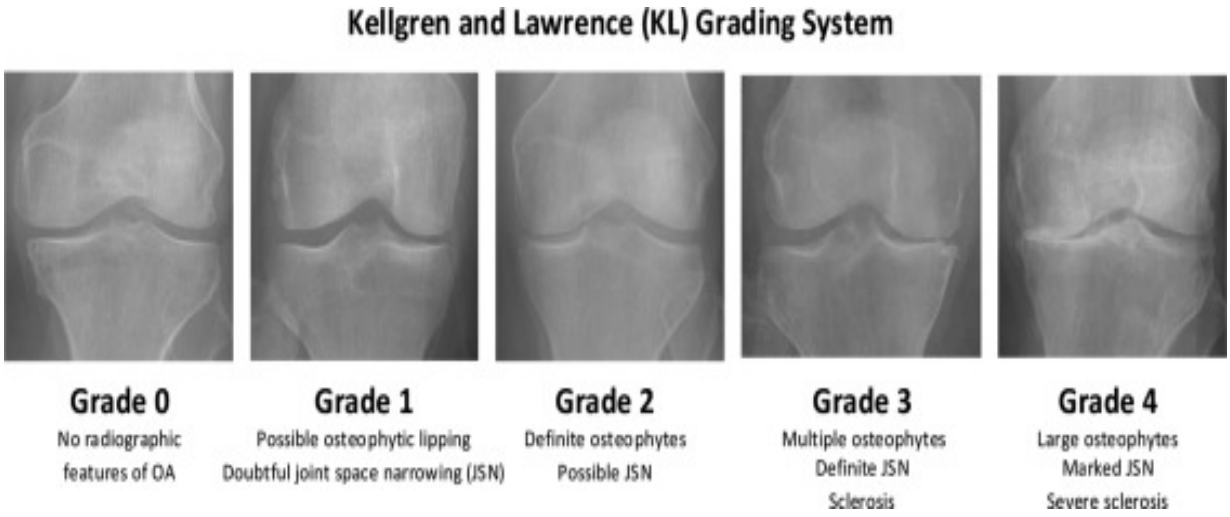

Figure 4-11. Radiographic images of the knee representing the different OA grades in the K&L system adapted from (291).

Another widely used grading system is the OARSI atlas criteria established by the Osteoarthritis Research Society International (286), which uses a semi-quantitative approach by grading the individual radiographic features present in each of the joints in the medial and lateral parts. It focuses on the presence of osteophytes and JSN by grading their presences from 0-3, where 0 is normal and 3 severe. The cut-off in this system is reached if the patient satisfies any of the following three criteria in each joint investigated: 1) JSN grade ≥2; 2) the sum of osteophyte grades ≥2; and 3) grade 1 JSN in combination with grade 1 osteophyte (286).

For hip OA the K&L grading system is generally used; however, a modification of that system was introduced by Croft, Cooper (14). Croft's grading system classifies the condition in six grades based on radiographic features, with each grade indicating different levels of severity as presented in table 4-2 below (274).

Table 4-2. Features of Croft's system for grading hip OA adapted from (14).

Grade	Radiographic features
0	Normal
1	Osteophytes noted
2	Joint space narrowing (JSN) noted
3	Two radiographic features present together: 1) osteophytes; 2) JSN; 3) bone sclerosis; 4) cyst
4	Three radiographic features present together: 1) osteophytes; 2) JSN; 3) bone sclerosis; 4) cyst
5	Grade 4 plus femoral head deformity

Even though a number of grading systems have been developed recently and are in use, the K&L grading system remains the one most widely used (261). The K&L classification has been regularly used as a main research method in OA epidemiological studies (292). A generally accepted threshold in defining a participant as having OA is to have an overall K&L grade ≥2. This grading system and threshold have been applied in key OA-related research that has had a significant impact on the understanding of the disease (12); for instance, in work undertaken to assess the prevalence of OA by Felson, Naimark (293) using data from the Framingham study, and also in a similar study conducted by Bagge, Bjelle (294) on two European populations. In addition, SCOTT JR, Lethbridge-Cejku (295) used the K&L grading system in producing atlases of the radiographic characteristics of OA.

The interobserver reliability of the K&L system has been evaluated alongside that of other classification systems by Wright, Ross (296). The study included knee radiographs of 632 participants in a Multicentre Revision Study. Three blinded observers graded the images independently of each other using different classification systems. The results showed that

the K&L system was the most popular method used and had moderate to very good interobserver reliability, with an intraclass correlation coefficient (ICC) ranging from 0.51-0.89.

Therefore, this system was chosen by the WHO to be the reference standard used in epidemiological studies that focus on OA (245). However, many researchers claim that, as with any other radiographic classification system, it may have limitations (297). A prominent example mentioned in the initial publication by Kellgren and Lawrence (298) is variability between observers when estimating the prevalence of OA.

4.2.5 Advantages and limitations of radiography in OA research

It is important to note that the role of radiography is not restricted to the clinical diagnosis of OA (298). Radiography has also played a vital part in research and clinical trials (272) due to several advantages such as that it provides good reliability and validity, is widely available and simple to use, and is the least expensive of all the diagnostic imaging modalities. By conducting a simple search for published papers in the Medline database over the last 5 years using the terms 'radiography' and 'osteoarthritis', 6442 papers were found. This clearly shows that this modality is widely used, particularly in research focusing on the prevalence, incidence, progression and classification of OA in different joints using the previously mentioned grading systems (261).

Even though it is the gold standard modality for the diagnosis of OA and is widely used in research, some researchers point out that the use of radiography in research associated with OA also has limitations, particularly, in studies that focus on the progression of OA in longitudinal studies (11). They also argue that radiography has other limitations in detecting the early pathogenesis of the disease and the early morphological features of an affected joint (18). This is due to factors such as its lack of sensitivity, particularly when aiming to detect cartilage damage (299). Moreover, while focusing on the monitoring of morphological features, radiography lacks the specificity to measure cartilage thickness, JSW, and changes in bone shape and area (299).

Radiography is known as the gold standard imaging modality used to determine a patient's eligibility for many clinical trials that focus on investigation of the progression of diseases or the development of modifying drugs (15). In the past two decades, several pharmaceutical companies have aimed to develop a disease-modifying osteoarthritis drug (DMOAD). The

estimated cost of developing such drugs and gaining market approval is high, at approximately US $ 2.6 billion (300). Despite, all of the efforts made and the high cost of such trials, no such pharmaceutical agents have been approved (18). Such unsuccessful approaches suggest that a deeper understanding of the process followed in such trials is vital.

The feasibility of the criteria for the inclusion of participants in DMOAD trials has been argued to be the main reason that such trials fail (301). As mentioned previously, radiography for severity, as defined by both JSW and the K&L grading system, is the main tool used for the criteria for inclusion in trials. The measures so produced are the only endpoint approved by the FDA for clinical trials in assessing a potential DMOAD (15). Therefore, the use of these classifications and this imaging modality may be responsible for the failure of trials (301). For example, the radiographic definition of severity in the K&L grading system includes grades 0 and 1 defined as normal, whereas other studies have proven that both grades may indicate structural OA in cases found not to be normal when evaluated using MRI (261).

In population-based observational research by Guermazi, Niu (302), 710 participants from the Framingham Osteoarthritis study were studied who were classed as having no radiographic evidence of OA after having been categorized as K&L grade 0. Knee MRI was then applied to assess the presence of any radiographic abnormalities, with the outcomes compared with those of K&L grading. Of the 710 participants, 89% (631) had abnormalities that were shown on MRI, among which the presence of osteophytes was the most common (524/710: 74%) (302).

Another study by Hayashi, Felson (303) confirmed those results using 696 participants from the same Framingham cohort, all of whom were given 0 K&L grades. The study aimed to investigate the presence of damage in knees using MRI in patients considered to have 'normal' knees according to K&L grading, and the analysis showed that the majority of participants had cartilage damage and osteophytes (303). Such results indicate that the use of K&L grading and radiography may not detect the early signs of OA. Therefore, the use of these techniques in epidemiological research, especially in evaluations of early changes in OA, longitudinal studies of disease progression, or tests of the effect of new drugs, may result in misclassifications of participants in groups which would not truly represent the state of their disease and thus lead to spurious results.

Similarly, another common problem with the radiographic definition of severity is the influence of knee position when acquiring radiographic images, which can also lead to misclassifications of participants during K&L grading (304). For example, variations in knee flexion can affect the measurement of JSW, potentially leading to inconsistency in categorisation during follow-ups, as shown in figure 4-12.

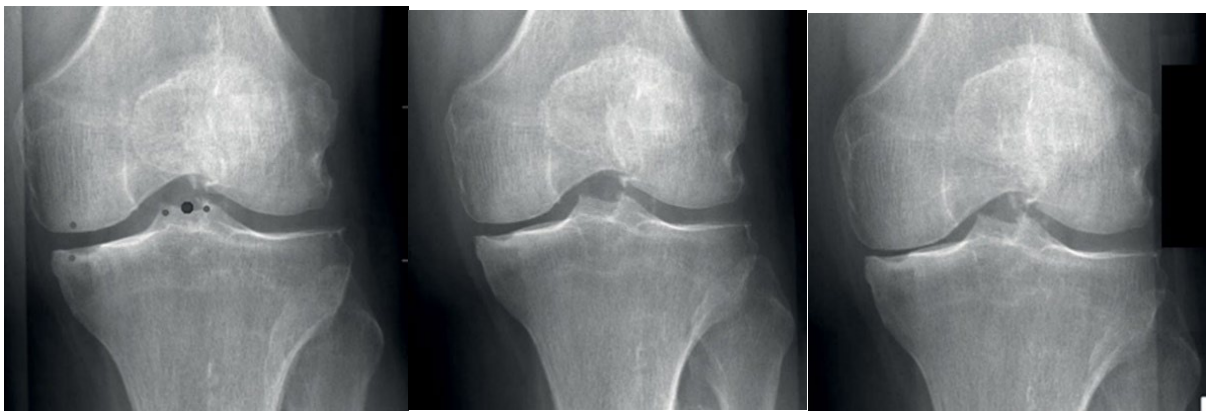

Figure 4-12. Variation in knee position during image acquisition affecting JSW and giving three different measurements for the same patient adapted from (304).

Furthermore, radiography is not a reliable method for the assessment of the morphological structure of the knee, hip, and ankle joints because it primarily relies on 2D image acquisition, which may not accurately represent the complex 3D morphologies of these joints (47, 50, 241, 242) which are 3D objects with varying levels of anatomical complexity (171). For example, the ankle joint is considered to be a more anatomically complex weight-bearing joint than the knee and hip as it contains several overlapping connected bones, as described in chapter 3. Radiographic assessment would not represent the true 3D morphology of this joint (47, 56, 171), or the knee and hip joints (242). Moreover, radiography has other limitations that affect its ability to accurately assess the morphology of the joints. Radiographic distortion may expand or compress the object imaged, leading to inaccurate assessment (243), and variations in patient positioning during imaging can also affect the morphological appearance of the imaged object (48).

Finally, although radiography, like any other imaging modality, has other advantages and disadvantages beside those mentioned above, it remains the gold standard imaging modality used to assess OA (261). Researchers should note the limitations associated with it and should aim to avoid them by applying more reliable imaging protocols and selecting experienced people to classify and assess the severity of OA (274). However, when aiming to assess the

morphology of joints or in studies that focus on the detection of the early signs of OA, more advanced imaging modalities such as MRI that can provide 3D images and more detailed morphological information should be used (262). The next section focuses on the use of MRI.

4.3 Magnetic resonance imaging (MRI)

4.3.1 A brief history of MRI

The fundamental work that encouraged scientists to work in the field of MRI goes back to 1938 when experiments by Isidor Isaac Rabi sent a molecular beam into a magnetic field, resulting in the emission of radio waves with specific frequencies (305). This is the first experiment that laid the foundations for the discovery of MRI, and in 1944 Isidor was awarded the Nobel prize for physics(306). Felix Bloch and Edward Purcell subsequently extended Isidor's work and applied it to materials such as solids and liquids (307). As a result of their work, they shared the 1952 Nobel Prize for physics (308). In 1971, an important breakthrough was made when Raymond Damadian discovered that relaxation time can be a significant tool in distinguishing between cancerous and healthy tissues (308, 309). Two years later, Paul Lauterbur elucidated the ability of the nuclear MR technique to create images (310).

The first MRI image was published in 1977 by Sir Peter Mansfield, who followed up the preliminary work of Lauterbur and developed an approach that resulted in the capture of an MRI image of the finger of a PhD student working in his laboratory (311). After obtaining the first image with a small machine, he received funds to build a full-size MRI machine that could be used to scan bigger organs (312). When the machine was ready, Mansfield volunteered to be the first person to be scanned (313). The process took approximately five hours and resulted in the first full abdominal cross-sectional MRI image (313). In 2003, both Mansfield and Lauterbur were awarded the Nobel Prize in Physiology for the discovery of MRI (313).

The first article that focused on the use of MRI as a diagnostic imaging modality was published in 1980, when only four other articles were published (307). One of these was led by Ronald Evans, who listed technological difficulties that could affect the use of the technology for diagnostic purposes without further research (314), and in the same year, the first commercial MRI system was introduced (314). Since then, there has been significant annual growth in the number of articles focussing on the use of MRI as a diagnostic tool, in 2013 alone, 240 published studies had MRI in their title compared with 4 in 1980 (315). This reflects the rapid development of this imaging modality, along with a parallel growth in interest in its use;

whereas in 1980 there only a small number of machines existed with low field strength (315). However, by 2010, it was reported that tens of thousands of MRI machines which were mostly of high field strength were in use in many healthcare facilities (307, 315). The development of the machines continued rapidly, resulting in very high-resolution images combined with fast acquisition times. A variety of image analysis software can be applied in the machines used now (315).

4.3.2 The use of MRI in OA

As mentioned previously, OA is now considered to be a whole-joint disease affecting all morphological aspects of the joint such as the bone, tissues and ligaments (65). The use of MRI in OA research has had a significant impact on the understanding of the disease process (262). Outcome measures in rheumatological clinical trials and the OARSI have identified MRI as the best imaging modality for the monitoring of early morphological changes (316). This is because MRI is the only imaging modality that can visualise all of the anatomical aspects of a joint, such as bone shape, cartilage changes, osteophytes, subchondral bone marrow lesions (BMLs) and joint effusion (262).

As with any imaging modality, MRI has numerous advantages and disadvantages that might limit or encourage its use in research and clinical diagnosis (11). The main concerns with regard to the use of MRI for the clinical diagnosis of OA relate to its availability and cost compared to radiography (317). Many primary healthcare facilities do not have MRI machines available to use and larger hospitals report numerous complaints regarding long waiting lists for MRI scans (318). In addition, the cost of an MRI scan is higher compared to a radiograph, especially when taking into consideration their minimal differences in sensitivity (317). In a meta-analysis by Menashe, Hirko (319) of studies of the diagnostic clinical performance of MRI in OA compared with the radiographic gold standard, it was found that MRI has higher specificity and moderate diagnostic sensitivity similar to that of radiography. Therefore, the authors concluded that the use of MRI as a clinical diagnostic modality for OA is not justified in terms of cost-effectiveness and availability (319).

Nevertheless, MRI has the benefit of not generating any ionising radiation, which is seen as an advantage over radiography (317). But taking into account the limitations of MRI mentioned above, as well as the low effective radiation dose from peripheral musculoskeletal radiography of approximately 0.001 mSv (equivalent to a few hours of background radiation),

this does not make MRI preferable for use in clinical examinations (320, 321). However, it is advisable to use MRI in the clinic when the patient has rapid or unexpected developments in the affected joint, such as continuous pain and inflammation (261, 317).

On the other hand, the use of MRI in OA research has had many advantages in the past, leading to a clearer understanding of how OA affects the entire structure of the joint (262, 322). Furthermore, when taking a broad view of relevant scientific papers, it can be seen that the focus is often not on the specific characteristics of the MRI machine or the protocols used, but rather the way that the resulting images are analysed (262, 323, 324). Three analytical approaches are widely used in research evaluations of OA using MRI: semi-quantitative, quantitative and compositional analysis (262). Such approaches are reviewed in the next sections.

4.3.3 Semi-quantitative MRI scoring

In 2004, Peterfy introduced a whole-organ semi-quantitative MRI scoring system. Since then, it has been applied in both clinical and research contexts related to OA (325). Such techniques have had a significant impact on the way that MRI images are analysed and provided greater clarity about the pathology of OA (326, 327). The semi-quantitative approach has been valuable method in evaluations of the performance of the multifeatured assessment of OA using MRI images (323). This technique simply scores different features of the joint that are thought to be associated with the pathophysiology and the progress of OA in a semi-quantitative manner (326). Several scoring systems have been published in the last decade that focus on different joints such as those in the knee, hand, shoulder, ankle, and spine(262, 272, 327). Various scoring systems are currently in use for each joint which may differ in the features that they assess (327). For example, several scoring systems associated with the knee joint have been published, which could be due to the fact that it is the joint most commonly affected by OA (272, 327).

The most common semi-quantitative knee scoring system that is currently used is the Whole Organ Magnetic Resonance Imaging Score (WORMS)(327). This was the first scoring system to be published which has been broadly used in many epidemiological studies for more than a decade (325). Since the development of WORMS, three more scoring systems have been established which are the Boston Leeds Osteoarthritis Knee Score (BLOKS) (328), the Knee Osteoarthritis Scoring System (KOSS)(329), and the MRI Osteoarthritis Knee Score (MOAKS)

(330). Both WORMS and BLOKS are commonly used semi-quantitative scoring systems (327), but each system has advantages and disadvantages which are reviewed in the following sections.

4.3.3.1 WORMS

This was the first scoring system to be published and it had been more widely cited than the other scoring systems, with 1161 citations by 2004 (325). In addition, it has been applied in several large epidemiological studies such as the Multicentre Osteoarthritis Study (MOST), OAI, and the Framingham study (331-333). Furthermore, this system depends on a unique protocol that divides the compartments of the knee into several sub-regions rather than depending on a lesion orientation approach (see figure 4-13) (325). This allows a focus on the essential parts of the knee in scoring the possibility of the existence of OA features such as BMLs, cartilage abnormalities, osteophytes, subchondral cysts and meniscus irregularities in the area examined (326). The advantage of this approach is that it allows several lesions in each sub-region to be scored at the same time, which enhances the analysis and interpretation of the data (332). Additionally, the definition of the precise size and location of each lesion is difficult when applying the regional approach because lesions close to each other can merge which could result in the presence of important OA features being missed(332). More details of this scoring system are provided in table 4-3 below.

4.3.3.2 KOSS

The Knee Osteoarthritis Scoring System was published by (329) and is another of the widely used systems, which has been cited 305 times. This system is similar to WORMS regarding its general purpose, which is to score and detect OA features in MRI images. However, differences include that the KOSS aims to individually score OA features such as the status of cartilage, subchondral BMLs and cysts rather than being measured in an additive manner as in WORMS (326). Bone lesions are also graded differently in the KOSS depending on the size of each lesion rather than its mere existence (272). Additionally, the KOSS focuses on scores of meniscal morphology and defines sub-regions differently compared with WORMS (272).

4.3.3.3 BLOKS

Hunter, Lo (328) published the more recent BLOKS system, which is used less commonly than WORMS and is cited in 444 studies. It depends on a regional approach when scoring OA features in the joint, and this is one of the main differences when compared with WORMS and

KOSS which use sub-regional approaches (261). The BLOKS system divides the knee into trochlear and weight-bearing regions, with greater focus on the weight-bearing components (326). Furthermore, in Hunter's (2008) original study, a comparison with WORMS concerning the association of BMLs with pain and cartilage loss showed that BLOKS performed better in scoring BMLs. This is considered to be the main advantage of the system (328), and BLOKS is also described in table 4-3 below.

4.3.3.4 MOAKS

WORMS, KOSS and BLOKS have now been available for several years and are widely used. However, few studies have compared these scoring systems and their weaknesses and strengths in any depth (326). Two studies compared the strengths and weakness in the approaches used to score specific OA features in WORMS and BLOKS (334, 335), and their findings formed the basis for the MOAKS scoring system proposed in 2011 by (330) with the aim to overcome some of the limitations of existing scoring systems. The refinements of the method used to score BMLs provide a more accurate delineation of their region, size, and shape (326). Additionally, a sub-regional assessment of cartilage is applied in this system to avoid areas of redundancy in the cartilage (Hunter, 2011). Furthermore, the MOAKS also refines the methods used in other systems to score meniscal morphology by adding the ability to score meniscal hypertrophy and progressive partial maceration. An extended description of this system is shown in table 4-3 below (330).

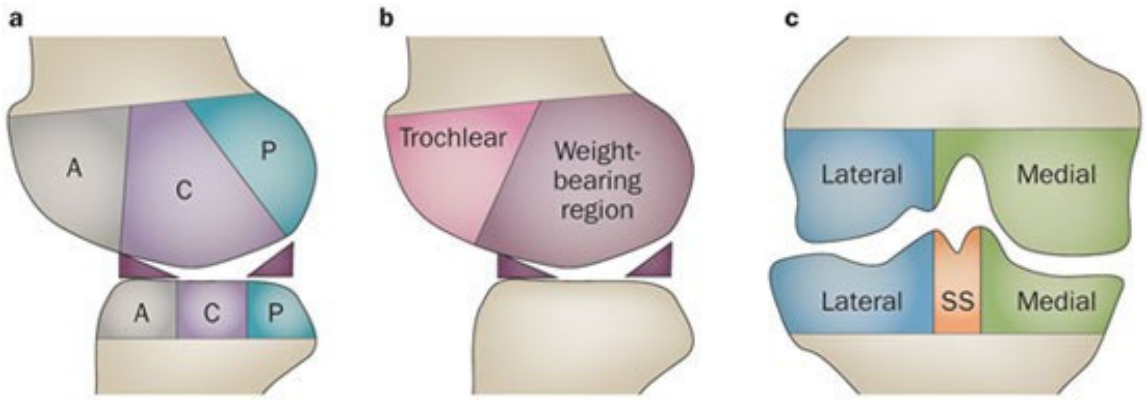

Figure 4-13. Definition of compartments of the knee depending on the type of scoring system used: a) WORMS and MOAKS divide the anatomical parts into the anterior, posterior and central; b) BLOKS divides them into trochlear and weight-bearing regions; c) the medio–lateral division of the femur as defined by all three scoring systems adapted from (326).

Table 4-3. OA features scored by the four-grading system with the grade range used to score knee MRI images for OA.

Scoring system	OA features scored (grades)
WORMS	• Cartilage (0–6). • BMLs (0–3). • Subchondral cysts (0–3). • Bone attrition (0–3). • Effusion and synovitis (0–3). • Per-articular cysts (0–3). • Bursitides (0–3); loose bodies (0–3). • Osteophytes (0–7). • Meniscal tear (0–4). • Cruciate and collateral ligaments (0–1).
KOSS	• Cartilage size and depth (0–3) • BMLs (0–3) • Subchondral cysts (0–3) • Osteophytes (0–3); effusion (0–3) • Meniscal tear (0–3) • Meniscal extrusion (0–3) • Popliteal cysts (0–3) • Synovial thickening (0–1)
BLOKS	• Cartilage size and depth (0–3, plus the extent of any cartilage loss at a specified point). • BMLs (0–3, for each lesion). • Osteophytes (0–3) • Effusion (0–3) and meniscal extrusion (0–3) • Synovitis (in Hoffa's fat pad 0–3 and at 5 additional sites 0–1). • Meniscal status (0–1 for intra-meniscal signal, tears, maceration, meniscal cyst, each scored individually) ligaments (0–1) • Periarticular cysts/bursitis (0–1) • Loose bodies (0–1)
MOAKS	• Cartilage size and depth (0–3) • BMLs (0–3, for each lesion) • Osteophytes (0–3) • Effusion--synovitis (0–3) • Hoffa synovitis (0–3) • Meniscal extrusion (0–3) • Meniscal status (0–1, for intra-meniscal signal, tears, maceration, meniscal cyst, Hypertrophy; scored individually) • Ligaments (0–1); Periarticular cysts/bursitides (0–1, scored individually)

4.3.4 Efficiency of semi-quantitative scoring systems

Several published studies show that the scoring systems used to score OA features in MRI images are reliable with good responsiveness (326, 336, 337). For instance, a meta-analysis of data from 243 studies published between 2009-2011 by Hunter, Zhang (336) assessed the responsiveness and reliability of quantitative and semi-quantitative MRI methods in the evaluation of knee OA. The results showed that, for semi-quantitative grading methods, the random-effects pooling of intra-reader ICC was excellent (ranging from 0.8-0.94) also, the Kappa values of intra-reader and inter-reader reliability ranging from 0.52-0.88 showed moderate to excellent agreement for semi-quantitative methods.

Regarding the responsiveness of the semi-quantitative methods, the results showed a value of polled standardised response mean (SRM) of 0.55 (95%CI 0.47–0.64) for cartilage, which was consistent with results obtained in studies using quantitative assessment. Also, in terms of the responsiveness to change, SRM values were calculated for BMLs of 0.43 (95% CI: 0.17-1.03) and synovial of 0.47 (95% CI: 0.18-0.77), which were considered to represent adequate to good responsiveness. The authors concluded that OA-related changes in the knee joint can be assessed reliably and with good responsiveness using semi-quantitative methods (336).

A recent study by Crema, Roemer (338) assessed the reliability of four expert readers of MRI images using the WORMS scoring system with data from the MOST study. The results showed that for cross-sectional data, the paired inter-reader weighted kappa values showed substantial to almost perfect agreement between readers, whereas moderate to high agreement was found for longitudinal data. The authors concluded that, for both cross-sectional and longitudinal data, semi-quantitative grading for knee OA features could achieve good reliability between different readers.

Although semi-quantitative scoring systems have had a positive impact in clarifying the diagnosis of OA in the joint, they also have some weaknesses (272, 323). One important weakness is the need to establish an imaging protocol, which might be time-consuming and difficult for patients when obtaining the images (262). Also, images should be at high resolution and obtained using advanced MRI machines in order to allow the reader to observe very good clarity when scoring images. Such machines might not be available in many medical facilities (326). Furthermore, OA research using such machines in large trials is more expensive than a less advanced machine. Another limitation is that the morphological changes

associated with bone shape and bone area measurements cannot be assessed using such systems (52). Recently the use of novel quantitative methods of image analysis has shown such changes to be good biomarkers for the onset and progression of OA in the knee and hip joints, as described in the next section (50, 52, 53).

4.4 Quantitative statistical shape modelling

Quantitative analysis is a powerful tool used to measure the various morphological aspects of joints from 3D medical images such as MRI and CT scans, including bone, cartilage thickness, effusion, osteophytes, and meniscus (339). In recent years, there has been growing interest in the use of machine learning for the analysis of medical images (340). This approach is becoming increasingly popular because of its potential advantages over manual scoring (341). For example, it allows for the exploration of an entire datasets in a more comprehensive way, reduces the dependence on human observers, and can detect subtle changes that might be missed in semi-quantitative analysis (51). Moreover, it is capable of the rapid recognition and classification of complex imaging patterns from multiple diagnostic modalities (340).

Given the rapid advances in imaging technology and the projected growth of research on machine learning, it is expected that these techniques will play a pivotal role in future clinical monitoring and decision-making processes (341, 342). In addition, machine learning algorithms can extract useful information not just from a single image but simultaneously from multiple medical images, thus enhancing the ability of clinicians to make accurate decisions about various pathologies (343).

Machine learning algorithms can be categorised into three types based on how they use labels in the training data: supervised, unsupervised, and semi-supervised learning (343). This section focuses on supervised learning, which is the most commonly used form of machine learning algorithm in musculoskeletal research, with particular emphasis on statistical shape models (SSMs)(344). Which are defined as *"geometric models that describe a collection of semantically similar objects in a very compact way … SSMs represent an average shape of many 3D objects as well as their variation in shape"* (51). SSMs were first introduced by Cootes, Taylor (345) and have since been widely used in the analysis of medical images, where the variability in shape of a group of objects such as bones is described and analysed using mathematical and statistical tools such as, principal component analysis to simplify a multifaceted 3D geometric shape into a single metric value that signifies the 3D shape (346).

SSM can be used in medical imaging to examine morphological variations between individuals in the shapes of bones and joints (347). Furthermore, SSM can assist in the identification of common patterns of variation and the understanding of the mechanisms that lead to such differences. Numerous clinical applications such as surgical planning, disease diagnosis, and treatment evaluation can benefit from the information provided from such novel method (51). More detailed descriptions of the reconstruction and utilisation of SSMs is provided in chapter 5. This section reviews the literature aiming to identify relevant studies that apply SSM to explore the morphology of the knee and ankle joints and assess its relationship with musculoskeletal pathologies such as OA.

4.4.1 Literature review

Initially, a systematic literature review had been planned but a preliminary search revealed few studies using such technology, especially in the analysis of MRI images. Also, only three research groups have published work using this method focusing on the knee and ankle joints. Regarding the knee joint, the majority of studies have been published by just one group, the Imorphics Manchester group. Similar papers focusing on the ankle were published using the same sample and research group. Therefore, a review that includes only papers the majority of which were published by one group with the analysis of data from the same population would be considered to be susceptible to bias. Therefore, a narrative review using a systematic search strategy is conducted here to ensure the inclusion of all relevant studies. Table 4-4 below summarises the search terms and databases used in this initial search.

Table 4-4 Summary of search terms, strategy and databases used.

Search terms	• Osteoarthritis, osteoarthritides, osteoarthrosis, osteoarthroses, osteoarthritis deformans, gonarthrosis and OA. • Magnetic resonance imaging and MRI. • Statistical shape modelling, SSM, active appearance modelling and AAM. • Knee, ankle, bone shape, bone area, subtalar joint, talocrural joint, joint space width and JSW.
Database results	• Scopus = 28 • PubMed = 52 • Google Scholar = 140 • EMBASE = 63 • Snowballing =5 • Total = 288

4.4.1.1 Search process

The databases mentioned in the table above were searched using the keywords listed. The first search included the relevant key words with the use of Boolean operators but did not identify any articles focusing on the ankle joint. Therefore, the search was repeated excluding key words for the diseases were removed and those for other types of 3D medical imaging such as CT were added. This search identified a total of 288 studies relevant to the search terms used. The search results were then filtered to remove all duplicates, which resulted in 214 relevant studies and their abstracts were then screened to focus on studies using SMM to assess the ankle and knee joints from MRI images. No studies were identified that used MRI images for the ankle, and therefore studies using CT were included. The screening process resulted in 71 studies that were assessed for eligibility by reading the full text. Of those, 58 studies were excluded for various reasons, leaving seven studies that investigated the knee joint and 8 studies that applied SSM to images of the ankle complex region which were relevant to this review. The PRISMA flowchart in figure 4-14 explains the search procedure.

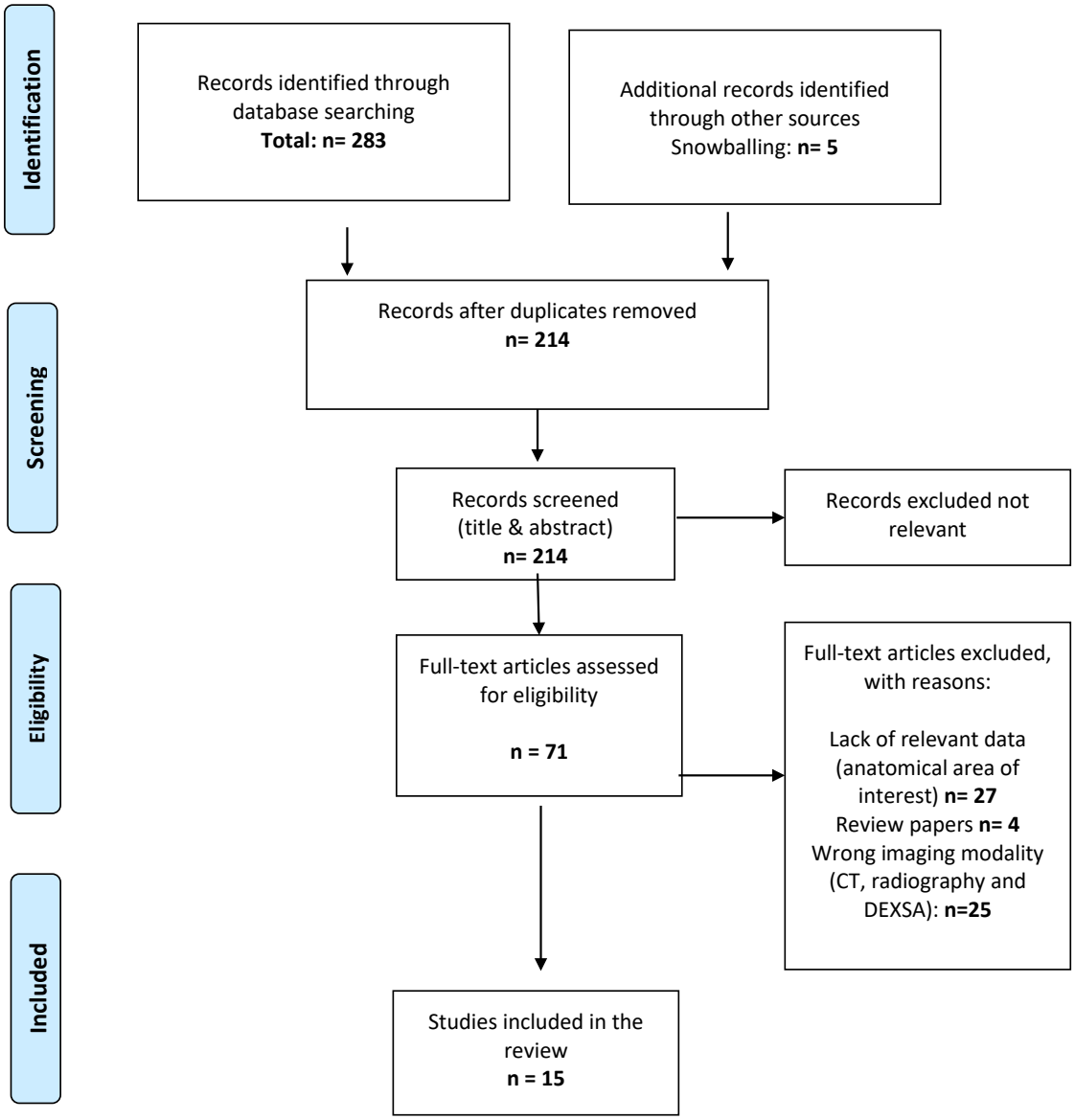

Figure 4-14. PRISMA flowchart of the search procedure used.

4.4.1.2 Selected studies

Of the 15 studies that were chosen for review, 7 used MRI images to assess the role of morphological variations in bone shape and bone area in the knee joint using an SSM method and they were all linked to OA. In the remaining 8 studies, SSMs were constructed from CT images in order to assess the bone shape of the ankle complex region with a variety of objectives, except for one study which analysed MRI images to validate the use of SSM. The studies included can be categorised into two main groups: those using SSM for the assessment of variations in the knee joint; and those that also used SSM in assessing variations in the ankle joint. Tables 4-5 and 4-6 provide a detailed summary of the studies reviewed.

Table 4-5. Summary of studies included in the review that used SSM to explore the knee joint.

Author	Aim	Sample size and population	Anatomical region	Method	Findings
Barr et al. (2014)	To investigate the association between 3D bone area, radiographic features of OA, and clinical characteristics	2588 participants from the OAI study	knee	3D MRI SSM bone area	3D bone are measurements provide more information that cannot be explained by current radiographic measurements
Bowes et al. (2015)	To investigate if 3D alterations in the knee bone area would be typical of OA and give an accurate indicator of progression.	1312 OA group 885 non-OA group from the OAI study	knee	3D MRI SSM bone area	People with OA were distinguished from controls by changes in bone area, which was more sensitive than the present imaging marker for disease progression JSW.
Bowes et al. (2016)	To examine the 3D knee bone area from an OA cohort that displays no change in cartilage thickness but with high risk of OA progression	27 participants from multicentre, observational OA cohort	Knee	3D MRI SSM bone area	While cartilage measurements were not affected at 3 and 6 months, the 3D SSM bone area did indicate that it is more sensitive in detecting OA progression
Neogi et al. (2013)	investigate whether 3D bone structure can forecast the development of radiographic knee (OA).	178 free of OA at baseline but at high risk of knee OA from OAI	knee	3D MRI SSM bone shape	3D knee bone shape was able to predict the radiographic OA's later onset.
Barr et al. (2016)	To establish a connection between total knee replacement and 3D MRI bone shape.	310 controls 310 TKR cases from OAI	Knee	3D MRI SSM bone shape	Baseline 3D bone shape for the TKR group was significantly different than the control group indicating that knee bone shape could be an imaging biomarker predicting TKR
Bredbenner et al. (2010)	To explore if variation in the 3D shape of the knee's bone will help distinguish between people who are at risk and those who are not for developing OA.	12 control group 12 high risk of OA group all female	Knee	3D MRI SSM bone shape	Significant 3D SSM bone shape variations were noted between controls and participants with high risk of OA.
Bowes et al. (2021)	To identify the advantages of 3D SSM bone shape of OA state for evaluating risks of clinically significant outcomes	4796 participants from the OAI	Knee	3D MRI SSM bone shape	This study's use 3D SSM provided an entirely novel, extremely accurate, and exact assessment of OA status: which is a quantified 3D femur bone shape known as the B-score.

Table 4-6. Summary of studies included in the review that used SSM to explore the ankle joint complex.

Author	Aim	Sample size and population	Anatomical region	Method	Findings
Grant et al. (2020)	To create and validate SSM of the foot bones ankle, midfoot, hindfoot and first metatarsal.	24 participants	Foot and ankle complex	3D MRI SSM	The SSM of the foot bones was successfully constructed and validated. Using segmentations from MRI scans, the bones of the foot can be rebuilt with minor inaccuracy.
Lenz et al. (2021)	To create a 3D SSM of healthy ankle joints using WBCT scans to analyse bone shape, joint coverage, and JSW.	27 asymptomatic individuals	Ankle complex (talocrural joint)	3D WBCT SSM	3D morphology of the ankle complex is somehow similar with minimal individual variations noted such information my improve the understanding of the ankle pathologies
Krähenbühl et al. (2020)	To create a 3D SSM of healthy subtalar joints using WBCT scans to analyse bone shape, joint coverage, and JSW.	27 asymptomatic individuals	Ankle complex (subtalar joint)	3D WBCT SSM	3D morphology of bones forming the subtalar joint show variations noted in the shape and JSW, such information indicates a potential for a 3D SSM clinical assessment of the subtalar joint.
Peterson et al. (2022)	To build a 3D SSM to assess morphological and alignment changes in the full ankle complex region in healthy people.	27 healthy individuals	Full Ankle complex region	3D WBCT SSM	A multi-level multi-domain 3D SSM can help clarify joint-level morphology and bone alignment differences. Further studies using bigger sample are warranted
Gabrielli et al. (2020)	To construct SSMs to exemplify ankle and hindfoot bone morphology for sex differences and side-to-side symmetry.	20 healthy participants	Ankle complex	3D CT SSM bone shape	No significant differences in morphology of both ankles, contralateral ankle may be used to guide surgery to restore natural morphology. Sex differences noted in tibia and calcaneus but not the talus
Tümer et al. (2019a)	To explore ankle complex bone shape variations between sexes and evaluate side to side symmetry using SSM	66 healthy individuals	Ankle complex	3D CT SSM bone shape	Similar shape patterns are seen on both sides of each bone type, with sex differences found in the tibial, calcaneal, and talus bone shapes.
Tümer et al. (2016)	To explore ankle complex bone shape variations between control and osteochondral defects using SSM	35-controls 37-with osteochondral defect	Ankle complex (talus and distal tibia bones)	3D CT SSM bone shape	Between the control and osteochondral defect groups, there are shape disparities. As a result, it seems possible that these observed shape differences could be a risk factor for osteochondral abnormalities.
Tümer et al. (2019b)	To examine using SSM 3D shape variations in subtalar joint bones among those with chronic ankle instability and healthy subjects.	26-controls 26-with chronic ankle instability	Ankle complex (Subtalar joint)	3D CT SSM bone shape	Significant bone shape variations between both gropes noted in the talus and calcaneus bone. Indicating that certain bone shapes may raise the chance of developing chronic ankle instability following a lateral ankle sprain.

4.4.2 Use of SSM to explore knee morphology

4.4.2.1 Change in bone area

Previous research has confirmed that change in the bone is fundamental in the development of OA (348). However, few researchers have focused on exploring the role of bone tissues in OA, because the process of precisely identifying and measuring changes in bone tissue has been challenging. In different stages of OA diseases, changes occur in bone size and shape. For example, some studies show that the bone area in the tibial condyles increases with OA (349), while (350) reported that the femorotibial bone area showed an increase in size when compared to healthy knees. Previous studies used 2D methods to measure such variation, but it is argued that such methods have the limitation of not measuring the full bone area with precision. However, with the development of new image analysis techniques such as 3D SSM, the measurement of changes in the bone area has become a focus of research in order to explore the possibility of new imaging biomarkers.

A study conducted by Bowes, Vincent (53) aimed to evaluate changes in the area of bones forming the knee joint. The authors hypothesised that such change represents a way of differentiating between participants with OA and those without. The study included MRI knee images from 1,312 participants who had confirmed radiographic OA and 885 non-OA participants from the OAI. The images were taken at baseline, and 1, 2 and 4 years. The MRI images were used to build a 3D SSM after the automatic segmentation of all the bones from the MRI images. The authors focused on the total area of subchondral bone (tAB) as the anatomical area of interest.

The results showed that bone area in the anatomical regions examined had increased more significantly over time in the OA compared with the non-OA groups. For example, the 4-year percentage increase in the medial femur bone area from baseline for the OA group was 1.87%, and for the non-OA group it was 0.43% ($p<0.0001$) (see figure 4-15). It was concluded that the novel 3D MRI SSM had succeeded in detecting and measuring the change in bone area and that such models could discriminate between people with OA and controls. Likewise, when compared with JSW, which is the radiographic gold standard for OA progression, the differences in bone measurements quantified using 3D MRI SSM were more effective in assigning OA progression status.

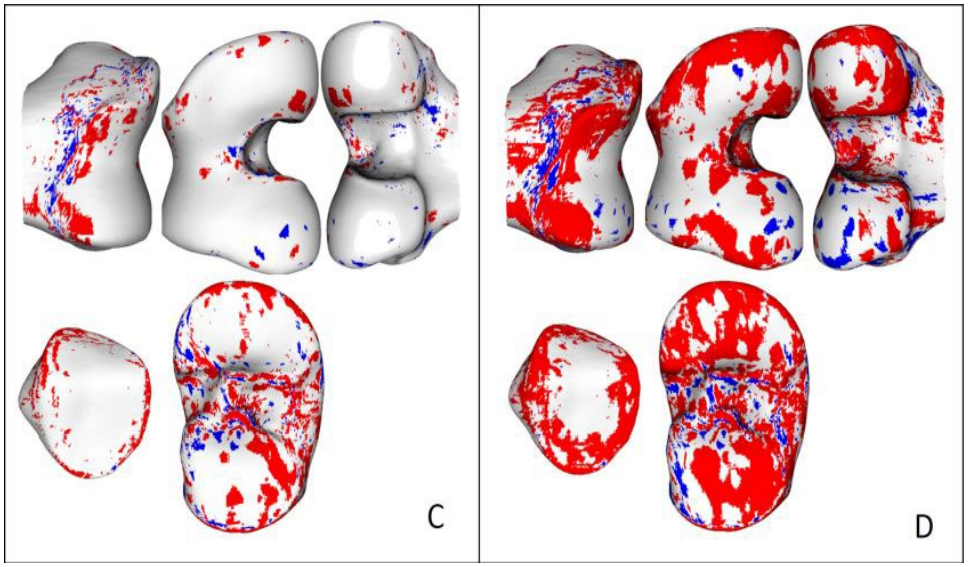

Figure 4-15. Heat maps showing changes over four years in the area of the bones forming the knee joint in participants with and without OA: (C) in the non-OA group; and D) in the OA group. The red colour represents increases in size and the blue decreases in size adapted from(53).

Additionally, the association between 3D area measurements of the bones forming the knee joint and clinical and radiographic OA characteristics was explored in a cross-sectional analysis published by Barr, Dube (351) of data for 2,588 participants also extracted from the OAI database including MRI images, radiographic OA measurements and several clinical characteristics such as height, weight, age and gender. The MRI images were divided into OA and non-OA groups according to radiographic criteria, and 96 random MRI images each representing the OA and non-OA groups were chosen to be manually segmented to train the SSM, and then automatic segmentation was applied to build the full model.

The full model was then used to quantify the area measurements of the bones in the knee joint, and the exact definition of the anatomical bone area used are shown in figure 4-16.

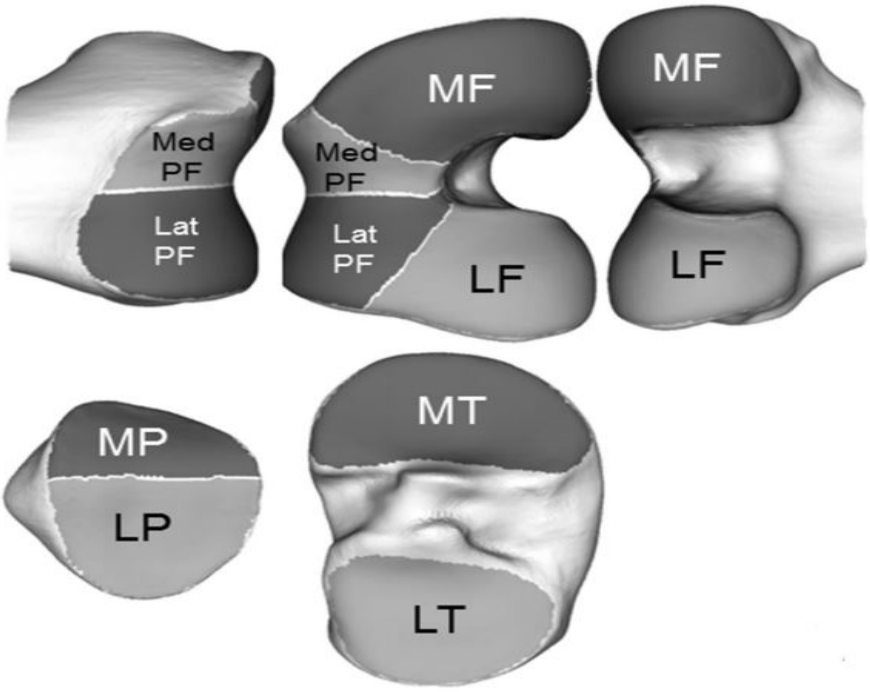

Figure 4-16. Anatomical bone areas chosen: MF (medial femur), LF (lateral femur), LT (lateral tibia), MT (medial tibia), LP (lateral patella), MP (medial patella), MedPF (medial trochlear) and LatPF (lateral trochlear) adapted from (351).

Results from linear regression models showed that the clinical covariates of height, weight and age together explained 22.5% of the variance in MF bone area in the male model and 43.1% in the female model. Furthermore, the variance in the MT bone area was similar to that of the MF in both genders.

The linear regression results also showed that the radiographic OA features JSW, sclerosis, osteophytes and K&L grade respectively described only 5.3%, 10.1%,14.9% and 20% of variance in the MF bone area, with similar results for the MT bone area. The authors concluded that a relationship exists between knee bone area measurements and body size in both sexes. Also, a week association was noted between the gold standard radiographic OA features as quantified from 2D x-ray images and the bone area measurements quantified using 3D SSM. This indicates the ability of the 3D measure to provide extra morphological information representing variations in the population and suggests that the traditional radiographic OA features lack sensitivity in detecting such morphological variations.

Finally, a observational cohort was used in a study by Bowes, Maciewicz (352) to analyse changes in the 3D morphological knee bone area in an OA cohort at different time points where no change had been reported in cartilage thickness, which would be an indicator for disease progression. The aim was to determine if bone area provides a better indicator of

disease progression than cartilage thickness. The sample comprised only 29 participants with knee pain but without any changes to the cartilage and with radiographic evidence of OA. MRI images for both knees at different time points of 1 week, 3 months and 6 months were obtained. However, only the knees with the higher K&L grade were selected to be automatically segmented using AAM. Later, a 3D model was constructed from the segmented images, with a focus on two specific anatomical areas of the femur: the MF and LF (see figure 4-17).

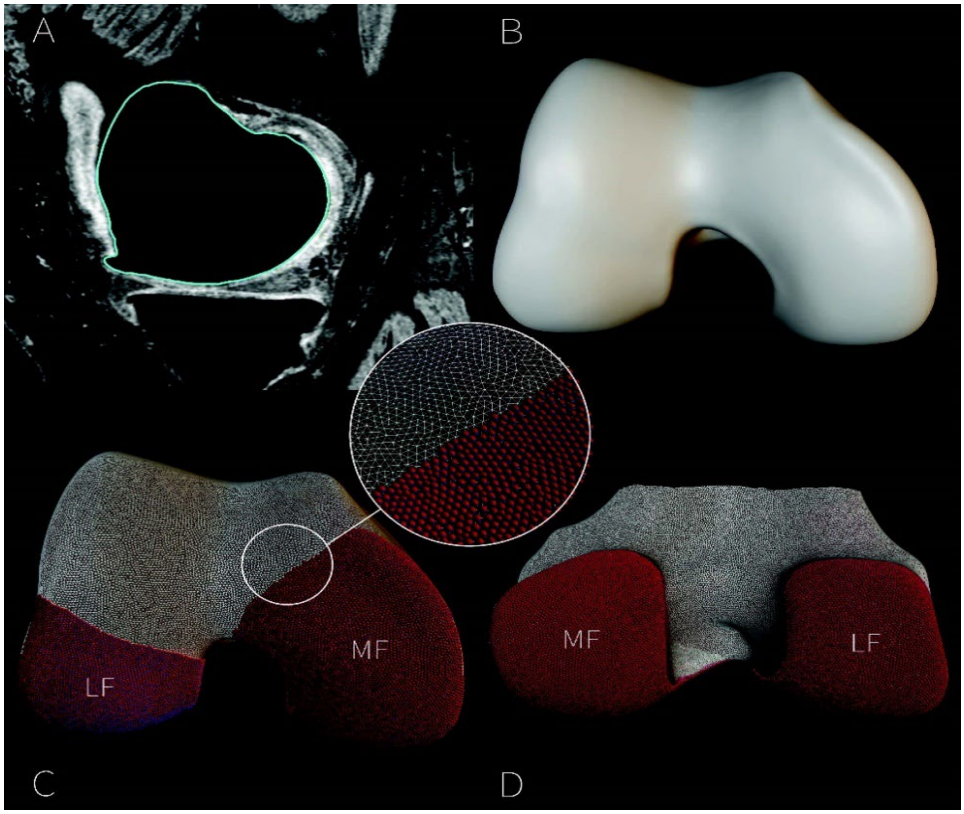

Figure 4-17. Steps in 3D SSM model production using MRI images: A) automatic segmentation of the MRI image; B) the 3D bone surface model produced from the segmented data; C) and D) the mean bone surface as a triangulated mesh in which each vertex represents an anatomically corresponded point or landmark. The anatomical regions chosen are in red: MF, medial femur; LF, lateral femur adapted from (352).

The outcomes showed that the mean MF bone area in the baseline image was 2,291 mm^2. At 3 months the MF bone area ratio of the value against the bassline value had increased by 0.34% (95% CI 0.04–0.64; p = 0.03), and at 6 months it had increased to 0.61% (95% CI 0.32–0.90; p = 0.0002). In addition, the LF bone area in the baseline image was 1,527 mm^2 and at 3 months no significant change was noted; however, at 6 months the ratio of the value against the bassline value had significantly increased by 0.49% (95% CI 0.18–0.80; p = 0.0021).

It was concluded that there were changes in bone area measurements quantified using 3D SSM at different time points. The increases in bone area in both selected anatomical regions were statistically significant, indicating that the use of 3D SSM bone area measurements can detect small changes which represent disease progression even when cartilage thickness, which is the current progression imaging marker, did not change.

Overall, the importance of the studies using 3D MRI SSM to explore morphological variations in bone area, particularly in the knee joint, lies in demonstrating the ability of a machine learning method to perform as a prognostic imaging biomarker for the onset of knee OA. They also show that evidence identified in this way of morphological variations in the bones forming the knee joint is likely to be more effective than radiographic features in detecting change and OA progression.

4.4.2.2 Change in Bone Shape

Changes in the shapes of bones have attracted significant interest among researchers exploring their association with OA, given that bone undergoes both structural and functional changes during the progression of OA disease (210). These changes are likely to be a result of adaptations by the bone when exposed to mechanical influences such as stress, as justified by Wolff's Law (353). Therefore, studies have aimed to explore if bone changes can be used as an OA imaging biomarker. Several studies using SSMs reconstructed from MRI images have explored variations in bone morphology focusing on the knee joint.

One of the first studies using 3D MRI SSM to study variations in knee bone morphology was carried out by Bredbenner, Eliason (354) to assess its potential as a method to distinguish between people at risk of developing knee OA and those not at risk. In this study, 24 female participants with matched ages and BMI for whom MRI images were available in the OAI database were selected from incident and control groups of 12 individuals each. The MRI images were then segmented in order to construct the SSM which was used to quantify morphological features from both groups.

The findings indicate that tibia bone height was lower on average in the incident group compared to the control group, while width measurements for the anterior-posterior and medial-lateral tibial plateau were greater in the incident group. These results demonstrate the ability of SSM technique to quantitatively demonstrate differences between groups and that

it can serve as an advanced tool to explain variations between participants with and without knee OA by statistically characterising the bone shape morphology of knee joints.

A subsequent case-control study by Neogi, Bowes (355) used the 3D SSM technique to build a 3D bone shape model and to explore whether or not such a method could predict the onset of knee OA prior to it being confirmed by radiography. Data from the OAI study used in the case included MRI images for 176 knees free of OA at baseline which later developed incident radiographic OA during follow-up, matched with 353 random knee MRI images in the control group. An SSM was constructed by firstly training the model using manual segmentation, and then automatic segmentation completed the reconstruction of the full SSM for the femur, tibia and patella bones of all of the MRI images (see figure 4-18).

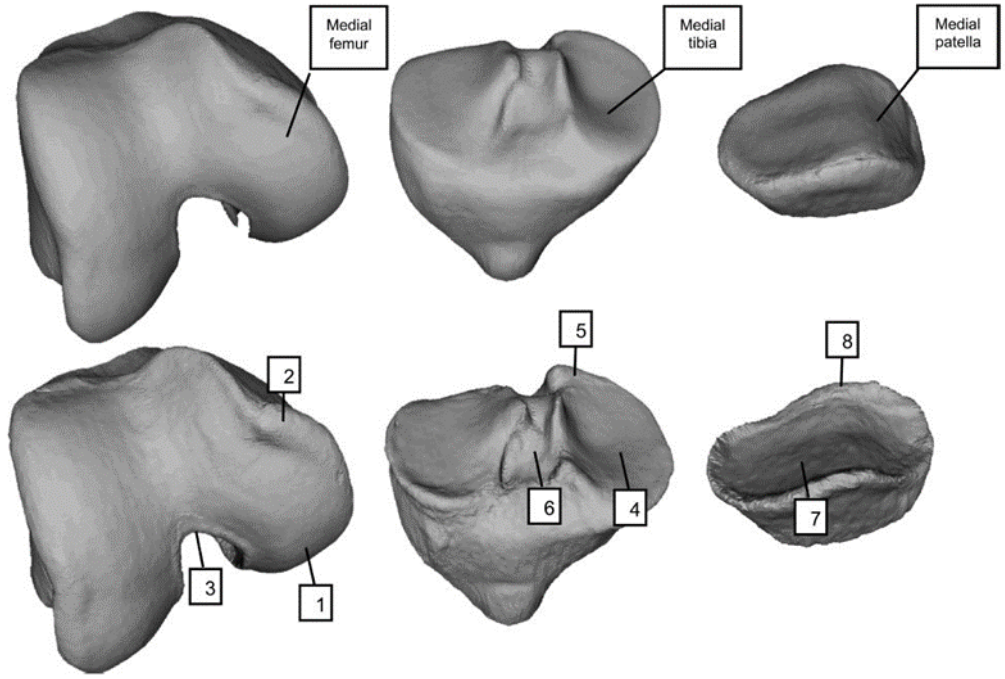

Figure 4-18. Illustration of the main differences in bone shape of the femur, tibia and patella bones in both OA bones (lower row) and controls (top row). Various morphological variations are clear: for the femur, 1 - winding of the femur condyles, 2 - increased osteophyte growth, 3- notch edge narrowing; in the tibia, 4 - winding of the tibia condyles, 5 - increased osteophyte growth, 6 - spines of the tibia moving together; for the patella, 7 - the cartilage plate is increased in size, 8 - osteophytic edge adapted from (355).

Linear discriminant analysis was used to distinguish between OA and non-OA groups, and this method can accurately identify the line in a multi-dimensional space that separates the OA and non-OA groups. The shape variation can then be reported as a single scalar value which represents the space along the LDA vector for each bone considered.

According to the study's findings, the 3D bone shape vectors of knees that eventually developed radiographic knee OA tended to become more 'OA-like' over the course of the study, from the baseline to the 12-month visit prior to the onset of OA and the visit where OA was detected. In contrast, there was no significant change in the 3D bone shape vectors of control knees across these three time-points. For example, in the full knee SSM the knees in the highest tertile were three times more likely to develop incident radiographic knee OA after a year than the knees in the lowest tertile OR 3.0 (95% CI: 1.8-5.0; $p<0.0001$). The findings imply that variations in bone shape could serve as an early indicator of the onset of knee OA.

The results of the two previous papers demonstrate the value of quantitative 3D MRI SSM in understanding the role of bone morphology in OA and its potential as a disease biomarker. Therefore, other studies have looked at different related aspects of bone pathology and clinical outcomes using 3D quantitative bone shape models.

Barr, Dube (52) conducted a nested case-control study aimed to examine the relationship between 3D MRI SSM bone shape and total knee replacement (TKR). Data in this study were collected using cumulative incidence sampling and extracted from the OAI cohort. The participants were separated into two groups: the case knee MRI group and the control group. The case group included 310 participants who had undergone TKR or who had confirmed OA indications of TKR during 72 months of follow-up. The control group included another 310 participants for whom there were no TKR reports.

MRI images at bassline for both groups were extracted from the database and used to construct the 3D MRI SSM using a similar method as mentioned above. After the training of the model by manual segmentation on a training set, the information learned was used to automatically segment the remaining images, and then the 3D SSM was constructed using the AAM. Following the AAM search, the knee bone shapes of all participant bones in the study were represented as principal components. The shape vector for each of the bones is determined by drawing a straight line between the principal components of the average shape of the OA and non-OA groups. The distance from the line is then reported: where the mean non-OA shape was -1 and the mean OA shape was +1 as shown in figure 4-19.

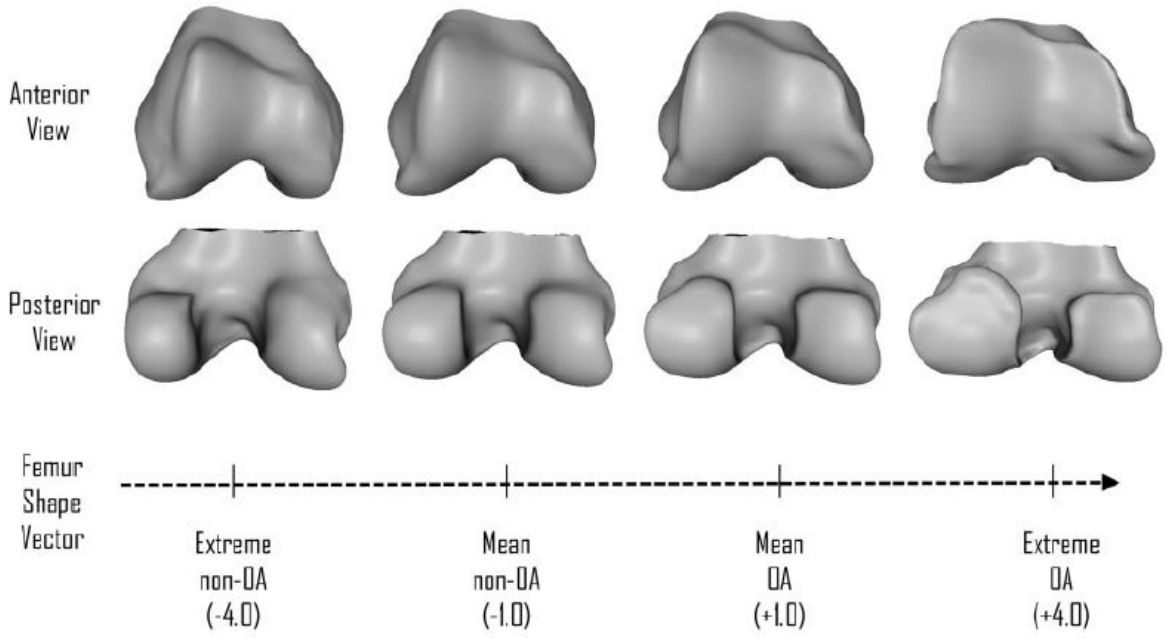

Figure 4-19. Femoral shape anterior and posterior views, where the shape vector -1 is the mean shape with no radiographic OA and +1 is the mean shape with reported radiographic OA adapted from (52).

The results of the study showed significant differences in the femoral bone shape of the knee joint at baseline between the group that had TKR during follow-up and the controls. The mean bone shape vector for the TKR group was 0.98 (SD 1.51) and for the control group the mean was -0.11 (SD 1.40) with an independent t-test p-value of <0.001, and the results for bone shapes of the tibia and patella gave similar results. The authors concluded that 3D bone shape was related to the critical patient outcome of TKR. The accuracy of prediction revealed here supports the value of SSM bone measurements for implementation in future therapy studies concerning disease-modifying OA treatments.

Given the promising results obtained from these studies, increasing numbers of researchers have investigated the effectiveness of 3D MRI SSM as a reliable and precise method of measuring the status of OA. A recent study by Bowes, Kacena (50) explored the benefits of 3D bone shape SSM for the measurement of several clinically important outcomes associated with OA. Baseline knee MRIs from 4791 participants in the OAI cohort, K&L gradings, pain scores and TKR data for all of the participants were extracted from the same cohort.

The focus of this study was only the bone changes occurring in the femur bone; therefore, all of the MRI images were automatically segmented to separate the femur using AAM. The SSM was constructed to identify the OA bone shape vector. To do that, the MRI images were divided into two groups according to the K&L grading for each participant. The OA group

included K&L grades ≥2 and the non-OA group included K&L grades of 0–1. When these groups had been identified in the SSM, the OA vector was defined as the line passing through the mean shapes of the groups with OA and those without it.

The authors aimed to generate a single quantitative measure to represent the variation in bone shape. This score is known as the B-score, and it is represented by the distance along the line of the OA bone shape vector as defined by the SSM. The initial B-score is 0 for the non-OA group. Each unit of change is then defined as 1 SD difference of from the non-OA group. This unit positively increases along the bone shape OA vector when moving towards the OA group and depends on the change in the bone shape (see figure 4-20).

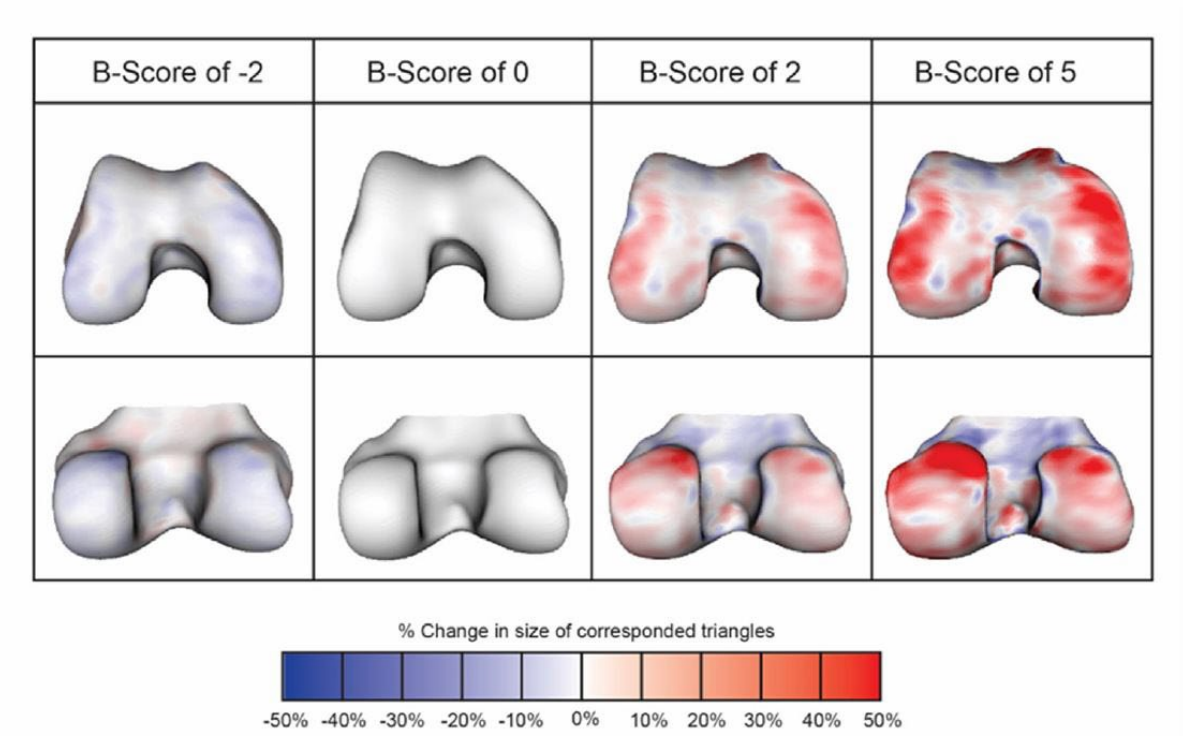

Figure 4-20. Change in femur bone shape in the anterior femur in the upper row and the posterior femur in the lower row. The red colours indicate increased changes in bone shape according to various B-score levels and blue indicates decreased changes in bone shape adapted from (50).

This study focused on an assessment of the risk of OA clinical outcomes such as in pain, function, K&L grade and TKR. The results showed that the risks of losing function and knee pain along the B-score increased from 10% to 60%. The same results were noted for the risk of TKR. On the other hand, logistic regression curves yielded similar results when the risk of increased knee pain, loss of function and TKR were calculated across the range of K&L grades. However, a wide range of B-scores was found for each K&L grade. For example, K&L grade 3 had a risk of pain of 34.4% (95% CI: 31.7 to 37.0) and the B-score ranging from 0-6 at this K&L

grade gave different pain risks in each range. For a B-score of 0 it was 17.0% (95% CI: 16.1 to 17.9) while for a B-score 6 it was 52.1% (95% CI: 48.8 to 55.4). Also, for the K&L grade 0, which is radiographically considered to be normal, the risk of pain was 12% but, in the B-score risk range from -2 to +2 it was 10% and 27%.

In conclusion, this study showed that, as a quantitative measure characterised by the B-score, the 3D MRI SSM can represent the severity of OA morphological diseases. Additionally, it can also detect early morphological changes associated with OA disease that are usually identified as at K&L grade 2 according to the current radiographic gold standard. However, it was shown that 31% of the participants in the OA group with a KL grade score of 2 had a B-score within the range of the non-OA group. Furthermore, 8% of the participants with K&L grades 0–1, which is the non-OA group, had a B-score range that classified them as being in the OA group. That proves that the bone shape B-score is more sensitive than the current gold standard in classifying patinates and detecting the severity of OA disease. It also has the advantage of being independent of the reader, unlike the other techniques, and this dependence frequently causes observational bias in the use of radiographic gold standard (50).

In summary, having reviewed the relevant studies, it is clear that the use of SSM has several advantages, and it has been shown to be a novel method for investigating the morphology of the knee joint. Moreover, the use of this method has helped to shift the focus towards the role of the bone in OA, whereas previously the focus was mainly on cartilage. The application of the 3D SSM shows that examining variations in bone shape over time provides a potential new biomarker of OA progression. The use of this method was also able to detect changes that occur in the early stages of OA which cannot be detected by radiography. Furthermore, it is important to be able to visualise the knee joint in 3D and to examine the morphology of the entire joint. Also, some of the studies reviewed categorised patients in an OA group when they would have been categorised differently using the radiographic gold standard, showing that this novel method is more sensitive in detecting changes associated with OA compared to the current radiographic gold standard. Also, it has the advantage of providing an objective analysis of measurements of bone area and shape, reducing the potential for bias in subjective evaluations and making such analysis easier when there are large volumes of data.

4.4.3 Use of SSM to explore ankle morphology

The success of SSM in research on knee OA has led to its use in musculoskeletal studies of other joints. The ankle joint complex is one of the most anatomically complicated joints in the human body, as described in chapter 3, and has recently attracted increasing attention. Research using novel SSM methods to explore morphological variations in the ankle joint has emerged in the past few years(218). Such studies identified in the literature search had different objectives and used different medical imaging modalities to reconstruct SSMs of the ankle. Only one of these studies used MRI, and the others used CT images.

The studies included in this review, as shown in Table 4-6, can be categorised as follows. Some aimed to create and validate the SSM of the ankle joint complex and describe normal ankle morphological variations, while others explored sex-related morphological variations and side-to-side symmetry or exploring the ankle's morphological variations in relation to ankle joint region pathologies. The next section reviews these studies in order to provide a comprehensive overview of morphological variations in the ankle joint complex using SSM. The objective is to establish the significance of these studies and their contributions to the field of musculoskeletal research.

4.4.3.1 Validation of ankle joint complex SSMs and normal variations

Only one study by Grant, Diamond (356) used MRI images to create and validate an SSM of the bones in the foot and ankle complex region. The study included 24 individuals whose foot and ankle MRI images were manually segmented to identify the outer contours of the bones. These contours were used to generate 3D point clouds, which were then registered and analysed using principal component analysis (PCA) to produce the SSM, which describes the variation in bone shape across the sample for all of the bones in the foot and ankle region.

To validate the accuracy of the SSM, the study used a leave-one-out test in which one participant's data were removed and the rest were used to reconstruct the model. The excluded data was then used to test the model's fit and generalisability using the root mean square error (RMSE) and the Jaccard index test. The Jaccard index measures the similarity between the model and the data, and a higher index value suggests a better model-data fit, while RMSE assess the difference between projected and actual values, where a lower RMSE indicates better prediction reliability for previously unseen bone shapes.

The study found that reconstructions made with sparse anatomical data had a higher Jaccard index and a lower RMSE, indicating the reliable and accurate reconstruction of the SSM. The authors concluded that the SSM of the bones forming the foot and ankle joint complex can be reconstructed with minimal error using full segmentation even with sparse anatomical landmarks.

The remaining studies used other medical imaging modalities rather than MRI. Of these, three studies published by a research group based at the University of Utah used weight-bearing computed tomography (WBCT) to reconstruct the SSM of the ankle joint complex (47, 56, 357). The studies used the same population of 27 healthy individuals and explored different anatomical parts of the ankle joint complex in each study.

The first study by Krähenbühl, Lenz (56) aimed to explore the morphology of the bones forming the subtalar joint and to assess JSW using SSM. To achieve this, the study used WBCT images to segment the calcaneus and talus bones and generate 3D bone surface meshes. These meshes were registered and transferred to volumetric datasets, and PCA was applied to generate mean shapes and modes of variation for both bones.

The SSM analysis revealed that, for both the talus and calcaneus bones, seven PC modes were found to be important, accounting for 65.5% and 69.3% of the total shape variation respectively. Considerable morphological variation was detected across these important modes for each bone. For instance, the first mode of variation of the talus bone, accounting for 16.5% of the total variation in the model, represented variation in the population regarding the existence or absence of the talar posterior process. The same mode of variation in the calcaneus model accounted for 24.1% of the total variance in the model, and mainly showed variation in the population regarding the AP length of the calcaneus accompanied by an increase in the superior slope of the posterior facet. Other mode of variations showed other forms of morphological variations in both bones.

In addition, the study quantified JSW for both the subtalar joint posterior and anteromedial facets, with mean + SD measurements of 2.07±0.44mm and 1.60±0.26 respectively. These findings suggest that, by using SSM, it is possible to quantify JSW in the subtalar joint and detect differences in bone morphology between healthy participants.

The second study by Lenz, Krähenbühl (47) used the same population and imaging modality as the first, but this time aimed to reconstruct the SSM in order to evaluate the morphology of the bones forming the talocrural joint and the articulation regions of the joint. Segmentation was performed on the three bones that form the talocrural joint: the distal tibia and fibula and the talus. The same method as described in the previous study was used to produce and analyse the SSM.

The results indicate that each bone has seven PC modes that represent variation within the population. The sum of the seven modes of variation in the tibia, fibula, and talus described 78.2%, 74.8%, and 65.5% respectively of the total variation noted in each SSM. In the tibia, the first PC mode represented variation in bone shape in the height of the medial malleoli. Similarly, in the fibula, the first mode varied in the population according to the angle of the articular facet of the lateral malleolus. For the talus bone, the first mode showed population variation in the superior/inferior height of the talus bone.

It was also found that the tibiotalar and talofibular articulation surfaces had values of mean + SD JSW of 2.15±0.41mm and 2.43±0.56mm respectively. The SSM demonstrated a highly symmetrical talocrural joint with few inter-individual morphological variations at the articular surfaces. Furthermore, the SSM was able to quantify the JSW of the two articulation surfaces in the talocrural joint.

The third study published by Peterson, Lisonbee (357) used the same participants and imaging modality to assess the subtalar, talonavicular, and calcaneocuboid joints by developing a multi-domain SSM that includes the four bones forming these joints (calcaneus, talus, navicular and cuboid). The model was then used to determine 3D joint measurements and evaluate morphological and alignment variations in the bones. Two SSMs were produced using similar methods as in the two previous studies but employing two different techniques to construct single-domain and multi-domain SSMs. The former involved creating an SSM for each of the four bones before integrating them into a single model, while the latter registered all four bones together and retained their anatomical alignments from the weight-bearing CT scans. The advantage of the latter approach is that it allows the assessment of both morphological and alignment variations.

The findings showed that three PC modes of variation accounted for 74.8% of the total variation in the model. The first mode accounted for 63.8% of the total variation in the model, while the second and third modes accounted for 6.3% and 4.7% respectively. In the analysis of morphological variation, the first PC mode revealed differences in the sizes of all four bones, while the second mode showed variations associated with the length of the calcaneus. Meanwhile, the first PC mode for variations in alignment involved overall outward and inward movement between the bones, whereas the second mode concerned superior and inferior movements of the four bones.

The values of joint space width (JSW) for the subtalar, talonavicular, and calcaneocuboid joints were reported to be means + SD of 3.33 ± 2.06, 1.32 ± 0.43, and 1.67 ± 0.62, respectively. These JSW measurements did not change when assessed across all modes of variation using both the alignment and morphological models. The authors concluded that the employment of a single multi-domain approach when producing the SSM allowed for the separate assessment of variations related to both alignment and morphology. Furthermore, both morphology and alignment variation models have the potential to predict similar and reliable JSW measurements within a population.

Overall, the three studies highlighted the potential of SSM as a tool in exploring morphology and alignment, as well as the easements, of the JSW in the anatomically complex ankle complex region, which comprises several overlapping bones that form joints that are essential but challenging to evaluate using conventional 2D methods. However, while these studies had the advantage of examining the ankle complex region in a weight-bearing position, they share some limitations mainly associated with the population studied. For example, all three studies showed significant variations in morphological and joint measurements across the population, but the generalisability of these results is limited owing to the small sample size and the absence of an explicit sampling frame.

Moreover, it is unclear if the morphological variations identified among participants were attributable to differences in sex or body size, since such associations were not tested. This is possibly due to the small sample size and unequal sex ratio (20 females and 7 males), which precluded full statistical analysis. Therefore, further research using larger samples is necessary to build on these findings and deepen our understanding of the morphology of the ankle complex region.

4.4.3.2 Use of SSM to assess variation due to sex and side symmetry in ankle morphology

As seen in chapter 3, sex-related morphological variations in the ankle joint are important and are normally assessed using pre-defined measurements from cadaveric specimens. The literature search revealed two studies that aimed to reconstruct SSMs to exemplify the bone morphology of the ankle complex and to evaluate sex differences and side-to-side symmetry. The first study was conducted by Tümer, Arbabi (57), who manually segmented 66 bilateral CT scans of the ankle (55 male and 11 female, ages: 61 ± 10 years) to produce separate SSMs for each of the four bones: the distal tibia and fibula, talus, and calcaneus. They then used PCA to generate a mean shape and modes of variation for each bone. To assess sex-related differences, the left and right bones were combined into a single group, and an analysis of covariance (ANCOVA) was used to adjust for age.

The results showed significant sex differences in bone shape, with different PC modes for each bone model. For example, in the first PC mode for the tibia, males had larger lateral and medial condyles than females ($P = 0.003$), whereas the first PC mode for the calcaneus showed that females tend to have longer and higher bones ($P < 0.001$) and for the talus the 8th PC mode showed that the posterior part of the bone was larger in males ($P = 0.001$). Additionally, no side-to-side morphological differences were found, indicating that both sides of the bones that make up the ankle complex region displayed identical shape patterns across genders.

The study concluded that there was no directional asymmetry in any of the bones studied. They also found sex-related variations in bone shape, but these did not account for a significant portion of the variation identified by the SSMs. In future studies, it may be useful to explore other factors that contribute to bone shape differences.

The second study was recently published by Gabrielli, Gale (55) and aimed to evaluate morphological differences between male and female ankles and to assess the symmetry of the left and right ankles using SSM. Bilateral ankle CT scans were used from 20 healthy individuals (10 males and 10 females, age 30.7 ± 6.3 years) to reconstruct an SSM of the bones in the ankle complex region. To create the SSM, the authors performed manual segmentation and registered all 3D surfaces, and then applied PCA to produce a mean shape and modes of variation.

The average distance between matching points on the left and right bones for each participant was calculated to evaluate side-to-side variation, and a t-test was used to analyse the differences. Also, to assess sex-related differences, the authors produced typical SSMs for males and females representing each bone in the ankle complex region (tibia, talus, and calcaneus), and co-registered the models for each bone for both sexes. The differences between male and female bones were calculated by subtracting points from the typical male bone model from points on the typical female bone.

No statistically significant side-to-side variations in bone morphology were found in this sample. Also, while there were no obvious differences between the sexes in the morphology of the talus bone, the distal tibia bones of males were generally larger than those of females. Additionally, there were sex-related differences in the calcaneus bone, with females having bones of greater length, but which were thinner compared to males.

The use of SSM can help in categorising bone morphology and may provide a more precise guide for the surgical restitution of native ankle morphology from an examination of the contralateral ankle. These findings have important implications for the understanding of ankle morphology and surgical intervention.

The studies by Gabrielli, Gale (55) and Tümer, Arbabi (57) both employed a novel method to investigate morphological differences in ankle bone structure between males and females and to assess side symmetry. Their findings offer valuable insights, particularly in relation to sex-related variations in a population. Furthermore, such findings can inform decisions on surgical intervention and contribute to our understanding of the morphology of the ankle complex. However, their limitations include small sample sizes and significant age differences among participants which may compromise the generalisability of the results. Tümer et al.'s small sample with a significant variation in the number of males and females (55 and 11 respectively) may also limit the accuracy of the model used to determine sex-related variation because it was trained on more examples of male bones. In addition, neither study explored the association between body anthropometry and variations in bone morphological in both sexes. it is important when investigating sex-related variation to differentiate between variability related to sex or body size.

Despite these limitations, it is important to gain a clearer understanding of sex-related variations in the morphology of the ankle joint complex. Doing so would be of great significance in various fields, including surgery planning, sports injury prevention, gait analysis, and forensic science. Future studies using SSM to assess sex-related variations in ankle bone structure should aim to overcome these limitations while providing greater clarity on whether variations observed are due to sex or body size.

4.4.3.3 Use of SSM to assess pathological variations in ankle morphology.

Another benefit of using SSM is that it makes it possible to quickly quantify and compare complicated anatomical areas and to analyse the bone shapes, which enables researchers to identify and characterise small variations in bone morphology that might be related to specific pathologies. Two studies have aimed to explore the differences between participants with ankle pathologies and healthy controls. The first study, by Tümer, Blankevoort (358), explored the morphological differences between 35 participants diagnosed with osteochondral defects matched to 35 controls. They used CT scans to reconstruct two SSMs for the talus and distal tibia bone, and PCA was used to derive the mean bone shape and modes of variance. The statistical ANOVA test was used to explore variations in bone shape represented by the modes of variance between the groups. Each PCA mode that a showed significant difference was then visualised and described.

The results showed that the first five modes of variation in the distal tibia SSM explained 40% of the variance and in the talus the SSM explained 49% of variance. In the distal tibia model, the first mode of variance showed significant difference between the groups ($p<0.0001$) where the osteochondral defect deviated towards the -SD of the first mode of variation, representing enlargement and narrowing in the tip of the medial malleolus bone. In the talus SSM, only the fifth PC mode yielded significant differences between the groups ($p=0.004$). The osteochondral defect deviated towards the -SD, which represents a decrease in the size of the talus dome and an increase in the vertical neck angle. The authors concluded that bone shape variations exist between the osteochondral defect and control groups, which suggests that the morphology of the talocrural joint as assessed by SSM can be used to identify bone variations that may represent a biomechanical risk factor for osteochondral defects.

The second study by Tümer, Vuurberg (359) explored morphological variations in the talus and calcaneus bones which form the subtalar joint in participants with chronic ankle instability

and healthy controls. Ankle CT scans of 26 participants diagnosed with chronic ankle instability and 26 healthy controls were used to produce two statistical shape models (SSMs), one for each bone. The SSMs were reconstructed and analysed using similar methods as the authors' previous study. Bone shape as represented by the principal component modes of variation was analysed using ANOVA to determine which modes showed significant variation.

The study found no significant difference in the bone shape of the calcaneus and talus bones between ipsilateral chronic ankle instability and their contralateral ankle. For the calcaneus, the first five principal component modes described 49% of the total variance, and for the talus, the first six modes described 40% of the total variance. These modes of variance were used for statistical analysis.

For the calcaneus, principal component mode 3 showed significant ($p=0.003$) bone shape differences between the disease and control groups. The former deviated towards the -SD, which represents a more distally located medial tuberosity and a centred lateral tuberosity, which is different from the control group that showed a less extended tuberosity. Regarding the talus bone, the second principal component mode showed significant differences ($p=0.001$) between the groups. The disease group deviated towards the +SD, representing anterior reductions in the angle of the neck of the talus relative to the body of the bone, whereas in the healthy group that angle increased.

These morphological variations in the shapes of both bones between healthy and diseased ankles indicate that such morphological variations may increase the risk of the development of chronic ankle instability. The findings suggest that the construction of SSMs using mixed data from the two groups enables the identification of variations in shape that may increase the risk of disease.

These studies by Tümer et al represent the only so far studies which assessed the morphological variations between pathological and normal ankles using SSM, using methods similar to those employed in assessing variations in knee joint morphology in OA and non-OA participants. SSM usually requires a substantial amount of data for training in order to be effective, and this can be difficult to acquire in some circumstances. Therefore, the main limitation of such studies is their low sample size, which may affect the ability of the model to identify in detail any variations between groups. When aiming to explore the differences

between a diseased group and healthy controls, a larger sample that includes participants with diseases at different stages will enable the model to better capture important variations. In general, however, the use of machine learning methods such as SSM makes it possible to quantify complex anatomical structures, giving researchers a more in-depth understanding of size and shape variations in diseased and healthy groups. One of the main advantages of SSM is its capability to precisely determine small variations in morphology that might be challenging to recognise using conventional manual methods. This can be especially helpful in the detection of the early symptoms of disease and the tracking of disease development over time.

4.4.4 Conclusion

This section has reviewed studies that have used SSM to evaluate the morphology of the knee and ankle joints. The findings clearly demonstrate the strong ability of SSM to quantitatively evaluate the morphological structure of joints, particularly in research focused on knee OA. Where SSM has been used on large datasets with participants from all stages of the disease, the production of such promising results qualifies it as a reliable imaging biomarker for OA.

Regarding the ankle, previous studies aiming to assess the morphological variations in the ankle complex have used 2D radiographs or measurements on cadaveric specimens, as described in chapter 3. Such methods have limitations in accurately assessing variations in the morphology of a 3D object such as the ankle complex region which involves triplane motion and multiple overlapping bones. However, the application of SSM can overcome these limitations in assessing the morphology of the ankle complex region. However, research using SSM to evaluate the morphological features of the ankle joint is still a new area of research. Even though the majority of studies reviewed were published within the last three years, they have already provided a deeper understanding of the normal and pathological morphology of the ankle joint complex compared to other conventional 2D methods, to an extent comparable to what has been shown in studies using SSM and focusing on the knee joint.

It is important to note that all of the studies reviewed here, and in particular those focusing on the ankle region, have limitations that should be taken into account. The most significant limitations are small sample size and sampling frame, where in some studies convenience sampling is used while others provide no explicit sampling frame, and this could affect the generalisability of the results. Also, a smaller sample may not detect or reflect all

morphological variations between populations, potentially leading to both type I false-positive errors or type II false-negative errors. Furthermore, as discussed in chapter 3 age, ethnicity, body size and sex are further important variables that should be taken into account when exploring these morphological variations. Such variables were not considered in the majority of the reviewed studies, and more comprehensive research could provide more accurate and detailed evaluations of morphology patterns and help in explaining differences between populations.

In addition, this review explored whether or not existing studies have used SSM to evaluate morphological variations in ankles between participants with knee and hip OA and those without. As explained in chapter 2, variations in ankle and foot morphology could lead to increased mechanical stress on both the knee and hip joints, potentially affecting the onset or progression of OA. To the best of the present author's knowledge, no studies have explored such associations. Therefore, the use for this purpose of data from the Newcastle Thousand Family Study (NTFS) presents a valuable opportunity to study morphological variations in the ankle complex region in a population-based study with a large and representative sample. The NTFS is discussed in more detail in chapter 5, and this study aimed to use its database to produce SSMs from ankle MRI images and to evaluate sex-related variations between participants of the same ethnicity background and age. The interrelation is also examined between morphological variations and OA in other lower limb joints as defined by radiographic and clinical data available for the same participants in the cohort.

Chapter 5 Methods

This chapter provides a detailed description of the methods used in this research. To begin, the NTFS cohort is introduced, which served as the primary data source for this study. The clinical assessment that was conducted and the types of data that were collected are described, and the specific data that were used in this research are clarified. Next, the methods that were employed to extract data from both the NHS and the NTFS databases are outlined. All necessary approvals that were obtained are listed. The methods used in reconstructing the SSM to quantify morphological variations are then detailed. Finally, a thorough description of the statistical analysis tests and methods that were used in the study is presented.

5.1 Primary data source: Newcastle Thousand Families Birth Cohort

5.1.1 Origin of the study

Spence and Miller (360) report concluded that high rates of infant mortality in Newcastle upon Tyne during the 1930s resulted from acute infections. To investigate further, the Newcastle Thousand Families Study (NTFS) was initiated. This unique study examines a cohort of babies born in May and June 1947 in the same city, providing valuable comparisons for the researchers involved (361). Later, researchers determined that they needed to follow participants throughout their lives, adding further value to the study.

In May and June of 1947, the Newcastle Thousand Families Study recruited all 1,142 babies born in the city of Newcastle upon Tyne, representing the entire social strata of the city (361). Although originally intended to follow participants for one year, the study continued through their childhood and now includes nearly 80 years of follow-up (58). This extensive follow-up has provided valuable insights into the causal relationships between childhood and adult health conditions.

In 1947, Newcastle upon Tyne had a population of nearly 300,000 people, with a high birth rate and migration from neighbouring towns and villages for work (362). The demand for unskilled labour was significant, as the area looked to rebuild itself after the destruction of the

Second World War. This period also saw an increase in marriage rates and the number of families in which children were born (362).

The sample for this study was influenced by the historical context in which it was conducted. The study was initiated two years after the war, when birth rates were lower resulting in smaller families. In fact, almost three-quarters of the cohort were from families with only one or two children, a much lower number than before the war. Living conditions in the city were challenging, with inadequate housing and sanitation. A report from 1865 revealed that many families lived in a single room, and most homes did not have indoor toilets. During this time, Newcastle had the highest annual death rate in the country, at 36.7 per 1000 people. However, infant mortality rates decreased significantly from 1873 to 1947, dropping from 186 per 1000 births to 44 per 1000 in 1947 (362).

The study's initial data set, collected over 15 years, was presented in three separate books(361-363). The researchers were initially required to visit families, observe living conditions, and discuss the children's health with their parents (361). At the time, the researchers determined that there was a strong need to follow these children as they grew up in and outside of the community. The research team, comprised of trained health visitors and paediatricians, made numerous follow-up visits to record data for antenatal records. These records were initially created during a visit from a clinician after birth (58). The team followed 967 babies until age one, 847 until age five, and 750 during their school years, with the intention to examine the relationship between weight, height, living situation, socioeconomic situation and health statues (58).

The family visits involved the observation of children and documentation of their socio-economic circumstances. The team conducted visits every six weeks when the children were babies and every three months until they turned five. In addition to observing the children, the team recorded details of the family's socio-economic situation and lifestyle. This assessment was made at the beginning of the study and updated regularly after visits from the research team. Furthermore, the children received formal examinations by a paediatrician at ages one, three, and five (58).

As the children entered school, their height, weight, and reported illnesses were recorded in addition to other data. The study team flagged participants' medical records in primary care

settings to identify healthcare incidents and code them appropriately. This approach resulted in detailed data collection, including marking GP records to inform the team of emerging health events. The use of a red dot on medical records earned the children the nickname 'red spot babies,' and this designation is still used today. During the period in which the study was dormant , the existing records were stored in the Newcastle City Archive (58).

In 1997 the study was resumed, and all members of the cohort who were traced were sent a health and lifestyle questionnaire and asked to attend for a health examination. Of the 574 who completed the questionnaire, 412 participated in a clinical examination that included assessments of serum, bone density, and other clinical measures(58). Those who participated in the ages 49-51 were representative of the original cohort, although the gender balance was slightly skewed (364). Notably, 18% of participants lived outside the North of England, enhancing sample representativeness (58).

A strength of the NTFS cohort is that it focused on children born in a single UK city after World War Two. The study was highly comprehensive due to its focused geographical region and minimal attrition rates. Notably, the study had very low dropout rates during childhood. The main strength of the study lies in the continued relationship between participants and the study team, allowing for lifelong tracking of the participants' development. This study is significant for its ability to provide detailed insights into the lives of individuals from a specific time and place (58).

Furthermore, the longitudinal design of the study has allowed for the collection of extensive data on lifestyles, health behaviours, and medical histories of participants(58). Multiple epidemiological studies have been published using such data. The common thread found in these studies is that risk factors in adulthood seem to have a much greater impact on the development of a variety of disease outcomes by the age of 50 than do variables from early life. The results of these studies have influenced public health policies and interventions targeted at lowering risk factors and enhancing adult health outcomes. In the context of this thesis, follow up data from the ages of 62-63 years were used. A detailed description of the specific data used is presented in the following sections.

5.1.2 Age 62/63 cohort follow up

The follow-up of those aged 49-50 that took place from 1997-98, resulted in 832 participants being traced using several methods. Of a total of 574 participants who returned the questionnaire, 412 engaged in the clinical assessment. The data collected from that review resulted in the publication of more than 45 peer-reviewed papers. Given the quality of the data produced from such a review in 2009-11, a follow-up of the 62-63 years age group was undertaken. Ethical approval was granted by Sunderland Research Ethics Committee (REC reference 09/H0904/40), and all participating study participants gave informed written consent.

The protocol for the most recent follow-up was similar to the age 50 follow-up. This included a health and lifestyle questionnaire and a clinical assessment visit. The number of study members traced for the most recent follow-up was 741. The self-completion questionnaire was posted to participants and, of the 741 approached, 433 returned the questionnaire and 350 attended for clinical assessment.

The clinical assessment took place at the Clinical Research Facility (CRF), Royal Victoria Infirmary (RVI), Newcastle upon Tyne. A wide range of assessments was carried out during the visit which included:

- Cardiovascular assessment
- Musculoskeletal assessment
- Assessment of cognition.
- Assessment of hearing function
- Assessment of respiratory function
- Assessment of oral health
- Collection of blood, serum, and urine samples.

5.1.2.1 Health and lifestyle questionnaire

During the age 62/63 cohort follow-up, 433 out of 741 study cohort members who had been traced completed the questionnaire. The questionnaire was printed and sent to the participants with clear instructions on how to answer each section. After completion of the questionnaire, the participants then sent it back to the NTFS team. Various aspects of the

participant's health and lifestyle were covered in the questionnaire, which contained a total of 214 questions divided into 12 general sections which are as follows:

1. Work, retirement, home, and family
2. Smoking
3. Alcohol use
4. Diet
5. General health
6. Women's health
7. Men's health
8. Physical health
9. Mood
10. Family health
11. Income
12. Updated contact information

After the questionnaire was returned, the NTFS team transcribed and saved all data electronically in a secure database while keeping all paper questionnaires stored as well. The focus in this thesis is only on data relevant to the aims and objectives of this research which were determined after a review of the literature. The data used from both the self-report questionnaire and clinical assessment visits are detailed below.

5.1.2.2 Dominant body side

According to the Miller-Keane Encyclopedia and Dictionary of Medicine, a person's dominant side is that which is stronger and more frequently used in daily activities. The determination of the dominant side has been a debated topic in the literature, but the self-report is considered to be one of the best methods (365). In the NTFS Health and lifestyle questionnaire, participants were asked which side they preferred in the use of their hands and feet in the section on physical activity. This information is relevant to this thesis because the MRI protocol requires the scanning of the dominant hand, wrist, knee, and ankle. Therefore, information about the dominant side of each participant was available both from scanning and the data extracted from the questionnaire.

5.1.2.3 Knee, and hip pain

In the general health section, questions included joint pain at the time of questionnaire completion. The questions focused on all joints; however, hip and knee joints were of particular interest. Participants who had pain on the day could tick which joint(s) were affected and on which side: left, right or both. However, data for these questions were extracted for

analysis only for the ipsilateral side of the MRI images and were used as categorical explanatory variables. This means that the answers for the side of each joint for each participant were chosen depending on the dominant side scanned by MRI.

5.1.2.4 WOMAC

The physical health section of the questionnaire included those for the Western Ontario and McMaster Universities Osteoarthritis Index (WOMAC; version 3.1) as part of the musculoskeletal assessment. As described in section 2.5.1, WOMAC is a validated tool which evaluates three domains: pain, functioning, and stiffness of the lower extremity joints. The tool is a questionnaire containing a total of 24 questions in three categories. The function section has 17 questions, and there are 5 and 2 questions respectively to assess joint pain and stiffness. The index uses a scale from 0-10 for each question. For example, pain questions scale from 0 (indicating no pain) to 10 (indicating extreme pain). The pain section includes questions assessing pain during specific activities, while the stiffness section assesses stiffness during a specific time of day whereas the function section scales difficulties with specific activities.

For this thesis, the data were analysed by calculating the sub-score for each category and generating a total WOMAC score representing the total of all three sections for each participant out of 240. Participants were separated into four categories of severity for each domain (none, mild, moderate, and severe). The data were used as categorical explanatory variables.

5.1.3 Age 62/63 clinical assessment

5.1.3.1 Height and weight

During the age 62/63 review, height and weight measurements were taken of all NTFS participants during visits to the CRF for clinical assessments. Weight was recorded using a calibrated SECA digital scale, with participants wearing light clothing and without jackets or shoes. Measurements were rounded to one decimal point according to the protocol. Height was measured using an electronic stadiometer, with participants standing upright without shoes, and recorded to the nearest centimetre. Before taking measurements, all electronic scales were calibrated according to the manufacturer's recommendations. Participants' BMI was calculated using weight (in kilograms) divided by height squared (in metres).

5.1.3.2 Magnetic resonance imaging (MRI)

Of 354 participants attending the clinical assessment, MRI scans of the knee, hand/wrist and ankle were performed on 281 participants. Not all participants had all three joints scanned due to prespecified exclusion criteria in the protocol. All 281 participants had hand/wrist scans, 258 had knee scans and 277 had ankle scans. Exclusion criteria included MRI contraindications (the presence of a pacemaker, ICD, aneurysm clip, cochlear implant, orbital metal fragments, metallic heart valve/stent, aortic stent, and joint metalwork).

MRI scans were performed on each joint on the dominant side and were carried out at the CRF in the Royal Victoria Infirmary (RVI). The scans were performed by a research radiographer using a 0.2T Esaote C-Scan dedicated extremity MRI scanner with gradient echo-based T1 imaging allowing 3D reconstruction. The MRI scanner's quality was assessed by following the quality assurance protocol established by the Radiology department at the RVI. Every week, a dedicated quality assurance test was conducted on the MRI machine, using a specialised MR phantom as per the manufacturer's operating specifications detailed in the user manual. Such tests primarily aimed to ensure the scanner's safety, evaluate image quality, and assess parameters like the signal-to-noise ratio. The regular performance of these quality assurance tests is crucial in ensuring the safety and reliability of the MRI scanner, as well as maintaining the quality of the images produced.

The peripheral scanner allowed the imaging of the relevant joints without the potential for inducing claustrophobia. The sequences included gradient echo-based T1 imaging allowing for 3D reconstruction. The MRI scanner had specific coils for each body part scanned. For the MRI scan of the ankle joint, the participants were positioned on a couch with the MRI machine centred on the tibiotalar joint. Soft sponges were used to help with immobilisation. Sagittal, coronal, and transverse images were obtained. Images of the knees, wrists and hands were also obtained. The scans took 45 minutes to complete, while an ankle joint scan required 6-7 minutes. All scans were then stored electronically in the Picture Archiving and Communication System (PACS) of the Royal Victoria Infirmary using the participants' NHS numbers.

5.1.3.3 Radiography for K&L grading and JSW of knee and hip

As part of the most recent clinical assessment, attending cohort members had radiographic images taken of the knee, foot, and hand/wrist. Of 354 participants attending for clinical assessment, 324 participants had both knee and foot radiographic images.

Radiographs were acquired in the RVI's radiology department. The imaging protocols used are as mentioned in section 4.2.3. Three weight-bearing radiographic views of the knee were obtained for each participant: bilateral PA, lateral and skyline images, while only the AP view was obtained for both feet. All radiographic images were obtained by a research radiographer and then stored in the hospital's PACS system using the participants' NHS numbers. For this study, only the radiographic images of the participants' knees were included.

5.1.3.4 Dual-energy X-ray absorptiometry (DXA) scan

The clinical assessment included dual-energy X-ray absorptiometry (DXA) in the Clinical Research Facility. Using an iDXA (GE Lunar, Madison, WI), patients were lying down in a supine position wearing only a medical gown. Images were obtained from several anatomical regions of the participant's body including the whole body, right and left hips, lower limbs, and spine. DXA scans allow the measurement of both bone mineral content (BMC) in grams (g) and bone mineral density (BMD) in g/cm^2.

DXA images are usually used clinically for the diagnosis and classification of conditions such as osteopenia and osteoporosis, and are not commonly used to classify or diagnose hip OA. However, in the NTFS, the advanced technology of a high-resolution DXA scanner (iDXA) was permitted for use in assessing OA features in the participants' hips. This can be justified based on the results of studies that have investigated its reliability which have been discussed in section 4.2.3. Also, since the NTFS aims to investigate multiple musculoskeletal diseases such as OA and osteoporosis, DXA scans can give the desired results while exposing subjects to less radiation, which is preferable ethically. Therefore, in the NTFS, DXA images were used to measure BMD, grade hip OA, and measure hip joint space width (JSW).

5.1.4 Assessment of radiography and iDXA images for OA

All radiographic images were assessed for OA within the joints. The tibiofemoral knee joint was assessed in an evaluation of the radiographic images for both sides according to the K&L scoring system (13), which is an internationally recognised standard radiographic grading system for OA as previously described in section 4.2.4. Key radiographic features such as the presence of osteophytes, bone sclerosis and other features in the knee x-ray images were taken into consideration when grading the participants. The original atlas of images published by Kellgren and Lawrence was used as a guide so as to ensure accurate scoring (13). Eventually, each joint was then given an overall score indicating the severity of OA in that specific joint.

The threshold used to determine the presence of radiographic OA in the joints was set at an overall K&L grade ≥2, which is similar to the generally accepted criteria in the literature as previously described in section 4.2.4.1.

As assessment of radiographic joint space width was used alongside the K&L scoring system for the knee joint. The measurements of minimum joint space width (mJSW) were scored to the nearest 0.1mm. This technique is used to measure the minimal distance between the two bones in the tibiofemoral joint, where the joint space width is determined as a composite surrogate for cartilage loss in the joint on both the femoral and tibial sides. This is a reliable method, according to studies mentioned in section 4.2.4.

The hip joint was assessed for the severity of OA in a different way than described above for the other joints. A modification of the internationally known K&L scoring system known as Croft's modification was used to grade the high-resolution iDXA images of the hip (Croft, Cooper (14). The Croft modification uses grades from 0 to 5, where 0 indicates no changes in osteoarthritis and 5 is categorised as end-stage OA. More details on this grading system and its reliability are discussed in section 4.2.4.1. The threshold used to determine the presence of radiographic OA in the hip was set at an overall Croft modification of K&L grade ≥2. Hip minimum joint space was also calculated to represent the minimum distance from the margin of the femoral head to the acetabulum using the same technique as described by Croft, Cooper (14).

Two independent trained researchers (Hussam Ahmed and Iain Goff) analysed and graded all of the radiographic images of the knee and hip joints. To ensure the reliability of radiographic assessment both inter-rater and intra-rater reliability were assessed for both individuals and all gradings used. The results showed that Kappa inter-rater reliability was moderate for radiographs of the knee, and moderate-to-strong for the hip images, and intra-rater agreements yielded similar results (366).

5.2 Data extraction

A protocol for the data extraction designed by the author explains the procedures followed to extract all relevant data needed for the research. Data was held in two separate databases: the secure database for the NTFS study; and the Royal Victoria Infirmary PACS system. Each database requires specific approval methods for data access that needed to be gained prior

to data collection. The next sections explain in detail the process of data extraction, describe the approval gained, and summarise the protocol used.

5.2.1 Data access approvals

5.2.1.1 NTFS data access agreement

The main source of data in this research is the NTFS cohort study. An agreement for access to this data was requested and approved. The research proposal was submitted to the NTFS management team stating the aim and objectives of the study and the type of data needed. After the completion of all of the procedures required, the data access agreement was signed by the NTFS management team and the author which allowed access to the data required to fulfil for the purpose of the research.

5.2.1.2 Collaboration agreement

The core MRI data used in this research is analysed using advanced machine learning technology. The technology allows the generation of 3D SSMs of anatomical areas and has an extensive evidence base. One of the leading companies that developed this technology is Imorphics Ltd, based in Manchester. Their previous work using this technology has been shown to be promising in several publications focusing on the knee joint which are reviewed in section 4.4. Therefore, a collaboration agreement was signed allowing for a collaboration to produce the SSM.

5.2.1.3 NHS research passport

To conduct this study, the author required access to radiographic and MRI medical imaging data. While the NTFS databases contained all of the other required data, these images were stored in the PACS system of the RVI where the latest cohort follow-up was undertaken. Previous analysis had been completed on DXA images which were already stored in the NTFS database and did not require re-extraction.

To gain access to the necessary medical imaging data, the author needed to obtain a 'research passport'. This process allows non-NHS staff to apply for access in order to conduct research activities within the NHS or using its data. The author completed and submitted a request to the NHS which briefly introduced the study and outlined the planned research activities. Approval of the request was delayed due to the COVID-19 outbreak as described in section 1.4 but was ultimately granted (Research Project No: 03748). Once the author had gained approval for the research passport, an NHS smart card was also obtained so that access could

be gained to NHS facilities. Additionally, an NHS IT account was set up to gain access to the relevant data.

5.2.2 Data extraction protocol and procedure

Before the extraction of data, a protocol was designed by the author to plan the work to be undertaken in order to provide assurance concerning the quality of all data extracted and to manage the data. The protocol has six sections as detailed below.

5.2.2.1 Extraction of initial NTFS information

In searching the PACS system for the MRI data required, the names, dates of birth, and NHS numbers of the 281 participants who underwent MRI scans during clinical assessment needed to be extracted from the NTFS database. The MRI images are the core data in this research, and so the data extraction process focused solely on those who had undergone MRI scanning. Once the initial information was extracted from the study database, the data were organised in a password-protected Excel sheet and stored on a password-protected external hard drive.

5.2.2.2 PACS training

In order to navigate the PACS system efficiently, the author attended two training sessions organised by the RVI PACS department. The first session involved learning how to use the INFINNIT PACS software and to navigate the system using an IT account. Knowledge was also gained on how to search for data using a participant's name, date of birth, and scanning dates. The second session covered the extraction of imaging data in DICOM format and operating the anonymisation feature to ensure participant privacy. The PACS manager, Keith Lennox, delivered the training sessions and authorised the author to extract the data required.

5.2.2.3 Organisation of the workload

Due to the large volume of data to be extracted, the protocol required the workload to be suitably organised. In order to ensure high-quality data extraction, data for only 10 participants were extracted per day. This approach minimised the risk of errors and allowed sufficient time to assess the quality of the MRI images for each participant.

5.2.2.4 Searching the PACS system

Specialized monitors are essential for accurate and consistent visualization of images from PACS. The EIZO RadiForce RX370 with a 3-megapixel resolution and DICOM compatibility was used to visualize and extract the images. This monitor undergoes a daily quality assurance test to ensure reliable and high-quality image interpretation. The built-in software, RadiCS,

automatically performs the test when the monitor is turned on. These tests include daily calibration, precision assessment, and evaluation of contrast and colour reproduction, all in accordance with the manufacturer's specifications.

To initiate the search process each day, the initial information for the 10 participants scheduled for data extraction that day was identified. The protocol required the PACS system to be searched using the participant's NHS number. The PACS system contains all previous imaging information for each participant, and the results were expected to contain procedures from various diagnostic imaging modalities. Therefore, the next step was to filter the results to include only those showing scans on a specific date. The scan date for each participant was available in the initial data extracted from the NTFS database.

Participants' names and dates of birth were also cross-checked to ensure that the information shown on the MRI image matched the information for each participant. This ensured the accuracy of the data extracted for each participant.

5.2.2.5 Image quality check

The quality of the images obtained needed to be checked during the extraction process, since they had not been reported or checked previously. Also, since the MRI device used in the NTFS is an extremity MRI scanner with a low field strength of 0.2T, which might affect the image resolution. The images were visualized and extracted in a dedicated workstation that provides a controlled viewing environment where the room lights are dimmed. This helps minimizes glare and reflections on the monitors, which could otherwise affect the assessment process. A checklist was developed to ensure the quality of the images which focused on the number of bones included in the scan, available views (axial, sagittal, and coronal), presence of image artefacts, and image resolution. Having identified each participant's image assessed its quality, its level of acceptability for inclusion was noted. All images were extracted, regardless of quality, in order to solicit additional input from the research team.

5.2.2.6 Anonymisation and storage of the data

Once each participant's MRI image had been identified and a quality assessment completed, and before transfer and storage of all of the images, they were 'de-identified' so as to protect the participants' personal information. The DICOM image anonymisation tool available in the PACS system automatically removes all information and labels from the header and image

pixel data. The use of this highly customisable tool allowed the author to rename the images using specific codes for each participant.

After anonymisation, the images were extracted as DICOM files and stored directly in a password-protected hard drive. When the steps described above had been completed for all 281 participants who underwent MRI scans during their clinical visits, all anonymised imaging data were transferred to the NTF study database.

5.3 MRI data included in the analysis

The aim of this study was to include all participants who had an ankle MRI scan taken during their clinical assessment visit. Inclusion criteria were systematically assessed and determined by the author and research team, based on the following criteria:

- Acceptable quality of ankle MRI images for the construction of 3D SSMs.
- Availability of clinical data (participants excluded if questionnaire data was missing).
- Availability of radiographic and DXA imaging for hip and knee assessment (participants excluded if images were not available).

The PRISMA chart in figure 5-1 shows the inclusion and exclusion of participants for whom ankle MRI images.

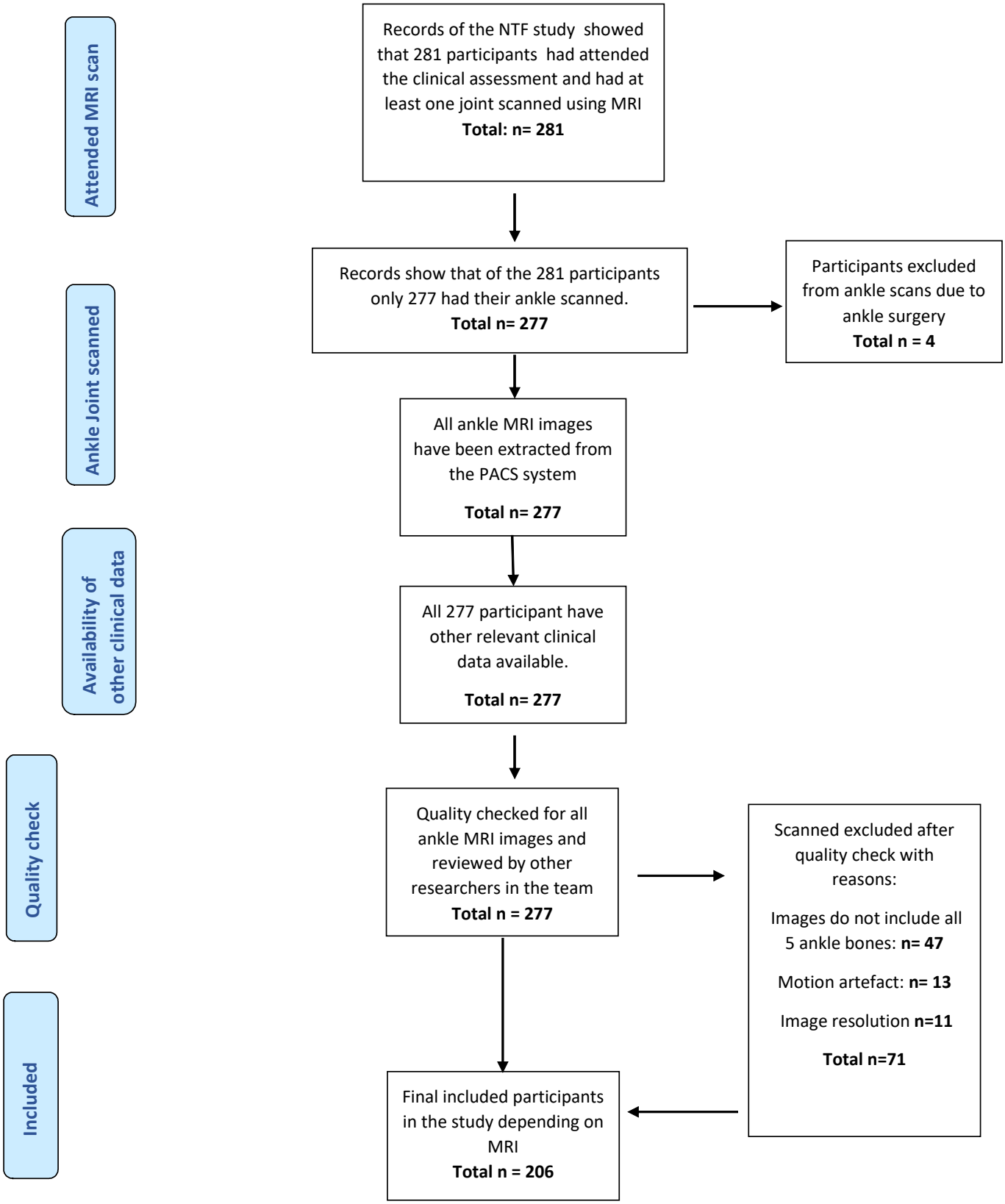

Figure 5-1. PRISMA chart showing the participants' ankle MRI scans which were included and excluded.

5.3.1 Extraction of clinically relevant data for the participants included

After the identification of the 206 participants, their relevant clinical, radiographic and DXA imaging data for the hip and knee joints were extracted. In this process, the NTFS database was searched using each participant's study number and cross-referencing with their name. Data for a total of 24 clinical variables for each participant were extracted and securely organised, coded, and saved on an electronic server. A summary of the variables involved is presented in table 5-1.

Table 5-1. Summary of the clinical variables considered in the research.

Variable name	**Variable name**
Gender	K&L score for left right, and dominant side knee
Height	Croft score for left right, and dominant side hip
Weight	BMD spine
BMI	BMD lower limbs
Dominance side	BMD right femur neck
WOMAC pain	BMD right femur total
WOMAC function	
WOMAC stiffness	
Left, right, and dominant side hip pain	
Left right, and dominant side knee pain	

5.4 Reconstruction of ankle SSM

Active appearance modelling (AAM) is a type of statistical shape modelling that incorporates both the shape of a structure and its appearance. AAM was introduced by (345) and has been widely used in the analysis of medical images. An AAM is developed using a supervised machine learning technique in which principal components analysis (PCA) is applied(367). The main aim is to use AAM to characterise and detect variation in shape by applying a set of examples that represent the variabilities of the shape and grey-scale texture (appearance) of any object, such as, in this case, the ankle joints from an MRI image.

Furthermore, AAM can be used to automatically segment a population of 3D images. However, to do that, the production of a trained AAM model is required which includes an example set from the population (367). This trains the model to learn the variations in shape and appearance of the object studied such as, in this study, MRI images of the ankle. The

trained model can then be used to automatically search and segment similar objects to the ones used in the trained model: for example, new ankle MRI images (367). A final SSM is then obtained that uses all of the MRI images included in the population and represents the anatomical object in the MRI scans in a 3D manner. In the present study, the final model was built using all 206 ankle MRI images. Such methods have been previously applied and published by the collaborating team on the knee joint (368). The steps applied in building the 3D SSM are described in detail in the following sections.

5.4.1 Trained 3D ankle AAM

The first step to produce the ankle AAM is to train the model to detect variability in the shape and appearance of the ankle joint in the population. The final trained model is built in three main steps (355): manual segmentation, production of the correspondence of points on bone surfaces; and the application of PCA. In the present study, these steps were applied by the research team and a detailed description of the methods used is given next, ending with a flowchart summarising the model-building process.

5.4.1.1 Manual segmentation

In order to obtain the morphological shape of an anatomical organ in a medical image such as an MRI image, the organ must be segmented to distinguish it from its surroundings. This process of segmentation is required to reconstruct the 3D SSM of the bones in the joint (369). In this research, manual segmentation was used to segment ankle MRIs from a training set of 30 randomly selected non-duplicated scans from the 206 ankle images available. Endpoint 1.20 software developed by IMorphics, Manchester, was used to perform the segmentation process. The distal tibia, fibula, calcaneus, talus, and navicular bones were segmented slice by slice using manual line drawing in the form of a stack of 2D contour lines and Live Wire software, which is a widely employed method (367). The images were segmented in the sagittal plane, although images were also available in the coronal and transverse planes. Figure 5-2 below shows a screen shot representing the manual segmentation process.

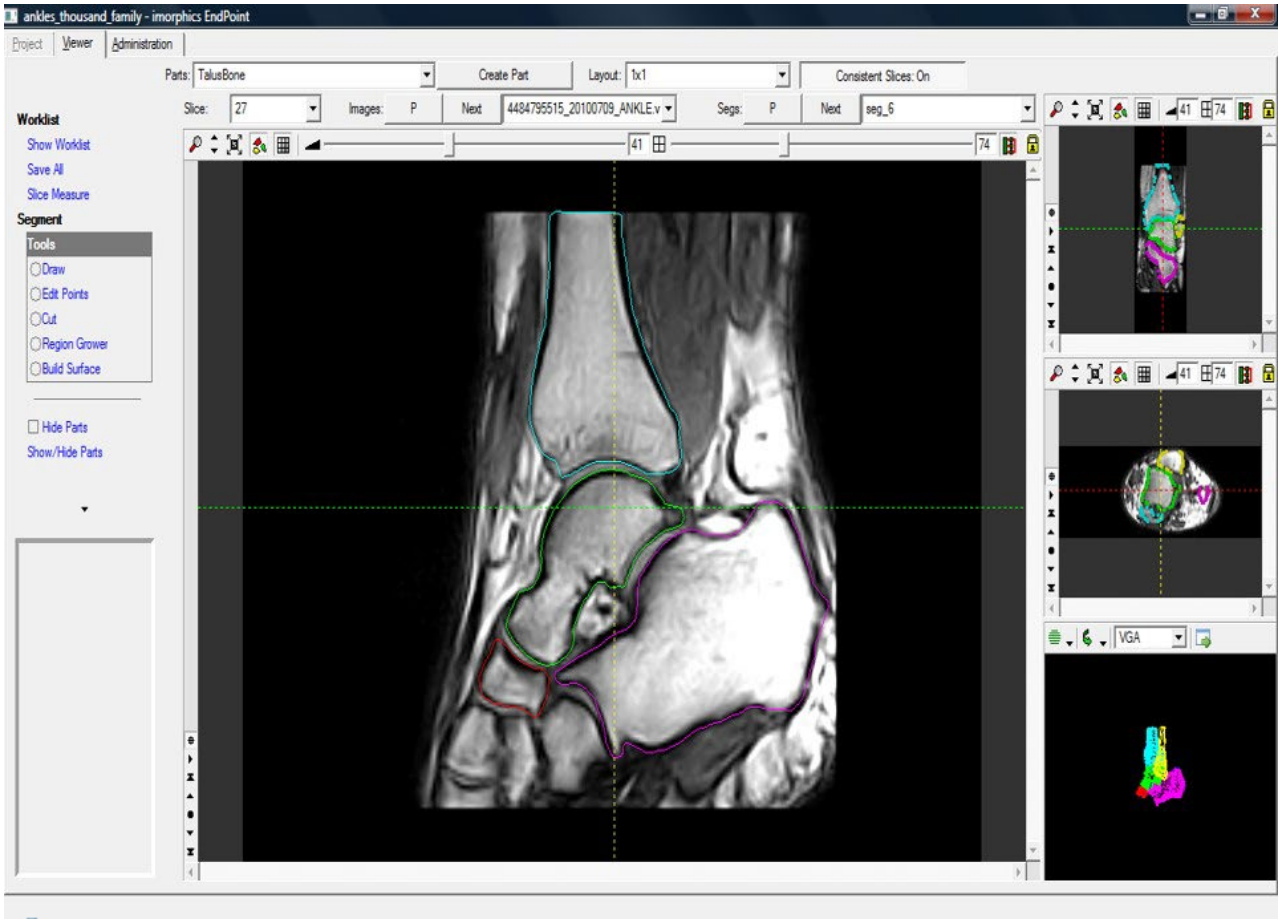

Figure 5-2. Screen shot of the program used for MRI manual segmentation. The figure shows an ankle MRI image and illustrates the software used for manual segmentation employing manual line drawing and the Live Wire method.

The aim of this part was to segment only the bones of the ankle and to exclude soft tissue. The segmentation process was carried out by a single trained researcher (rheumatologist 'KC') who underwent extensive training conducted by an expert in segmentation. Both the author and 'MB', a collaborating expert in segmentation and machine learning, reviewed the segmentation results so as to ensure accuracy. The research team comprised experts with diverse backgrounds, including a rheumatologist, a senior radiographer, and a machine learning expert, which facilitated effective manual segmentation by consensus. The team reviewed any challenging or incomplete images. The manual segmentation was checked by two different experts to ensure the identification of errors as shown in Figure 5-3.

If any of the reviewers noticed a mistake, it was discussed with the team and amendments were made upon agreement. Finally, the manual segmentation of all 30 scans was completed and reviewed by the team and the best quality was agreed upon.

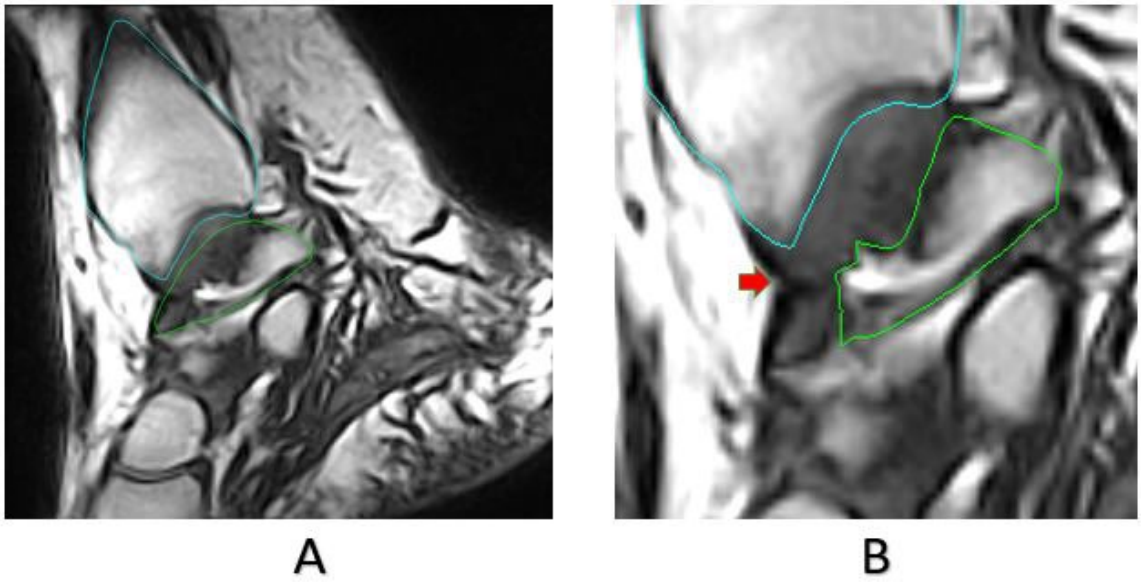

Figure 5-3. Example of the checking of manual segmentation for errors: A) segmentation completed by the trained researcher, which shows a mistake in the identification of the correct boundaries of the bone; B) the correct boundary of the bone in the same slice amended after the agreement of the research team. The red arrow shows the black line that misled the researcher into thinking that it was the bone boundary.

5.4.1.2 Registration of bone surfaces

The manual segmentation of the training set was used to extract the stack of 2D contour lines used in the segmentation. These were then converted into a 3D bone surface using the marching cubes algorithm, which is a well-known technique used in medical visualisation (370). It aims to extract the triangulated surface mesh (a type of polygonal mesh) bounding a 3D solid object (the bone surfaces) showing a discrete representation of the geometric information acquired from the segmentation process. Once the triangulated bone surface mesh shown in figure 5-4 below had been acquired, the marching cubes algorithm then automatically covered the mesh with random points (vertex) which then represent contours as surfaces with signed distance 3D images for each participant in the training set. The quality of the signed distance 3D images is then assessed using geometrical smoothing which aims to reposition the random points so as to improve the overall quality of the 3D images in representing the shape of the ankle joint complex of each participant in the training set.

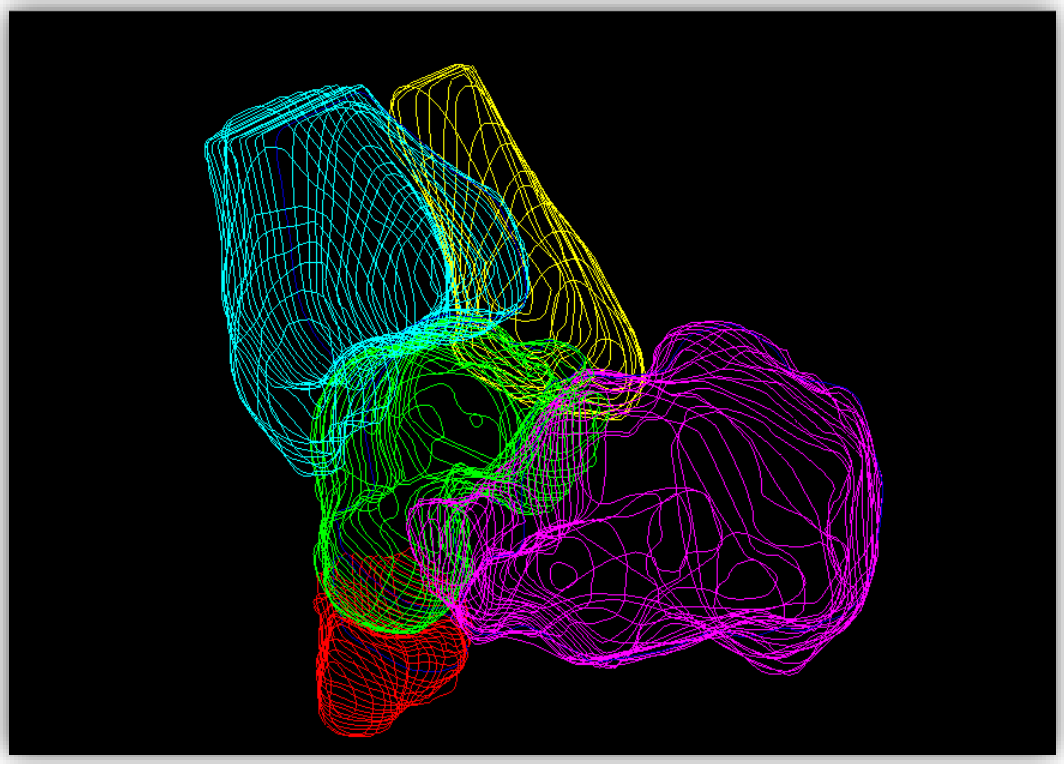

Figure 5-4. An ankle complex triangulated surface mesh bounding a 3D bone surface of all five bones: navicular (in red); distal tibia (blue); talus (green); yellow, distal fibula (yellow); and calcaneus (purple).

To create a shape model, a correspondence between the points of the bone surface mesh obtained from each participant in the data set should be established. Additionally, to work as a correspondence guide, consistency is required for each bone of each participant included in the training set. To establish such a correspondence system, the registration of all included images is needed (371).

Image registration is a crucial step in the construction of an SSM, and is a widely used technique in medical imaging data processing which aims to align two or more images for joint processing or model building (371). The registration process involves aligning multiple images to create a mean image and a mean 3D triangular mesh. Numerous methods of image registration are used in medical imaging, which vary depending on the type of images involved and the purpose of registration (372). In this study, a variant of the Minimum Description Length Approach to Groupwise Image Registration (MDL-GIR) algorithm (373) was used to register all images in the group simultaneously utilising information about their shapes. Once registration is completed, correspondence landmarks are generated for each participant as elements in a high-dimensional space which incorporate 36,838 landmarks representing the

shape of the ankle complex region. The landmarks are projected onto the 3D bone surface for each participant, as seen in figure 5-5 below. They are also represented as a cloud of points in a shape space, such as a shape matrix that contains all participants in the training set. The outcome of this process is a shape model that describes the geometric form of the ankle complex, and its orientation, scale, and position in 3D space, and a similar method has been used for models of the knee (53, 367, 368). The registration process was completed automatically using specialised software provided by our collaborators and under the supervision of MB.

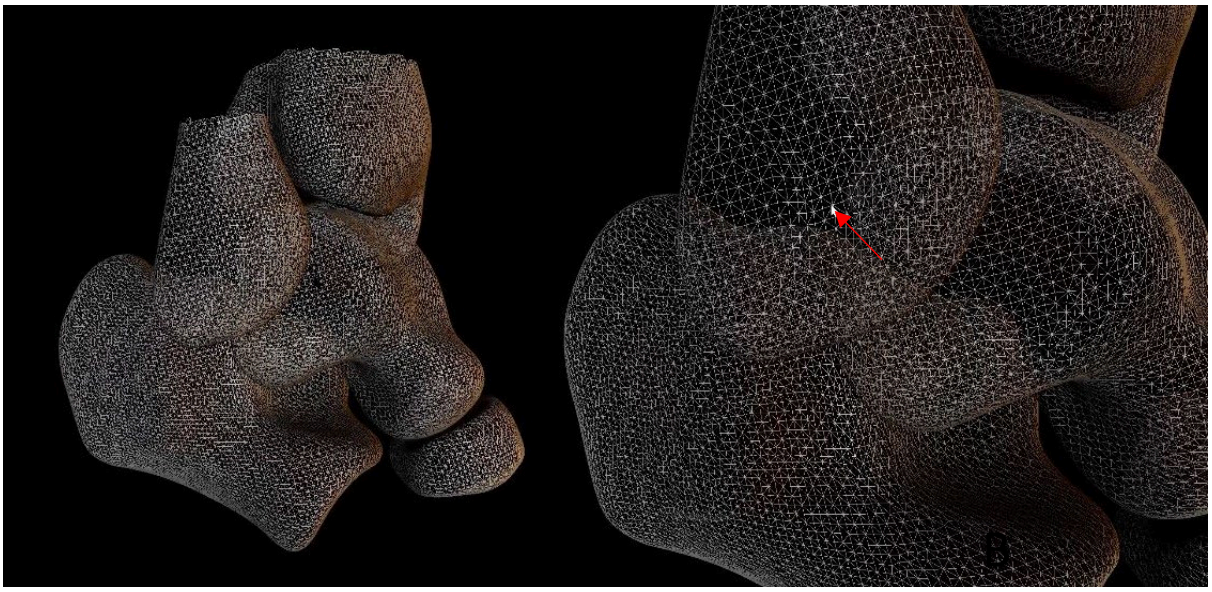

Figure 5-5. Anatomical correspondences landmarks (points) covering the 3D surface of the ankle complex model: A) full ankle complex model covered with sets of landmarks; B) zoomed image which clearly shows the correspondence landmarks. The red arrow points to an example of a landmark, and such landmarks after the completion of registration have the same ID in each participant.

5.4.1.3 Principal components analysis (PCA)

The outcome of the registration of the trained model and lining up of all landmarks is an immense and complex data set. PCA, which is an extensively used dimensionality reduction technique, is applied in order to analyse such landmarks, and capture the geometric variability that they represent. It was initially introduced by Pearson (374) and later adapted and named by Hotelling (375). PCA aims to decrease the size of a multidimensional data set to one of lower dimensions that retains much of the original information and to present it in terms of modes of variance that can be easily visualised and analysed. More information on this

method and its application and the mathematical algorithms used can be found elsewhere (376).

PCA is a technique used to analyse the variability in data by identifying patterns and trends and was applied to the shape matrix that contains a coordinate vector for each example resulting from the image registration process. In this case, it was used to analyse the shape of the ankle complex across all examples in the dataset. The analysis yielded two important results: the shape of the mean ankle complex, representing its average shape across all examples in the dataset; and a covariance matrix which represents the linear relationships among all coordinates and can be used to identify the most important directions of variability in the data.

Eigenvectors and eigenvalues are then calculated from the covariance matrix. The eigenvectors define the principal component modes of variation, and eigenvalues signify the percentage of variance that can be explained by each eigenvector. The goal of the process is to reduce the dimensions of the shape space while retaining as much of the original variation as possible. PCA aims to retain the leading PC modes that describe 95% of the variance and discard other modes. This results in a new space with reduced dimensions that explains 95% of the variance in the data. The shape model using the results of PCA in this study includes the mean shape of the ankle complex bones and 59 PC modes of variation. Any new ankle shape can be predicted using a specific formula that includes the information gained from the PCA. This information was then used in the automatic segmentation of the remaining participants. The process was completed automatically using specialized software in an attempt to find the best possible direction that allows the first PC to pass through the maximum number of points.

5.4.2 Automatic segmentation

The manual segmentation of a large set of ankle MRIs is not practicable for several reasons, which include the laborious and time-consuming nature of the process, its dependence on observers, and the inability to accurately capture the variation in shape of the object being studied. Additionally, manual acquisition of corresponding anatomical landmarks on a large number of 3D objects would be impossible because several thousand landmarks would need to be distributed manually on each 3D object is necessary and this process which would need repeated for all of the participants so as to ensure anatomical correspondence. Such a method

might be potentially feasible with 2D images since the number of landmarks required is far fewer than those needed to cover a 3D object.

One major advantage of using AAMs is that they allow for the acquisition of a mean appearance and shape of the ankle complex bones, along with learned mathematical information that provides a mathematical description of the variability of each training sample(369). This mathematical information enables the model to apply a unique search and match algorithm that aims to interpolate the mathematical information learned from the training sample to a new set of MRI images of the same object. As a result, instances of shape and appearance can be found which permits automatic segmentation and the application of the same set of corresponding landmarks to the new segmented images. This depends on the patterns of variability in shape and appearance learned from the training set and uses mathematical information about shape and appearance from the training model (367).

For the models in this study, the automatic segmentation of the ankle MRIs of the remaining participants in the population studied was initiated using mathematical information about the learned shape and appearance in the form of principal components of shape and appearance derived by the trained model. Automatic segmentation was completed using a specific algorithm developed by collaborators in this research (details of which cannot be provided here due to a non-disclosure agreement) that focuses on searching and matching the resultant principal components of shape and appearance from the trained model to the new ankle MRI images, as shown in figure 5-6 below. The process is then concluded by obtaining a mean shape and PC modes of variation for each of the 206 ankle MRI images. This culminates in the construction of the full ankle complex model represented by PC modes and anatomical correspondence landmarks.

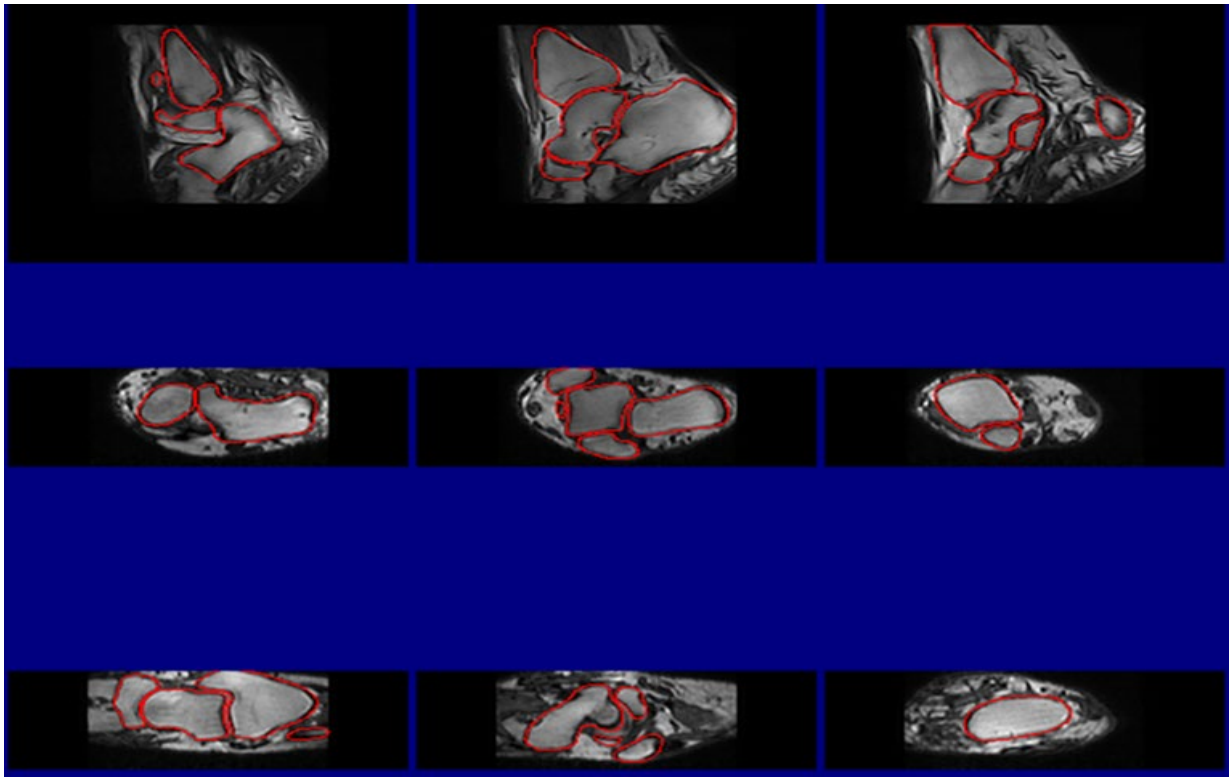

Figure 5-6. Screenshots of the front page of the software used for automatic segmentation showing the search process conducted by the algorithm that results in the simultaneous segmentation of a new set of ankle MRI images using sagittal, coronal, and axial planes.

The accuracy of the automatic segmentation method used had previously been assessed by the collaborators, and the results showed that it was able to automatically segment new knee MRI images with point-to-surface accuracy of < 1 mm (377). This algorithm has been previously applied to images of knee joints as described in publications by the research collaborators (50, 52, 53, 367, 368).

Furthermore, a final review of all automatic segmentations for the ankle model was completed so as to ensure model accuracy. All of the 206 images used in this study were carefully visually reviewed for errors resulting from automated segmentation. The revision process was conducted by the same members of the research team who reviewed the initial manual segmentation. If a segmentation error was noticed, the reviewers together with the expert checked if the error could be fixed by manual segmentation. During the review process, minor errors were noted in 11 scans, and the research team decided that manual segmentation could improve those errors. Therefore, manual segmentation techniques were used to complete the necessary amendments to the results of the automatic process.

5.4.3 Summary and final models

The model-building procedure is summarised in figure 5-7 below, which shows that the outcome is a 3D ankle complex SSM that contains all five bones of the ankle complex joint for both males and females and all 206 participants in this study. All PC modes for each participant were obtained and stored electronically.

In the analysis of bone shape, other models that focus on a particular set of bones were generated using the same method. For example, models were generated that contain only the tibia-talus-navicular bones or the calcaneus bone alone. Finally, separate models for males and females were also obtained and used in exploring the association between bone shape and the state of OA in the knee and hip.

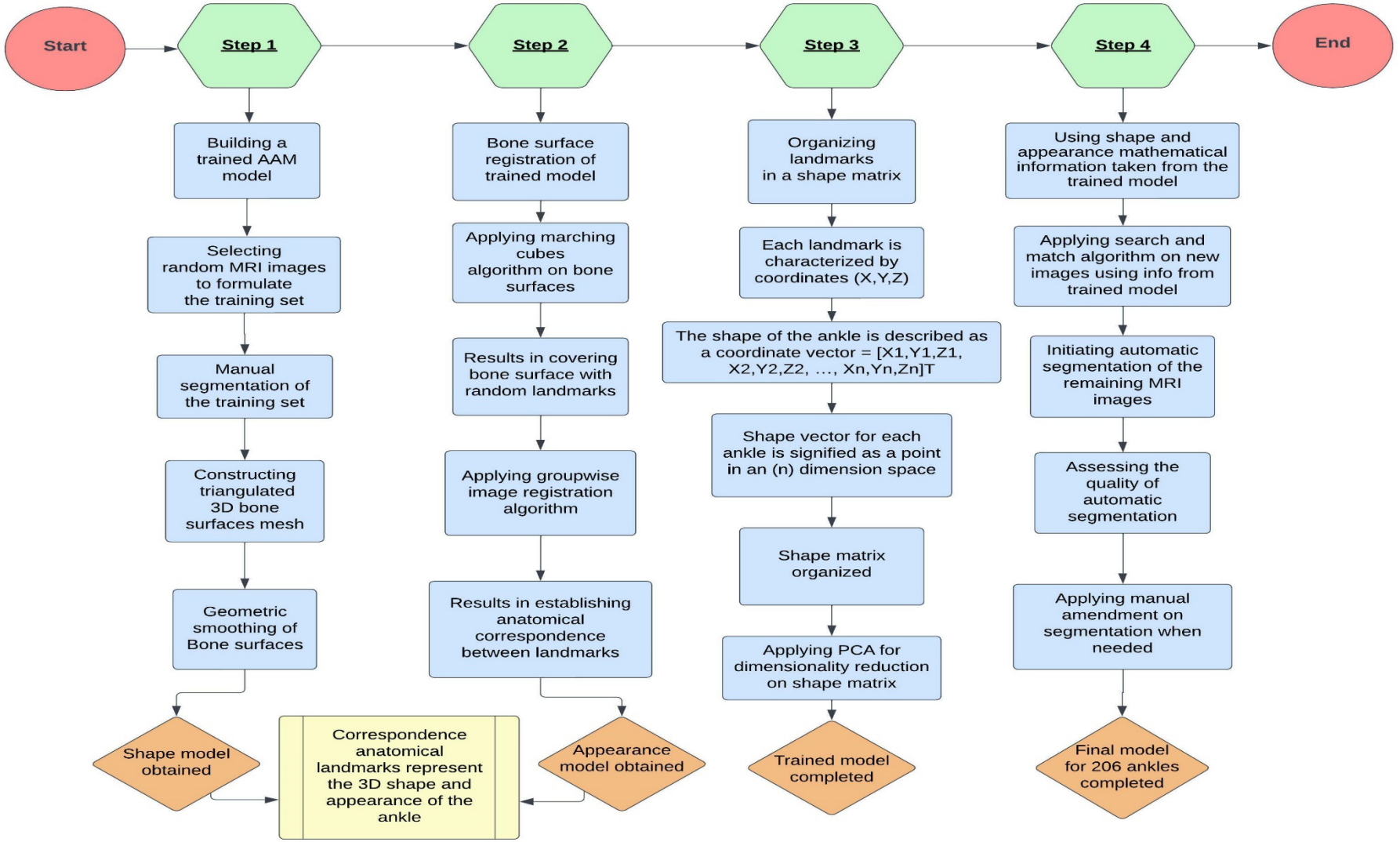

Figure 5-7. Flowchart summarising the model building process divided into four main steps.

5.5 Measurements obtained from the model

One of the significant advantages of using SSM in analysing MRI population data is that the model has the capability to measure any part of the object that the researcher is interested in, from all participants at the same time. The resulting bone surface is a triangulation in which the vertices are a dense set of anatomically corresponding landmarks, as each bone is fitted with the same points. Additionally, masks created on these points can be used to take measurements consistently across the population.

By selecting the landmarks representing the anatomical area of interest on the main shape, measurements of that area for all other participants included in the model can be produced. The resulting measurements for the area of interest can be assumed to represent the same area for all participants. Thanks to the correspondence, anatomical landmarks are established in the model building process, as explained previously in section 5.4.1.2.

In this thesis, several anatomical areas were measured with the aim to assess variation in the morphology of the ankle complex in the population studied. The methodology relating to the measurements conducted is detailed next.

5.5.1 Measurement of ankle joint space width

The ankle is a complex anatomical region of the body which contains several articulations, as discussed in chapter 3. One aim of this study, as stated in section 1.2, is to use the 3D SSM to quantify JSW in the joints formed by the five bones in the ankle complex region. These joints were selected after a review of the anatomy of the ankle as described in section 3.2.2, namely the tibial plafond (tibia-talus JSW), medial malleolus (medial side of the tibia-talus JSW), talonavicular (talus-navicular JSW), talofibular (lateral malleolus distal part of the fibula-talus JSW), subtalar posterior facet (posterior part of the calcaneus-talus JSW) and subtalar medial facet (medial part of the calcaneus-talus JSW).

To conduct the quantification, the anatomical areas representing JSW between the bones included were chosen and then discussed with the research team and agreed upon. A set of landmarks covering the bone surface area of the JSW on one bone that formed the articulation was selected. Using a specific code, the model was instructed to automatically produce a perpendicular line for each landmark that extends to the opposite bone surface in the joint, as shown in figure 5-8.

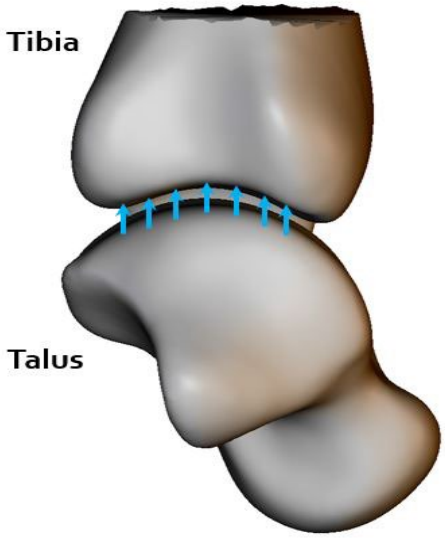

Figure 5-8. Lateral view of the tibial plafond joint where measures are taken from multiple points across the joint using a correspondence point, where the points then produce a perpendicular line that extends to the upset bone surface (tibia).

Figures of average JSW across the joints were produced with a heat map showing the measurement in millimetres from each correspondence point in the selected bone area of the model. These figures were then reviewed using this heat map to extract only the average values of JSW across each joint. Appropriate masks were created on each bone so that only the selected average bone area was included. Figure 5-9 illustrates this process for the bone surface of the talus dome, where the left-hand box shows the initially chosen bone area covering the anatomical area that forms the JSW of the tibial plafond joint. A mask was then chosen that only includes the average measurement, as seen in the middle box. The figure in the right-hand box shows the final chosen mask.

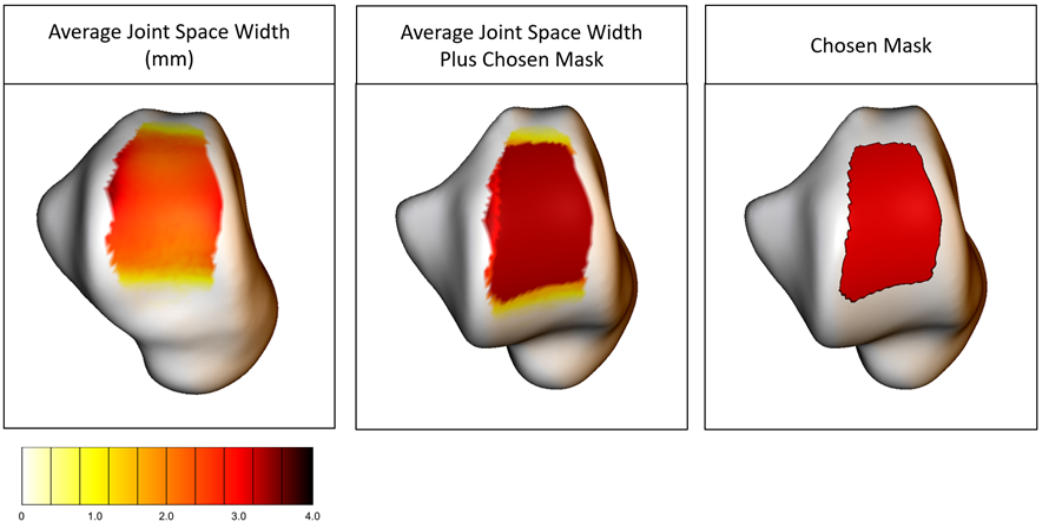

Figure 5-9. Use of the average 3D JSW map to choose an appropriate mask for measurements to be taken.

The final masks were selected in order to reproduce the JSW measurements representing the average coverage area of the six joints, using the same method to generate a perpendicular line from each landmark in the final chosen masks. To clarify this process further, the first images in figure 5-10 displays all of the correspondence points on the talus and the second shows the position of the mask which is bounded by correspondence points.

Finally, mean, median, and various percentiles for each participant were calculated and recorded to assess minima and maxima.

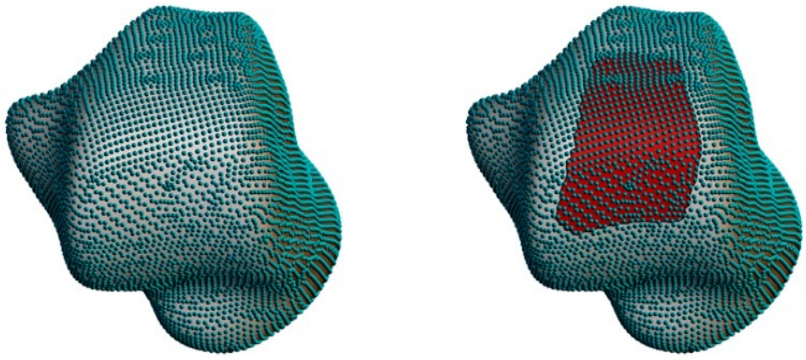

Figure 5-10. 3D model of the talus bone covered with anatomical correspondence points: on the left is the model without the mask chosen to take the JSW measurements; and on the right image the location of the chosen mask is shown by the red area covered with the anatomical correspondence points.

5.5.2 Measurements of bone area

An advantage of SSM is that it can provide accurate measurements of bone morphology from all participants simultaneously and from the same location. Several of the studies reviewed in section 4.3.2 used SSM of the knee joint in aiming to quantify the subchondral bone area and assess its morphological association with OA. Such studies have concluded that variations between participants in the knee joint bone area provide a prognostic biomarker for knee OA (53, 378).

The present study aimed to assess the morphological variations in the ankle complex region among the studied population, as stated in section 1.2, and ankle bone area is one such variation. However, only bone area measurements from the talus and calcaneus bones were quantified in this study since they are the largest bones in the ankle complex and have a significant impact on ankle biomechanics, as stated in section 3.2.1 (379). Also, these bones showed greater variation in shape compared to others when visualised in the model. This research focussed on the total area of the subchondral bone, which has been designated as tAB by a nomenclature committee which has established a commonly accepted terminology for reporting musculoskeletal MRI morphological variations as explained in section 4.3.2.1.

For the talus bone, tAB measurements from three anatomical parts were quantified which represent the articulation surface of the bone, as reviewed in section 3.2.1.2. These are the articular surface of the tibia (talar dome), the articular surface of the posterior facet of the calcaneus, and the bone area of the taler head (articular surface of the navicular), as presented in figure 5-11.

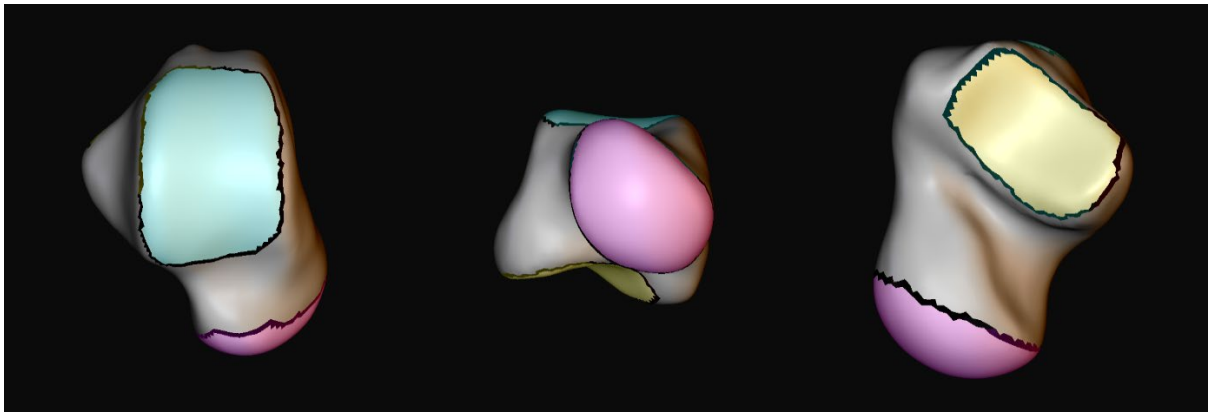

Figure 5-11. Subchondral bone area of the three joints of the talus selected for bone area measurements. The left image shows the area of the taler dome coloured in light blue, the middle image shows the area of the taler head in pink, and the right image shows the area of the posterior facet in gold.

Measurements of talus height, width and length show significant variations between individuals, as noted in the studies reviewed in section 3.3. Therefore, these features were quantified for all participants from the SSM. However, the quantification of measurements for a bone that is known to have such an irregular shape, which can be represented as approximately cuboid as described in section 3.2.1.2, is rather complicated. It was accomplished in this study by drawing a bounding box on the mean shape of the talus bone in the SSM. The box includes the entire talus bone within it, as seen in figure 5-12.

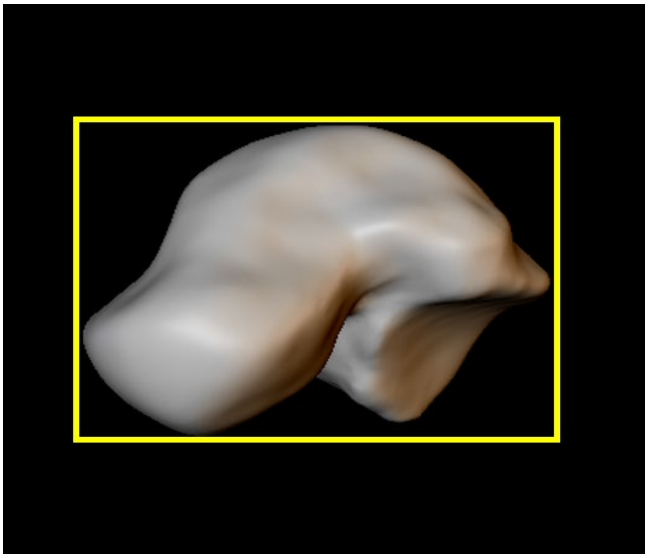

Figure 5-12. 3D representation of the 3D bounding box applied on the mean shape of the talus bone from the SSM.

In this way, a coordinate system was established that defines the X, Y, and Z axes within the bounding box as presented in figure 5-13 below, with the following definitions of the axes:

- X-axis: represents the width of the talus and passes from the middle of the articular surface of the medial malleolus to the middle of the lateral process on the opposite side.
- Y-axis: represents the height of the talus and is perpendicular to the X-axis. It passes from the inferior part of the talus through the centre of the talus dome.
- Z-axis: represents the length of the talus and is perpendicular to both the X and Y axes. It passes from the posterior process to the centre of the talus head.

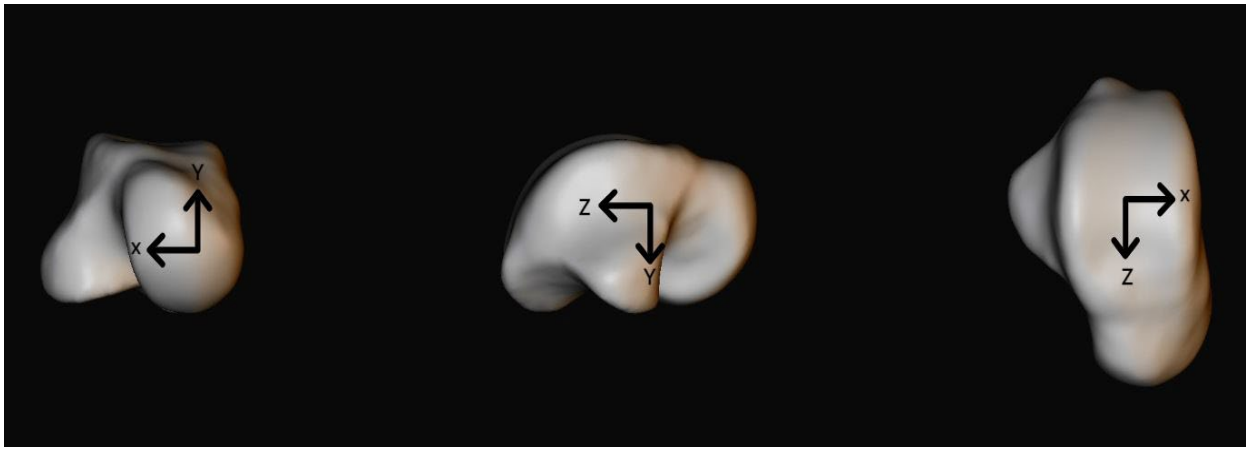

Figure 5-13. Location of the X, Y, and Z axes used to quantify talus height, width and length within the bounding box from the mean talus shape reconstructed using the SSM.

Only three measurements were quantified for the calcaneus bone, which are the bone area and width of the posterior tuberosity and the overall anterior-posterior length of the bone. A coordinate system similar that for the talus bone that defines the X, Y, and Z axis was established for the calcaneus. The axes shown in figure 5-14 below are defined as follows:

- X-axis: represents the length of the calcaneus and passes from the middle of the anterior articular surface of the cuboid to the middle of the posterior tuberosity.
- Y-axis: represents the height of the calcaneus and is perpendicular to the X-axis. It passes from the inferior part through the centre of the calcaneus body.
- Z-axis: represents the width of the talus and passes from the medial surface through the body and out from the lateral surface of the calcaneus bone.

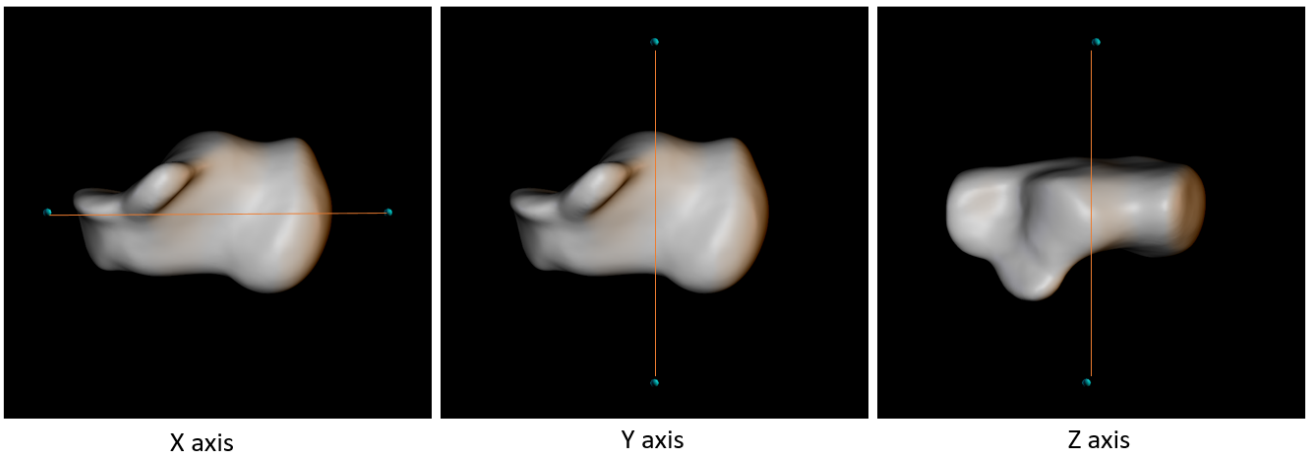

Figure 5-14. Location of the axes used as a coordinate system for the calcaneus bone represented on the mean calcaneus bone shape reconstructed using the SSM.

The bone area of the posterior tuberosity was also quantified using similar methods as mentioned previously for the bone area of the talus. The mean calcaneus bone shape was used to outline the correspondence landmarks of the area of the calcaneus tuberosity, as seen in figure 5-15, while the width of this area was quantified using the Z axis.

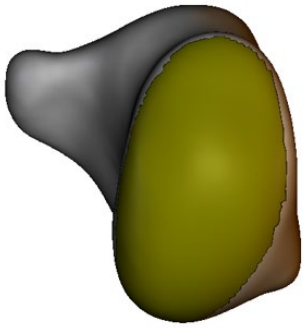

Figure 5-15. Mask chosen to quantify the area and width of the posterior tuberosity from the correspondence points on the mean calcaneus bone shape reconstructed from the SSM.

The two collaborating researchers ME and MB reviewed the anatomical location selected for the tAB measurements and for the coordinate definitions separately using a guided anatomical book, and then discussed and agreed upon the best to use. The tAB regions were outlined using landmarks on the mean bone shape in the SSM, which has established correspondence landmarks. Also, the coordinate axes were fitted using specific landmarks on the mean talus and calcaneus bone shapes. This enabled the quantification of all measurements from the same location for all participants. Using a specific code, the model was instructed to automatically produce and store the measurements for each participant using their study number, in mm^2 for tAb and in mm for the length, width and height of bones.

5.5.3 Assessment of variation in bone shape

During the building of the SSM, the mean shape and the variance modes for the ankle complex were extracted and saved. Two methods were used to assess variations in bone shape. The first evaluates all variance (PC) modes together, while the second assesses the top-ranking ten PC modes that together explain the majority of variation in the model. Both methods are explained in detail next.

The first method focuses on the combination of all PC modes of variation into one shape vector, the population bone shape vector. The shape vector for each bone is calculated by taking the principal components of the mean shape of, for example, the male and female groups and the OA and non-OA groups and drawing a straight line through them. Individual bone shapes from ankles in this study represented as principal components following the AAM search were projected orthogonally onto the new vector. The distance along the vector was normalised by treating the mean non-OA shape as -1 and the mean OA shape as +1. The same normalisation was applied to the male and female groups. Such method was used by the collaborators on research focusing on the knee joint (378)

This method is then presented on a histogram to show the distributional variation in bone shape between the groups on the new population bone shape vector. Also, in a further exploration of the distributional differences between, for example, the sexes, independent t-tests were applied to compare the difference in the mean of the population bone shape vector between males and females. This method has been previously used on the knee joint and published by the research collaborators (378, 380). The advantage of this method is that it uses all PC modes of variation in the model and does not neglect modes representing small variations. However, it lacks the ability to specifically visualise and report actual shape variations between groups and cannot create 3D images.

The second method involves taking into account the main PC modes of variation in the 3D model that explain approximately 80% of the total variation, where for some models the first 10 PC modes and for others the first 5 PC modes are included. Custom software for this purpose was provided by the collaborators. Prior to that, t-tests were applied to the values for each PC mode so as to explore differences between groups. The PC modes for which significant differences were found were then visualised and assessed using the software, which allowed the research team to interactively visualize bone shape variations in an animated 3D model for each of those modes. The author and two other team members documented their own observations for each bone in the model, and their descriptions were compared to achieve consensus on the bone shape variations for each mode. Images that illustrated bone shape variation were extracted from the model for PC modes that showed significant differences between groups, such as male and female or OA and non-OA,

accompanied by a description of the variation observed. Three images for each mode of variation were extracted: the mean image and images for both ± 2SD.

This method allows the individual PC modes to be explored and provides images to illustrate differences between groups. However, it only considers the top-ranking 10 modes of variation which explain approximately 80% of the variation in the model, and other modes that account for small percentages of variation are disregarded. Therefore, both methods were used in this study so as to optimise and internally validate the approach.

5.6 Statistical analysis

Data analysis was performed using STATA 16.0 statistical software. Categorical data were reported as frequencies and totals using bar charts. Numerical variables were expressed using mean and SD or median and interquartile range (IQR) according to their distribution. Normality of distribution for all continuous variables was assessed graphically using histograms, numerically from values of skewness and kurtosis, and statistically using the Shapiro-Wilk test.

In this analysis, student's t- and Mann-Whitney U tests were chosen as appropriate for the examination of differences in the categorical characteristics of gender, ankle pain, and radiographic diagnosis of OA, with morphological variables extracted from the 3D SSM such as the bone shape variables represented by the value of the PC mode for each participant and JSW, with bone area measurements represented as distance in mm^2.

Linear regression models were also applied in the bone shape analysis to explore the association between bone shape represented by the value of PC mode and body anthropometry. The analyses were then repeated to adjust for potential confounding variables such as the participant's sex.

The JSW analysis considered the association between ankle JSWs as the dependent variable and several independent clinical variables including gender, body anthropometry, BMD values, and knee and hip JSW measurements. A multi-step approach was used to achieve this. Firstly, simple linear regression was applied to establish any significant relationships between the variables. This provided a baseline for comparison in the analysis of the effects of other variables on the dependent variable. Subsequently, multiple linear regression was applied to control for potential confounding factors and to evaluate the association between the

dependent and independent variables while accounting for the impact of other variables. Possible confounders were identified in a review of the relevant literature. Then, a graphical representation known as a DAG (Directed Acyclic Graph) was employed to model the relationships between the variables. A DAG can assist in demonstrating how one variable may affect both the exposure and the desired outcome when confounding variables are present (381).

In addition, regression analysis was employed to test for interactions between variables in order to examine whether or not the relationships between dependent and independent variables were influenced by the levels of other factors. This stage was vital for the identification of any potential effect modifiers in the associations between variables. Finally, the data was stratified by gender, and the analyses were repeated in order to investigate any potential sex-specific effects of the independent variable on the dependent variable.

All examined associations with ankle JSWs as the dependent variable were subject to this procedure, and a further backward regression step was added for the BMD measurements. This required the inclusion of each association with a significance threshold of p=0.15 in the model and using the p-value for each variable to determine which variables were not significantly associated with the dependent variable. These variables were then removed from the model one at a time until all remaining variables in the model were significant. Finally, 95% confidence intervals were calculated in all cases, and a p-value of 0.05 or lower was considered to be statistically significant.

It is important to note that, in reporting the p-values in the results section, no adjustments for multiple testing were applied. Multiple testing is a known problem in many epidemiological and biomedical studies because it increases the odds of false-positive results and biased conclusions being drawn (382). One way to deal with this issue is to employ the Bonferroni procedure which is applied by dividing the number of hypotheses tested on the predefined threshold of the p-value, resulting in the setting of a new adjusted p-value threshold (383). This threshold can be used to decide whether or not to reject the null hypothesis, resulting in a lower risk of reporting false-positive results (384). However, such multiple testing and use of adjustment methods is a controversial topic in the literature. Some question the efficiency of such methods owing to the fact that, when it is applied, it aims to limit type 1 errors. However, it also increases type 2 errors. Likewise, many debates, has focussed on when to use

such a method and when to avoid it, depending on the research area concerned and the type of data involved (385-388). Therefore, in this study the results of the statistical tests were reported without adjustment.

Chapter 6 Results for bone shape

in this chapter, descriptive statistics which summarises the dataset used is presented using table and figures. Then the results from both the bone shape analyses and the bone area measurements are presented in a clear and concise manner also using figures and tables.

6.1 Descriptive Statistics

In the analysis of data, 206 participants met the inclusion criteria and were 62 years old at the time of data collection. Of these, 123 (59.7%) were female and 83 (40.3%) male. The frequencies of hip, knee, and ankle pain and hip and knee OA are presented in figure 6-1.

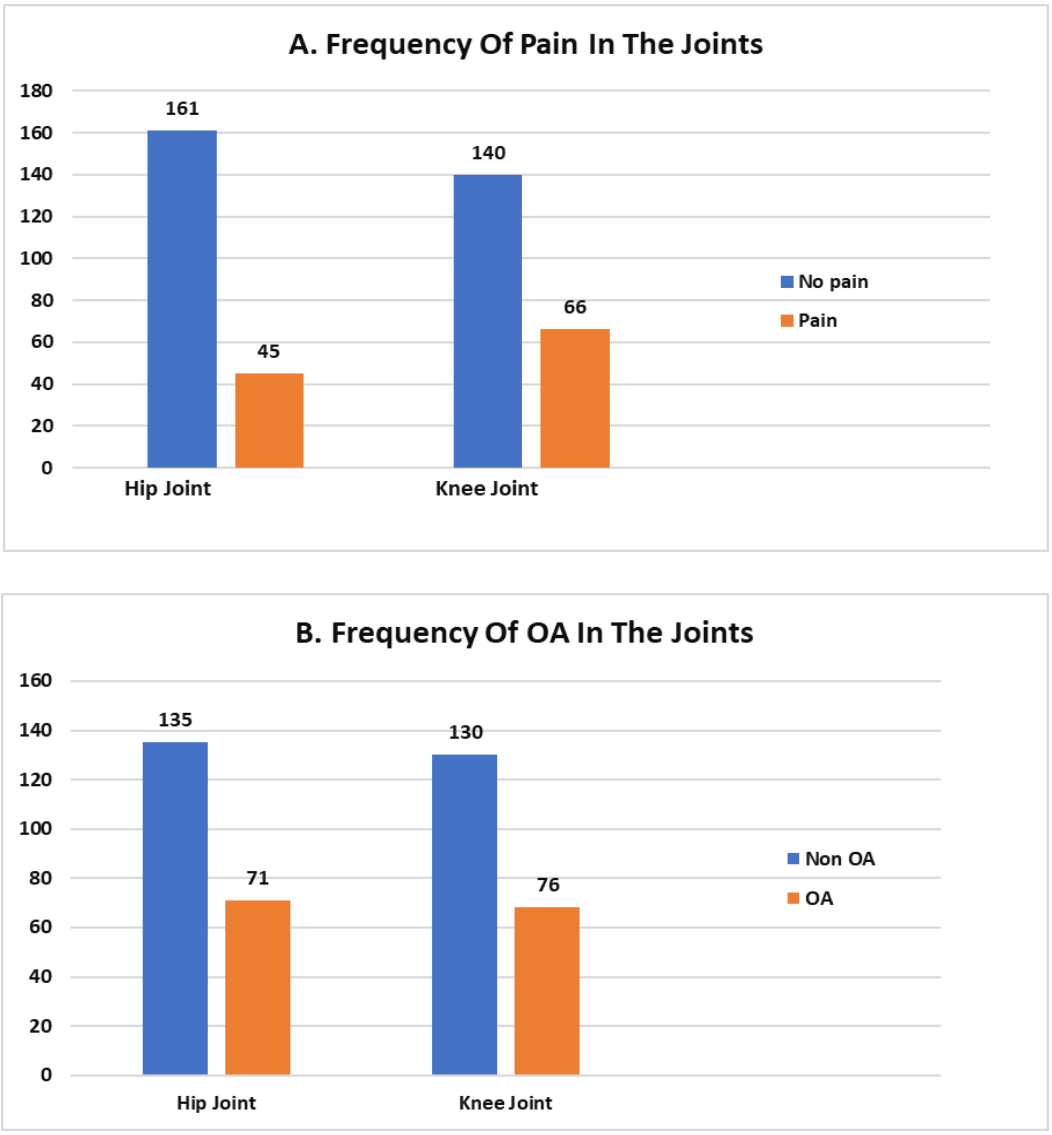

Figure 6-1. Frequency of pain (A) and OA (B) in the studied cohort, as reported in the dominant foot and ipsilateral hip and knee joints.

The frequencies of the categorical clinical variables are illustrated in Table 6-1, including sex, dominant foot, hip and knee pain, and knee OA incidence according to K&L radiographic grade where knee OA = (K&L grade ≥ grade 2) and hip OA incidence according to Croft grade for the hip where hip OA = (K&L grade ≥ grade 2). The central tendencies and dispersion of data for the continuous variables are summarised in Table 6-2.

Table 6-1. Frequencies of the categorical clinical variables.

Sex	**N=206**	**%**
Male	83	40.3
Female	123	59.7
Dominant foot	**N=206**	**%**
Right	186	90.3
Left	20	9.7
Hip pain	**N=206**	**%**
No	161	78
Yes	45	22
Knee pain	N=206	%
No	140	68
Yes	66	32
Knee OA	**N=206**	**%**
Yes	76	36.8
No	130	63.2
Hip OA	**N=206**	**%**
Yes	71	34.5
No	135	65.5

Note: Dominant foot as determined by MRI scan; ankle pain data obtained from questionnaire responses.

Table 6-2. Summary of descriptive statistics for all continuous variables included in the analysis.

Variable	Mean	SD	Min.	Max.
Height (cm)	166.3	8.2	145	187
Weight (kg)	77.4	14.9	49.4	130.4
BMI (kg/m^2)	27.9	4.9	18.4	47.6
Pain score (0-50)	8.6	11.9	0	50
Stiffness score (0-20)	3.4	4.8	0	20
Physical activity score (0-170)	24.3	36.2	0	143
Overall WOMAC index (0-240)	36.3	51.8	0	206
Ankle JSW (mm)				
1. Tibial plafond	2.4	0.56	1.2	4.4
2. Medial malleolus	3.1	0.79	1.2	5.6
3. Talonavicular	1.4	0.35	0.5	2.6
4. Tibiofibular	2.4	0.55	0.8	4.2
5. Subtalar posterior facet	2.8	0.97	0.9	6.8
6. Subtalar medial facet	4.2	2.2	1.1	7.4
Hip JSW (mm)				
Right hip JSW	3.10	0.72	1.10	5.2
Left hip JSW	3.07	0.74	0.95	4.7
Knee mJSW (mm)				
Right knee mJSW	3.89	0.88	1.1	5.8
Left knee mJSW	3.93	0.90	1.2	5.7
BMD (g/cm^2)				
1. Spine	1.06	0.15	0.72	1.50
2. Lower limbs	1.19	0.15	0.85	1.65
3. Right femur neck	0.92	0.13	0.57	1.31
4. Right femur total	1.00	0.15	0.5	1.63

6.2 Bone shape results

6.2.1 Full ankle complex model

The full ankle complex SSM was reconstructed using 59 PC modes where, as the number of modes increases, the SSM could describe 95% of the variation in ankle complex bone shape. Figure 6-2 below shows a cumulative variance plot which demonstrates the percentage variance accounted for by each PC mode. These values of variance decline towards the right-hand end on the x-axis; in other words, the first PC accounts for the largest variance and each one to the right accounts for less variance.

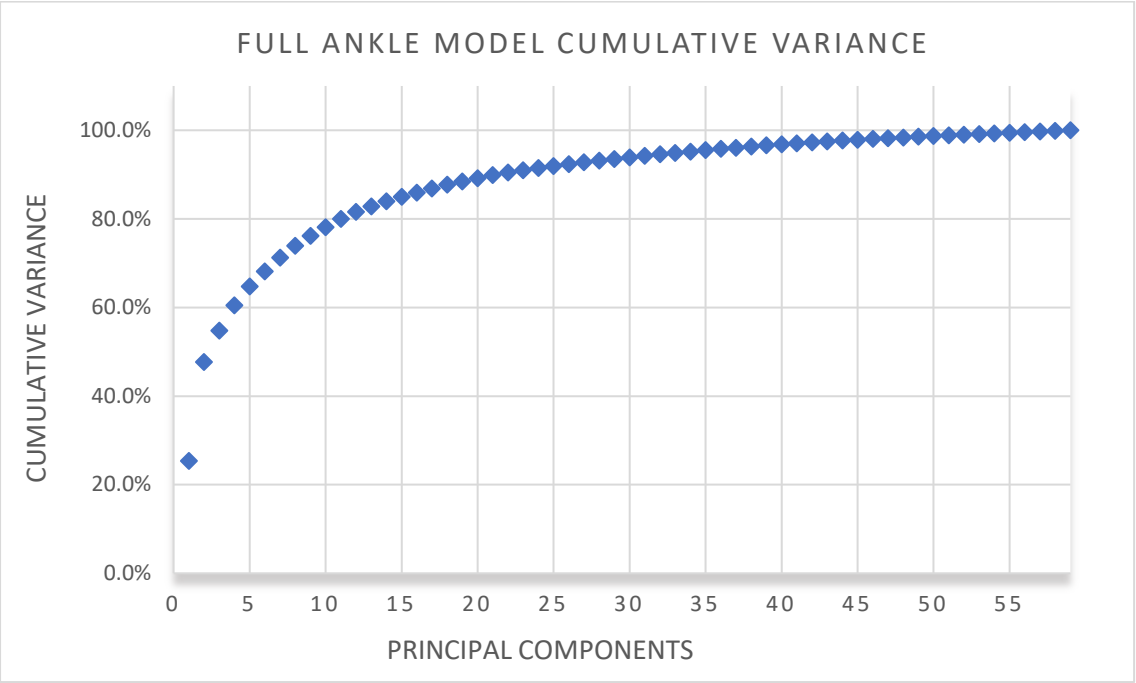

Figure 6-2. Cumulative variance plot showing percentage variance for each additional PC mode used in building the full ankle SSM.

6.2.1.1 Bone shape variations between sexes

The average of all 59 PC modes that represent the 3D bone shape for each participant, were projected orthogonally onto a bone shape vector using the method described in section 5.5.3 in chapter 5. The population bone shape vector represents a line between the mean shape of the male and female groups. The histogram in figure 6-3 shows the distribution differences between males and females along the population bone shape vector.

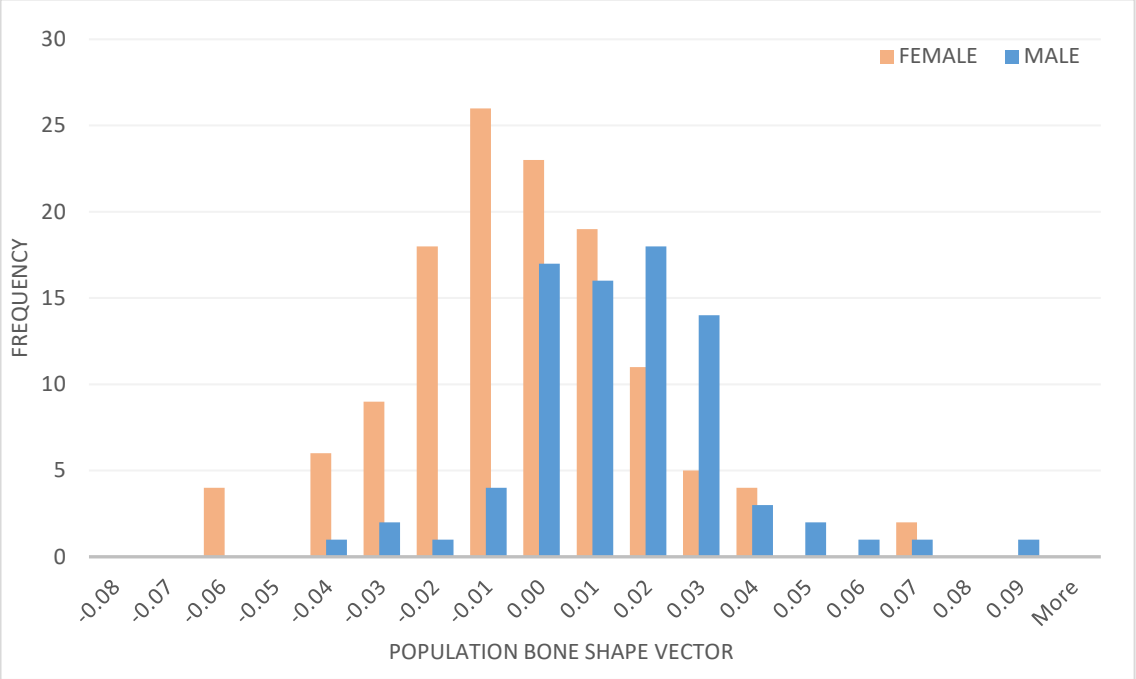

Figure 6-3. Histogram showing the distribution of male and female participants for the population bone shape vector for the full ankle complex model.

To further explore the distributional differences between the sexes shown in figure 6-3, an independent t-test was applied, and a significant difference was found in the means of the population bone shape vector between males and females. This indicate that there is variation in bone shape in the ankle complex between males and females when the average of all PC modes is used to reconstruct the model. Full results are shown in table 6-3.

Table 6-3. Independent t-test results showing the difference between the sexes for mean population bone shape vector.

Participant's Sex	Mean ± (SD) Bone shape vector	P value
Males (N=83)	0.0094 ± 0.02	<0.0001*
Females (N=123)	-0.0095 ± 0.02	

To explore and visualise the specific morphological variations in bone shape between the sexes in the ankle, an independent t-test was used to analyse the first 10 PC modes of variance from the 59 PC modes used to reconstruct the 3D ankle SSM which represent 79% of the variation in the SSM. PC modes beyond PC 10 were excluded from this analysis since they represent only a small amount of the total variance observed in the cumulative plot in Figure 6-2.

All PC modes met the assumption of homogeneity of variances using Levene's Test. However, PC 10 and PC 11 were not normally distributed, and so the Mann Whitney U test was used for the non-normal data. The results show that the variation in ankle bone shape between males and females is statistically significant in the following PC modes: PC 2, PC 5, PC 7, PC 9, PC 13, and PC 14 with p-values of 0.013, 0.002, 0.009, 0.010, 0.0006, and <0.0001 respectively. The full results are presented in Table 6-4.

Table 6-4. Results of independent t-tests and Mann Whitney U tests used to test the significance of the difference in PC modes representing variation in ankle bone shape between the sexes.

PC mode (mm)	Male N=83 Mean ± (SD)	Female N=123 Mean ± (SD)	P value
PC 1	0.0020 ± 0.04	-0.0025 ± 0.05	0.472
PC 2	-0.002 ± 0.04	0.010 ± 0.04	0.013*
PC 3	0.003 ± 0.02	- 0.001 ± 0.02	0.195
PC 4	0.0014 ± 0.02	-0.0010 ± 0.02	0.439
PC 5	0.004 ± 0.02	-0.003 ± 0.01	0.002*
PC 6	0.001 ± 0.01	-0.0006 ± 0.01	0.487
PC 7	-0.003 ± 0.01	0.002 ± 0.01	0.009*
PC 8	0.0006 ± 0.01	-0.0009 ± 0.01	0.465
PC 9	0.002 ± 0.01	-0.002 ± 0.01	0.010*
PC10	Median -0.0008 IQR -0.0009 to -0.0005	Median 0.0005 IQR 0.008 to 0.009	0.702
PC11	Median 0.002 IQR 0.005 to 0.008	Median -0.0004 IQR -0.007 to -0.005	0.145
PC 12	0.0005 ± 0.011	-0.0004 ± 0.011	0.558
PC 13	-0.003 ± 0.009	0.002 ± 0.010	0.0006*
PC 14	0.003 ± 0.008	-0.002 ± 0.009	<0.0001*
PC 15	0.001 ± 0.009	-0.0008 ± 0.009	0.130

Furthermore, it was investigated whether or not the statistically significant results obtained from the above independent t-tests were influenced by the variations in height and weight between the sexes. All PC modes that showed significant bone shape variation between the sexes (PCs 2, 5, 7, 9, 13 and PC 14) were tested separately using linear regression adjusting for possible confounders of height and weight.

Firstly, the association was examined between PC modes as the dependent variable and height as the independent variable which showed significant association. However, after controlling for sex, the association became non-significant indicating that a significant association in the univariable models was driven by the effect of sex in the population. Similar results were

noted regarding the association with weight. Therefore, no adjustment concerning height or weight was deemed necessary in further models since no effect was noticed in the baseline full ankle model. Full results are shown in table 6-5.

Table 6-5. Results of the linear regression models applied to assess the relationship between height and weight with PC modes adjusted for sex.

PC Mode (mm) (N=206)	Height (cm)			Weight (kg)		
	Coeff.	95% CI	P	Coeff.	95% CI	P
PC 2	-0.0004	[-0.001, 0.0001]	0.126	0.0001	[-0.0002, 0.0006]	0.400
PC 5	0.00005	[-0.0002, 0.0003]	0.737	0.0001	[-0.00008, 0.0003]	0.230
PC 7	-0.0001	[-0.0004, 0.00009]	0.208	-0.00008	[-0.00001, 0.0002]	0.251
PC 9	0.0001	[-0.00009, 0.0003]	0.261	0.0001	[-0.00001, 0.0002]	0.097
PC 13	-0.0001	[-0.0003, 0.00004]	0.068	-0.00006	[-0.0001, 0.00003]	0.222
PC 14	0.0001	[-0.00002, 0.0002]	0.106	-0.00006	[-0.0001, 0.00002]	0.152

All PC modes that showed significant bone shape variation between males and females were then interactively visualised in an animated 3D model. The differences are represented in figure 6-4, which displays 4 anatomical views (anterior, posterior, medial, and lateral) of the full ankle complex SSM where the male shape is coloured blue. The difference is seen in all bones, where larger bones such as the calcaneus exhibited more bone shape variation.

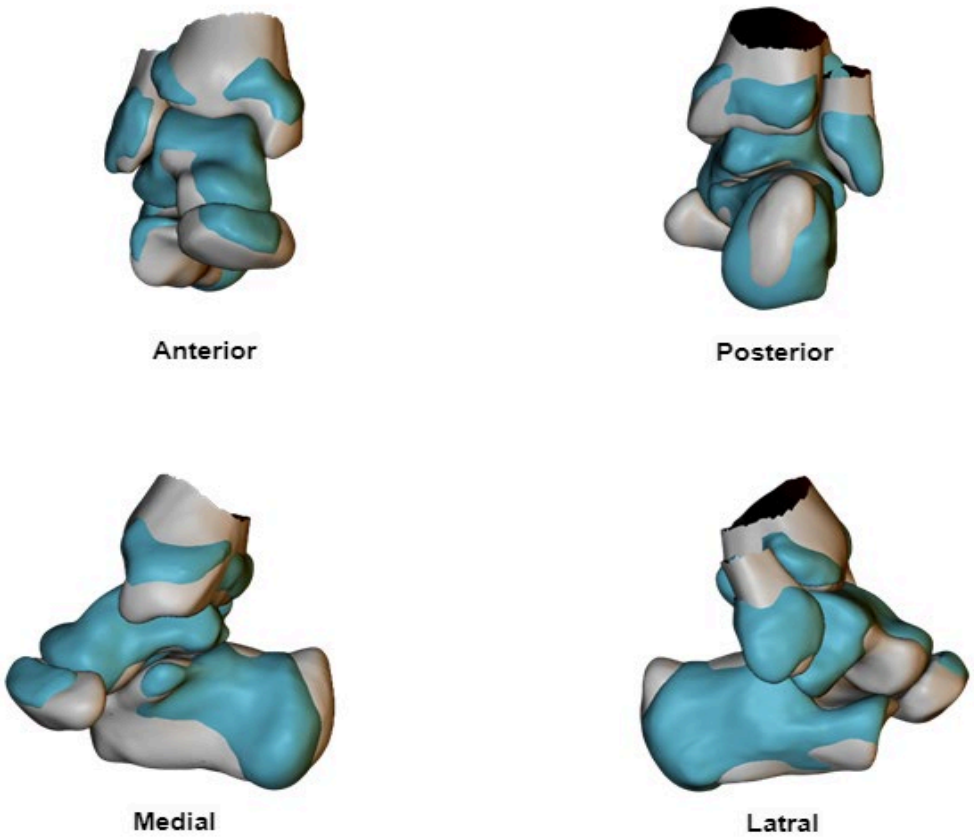

Figure 6-4. Variations between the sexes in ankle complex bone shape as seen in the animated model of the full ankle complex which includes all PC modes used to reconstruct the model. The blue colour represents the male bone shape, while the grey colour represents the female bone shape.

The full ankle model was used to compare morphological variations between sexes in all the bones of the ankle joint complex. To further assess sex differences in bone shape, two separate models were reconstructed. The first model included the distal tibia, talus, and navicular bone, while the second included only the calcaneus. The distal fibula bone was excluded since it showed minimal variation between sexes. However, the calcaneus bone was reconstructed separately due to its significant variation between sexes in all principal component modes of the full ankle SSM. By separating the calcaneus bone, its influence on other bones was eliminated and sex differences in all bones were better represented. The detailed results for these two models are presented below.

6.2.2 Distal Tibia-Talus-Navicular 3D SSM

The SSM was reconstructed using 53 PC modes of variations, which in total account for 95% of the variation in the shape of the bones concerned. Figure 6-5 shows a cumulative variance plot that represents the variances accounted for by each PC mode. The first PC accounts for the highest percentage of variance and each one afterwards accounts for less variance.

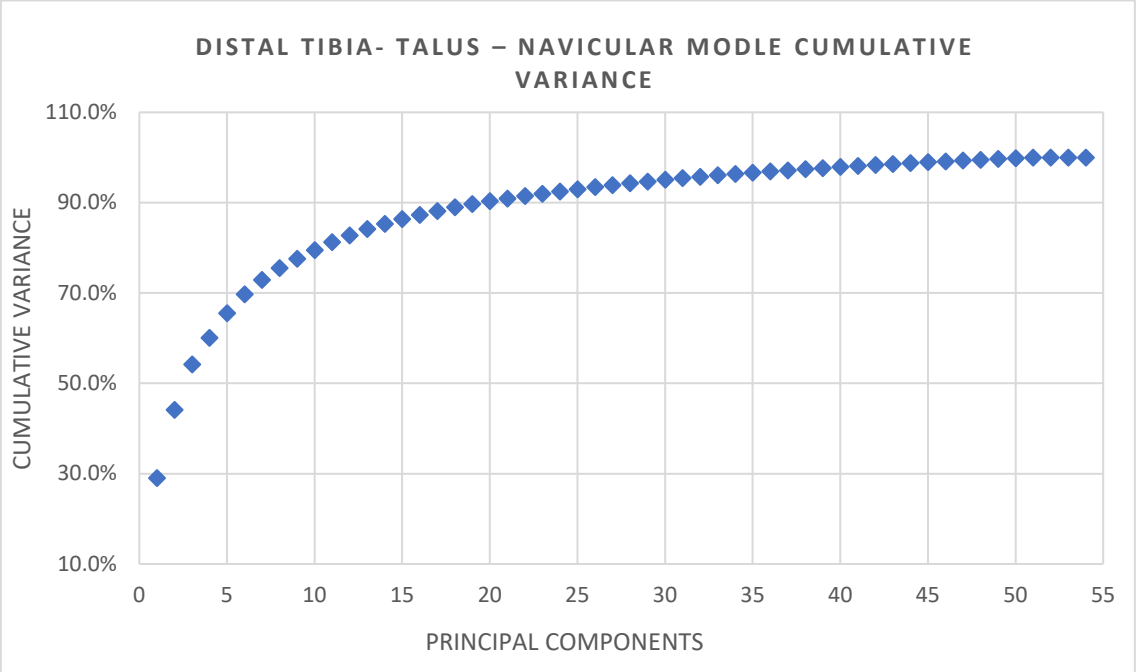

Figure 6-5. Cumulative variance plot showing the percentage of variance accounted for each PC mode in the distal tibia-talus-navicular 3D model.

6.2.2.1 Variations in distal tibia-talus-navicular bone shape and area between sexes

The histogram in figure 6-6 shows the differences in distribution between males and females along the population bone shape vector. Which represents a line between the mean shape of the male and female groups, the average of all 53 PC modes produced from 3D SSM for each participant, was projected orthogonally onto the vector.

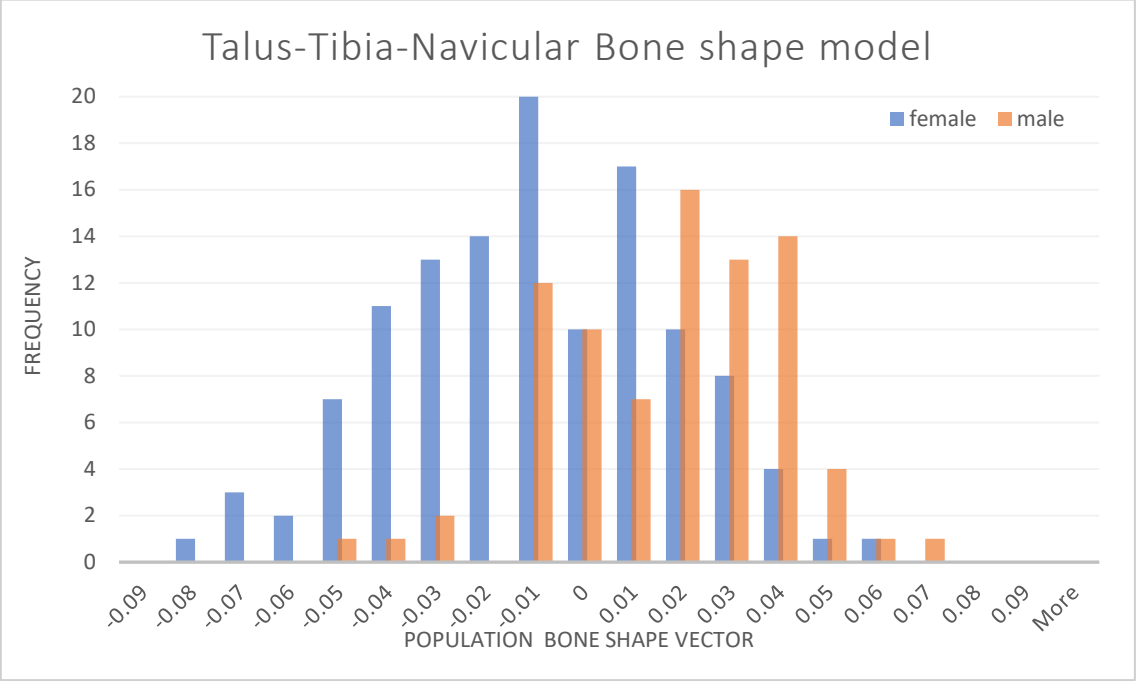

Figure 6-6. Histogram showing the separation of males and females for the population bone shape vector for the tibia, talus, and navicular bone.

To further explore the distributional differences between sexes shown in figure 6-6 above, an independent t-test was applied to compare the means of the population bone shape vector of the distal tibia, talus, and navicular bone shape of the different sexes. The results show significant morphological bone shape variations between males and females when using the average of all PC modes used to reconstruct the SSM. The results are shown in Table 6-6.

Table 6-6. Independent t-tests results showing the difference between sexes associated with the means of the population bone shape vector of the distal tibia, talus, and navicular SSM.

Participants Sex	**Mean ± (SD)** **Bone shape vector**	**P value**
Males (N=83)	-0.013± 0.025	
Females (N=123)	0.012 ± 0.023	<0.0001*

The previous findings indicated significant differences between the sexes in the shapes of the bones included in the model when using the average of all PC modes used to reconstruct the SSM. To represent bone shape variations and sex differences more accurately, an independent t-test was conducted on the first 10 PC modes which account for 78.6% of the total variation in the model. These first 10 PC modes were selected out of the 53 modes used in the reconstruction process because they account for most of the variation, while the remaining PC modes account for only negligible proportion of the variation.

All PC modes satisfied the assumption of the homogeneity of variances as measured using Levene's Test as well as the normality assumption using the Shapiro–Wilk test. The results show that the difference in ankle bone shape between males and females is statistically significant in PC modes 2, 3, and 7 with p-values of <0.0001, 0.0002, 0.035 respectively. Detailed results are presented in table 6-7.

Table 6-7. Results of independent t-tests used to test the difference in 3D SSM PC modes representing differences in the shape of the distal tibia-talus–navicular bones between the sexes.

PC mode (mm)	Male N=83 Mean ± (SD)	Female N=123 Mean ± (SD)	p value
PC 1	-0.003 ± 0.034	0.002 ± 0.046	0.359
PC 2	-0.011 ± 0.030	0.008 ± 0.036	<0.0001*
PC 3	-0.007 ± 0.023	0.005 ± 0.025	0.0002*
PC 4	0.0001 ± 0.023	-0.0002 ± 0.023	0.902
PC 5	0.002 ± 0.018	-0.002 ± 0.020	0.095
PC 6	-0.002 ± 0.018	0.001 ± 0.18	0.162
PC 7	-0.003 ± 0.016	0.002 ± 0.015	0.035*
PC 8	0.001 ± 0.012	-0.001 ± 0.015	0.201
PC 9	-0.0008 ± 0.013	-0.0005 ± 0.014	0.475
PC10	-0.001 ± 0.012	0.001 ± 0.012	0.068

All PC modes that show significant differences in bone shape between males and females were interactively visualised in an animated 3D model. PC 2 showed statistically different bone shape between sexes at $P < 0.0001$, where the variation was mainly represented in the shape of the distal tibia.

The shapes of the distal tibia for females deviated from the mean distal tibia shape in a positive direction with a mean of 0.008 mm. These positive deviations from the mean represent a decrease in the width of the distal tibia bone mainly in the anterior and posterior portions in females when compared to males in the negative direction (-2SD). Also, the positive direction shows a longer and thinner medial malleolus bone which points more inferiorly when compared with the negative direction which relates to a shorter and wider medial malleolus bone shape. Full results are presented in figure 6-7 using 4 anatomical views, with each including three images (-2SD, mean and +2SD) extracted directly from the SSM presented in a colour map of mean bone shape.

PC 3 showed statistically different bone shape variations between sexes ($P= 0.0002$) and the variation was mainly represented by the shape of the talus. From the interactively visualisation of the animated 3D SSM, the talus bone shape variation was extracted and is shown in figure 6-8. The mean of PC 3 for males deviates from that in the population in a negative direction with a mean of –0.007 mm. Such a deviation represents a longer and wider talus bone in males compared to females who deviated in the positive direction (+2SD) with a shorter and thinner talus bone. Also, the negative direction shows a wider tibia articular surface (talus dome) and a larger posterior articular surface in males when compared to females in the positive direction, who tend to have a thinner talus dome and smaller posterior articular surface.

PC7 showed statistically significant differences between the sexes at $p = 0.03$, and this mode represents only a small variation between the sexes mainly in the shape of the navicular bone. For females, this mode deviated in a positive direction with a mean of 0.002 mm, which represents a smaller and thinner bone mostly in the anterior portion of the bone with a less deep articular surface in contact with the talus head when compared to the negative shape in the male population. The shape variations were also extracted from the model and are presented in figure 6-8.

PC mode & view	-2SD bone shape	Mean bone shape with colour map	+2SD bone shape	Observed variation
PC 2 Distal Tibia bone Medial view	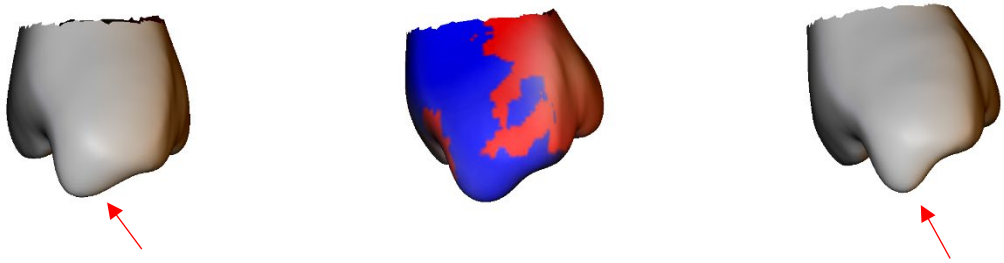			The medial malleolus is thinner and longer at +2SD and thicker and shorter at -2SD
PC 2 Distal Tibia bone Anterior View	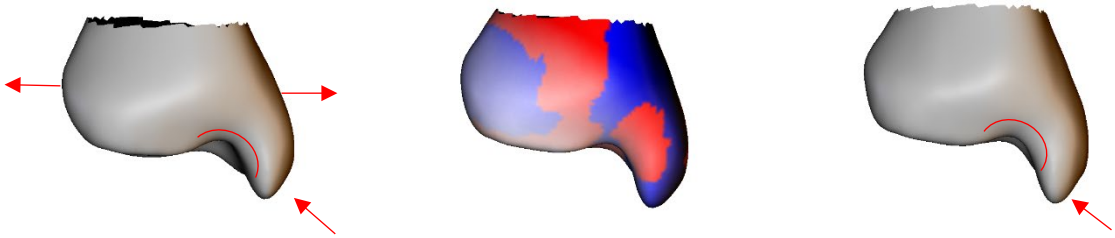			A wider distal tibia bone in the -2SD when compared with the +2SD.
PC 2 Distal Tibia bone Posterior View	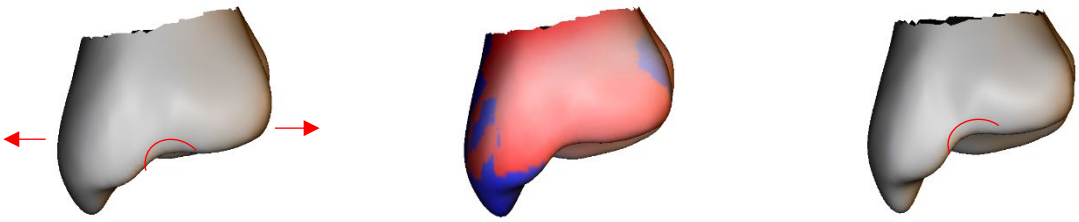			A wider distal tibia bone body when compared with the +2SD.
PC 2 Distal Tibia bone Lateral view	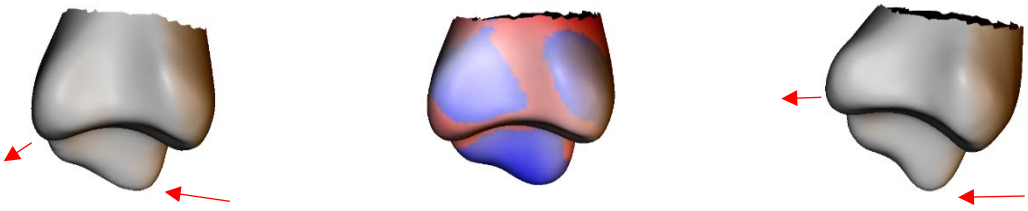			Similar variations as noted in the medial view plus curvature difference at tipial-plafond articulation surface, between ±2SD.

Figure 6-7. Differences in distal tibia bone shape seen for the PC 2 mode that significantly differentiate between participants according to sex.

Note: All images were extracted from the animated model focusing on the mean and +2SD and -2SD of bone shape. The mean bone shape image includes a colour map that represents the point-to-point difference between the +2SD results shown in blue and -2SD shown in red.

PC mode & view	-2SD bone shape	Mean bone shape with colour map	+2SD bone shape	Observed variation
PC 3 Talus bone Medial view	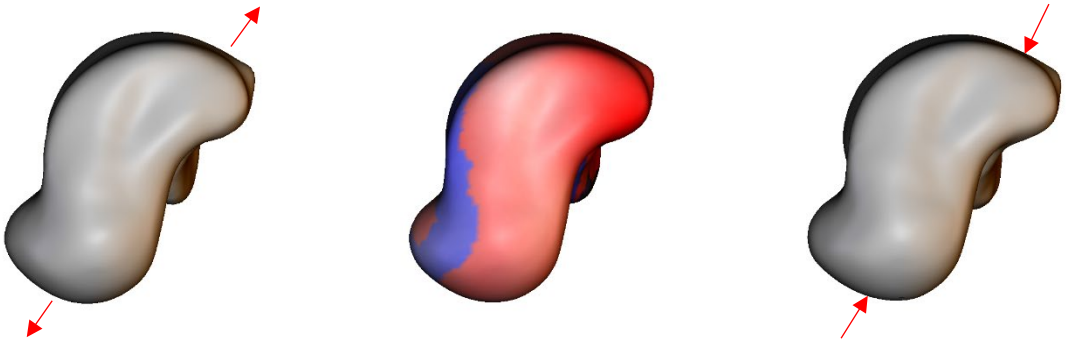			The -2SD talus shape is longer and wider compared to the mean and +2SD bone shape
PC 3 Talus bone Superior View	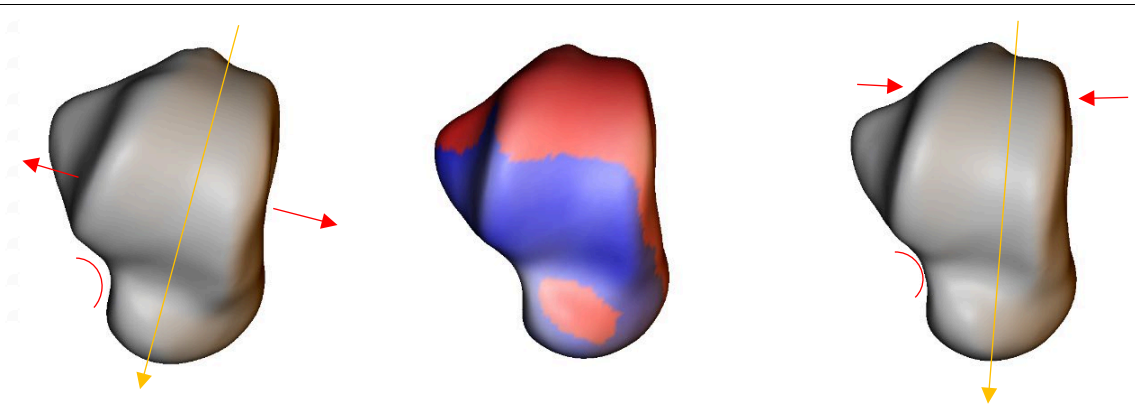			The -2sd has a wider talus dome with a narrower talus neck compared to the +2SD shape.
PC 3 Talus bone Inferior View	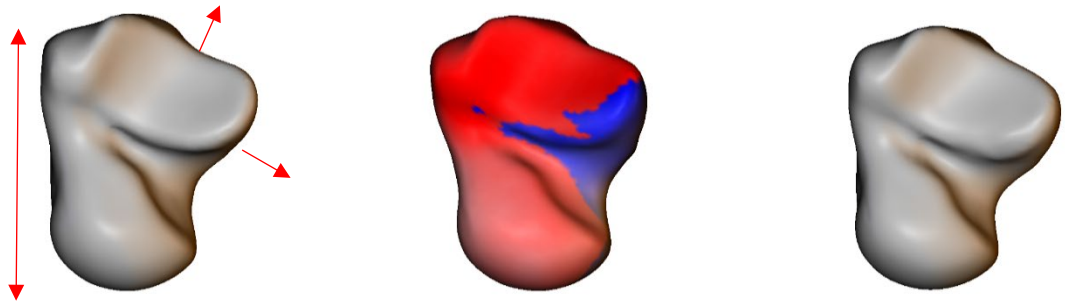			The -2SD talus shape is longer with bigger posterior articulation bone area compared with the +2SD shape
PC 7 Navicular bone Anterior view **PC 7 Navicular bone Medial view**	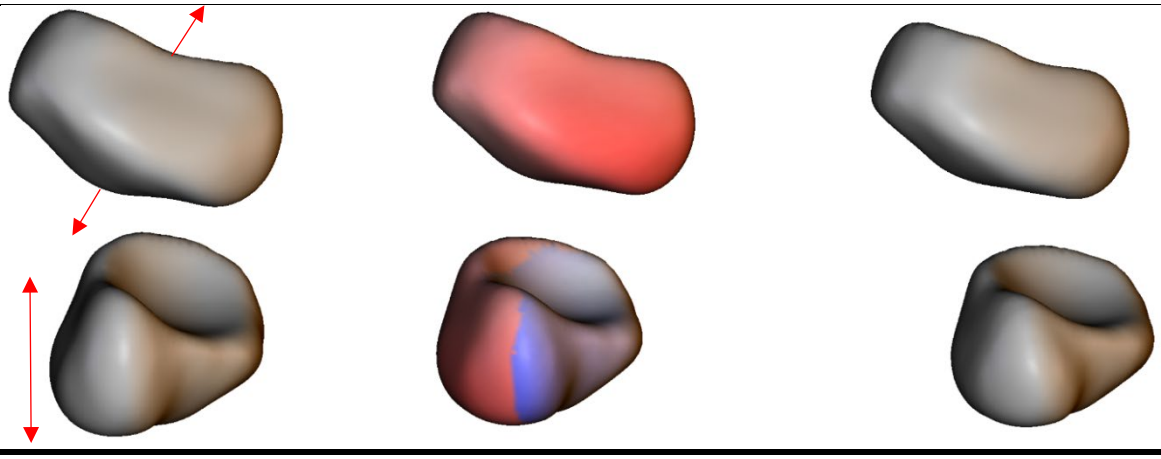			The -2SD anterior navicular shape is larger and has a wider and dipper articulation bone area when compared to the +SD shape.

Figure 6-8. Differences in the talus and navicular bone shape seen for PC modes 3-7 that significantly differentiate between participants according to sex.

Note: All images were extracted from the animated model focusing on the mean and +2SD and -2SD of bone shape. The mean bone shape image includes a colour map that represents the point-to-point difference between the +2SD results shown in blue and -2SD shown in red.

6.2.2.2 Variations in talus bone area and dimensions between sexes

The length, height, and width of the talus bone, as well as three specific bone areas, were measured using the SSM, as described in section 5.5.2. The previous bone shape analysis using PC modes showed significant variations between the sexes in these bone areas, as well as in the length and width of the bone (Figure 6-8). In this analysis, the aim was to quantify the exact measurements for each variable and to explore sex-related differences. After testing for the homogeneity of variances and normality, independent t-tests were conducted to compare the mean bone area of the talus dome, talus head, and posterior facet between males and females, as well as for the remaining measurements. The results shown in Table 6-8 demonstrate significant morphological differences between the sexes, with males having larger bone areas and dimensions compared to females. These findings are consistent with those noted in the previous bone shape analysis.

Table 6-8. Results of independent t test used to test for differences between the sexes in bone areas and dimensions quantified from the distal tibia-talus-navicular 3D SSM.

Bone measurements (mm/mm²)	**Male N=83 Mean ± (SD)**	**Female N=123 Mean ± (SD)**	**P value**
Talus dome (bone area)	1154 ± 11.5	954.3 ± 7.5	<0.0001*
Talus head (bone area)	971.5 ± 11.6	815.5 ± 7.7	<0.0001*
Posterior facet (bone area)	621.3 ± 7.3	510.4 ± 5.1	<0.0001*
Talus length	60.3 ± 0.3	54.8 ± 0.2	<0.0001*
Talus width	44.8 ± 0.2	40.7 ± 0.1	<0.0001*
Talus height	38.1 ± 0.2	35.07 ± 0.1	<0.0001*

6.2.3 Calcaneus 3D statistical shape model

The SSM was reconstructed using 50 PC modes, which in total account for 95% of the variation in the shape of the bones included. Figure 6-9 shows a cumulative variance plot that represents the variances accounted for by each PC mode. The first PC accounts for the highest percentage of variance and each one after it accounts for less variance.

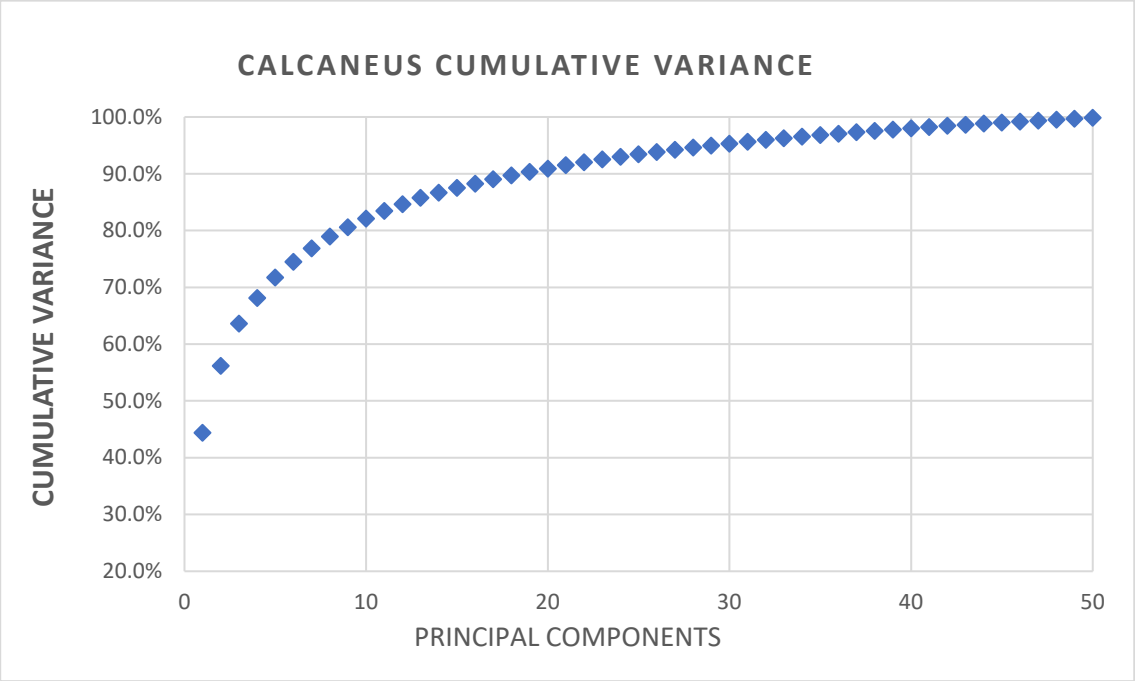

Figure 6-9 Cumulative variance plot shows percentage of variance accounted for each PC mode in calcaneus 3D SSM.

6.2.3.1 Calcaneus bone shape variations between sexes

The histogram in figure 6-10 shows the differences in distribution between males and females along the population bone shape vector which represents a line drawn between the mean shapes of the male and female groups, and the averages of all 53 PC modes produced from the 3D SSM for each participant were projected orthogonally onto the vector.

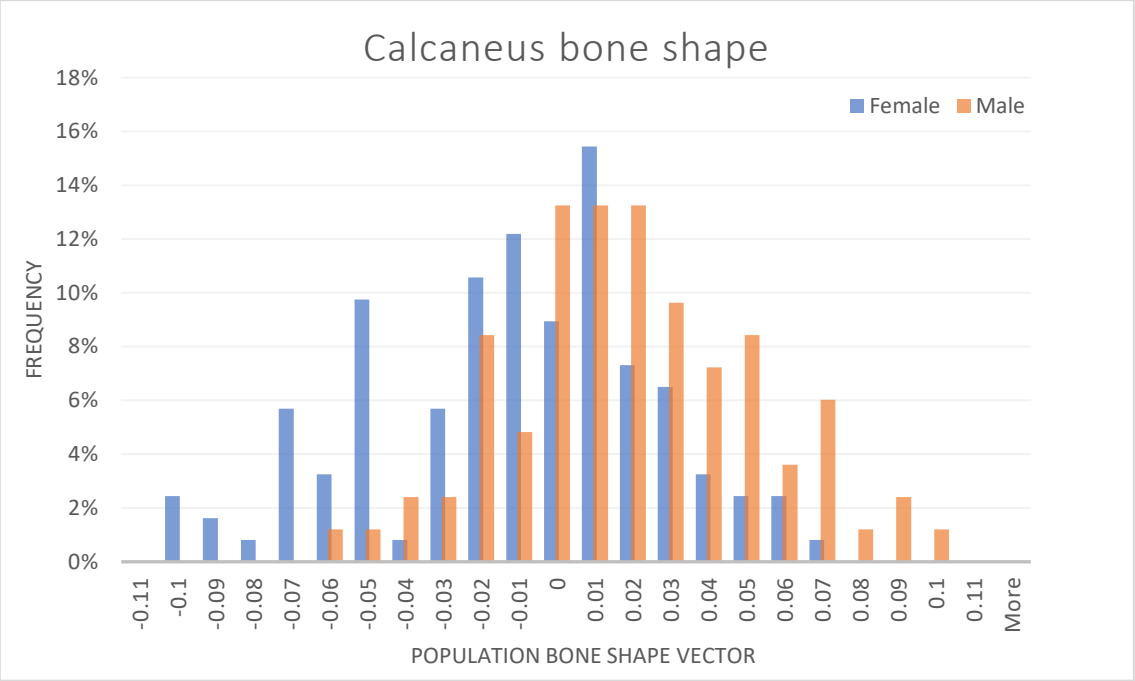

Figure 6-10. Histogram showing the distribution of the averages of all PC modes used to reconstruct the calcaneus SSM, for males and females on the population's bone shape vector.

To further explore the distributional differences between sexes shown in figure 6-10, an independent t-test was applied to compare the means of the population bone shape vector for the calcaneus between males and females. The results indicate significant morphological bone shape variations between the sexes as shown in table 6-9.

Table 6-9 Differences between means for males and females on the ankle bone shape vector.

Sex of participants	**Mean ± (SD) Bone shape vector**	**P value**
Males (N=83)	-0.009 ± 0.037	0.0003*
Females (N=123)	0.009 ± 0.034	

To assess the variation in bone shape between the sexes represented by the PC modes, an independent t-test was applied. Like the previous model including the remaining bones, only the first 5 PC modes of the total of 50 PC modes used to reconstruct the model were included in the analysis because they describe most of the variation noted in the model at approximately 76.9%.

All PC modes met the assumptions of the homogeneity of variances using Levene's Test and normality using the Shapiro–Wilk test. The results show that the difference in calcaneus bone shape between males and females is statistically significant in the PC modes 1, 4, and 5 with p-values of 0.017, 0.005 and <0.0001 respectively. Results are presented in Table 6-10.

Table 6-10. Results of independent t-tests used to test the difference in PC modes representing variation in the 3D SSM bone shape of the calcaneus between sexes.

PC mode (mm)	Male N=83 Mean ± (SD)	Female N=123 Mean ± (SD)	P value
PC 1	0.008 ± 0.057	-0.009 ± 0.064	0.017*
PC 2	0.002 ± 0.019	0.0001 ± 0.016	0.274
PC 3	-0.0003 ± 0.018	0.0005 ± 0.021	0.734
PC 4	0.004 ± 0.018	-0.002 ± 0.019	0.005*
PC 5	0.005 ± 0.014	-0.003 ± 0.014	<0.0001*

The PC modes representing bone shape variation that showed significant differences between the means of males and females from the independent t-tests were interactively visualized in the animated 3D SSM, and then images were extracted that represent the variations noted which are illustrated in figure 6-11. The first PC mode revealed a significant difference in calcaneus bone shape between the sexes (P = 0.017). The shapes of the calcaneus for females deviated from the mean calcaneus shape in the negative direction for the first PC mode, with a mean of -0.009 mm.

As shown in the lateral view, females exhibited a narrower main calcaneus body width than males. Additionally, the calcaneus tuberosity shows difference in the area where the achilles tendon is attached; in females it is more superiorly prominent when compared to males at +2SD. Moreover, the Gissane and Bohler's angles varied between the sexes at ±2SD, with

females showing smaller angles in the -2SD and males having larger angles in the +2SD. In the anterior view for PC 1, females at -2SD exhibited thinner posterior facet surfaces and thinner cuboid facets compared to males at +2SD. Figure 6-11 illustrates these variations with red arrows pointing to the specific differences.

Furthermore, PC 4 showed a significant difference in calcaneus bone shape between the sexes ($P = 0.005$), particularly in the length of the calcaneus and the prominence of the medial process. Females exhibited negative deviations from the mean calcaneus shape for PC 4 at -0.002 mm, indicating a relatively shorter calcaneus bone in comparison to males in the medial view. Additionally, the medial process of the calcaneus tuberosity was larger in females and more inferiorly prominent than in males for the +2SD bone shape, as also observed in the medial view.

PC 5 revealed significant differences in calcaneus bone shape between males and females ($P < 0.0001$), primarily in terms of size. The shapes of the female calcanei also deviated negatively from the mean for PC 5, with a mean deviation of -0.003 mm (see table 6-10). When visualising the variation in PC 5 using the SSM, differences were noted in the width of the calcaneus body in the inferior view. Females tended to have a thinner calcaneus body, while males deviated towards a wider bone area in the positive direction. Additionally, in the posterior view for PC 5, differences in overall calcaneus tuberosity size were noted. Females had a thinner calcaneus tuberosity, while males showed wider bone areas at +2SD in shape. Finally, the lateral process of the calcaneus tuberosity was more laterally prominent in males (+2SD) than in females in the negative direction.

All images showing the previously described variations were extracted from the model and are presented in figure 6-11 using 5 anatomical views of the calcaneus (anterior, posterior, medial, lateral and inferior) from all PC modes that showed significant differences between the sexes. Each view includes three images (-2SD, mean and +2SD), presented with a colour map for the mean bone shape.

PC mode & view	shape -2SD	Mean shape with colour map	shape +2SD	Observed variation
PC 1 Lateral view	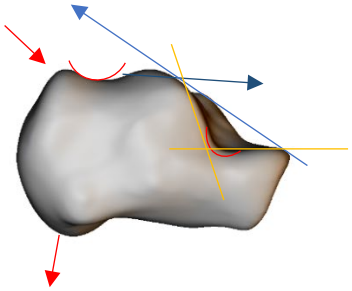	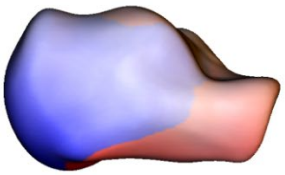	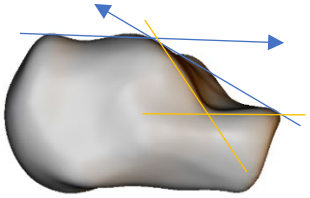	Variations noted in the main body and in the degree of Gaussian angle. (blue lines) and Bohler's angles (yellow lines) also variations in the shape of the calcaneus tuberosity
PC 1 Anterior View	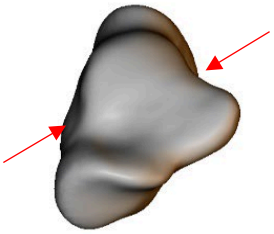	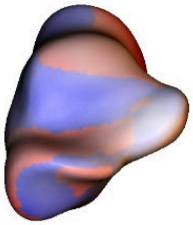	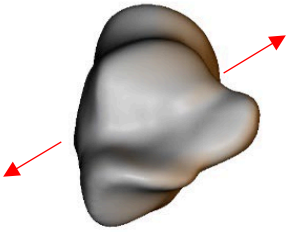	The articular surface of the subtalar joint is showing variation in bone shape were +2sd has a wider posterior facet area.
PC 4 Medial View	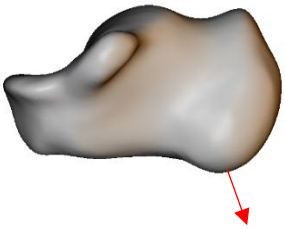	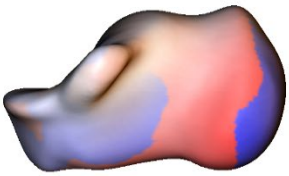		Variation in length of the bone where it is relatively longer in the +2SD. Also, variation in the medial process of the calcaneal tuberosity were in the -2SD it is extended more inferiorly
PC 5 Inferior view	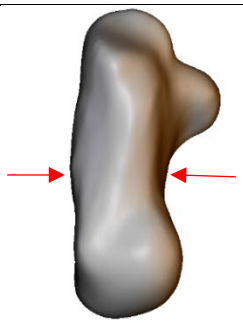	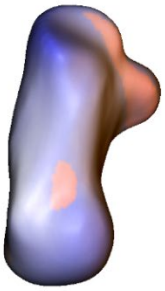	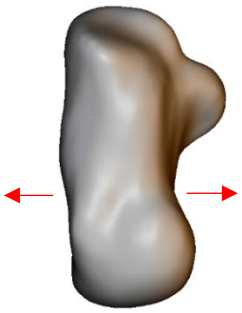	Variations in the width of the bone where it is wider in the +2SD. the posterior view also shows wider calcaneus tuberosity in +2SD with a more prominent lateral process
PC 5 Posterior view	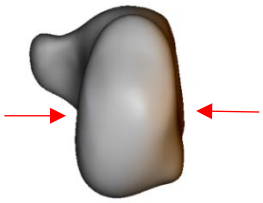	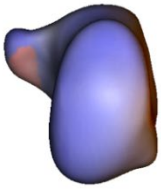	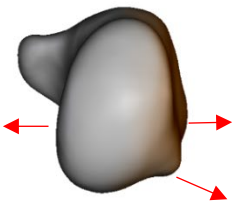	

Figure 6-11. *Differences in calcaneus bone shape seen for PC modes 1,4, and 5 that significantly differentiate between participants according to sex.*

Note: All images were extracted from the animated model focusing on the mean and +2SD and -2SD of bone shape. The mean bone shape image includes a colour map that represents the point-to-point difference between the +2SD results shown in blue and -2SD shown in red.

6.2.3.2 Variations in calcaneus bone area between sexes

Three calcaneus bone measurements (calcaneus length, tuberosity bone area, and posterior tuberosity width), were measured using the SSM, as described in section 5.5.2. The previous analysis of bone shape using PC modes showed significant variations between the sexes in these measurements (see Figure 6-11). In this analysis, the aim was to quantify the exact measurements for each variable and to explore differences related to sex. After testing for the homogeneity of variances and normality, independent t-tests were conducted to compare the means of calcaneus length, tuberosity bone area, and posterior tuberosity width between the sexes. The results shown in Table 6-11 demonstrate significant morphological differences between the sexes, with males having larger and wider bone area and longer calcanei compared to females. These findings are consistent with those of the previous bone shape analysis.

Table 6-11. Results of independent t-tests used to test differences between sexes in three bone areas quantified from the calcaneus 3D SSM.

Bone area (mm)	**Male N=83** **Mean ± (SD)**	**Female N=123** **Mean ± (SD)**	**p value**
Calcaneus length	85.02 ± 4.1	78.6 ± 4.1	<0.0001*
tuberosity bone area	1587.9 ± 18.2	1288.6 ± 13.8	<0.0001*
Tuberosity width	29.3 ± 1.9	25.4 ± 1.6	<0.0001*

6.2.4 Association between ankle bone shape variations and knee/hip OA:

To assess differences in ankle bone shape between participants with and without OA in the hip and knee joints, separate models were constructed for male and female participants. The incidence of knee OA for each participant was determined using the K&L grading system, where participants diagnosed with OA (K&L grade ≥ 2 in the dominant knee) were considered to have OA and those without OA (K&L grade < 2) were not. For hip OA, an overall Croft modification of K&L grade ≥2 was used to determine the presence of radiographic OA.

The PC modes representing bone shape from each model were analysed separately, and the variations in each model were extracted. In the male model, independent t-tests were used to examine differences in ankle complex bone shape represented by the first 5 PC modes of variation between participants with knee or hip OA and those without. All PC modes met the assumptions of homogeneity of variances and normality. The first 5 PC modes included in this analysis represent 76.34% of the total variation in the 3D ankle shape model. Other PC modes of variation were not included as each represents only a small amount (<5%) of the total variance shown in figures 6-12.

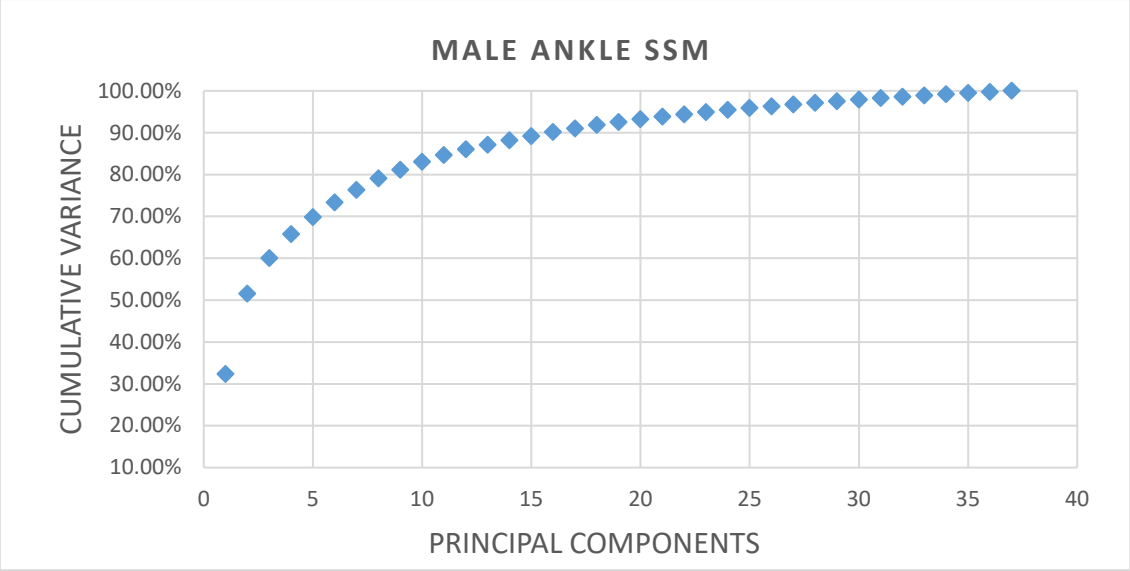

Figure 6-12. Cumulative variance plot showing percentages of variance accounted for by each PC mode in full ankle male SSM.

The statistical analysis revealed a significant difference in the full ankle complex bone shape between participants with knee OA and those without OA, specifically for PC 3 (p = 0.009), and the full results are shown in table 6-12. Furthermore, the t-tests applied to the first five PC modes in table 6-13 showed a significant difference (P = 0.01) in ankle bone shape between participants with and without hip OA, specifically for PC 4.

Table 6-12. Results of independent t-tests used to test the difference in ankle bone shape (represented by the PC modes of variation resulting from the male 3D SSM) between male participants with and without knee OA.

Male N=83	**Knee OA N=31**	**Non-Knee OA =52**	**p value**
PC mode (mm)	**Mean ± (SD)**	**Mean ± (SD)**	
PC 1	-0.003 ± 0.03	-0.002 ± 0.03	0.821
PC 2	-0.005± 0.03	0.0004 ± 0.03	0.433
PC 3	-0.009 ± 0.02	0.007 ± 0.02	0.009*
PC 4	0.003 ± 0.02	-0.002 ± 0.02	0.264
PC 5	0.003 ± 0.01	-0.002 ± 0.01	0.157

Table 6-13. Results of independent t-tests used to test the difference in ankle bone shape represented by the PC modes of variation resulting from the male 3D SSM between male participants with and without hip OA.

Male N=83	**Hip OA N=26**	**Non-Hip OA N=57**	**p value**
PC mode (mm)	**Mean ± (SD)**	**Mean ± (SD)**	
PC 1	-0.005 ± 0.03	-0.001 ± 0.03	0.690
PC 2	-0.006 ± 0.03	-0.0001 ± 0.03	0.421
PC 3	-0.001 ± 0.02	0.0005 ± 0.02	0.785
PC 4	-0.009 ± 0.02	0.004 ± 0.02	0.010*
PC 5	0.0007 ± 0.01	0.0003 ± 0.01	0.927

The PC modes that exhibited significant bone shape variation between male participants with and without knee and hip OA were visualised in an animated male 3D SSM. Images representing the variation were then extracted from the model and are shown in figure 6-13 using different anatomical views of the full ankle complex from both PC modes that showed significant differences between knee OA and non OA male particpents. Each view includes three images (-2SD, mean and +2SD). PC 3 showed a statistically significant difference in bone shape variation between knee OA and non-OA male participants (P = 0.009), where OA

participants deviated from the mean ankle complex shape in the negative direction for PC 3 with a mean of -0.009 mm.

Negative deviations from the mean ankle complex shape, as shown in figure 6-13, primarily represent variations in articulation and bone alignment which indicate foot posture. The -2SD group displayed a more pronated ankle shape, with the calcaneus more everted than in the +2SD group. Moreover, the height of the navicular bone differed, with the -2SD group showing a greater decline than that in the +2SD group, as seen in the lateral oblique view in figure 6-13. For more clarity, an extracted video from the modle showing the variations is found in this link https://vimeo.com/819372861?share=copy

Additionally, the results indicate that PC 4 was associated with a statistically significant difference in bone shape between male participants with hip OA and those without (P = 0.010), where OA participants exhibited a negative deviation from the mean ankle complex shape direction with a mean of -0.009 mm. The negative deviation primarily indicates a more supinated foot posture, as observed in the main and +2SD images extracted from the 3D SSM, as well as a calcaneus bone inversion motion combined with the external rotation of the distal tibia, as observed in the superior view in figure 6-13. Additionally, the talus bone showed more abduction and dorsiflexion compared to the +2SD. A video showing the variations is found here https://vimeo.com/819373807?share=copy

Male PC mode & view	-2SD	Mean shape	+2SD	Observed variation
PC 3 Lateral oblique view	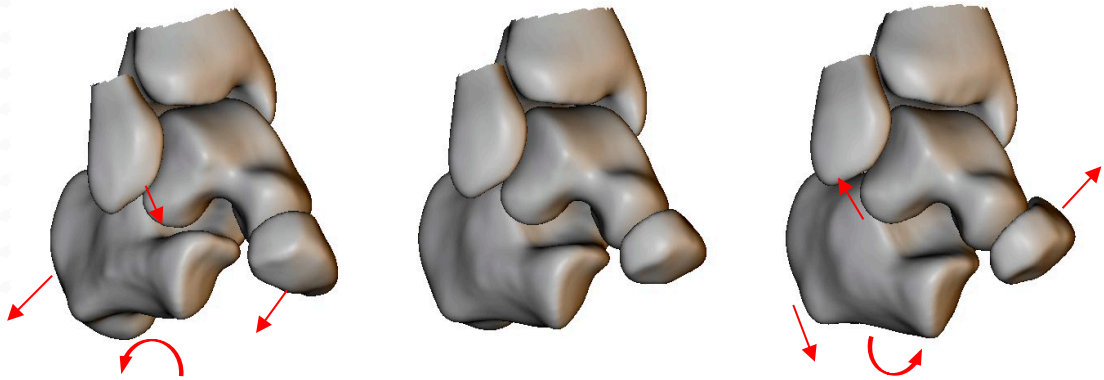			Two views extracted from PC3 of the male model a posterior view and a lateral oblique view. The -2SD showed a pronated foot type with an everted calcaneus, dropped navicular and plantarflexion of the talus compared to the main and +2SD. *Red arrows used to explain the noted motions
PC 3 Posterior View	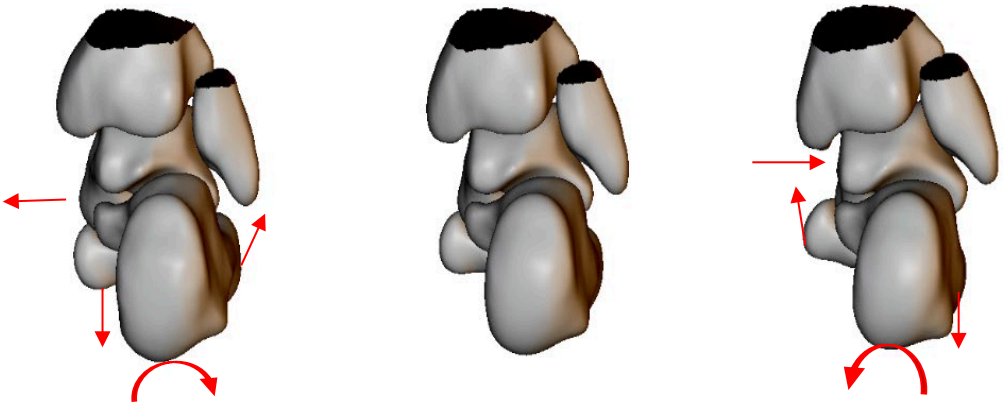			
PC 4 Posterior view	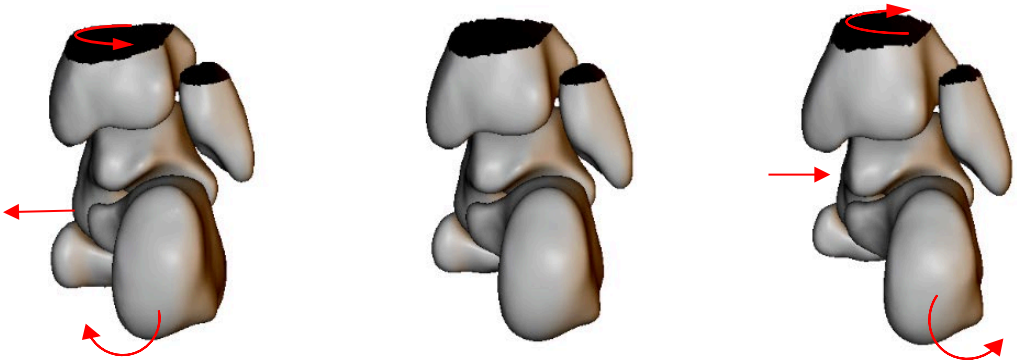			Both the posterior and superior views show In - 2SD the calcaneus is more inverted forming a more supinated rearfoot with a distal tibia that is more rotated internally compered to both the main and the +2SD
PC 4 Superior view	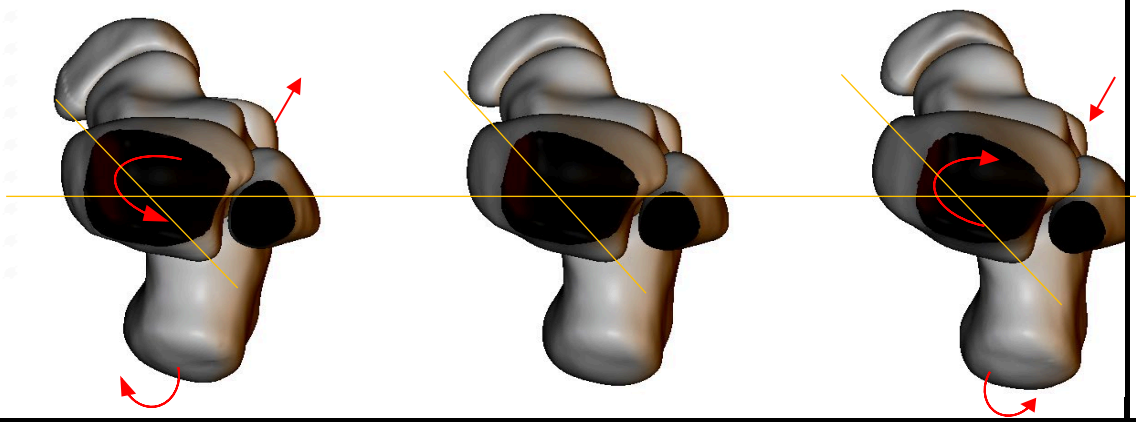			

Figure 6-13. Differences in bone shape for PC modes that significantly differentiate between male participants with knee and hip OA and those without OA. The images were extracted from the animated male 3D SSM and focus on the mean, +2SD, and -2SD of bone shape. PC3 showed significant differences between participants with knee OA and those without, and PC4 showed significant differences between participants with hip OA and those without.

Independent t-tests were also used to examine the differences in the ankle complex bone shape represented by the PC modes of variation between female participants with knee OA and others without knee OA, as well as between participants with and without hip OA. The assumptions of the homogeneity of variances and normality were tested, and all PC modes satisfied those assumptions.

The analysis included only the first 5 PC modes, which accounted for 77.18% of the variation in the female 3D ankle shape model. Other PC modes were not included because each represented less than 5% of the total variance as shown in figure 6-14.

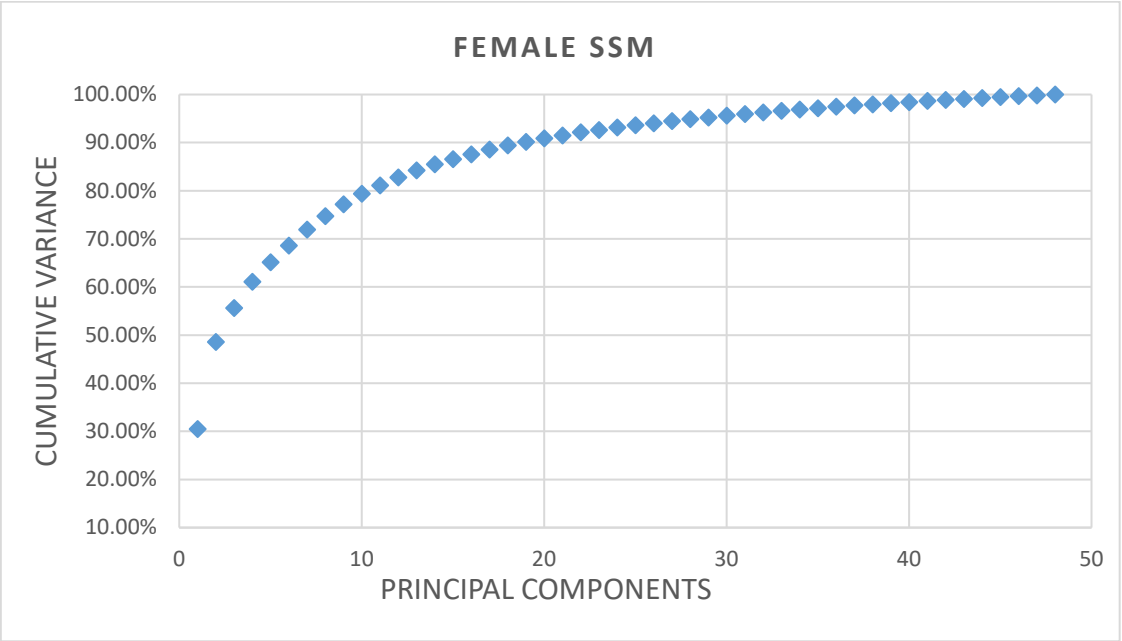

Figure 6-14. Cumulative variance plot showing percentage of variance accounted for by each PC mode in the full ankle female SSM.

The results show that the differences in the full ankle complex bone shape between female participants with knee OA and without are statistically significant only for PC 4 ($p = 0.012$), and the full results are shown in table 6-14. Furthermore, the results from the t-tests applied on the first five PC modes shown in table 6-15 show that only PC 5 showed significant differences ($p=0.013$) in ankle complex bone shape between female participants with and without hip OA.

Table 6-14. Results of independent t-tests used to test the difference in ankle bone shape represented by the PC modes of variation resulting from the female 3D SSM between female participants with and without knee OA.

Female N=123	**Knee OA N=38**	**Non-Knee OA N=85**	**p value**
PC mode (mm)	**Mean ± (SD)**	**Mean ± (SD)**	
PC 1	0.003 ± 0.03	-0.001 ± 0.03	0.579
PC 2	-0.008 ± 0.03	0.003 ± 0.03	0.107
PC 3	-0.001 ± 0.02	0.0006 ± 0.02	0.643
PC 4	-0.006 ± 0.02	0.003 ± 0.02	0.012*
PC 5	-0.002 ± 0.01	0.0009 ± 0.01	0.363

Table 6-15 Results of independent t-tests used to test the differences in ankle bone shape represented by the PC modes of variation resulting from the female 3D SSM between female participants with and without hip OA.

Female N=123	**Hip OA N=45**	**Non-Hip OA N=78**	**p value**
PC mode (mm)	**Mean ± (SD)**	**Mean ± (SD)**	
PC 1	-0.006 ± 0.03	0.004 ± 0.03	0.240
PC 2	0.004 ± 0.03	-0.002 ± 0.03	0.337
PC 3	0.001 ± 0.02	-0.0008 ± 0.02	0.632
PC 4	-0.0006 ± 0.02	-0.001 ± 0.02	0.800
PC 5	-0.005 ± 0.01	0.003 ± 0.01	0.013*

Both PC modes that show significant bone shape variation between female participants with and without OA were then interactively visualized in the animated female 3D SSM. PC 4 showed a statistically significant difference in bone shape variation between knee OA and non-OA female participants (P = 0.012) where OA participants deviated from the mean ankle complex shape in the negative direction of PC 4 with a mean of -0.006 mm. Negative deviations from the mean ankle complex shape described in figure 6-15 show variations in articulation and bone alignment representing foot posture, where the -2SD results showed that the calcaneus was more everted compared to that at +2SD. Also, the height of the navicular bone was different, as seen in the anterior view in figure 6-15, where in the -2SD results the height declined more when compared with +2SD. Such variations show a more pronated ankle shape in the -2SD.

PC 5 showed a statistically significant difference in bone shape between female participants with hip OA and those without (P = 0.013) where OA participants deviated from the mean ankle complex shape in the negative direction of PC 4 with a mean of -0.005 mm. Negative deviation from the mean ankle complex shape direction as described in figure 6-15 mostly shows a more supinated foot posture when compared to the mean and +2SD images extracted from the 3D SSM, where the calcaneus bone showed a greater inversion motion combined with the internal rotation of the distal tibia seen in the superior view in figure 6-15.

Female PC mode & view	-2SD	Mean shape	+2SD	Observed variation
PC 4 Anterior view	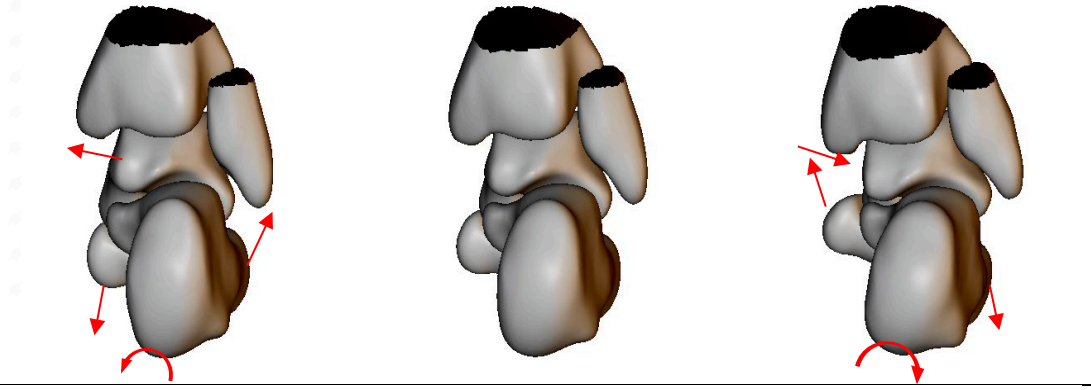			Two views extracted from PC4 of the female model in the posterior view and lateral oblique view. The -2SD showed a pronated foot type with an everted calcaneus, dropped navicular and plantarflexion of the talus compared to the main and +2SD. *Red arrows used to explain the noted motions
PC 4 Posterior View	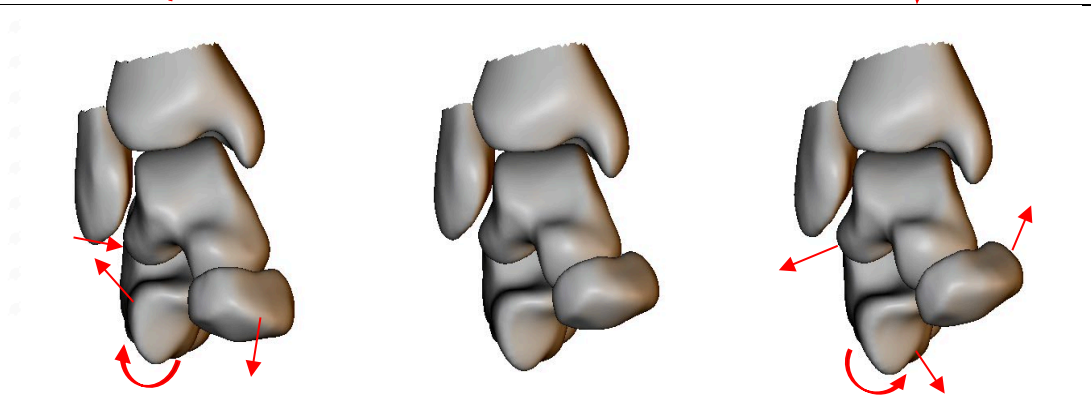			
PC 4 Posterior view	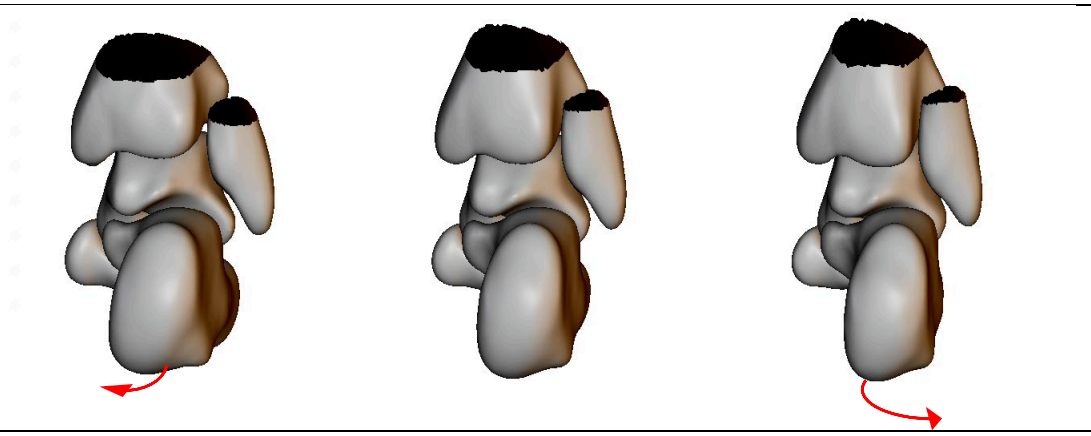			Both the posterior and superior views show In - 2SD the calcaneus is more inverted showing a more supinated rearfoot with a distal tibia that is more rotated internally compered to both the main and the +2SD
PC 4 Superior view	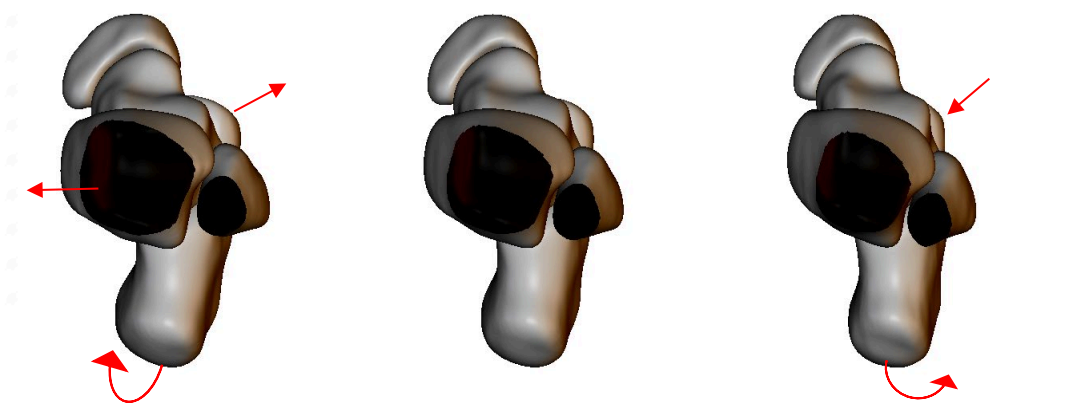			

Figure 6-15. Differences in the bone shape for PC modes that significantly differentiate between female participants with knee and hip OA and those without. All images are extracted from the animated female 3D SSM focusing on the mean, +2SD, and -2SD of bone shape. PC3 showed significant differences between female participants with knee OA and those without, while PC4 showed significant differences between female participants with hip OA and those without.

Chapter 7 Joint space width results

in this chapter, the results of the association between the ankle JSW measurements and other relevant clinical variables are presented using figures and tables. Starting by exploring the confounding variables and then the results of each relationship examined is presented in a separate section.

7.1 Confounding factors

Confounders can distort the association between predictor and outcome variables in cases where the study groups differ significantly with respect to these factors(389). They can be controlled for in the analysis if sufficient information about their status is available(389). The main outcome variables in this analysis are the six JSWs of the ankle joint, which are likely influenced by sex, ethnicity, age, and BMI based on what is seen in studies mentioned in chapter 3. The aim is to explore the association between ankle JSW and other clinical variables, including BMD, knee JSW, and hip JSW, which may also be influenced by sex, age, and BMI (85, 390, 391).

To identify potential confounding factors for example, in the association between ankle JSW and knee JSW, a DAG analysis was performed. The DAG suggested that BMI, sex, age and ethnicity could be confounding factors in this relationship. Since they were found to be associated with both ankle and knee JSW as seen in figure 7-1 below. However, all the participants recruited in this cohort were born in the same year, so controlling for age is not necessary. Also, they all share the same ethnicity background as they are members of a birth cohort. Therefore, only BMI and sex were thought to be potential confounding factors in this analysis. Statistical adjustment was performed by including BMI and sex as covariates in the regression model, which allowed for examination of the association between ankle JSW and knee JSW while controlling for these potential confounding factors.

The DAG analysis for other associations, such as BMD and hip JSW, yielded similar results to that for the knee JSW. As all participants in this cohort were born in the same year and share the same ethnicity background, controlling for age is not necessary in this analysis.

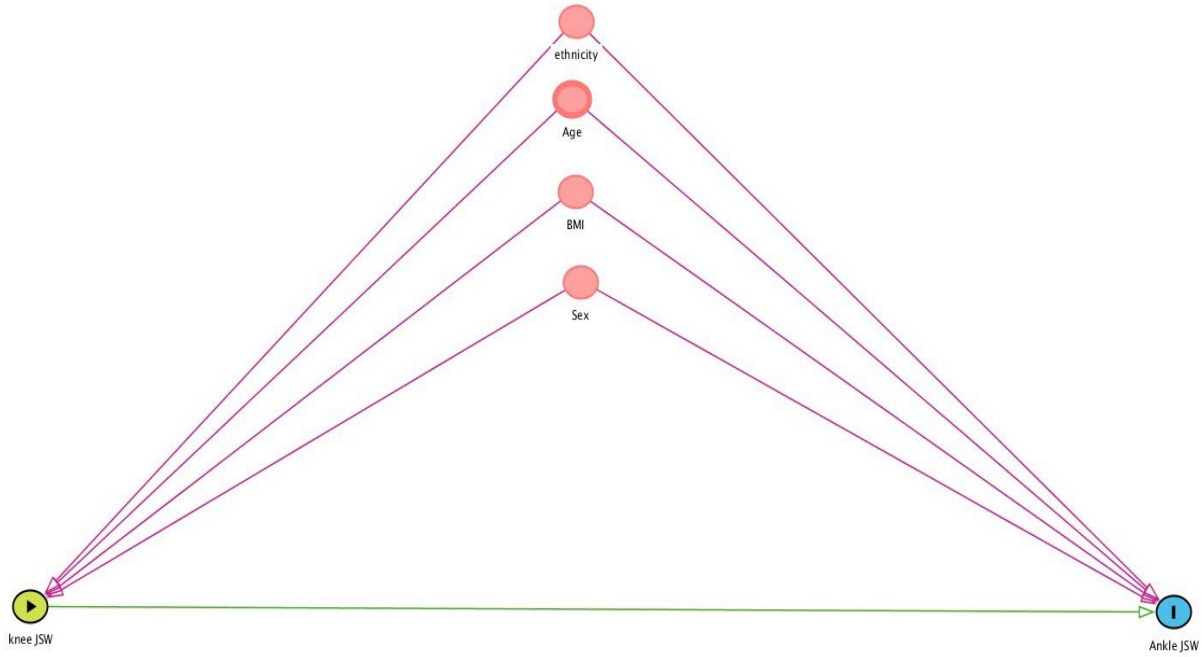

Figure 7-1 shows a Directed Acyclic Graph (DAG) depicting the causal relationships between ankle joint space width (JSW), knee JSW, and potential confounding variables. The graph shows that BMI, age, sex, and ethnicity may be confounding factors in the relationship between ankle JSW and knee JSW. Adjusting for these variables in the statistical analysis can help to control for their effects.

Furthermore, the following section summarizes the relationship between sex and other exposure variables considered for the analysis, such as body scale measurements, joint pain scores, WOMAC scores, OA in the joints and BMD. To assess if sex showed be controlled for when exploring the association with such variables.

7.1.1 Body scale measurements for each sex

Table 7-1 shows the descriptive statistics for the three body scale measurements of height, weight, and BMI in each sex. Differences between males and females regarding those features were assessed using the independent t-test for normally distributed data (height), and the non-parametric alternative Mann Whitney U test was used for the data which is not normally distributed (weight and BMI). Height and weight showed significant differences between sex, but BMI did not as present in figure 7-2 below. Therefore, adjusting for the confounding effect of sex in the subsequent analysis is necessary.

Table 7-1 Descriptive statistics for the three body scale measurements in each

Variable	Male N=83	Female N=123
Height (m) (mean ± SD)	1.73 ± 0.055	1.61 ± 0.06
Weight (Kg) median (IQR)	82.9 (76.1-93.2)	70.2 (62-81.1)
BMI (Kg/m^2) median (IQR)	27.44 (25.30-31.06)	26.79 (23.85-30.63)

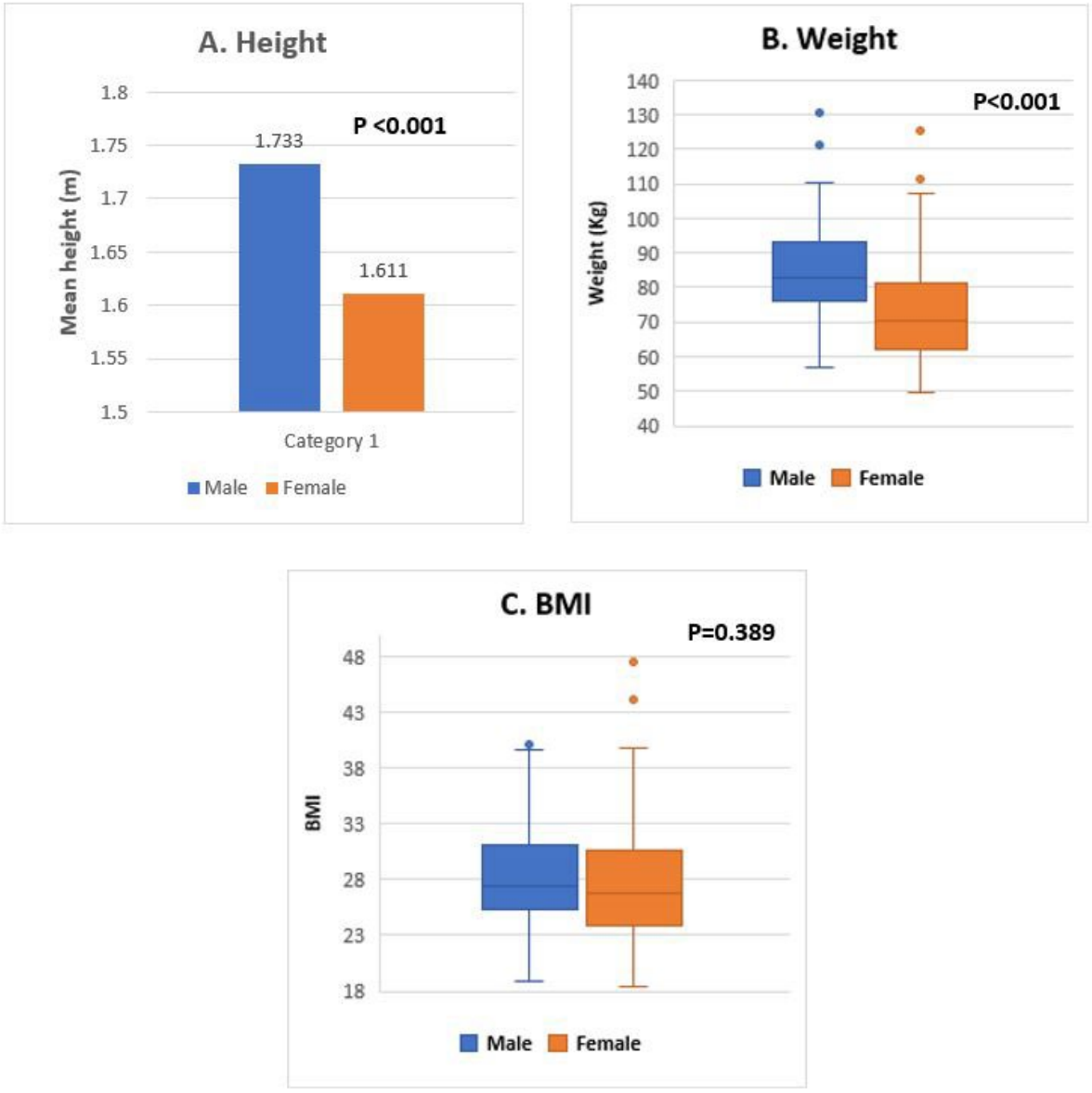

Figure 7-2. Differences in body scale measurements between the sexes: A) bar chart representing mean height (p<0.001); and box plots showing the median and inter-quartile range (IQR) for B) weight (p<0.001) and C) BMI (p=0.389).

To determine if males and females differed significantly regarding the incidence of OA (Figure 7-3) or occurrence of pain in the hip and knee (Figure 7-4), an analysis using Pearson's chi-squared test was conducted. The results showed no significant association between sex and either pain or OA in the joints. Therefore, adjusting for the confounding effect of sex in the subsequent analysis was not deemed to be necessary.

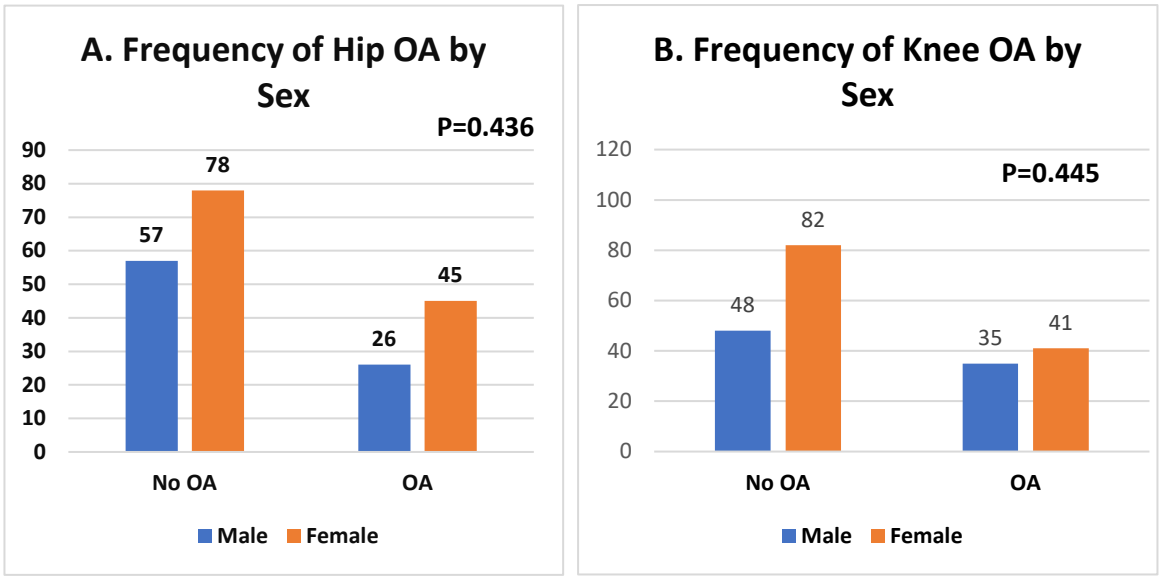

Figure 7-3. Bar charts representing the association between sex and the frequency of OA in: A) the hip (p=0.436) (A); and knee (p=0.445).

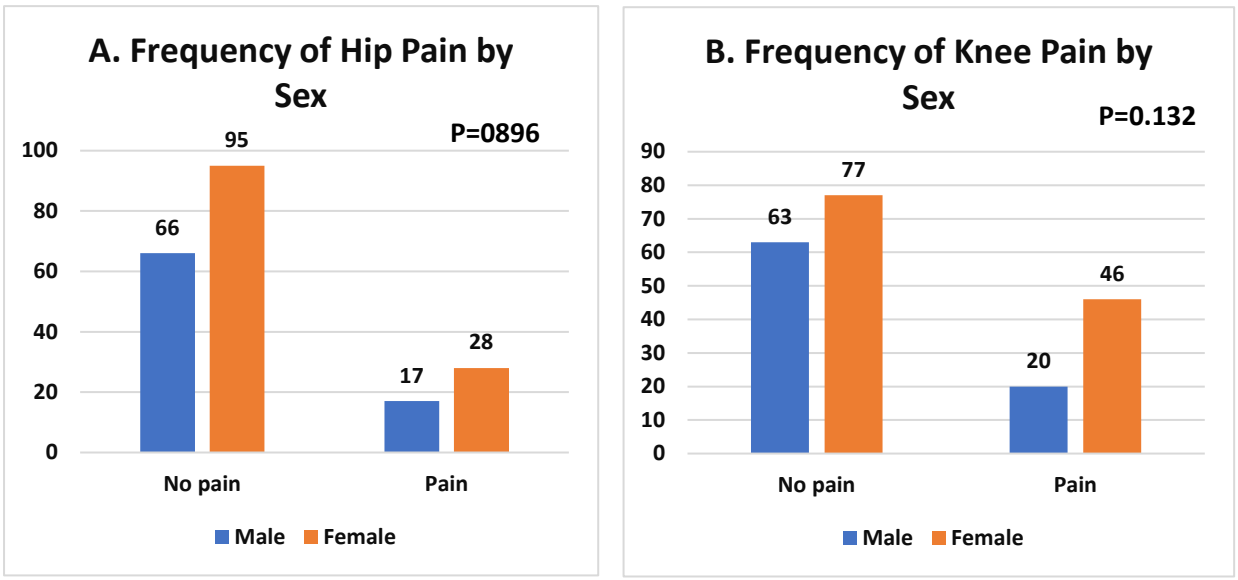

Figure 7-4. Bar charts representing the association between sex and the frequency of joint pain in: A) the hip (p=0.896); and knee (p=0.132).

7.1.2 Sex differences in pain, stiffness. physical activity and overall WOMAC score

The Mann Whitney U test was used to determine whether there were any significant differences between the sexes in the population in four variables obtained from the WOMAC scoring system: pain, stiffness, physical activity and overall WOMAC score. The results presented in table 7-2 below indicate no statistically significant differences between males and females in the variables tested. Therefore, adjusting for the confounding effect of sex in the subsequent analysis was not deemed to be necessary.

Table 7-2. Descriptive statistics for each sex regarding the four potential confounding variables and the results of the Mann Whitney U test.

Variable	Male		Female		p-value
	Median	IQR	Median	IQR	
Pain	4	0-12	3	0-14	0.669
Stiffness	0	0-6	0	0-5	0.818
Physical activity	8	0-25	4	0-41	0.883
Overall WOMAC	12	0-43	11	0-58	0.833

7.1.3 BMD measurements for each sex

Differences between males and females were examined in each of the four BMD measurements. Student's t-test or Mann-Whitney U tests were used according to whether the assumptions of the normality or homogeneity of variance of the data were satisfied. Table 7-3 shows very strongly statistically significant differences in all BMD measures except those for the necks of the right femurs (p= 0.148). Therefore, adjusting for the confounding effect of sex in the subsequent analysis is needed.

Table 7-3 Descriptive statistics and the significance of differences in BMD measurements among each sex.

BMD (g/cm^2)	**Male N=83**	**Female N=123**	**p value**
Spine (mean ± SD)	1.15 ± 0.12	1.00 ± 0.14	<0.001*
Lower limbs (mean ± SD)	1.31 ± 0.12	1.11 ± 0.11	<0.001*
Right femur neck (mean ± SD)	0.93 ± 0.12	0.91 ± 0.13	0.148
Total right femur (median, IQR)	1.03 0.95-1.15	0.95 0.88-1.04	<0.001*

7.2 Association of 3D MRI ankle JSW with participant's sex.

The association between JSW measurements produced from the 3D SSM and participants' sex was assessed using independent t-tests for data which was normally distributed and the non-parametric Mann Whitney U test for that which was not. The results indicate that females had statistically significantly smaller JSWs than males across all six JSW measures which were analyzed, as shown in table 7-4. The Mann Whitney U test compares the entire distributions of the two groups whereas the median values indicate the direction of the difference, and the findings suggest that sex is a significant factor influencing JSW.

Table 7-4. Results of independent t-test and Mann Whitney U test used to test the difference in JSWs between sexes

Ankle JSW (mm)	Male N=83	Female N=123	p value
Tibial plafond (median, IQR)	2.56 (2.26-3.00)	2.19 (1.85-2.59)	<0.001*
Medial malleolus (median, IQR)	3.2 (2.75-3.77)	2.83 (2.34-3.28)	<0.001*
Talonavicular (mean ± SD)	1.50 ± 0.33	1.29 ± 0.34	<0.001*
Tibiofibular (median, IQR)	2.53 (2.18-2.92)	2.29 (1.97-2.71)	0.003*
Subtalar posterior facet (median, IQR)	3.08 (2.56-3.62)	2.49 (2.12-3.00)	<0.001*
Subtalar medial facet (mean ± SD)	4.44 ± 1.28	3.7 ± 1.20	<0.001*

7.3 Association of ankle JSWs with the body anthropometry variables of height, weight, and BMI

To explore the association between ankle JSW measurements produced from the SSM and body anthropometry variables, linear regression modelling was used to determine the relationship between JSW and height, weight, and BMI. That the assumptions of the normality and homoscedasticity of the data were met was ensured by obtaining log values for the tibial plafond, medial malleolus, tibiofibular, and subtalar posterior facet in all models. Two separate models were fitted for each scale: a univariable model and a multivariable model adjusted for sex to remove any confounding effect of this variable.

Univariable models were fitted separately for each JSW measurement as the outcome variable was regressed against height as the predictor variable. The results from the univariable modelling shown as Model 1 in table 7-5 showed a significant association between height and all JSW measurements. However, in the multivariable model adjusted for sex (Model 2 in table 7-5), there were no significant associations between any of the JSW measurements and height. This suggests that the significant association found in the univariable models was driven by the effect of sex in the population.

Univariable models were used to explore the association between weight and each JSW measurement, and significant relationships were found for all JSW measurements except the subtalar medial facet. Full results are designated as Model 1 in table 7-6. However, in the multivariable models adjusted for sex, there were again no significant associations between any of the JSW measurements and weight (Model 2 in table 7-6). These findings are like those for height and indicate that the significant relationship found in the univariable models was driven by the effect of sex in the population.

Statistically significant associations were found between BMI and the ankle joint width space measurements for the talonavicular and medial malleolus. These associations remained significant even after adjustment for sex in the multivariable models. However, no significant relationships were found between BMI and the remaining four ankle JSW. In the multivariable model, the medial malleolus JSW showed a weak positive association with BMI, with a

regression coefficient of 0.006 (P = 0.04), suggesting that a one-unit increase in BMI is associated with an approximate 0.7% increase in medial malleolus JSW. Similarly, the talonavicular JSW showed a weak positive association with BMI, with a coefficient of 0.001 (P = 0.01). Results for both univariable and multivariable models are presented in table 7-7.

It was also important to investigate potential interactions between body anthropometry variables and sex to determine if the effects of these variables on ankle JSWs differ between males and females. Multiple regression models were used to identify any such potential interactions. The results presented in table 7-8 indicate that there were no significant interactions between sex and any of the body scale variables of height, weight, and BMI for any of the JSW measurements.

Table 7-5. Results of the linear regression modelling applied to assess the relationship between height and all ankle JSWs.

Ankle JSW (mm) N=206	Height (cm)							
	Model 1				Model 2			
	Coefficient	95% CI	P	R^2	Coefficient	95% CI	P	R^2
Tibial plafond	0.004	[0.0009, 0.008]	0.015*	0.03	0.003	[-0.001, 0.008]	0.177	0.13
Medial malleolus	0.007	[0.002, 0.011]	0.002*	0.04	0.0009	[-0.006, 0.005]	0.712	0.12
Talonavicular	0.008	[0.002, 0.013]	0.006*	0.03	0.0006	[-0.008, 0.007]	0.864	0.09
Tibiofibular	0.003	[0.0001, 0.007]	0.041*	0.01	0.002	[-0.001, 0.008]	0.206	0.05
Subtalar posterior facet	0.009	[0.003, 0.014]	0.001*	0.04	0.003	[-0.004, 0.010]	0.397	0.09
Subtalar medial facet	0.022	[0.001, 0.043]	0.037*	0.02	0.009	[-0.019, 0.039]	0.510	0.07

Model 1 is the univariable analysis, and Model 2 the multivariable analysis adjusted for sex. Log values were used of the JSWs for the tibial plafond, medial malleolus, tibiofibular and subtalar posterior facets.

Table 7-6. Results of the linear regression modelling applied to assess the relationship between weight and all ankle JSWs.

Ankle JSW (mm) N=206	weight (kg)							
	Model 1				Model 2			
	Coefficient	95% CI	P	R^2	Coefficient	95% CI	P	R^2
Tibial plafond	0.003	[0.0008, 0.005]	0.006*	0.04	0.001	[-0.001, 0.003]	0.298	0.13
Medial malleolus	0.004	[0.001, 0.006]	0.001*	0.06	0.002	[-0.0002, 0.004]	0.080	0.14
Talonavicular	0.006	[0.003, 0.009]	0.001*	0.07	0.004	[-0.0007, 0.007]	0.073	0.12
Tibiofibular	0.001	[0.0005, 0.003]	0.004*	0.01	0.0003	[-0.001, 0.002]	0.770	0.05
Subtalar posterior facet	0.004	[0.002, 0.007]	0.001*	0.09	0.003	[-0.001, 0.006]	0.064	0.11
Subtalar medial facet	0.004	[-0.006, 0.016]	0.402	0.01	0.004	[-0.01, 0.008]	0.529	0.06

Model 1 is the univariable analysis, and Model 2 the multivariable analysis adjusted for sex. Log values were used for the JSWs of the tibial plafond, medial malleolus, tibiofibular, and sub talar posterior facet.

Table 7-7. Results of the linear regression modelling applied to assess the relationship between BMI and all JSWs.

Ankle JSW (mm) N=206	BMI (kg/m²)							
	Model 1				Model 2			
	Coefficient	95% CI	P	R^2	Coefficient	95% CI	P	R^2
Tibial plafond	0.006	[-0.006, 0.01]	0.077	0.03	0.004	[-0.01, 0.01]	0.114	0.12
Medial malleolus	0.007	[0.0003, 0.01]	0.041*	0.04	0.006	[0.001, 0.01]	0.045*	0.13
Talonavicular	0.002	[0.002, 0.02]	0.015*	0.05	0.001	[0.002, 0.02]	0. 016*	0.11
Tibiofibular	0.002	[-0.003, 0.009]	0.375	0.01	0.002	[-0.003, 0.008]	0.417	0.06
Subtalar posterior facet	0.007	[0.0009, 0.01]	0.081	0.03	0.007	[-0.001, 0.01]	0.092	0.10
Subtalar medial facet	-0.007	[-0.04, 0.03]	0.700	0.003	-0.009	[-0.03, 0.02]	0.615	0.07

Model 1 is the univariable analysis, and Model 2 the multivariable analysis adjusted for sex. Log values were used for the JSWs of the tibial plafond, medial malleolus, tibiofibular, and subtalar posterior.

Table 7-8. Results from linear regression applied to assess the interaction between sex and body scale variables: the p values presented are for the interaction term.

Ankle JSW (mm) N=206	Interaction term P value for sex with body scale variables on ankle JSW		
	Height	Weight	BMI
	P-value	P-value	P-value
Tibial plafond	p=0.369	p=0.408	p=0.299
Medial malleolus	p=0.416	p=0.351	p=0.263
Talonavicular	p=0.090	p=0.933	p=0.343
Tibiofibular	p=0.871	p=0.503	p=0.487
Subtalar posterior facet	p=0.307	p=0.935	p=0.843
Subtalar medial facet	p=0.498	p=0.252	p=0.425

Owing to the potential lack of statistical power relating to the interaction term, the decision was made to stratify the data according to the participant's sex. The aim of this was to provide a more detailed explanation of the relationships between the three body scale measurements and the morphological variation in JSW in both sexes. Therefore, linear regression models were applied after separating the data according to sex so as to assess the relationships between height, weight, and BMI and the JSW of all ankle joints for each sex separately.

No significant associations were found in either sex between any of the JSWs and height or weight, as shown in tables 7-9 and 7-10 respectively. The stratified results are thus fully consistent with the results of the multivariable analysis where the data were adjusted for sex as presented above.

Only the JSWs for the medial malleolus and the talonavicular showed significant associations with BMI in females, but this was not the case in males and no other associations were found in either males or females in the remaining joints. These results indicate that the significant associations noted in the combined model with BMI shown in table 7-7 were stronger in the female population. These findings are illustrated in table 7-11.

Table 7-9. Results of the linear regression modelling applied to assess the relationship between height and all JSWs for males and females separately.

Ankle JSW (mm)	Height (cm)					
	Male (N=83)			Female (N=123)		
	Coefficient	95% CI	P	Coefficient	95% CI	P
Tibial plafond	0.002	[-0.0005, 0.005]	0.108	0.005	[-0.001, 0.011]	0.113
Medial malleolus	0.008	[-0.019, 0.035]	0.569	0.013	[-0.005, 0.031]	0.164
Talonavicular	0.009	[-0.004, 0.022]	0.179	0.006	[-0.003, 0.019]	0.241
Tibiofibular	0.007	[-0.012, 0.027]	0.461	0.008	[-0.009, 0.024]	0.353
Subtalar posterior facet	0.006	[-0.006, 0.018]	0.339	0.0006	[-0.007, 0.008]	0.875
Subtalar medial facet	0.004	[-0.035, 0.046]	0.882	0.017	[-0.018, 0.052]	0.338

Log values were used for the JSWs of the tibial plafond and subtalar posterior facets.

Table 7-10. Results of the linear regression modelling applied to assess the relationship between weight and all JSWs for males and females separately.

Ankle JSW (mm)	Weight (kg)					
	Male (N=83)			Female (N=123)		
	Coefficient	95% CI	P	Coefficient	95% CI	P
Tibial plafond	0.0005	[-0.008, 0.009]	0.911	0.001	[-0.001, 0.003]	0.193
Medial malleolus	0.006	[-0.003, 0.004]	0.730	0.008	[-0.002, 0.011]	0.060
Talonavicular	0.003	[-0.001, 0.009]	0.163	0.004	[-0.0003, 0.001]	0.057
Tibiofibular	0.002	[-0.010, 0.006]	0.635	0.009	[-0.005, 0.003]	0.552
Subtalar posterior facet	0.003	[-0.002, 0.008]	0.253	0.003	[-0.0006, 0.006]	0.086
Subtalar medial facet	0.005	[-0.02, 0.15]	0.613	0.009	[-0.005, 0.024]	0.219

Log values were used for the JSWs of the tibial plafond, medial malleolus, and subtalar posterior facets.

Table 7-11. Results of the linear regression modelling applied to assess the relationship between BMI and all JSWs for males and females separately.

Ankle JSW (mm)	BMI (kg2M)					
	Male (N=83)			Female (N=123)		
	Coefficient	95% CI	P	Coefficient	95% CI	P
Tibial plafond	0.002	[-0.02, 0.03]	0.852	0.007	[-0.0004, 0.014]	0.063
Medial malleolus	0.002	[-0.01, 0.012]	0.758	0.028	[0.004, 0.051]	0.018*
Talonavicular	0.007	[-0.001, 0.24]	0.372	0.013	[0.001, 0.024]	0.025*
Tibiofibular	0.0007	[-0.01, 0.001]	0.881	0.004	[-0.003, 0.010]	0.323
Subtalar posterior facet	0.005	[-0.01, 0.02]	0.522	0.008	[-0.001, 0.01]	0.096
Subtalar medial facet	-0.012	[-0.05, 0.07]	0.709	-0.018	[-0.05, 0.02]	0.378

Log values were used for the JSWs of the tibial plafond, medial malleolus, and subtalar posterior facets.

7.4 Association of ankle JSW with knee clinical variables of pain, OA, and radiographic mJSW

The relationship between contemporaneously reported knee pain and morphological variations in ankle JSWs for all joints included was examined. The aim was to investigate if participants with knee pain had different ankle JSW values compared to those without knee pain. Independent t-tests were used when both groups of data were normally distributed with homogeneity of variances. When these assumptions were not met, the non-parametric Mann Whitney U test was used. The results presented in table 7-12 below indicate that ankle JSWs did not differ significantly between participants with and without reported knee pain.

The differences in ankle JSWs between participants with and without knee OA was then explored, with independent t-tests or Mann-Whitney U tests used to investigate the differences between all ankle JSWs and OA of the knee joint. As shown in table 7-13, the OA group showed narrower JSW in most of the joints compared to the non-OA. However, no significant differences were found in between participants diagnosed with OA (K&L grade ≥ 2 in the dominant knee) and those without OA (K&L grade < 2) in any of the ankle JSW.

Table 7-12. Results of tests for differences in ankle JSWs based on knee pain.

Ankle JSW (mm)	Pain in the knee No N=140	Pain in the knee Yes N=66	P-value
Tibial plafond (mean ± SD)	2.42 ± 0.59	2.41 ± 0.55	0.907
Medial malleolus (median, IQR)	3.00 (2.51-3.44)	3.07 (2.55-3.58)	0.800
Talonavicular (mean ± SD)	1.37 ± 0.35	1.39 ± 0.34	0.717
Tibiofibular (median, IQR)	2.40 (2.07-2.85)	2.24 (1.87-2.94)	0.303
Subtalar posterior facet (median, IQR)	2.70 (2.25-3.32)	2.65 (2.17-3.16)	0.550
Subtalar medial facet (mean ± SD)	4.12 ± 1.36	4.02 ± 1.23	0.626

Table 7-13. Results of tests for differences in JSWs based on knee OA status.

Ankle JSW (mm)	Non-OA N=130	OA N=76	P value
Tibial plafond (mean ± SD)	2.44 ± 0.55	2.36 ± 0.57	0.321
Medial malleolus (median, IQR)	3.01 (2.43 - 3.44)	3.09 (2.70 - 3.50)	0.171
Talonavicular (mean ± SD)	1.40 ± 0.33	1.35 ± 0.37	0.491
Tibiofibular (median, IQR)	2.49 (2.07-2.85)	2.36 (1.87-2.94)	0.316
Subtalar posterior facet (median, IQR)	2.78 (2.29-3.34)	2.61 (2.08-3.17)	0.096
Subtalar medial facet (mean ± SD)	3.99 ± 1.23	4.17 ± 1.29	0.879

Another aim of this study was to investigate the relationship between the JSWs of the joints in the ankle complex region and knee mJSWs using linear regression models. The log values for the tibial plafond, medial malleolus, and subtalar posterior facet were obtained since the assumptions of the normality and homoscedasticity were not met, and two models were fitted for each side: a univariable model and a multivariable model adjusted for sex and BMI.

The results presented in table 7-14 show that all ankle JSWs were significantly associated with the right knee mJSWs in the univariable model, except for the tibiofibular and subtalar medial facet. After adjustment for sex and BMI in the multivariable model, only the associations of the JSWs of the tibial plafond and subtalar posterior facet remained significant at b= 0.04 (P = 0.035) and b= 0.08 (P = 0.001) respectively. This suggests that a 4% increase in tibial plafond JSW and an 8% increase in subtalar posterior facet JSW is associated with a 1 mm increase in right knee mJSW, as the regression models were applied using log values of data for these joint space widths.

For the left knee mJSW, the univariable model showed significant associations with all ankle JSWs except for that of the subtalar medial facet. However, after adjusting for confounders in the multivariable model, no significant associations were noted with any ankle JSWs. The results are presented in table 7-15.

Finally, the association between ankle JSWs and the ipsilateral knee mJSW (also the side of the dominant ankle that was scanned) was also examined. The univariable model showed significant associations between all ankle JSWs and ipsilateral knee mJSW, except for that of the subtalar medial facet. However, the multivariable model adjusted for sex and BMI showed similar results as for the right knee JSW model, with only the JSWs of the tibial plafond and subtalar posterior facet retaining significant relationships. This may be because only 20 participants had the left dominant ankle scanned and therefore did not differ significantly from the results for the right knee mJSW. The results are presented in table 7-16.

Table 7-14. Results of the linear regression modelling applied to assess the relationships between right knee mJSW and all ankle JSWs.

Ankle JSW (mm) N=206	Right knee mJSW (mm)							
	Model 1				Model 2			
	Coefficient	95% CI	P	R^2	Coefficient	95% CI	P	R^2
Tibial plafond	0.05	[0.018, 0.091]	0.003*	0.05	0.04	[0.0008, 0.07]	0.035*	0.15
Medial malleolus	0.05	[0.008, 0.09]	0.017*	0.03	0.03	[-0.01, 0.06]	0.168	0.14
Talonavicular	0.06	[0.004, 0.11]	0.034*	0.03	0.03	[-0.02, 0.09]	0. 195	0.14
Tibiofibular	0.06	[-0.02, 0.15]	0.152	0.01	0.04	[-0.05, 0.13]	0.404	0.06
Subtalar posterior facet	0.094	[0.07, 0.12]	<0.001*	0.07	0.089	[0.03, 0.14]	0.001*	0.14
Subtalar medial facet	-0.05	[-0.26, 0.14]	0.582	0.004	-0.07	[-0.28, 0.13]	0.490	0.09

Model 1 represents the univariable analysis, while Model 2 is the multivariable analysis adjusted for sex and BMI. Log values were obtained of the JSWs for the tibial plafond, medial malleolus, tibiofibular, and subtalar posterior facet.

Table 7-15. Results of the linear regression modelling applied to assess the relationships between left knee mJSW and all ankle JSWs.

Ankle JSW (mm) N=206	Left knee mJSW (mm)							
	Model 1				Model 2			
	Coefficient	95% CI	P	R^2	Coefficient	95% CI	P	R^2
Tibial plafond	-0.36	[-0.56, -0.17]	0.002*	0.06	-0.19	[-0.37, 0.002]	0.055	0.20
Medial malleolus	0.046	[0.016, 0.076]	0.005*	0.04	0.020	[-0.009, 0.049]	0.182	0.18
Talonavicular	0.056	[0.018, 0.095]	0.009*	0.04	0.027	[-0.010, 0.066]	0.159	0.14
Tibiofibular	-0.12	[-0.31, 0.05]	0.172	0.01	-0.07	[-0.25, 0.11]	0.457	0.14
Subtalar posterior facet	0.047	[0.002, 0.093]	0.039*	0.02	0.033	[-0.010, 0.077]	0.135	0.15
Subtalar medial facet	-0.078	[-0.27, 0.11]	0.429	0.003	-0.18	[-0.37, 0.005]	0.057	0.10

Model 1 represents the univariate analysis, and Model 2 is the multivariate analysis adjusted for sex and BMI. Log values were obtained of the JSWs for the tibial plafond, medial malleolus, and subtalar posterior facet.

Table 7-16. Results of the linear regression modelling applied to assess the relationships between Ipsilateral knee mJSW and all ankle JSWs.

Ankle JSW (mm) N=206	Ipsilateral knee mJSW (mm)							
	Model 1				Model 2			
	Coefficient	95% CI	P	R^2	Coefficient	95% CI	P	R^2
Tibial plafond	0.055	[0.019, 0.091]	0.003*	0.04	0.038	[0.002, 0.074]	0.038*	0.15
Medial malleolus	0.049	[0.009, 0.089]	0.016*	0.03	0.028	[-0.011, 0.068]	0.160	0.14
Talonavicular	0.063	[0.008, 0.11]	0.024*	0.02	0.040	[-0.014, 0.096]	0.151	0.13
Tibiofibular	0.063	[-0.023, 0.15]	0.153	0.01	0.041	[-0.049, 0.13]	0.374	0.06
Subtalar posterior facet	0.094	[0.046, 0.14]	<0.001*	0.07	0.082	[0.032, 0.13]	0.001*	0.13
Subtalar medial facet	-0.054	[-0.26, 0.15]	0.602	0.002	-0.078	[-0.28, 0.13]	0.462	0.09

Model 1 represents the univariate analysis, and Model 2 is the multivariate analysis adjusted for sex and BMI. Log values were obtained of the JSWs for the tibial plafond, medial malleolus, and subtalar posterior facet.

To explore the potential effect modification of sex on the relationship between knee mJSW variables quantified from the right, left and ipsilateral knee and ankle JSWs, a linear regression analysis was conducted which included an interaction term between knee JSW and sex. The results presented in table 7-17 show that the interaction term was not statistically significant in any of the analyses, indicating that no evidence could be found of sex modifying the association between ankle JSWs and knee mJSW.

Table 7-17. Results for the interaction term from linear regression applied to assess the interaction between sex and knee mJSW: the P values presented are for the interaction term.

	Interaction term P value for sex with knee joints on ankle JSW		
Ankle JSWs (mm) N=206	**Right knee mJSW**	**Left knee mJSW**	**Ipsilateral knee mJSW**
	P-value	**P-value**	**P-value**
Tibial plafond	p=0.574	p=0.389	p=0.593
Medial malleolus	p=0.669	p=0.553	p=0.656
Talonavicular	p=0.725	p=0.255	p=0.774
Tibiofibular	p=0.932	p=0.793	p=0.866
Subtalar posterior facet	p=0.447	p=0.462	p=0.442
Subtalar medial facet	p=0.749	p=0.653	p=0.721

Even though no significant interaction was observed, the data were stratified according to each participant's sex to gain a more in-depth explanation of the effect of sex on the association between knee mJSW and ankle JSW. The regression models were then run again for each sex separately to assess the association between ankle JSWs and Knee mJSW quantified from the right, left, and ipsilateral knee to the scanned ankle. For each group, two models were produced: a univariable Model 1; and a multivariable Model 2 adjusted for BMI.

Because assumptions of the normality and homoscedasticity of the data were not met, log values for the female participants of the tibial plafond, medial malleolus, and subtalar posterior facet were obtained. Table 7-18 shows that only the tibial plafond JSW had a significant association with left knee mJSW in the univariable model (R^2 = 0.04, *b* = -0.053, P = 0.04). However, this association disappeared in the multivariable model (R^2 = 0.06, *b* = -0.043, P = 0.113). The subtalar posterior facet was the only joint that showed significant association before and after adjustment with the right knee JSW (R^2 = 0.07, *b* = 0.077, P = 0.025). Similar results were noted in the ipsilateral knee, as only 10 females had their left dominant ankles scanned.

In the male population, after the normality and homoscedasticity assumptions were not supported, log values of the JSWs of the tibial plafond, medial malleolus, and subtalar posterior facet were obtained. For each ankle JSW, linear regression models were applied with the right, left, and ipsilateral knee mJSW as the independent variable. Table 7-19 shows that the tibial plafond had a trend similar to what is noted with the right knee mJSW in the combined analysis for both sexes. However, the association was not significant (R^2 = 0.05, *b* = 0.044, P = 0.08). In contrast, the subtalar posterior facet did have a significant association with the right knee mJSW measurements (R^2 = 0.09, *b* = 0.098, P = 0.015).

The left knee mJSW did not show any significant association with any of the ankle JSWs. However, the mJSW value of ipsilateral knee to the ankle scanned showed similar results as the right knee model, possibly due to only 10 participants having their left ankle scanned.

Overall, the results from the stratified data follow a similar trend to the combined data, where the data did not show differences in the association between both males and females. The only slight differences are related to the p-value, where it is higher in the stratified data which could be due to the loss of statistical power after stratifying the data. However, the magnitude and direction of the association were comparable especially for both the tibial plafond and the subtalar posterior facet, as seen in the results of the combined model.

Table 7-18. Results of the linear regression modelling applied to assess the relationship between right, left, and ipsilateral knee mJSW with ankle JSWs in the female population.

Ankle JSWs (mm) Female n= (123)	Right knee mJSW		Left knee mJSW		Ipsilateral knee mJSW	
	Model 1	Model2	Model 1	Model2	Model 1	Model 2
	Coefficient 95%CI	Coefficient 95%CI	Coefficient 95%CI	Coefficient 95%CI	Coefficient 95%CI	Coefficient 95%CI
Tibial plafond	0.033 (-0.03, 0.08)	0.036 (-0.035, 0.08)	-0.053* (-0.10, -0.0003)	-0.043 (-0.09, 0.01)	0.052 (-0.001, 0.10)	0.049 (-0.004, 0.10)
Medial malleolus	0.013 (-0.04, 0.07)	0.019 (-0.03, 0.07)	0.013 (-0.04, 0.07)	0.002 (-0.05, 0.06)	0.014 (-0.05, 0.07)	0.018 (-0.04, 0.07)
Talonavicular	0.036 (-0.04, 0.10)	0.043 (-0.03, 0.12)	0.03 (-0.05, 0.11)	0.008 (-0.07, 0.09)	0.038 (-0.04, 0.11)	0.044 (-0.03, 0.12)
Tibiofibular	0.027 (-0.10, 0.15)	0.033 (-0.09, 0.016)	-0.07 (-0.20, 0.06)	-0.056 (-0.19, 0.08)	0.022 (-0.10, 0.15)	0.028 (-0.10, 0.15)
Subtalar posterior facet	0.08* (0.01, 0.14)	0.077* (0.009, 0.14)	0.004 (-0.06, 0.06)	0.013 (-0.05, 0.08)	0.082* (0.01, 0.15)	0.079* (0.011, 0.14)
Subtalar medial facet	-0.09 (-0.37, 0.18)	-0.10 (-0.38, 0.17)	-0.15 (-0.44, 0.13)	-0.19 (-0.49, 0.10)	-0.10 (-0.38, 0.17)	-0.11 (-0.39, 0.16)

Model 1 represents the univariable analysis, and Model 2 is the multivariable analysis adjusted for BMI. Log values of the JSWs were obtained for the tibial plafond, medial malleolus, and subtalar posterior facet.

Table 7-19. Results of the linear regression modelling applied to assess the relationship between right, left, and ipsilateral knee mJSW with ankle JSWs in the female population.

Ankle JSWs (mm) Male N = (83)	Right knee mJSW		Left knee mJSW		Ipsilateral knee mJSW	
	Model 1	Model2	Model 1	Model2	Model 1	Model 2
	Coefficient 95%CI	Coefficient 95%CI	Coefficient 95%CI	Coefficient 95%CI	Coefficient 95%CI	Coefficient 95%CI
Tibial plafond	0.041 (-0.007, 0.09)	0.045 (-0.005, 0.09)	-0.022 (-0.07, 0.02)	-0.022 (-0.07, 0.02)	0.041 (-0.007, 0.09)	0.048 (-0.003, 0.10)
Medial malleolus	0.026 (-0.02, 0.07)	0.030 (-0.02, 0.08)	0.011 (-0.03, 0.06)	0.014 (-0.03, 0.06)	0.26 (-0.02, 0.07)	0.031 (-0.02, 0.08)
Talonavicular	0.027 (-0.05, 0.10)	0.040 (-0.04, 0.12)	0.035 (-0.04, 0.11)	0.046 (-0.03, 0.12)	0.32 (-0.04, 0.11)	0.44 (-0.03, 0.12)
Tibiofibular	0.044 (-0.08, 0.17)	0.48 (-0.08, 0.18)	-0.046 (-0.17, 0.07)	-0.048 (-0.17, -0.08)	0.048 (-0.07, 0.17)	0.052 (-0.07, 0.18)
Subtalar posterior facet	0.089* (0.012, 0.16)	0.98* (0.019, 0.17)	0.044 (-0.03, 0.12)	0.049 (-0.03, 0.13)	0.087* (0.011, 0.16)	0.096* (0.02, 0.17)
Subtalar medial facet	-0.037 (-0.34, 0.27)	-0.013 (-0.33, 0.30)	-0.25 (-0.55, 0.04)	-0.24 (-0.55, 0.06)	-0.031 (-0.33, 0.27)	-0.008 (-0.32, 0.31)

Model 1 represents the univariable analysis, and Model 2 is the multivarible analysis adjusted for BMI. Log values of the JSWs were obtained for the tibial plafond, medial malleolus and subtalar posterior facet.

7.5 Association of ankle JSW with clinical variables of hip pain, OA, and radiographic JSW

One of the aims in this study is to investigate the differences in ankle JSWs between participants with hip pain and those without. Data for hip pain were obtained from a clinical questionnaire in which participants were asked to report whether or not they experienced hip pain. The independent t-test was used when date for both was normally distributed and had homogeneous variance. When these conditions were not met, the Mann-Whitney U test was applied. The results presented in table 7-20 show no statistically significant differences in ankle JSWs between participants with and without hip pain.

In addition, the differences in ankle JSWs between participants with hip OA (Croft grade ≥2 in the dominant hip) and those without (Croft grade <2) were explored using t-tests or Mann-Whitney U tests. The results show significant differences in the JSWs of three of the six ankle joints: the tibial plafond, tibiofibular, and subtalar posterior facets (P = 0.035, 0.015, and 0.002 respectively). The participants with hip OA had smaller joint spaces in all ankle joints compared to those without hip OA; more detailed results are presented in table 7-21.

To determine whether the differences in ankle JSWs between participants with and without hip OA varied according to sex, the data were stratified according to sex and the same tests as before were applied. The results in table 7-22 show that male OA participants had smaller ankle JSWs compared to the non-OA group across all ankle joints, with the most significant differences observed in the tibial plafond, tibiofibular, and subtalar posterior facets JSW (P = 0.042, 0.014, and 0.005, respectively). Moreover, similar trends were observed in the female population, where those with hip OA had narrower ankle JSWs as shown in table 7-23, but no significant differences in mean ankle JSWs were observed between the hip OA and non-OA groups. This indicates that the significant differences in the combined analysis are related more to the male population.

Table 7-20. Results of tests for differences in ankle JSWs based on hip pain.

Ankle JSW (mm)	No N=161	Yes N=45	P value
Tibial plafond (median, IQR)	2.39 (1.97 - 2.81)	2.37 (2.05-2.66)	0.796
Medial malleolus (median, IQR)	3.08 (2.58-3.48)	2.83 (2.52, 3.38)	0.403
Talonavicular (mean ± SD)	1.37 ± 0.30	1.38 ± 0.36	0.972
Tibiofibular (median, IQR)	2.37 (2.03-2.85)	2.49 (2.18-2.93)	0.476
Subtalar posterior facet (median, IQR)	2.69 (2.25-3.32)	2.69 (2.14-3.13)	0.429
Subtalar medial facet (mean ± SD)	4.23 ± 1.43	4.00 ± 1.22	0.294

Table 7-21. Results of tests for differences in ankle JSWs based on hip OA status.

Ankle JSW (mm)	No N=135	Yes N=71	P value
Tibial plafond (median, IQR)	2.45 (2.11-2.78)	2.14 (1.84-2.70)	0.035*
Medial malleolus (median, IQR)	3.09 (2.61-3.59)	3.02 (2.35-3.38)	0.134
Talonavicular (mean ± SD)	1.40 ± 0.34	1.33 ± 0.36	0.211
Tibiofibular (median, IQR)	2.48 (2.12-2.92)	2.23 (1.97-2.63)	0.015*
Subtalar posterior facet (median, IQR)	2.83 (2.32-3.34)	2.52 (2.03-3.08)	0.002*
Subtalar medial facet (mean ± SD)	4.09 ± 1.31	3.99 ± 1.19	0.589

Table 7-22. Results of tests for differences in JSWs based on hip OA in the male population.

Ankle JSW (mm) Male N=83	Non-hip OA N=57	Hip OA N=26	P value
Tibial plafond (mean ± SD)	(2.72 ± 0.55)	(2.46 ± 0.54)	0.042*
Medial malleolus (median, IQR)	3.33 (2.83-3.51)	3.25 (2.63-3.39)	0.599
Talonavicular (mean ± SD)	(1.52 ± 0.35)	(1.45 ± 0.28)	0.393
Tibiofibular (mean ± SD)	(2.68 ± 0.47)	(2.38 ± 0.50)	0.014*
Subtalar posterior facet (median, IQR)	3.17 (2.73-3.42)	2.06 (1.92-2.78)	0.005*
Subtalar medial facet (mean ± SD)	4.53 ± 1.31	4.25 ± 1.19	0.368

Table 7-23. Results tests for the difference in JSWs based on hip OA in the female population.

Ankle JSW (mm) Female N=123	Non-OA N=78	OA N=45	P value
Tibial plafond (median, IQR)	2.27 (2.12-2.64)	2.11 (1.96-2.44)	0.227
Medial malleolus (median, IQR)	2.94 ± 0.70	2.73 ± 0.71	0.113
Talonavicular (mean ± SD)	1.31 ± 0.31	1.27 ± 0.38	0.481
Tibiofibular (median, IQR)	2.41 ± 0.54	2.28 ± 0.59	0.225
Subtalar posterior facet (median, IQR)	2.59 (2.30- 2.71)	2.25 (2.04-2.55)	0.105
Subtalar medial facet (mean ± SD)	3.77 ± 1.22	3.83 ± 1.18	0.768

Another aim of this study was to investigate the relationship between the JSWs of the joints in the ankle complex region and radiographic hip JSW using linear regression models. The log values for the tibial plafond, medial malleolus, tibiofibular, and subtalar posterior facet were obtained since assumptions of the normality and homoscedasticity of this data were not supported. Two models were fitted for each side separately: a univariable model and a multivariable model adjusted for sex and BMI.

Table 7-24 below shows that only the medial malleolus and subtalar medial facet showed no significant associations with the JSW measured in the right hip; however, all of the remaining ankle JSWs showed significant positive association with the right hip's JSW in the univariable model. Also, after adjustment for the confounding effects of sex and BMI, the associations found remained significant, to the greatest extent for the subtalar posterior at a p-value 0.003 with a coefficient of 0.08 and an R^2 of 18%. As the regression model was applied to the log value of this JSW, a coefficient of 0.08 should be interpreted as an 8% increase in the subtalar posterior JSW for every 1mm increase in the right hip's JSW.

Furthermore, none of the associations between ankle JSWs and the left hip's JSW were statistically significant in either the univariable or multivariable models. Only the talonavicular JSW showed a borderline significant association with the left hip's JSW in the final adjusted model (R^2 = 0.14, *b* = 0.06, P = 0.052). The results are shown in table 7-25.

Finally, the associations between all ankle JSWs and the JSW of the hip on the same side as the dominant foot (ipsilateral hip) were examined. The results of the fitting of the regression models were consistent with those obtained from the right hip JSW measurements, but since only 20 participants had a left-dominant foot this scarcely affected the results. Results of both models are presented in table 7-26.

Table 7-24. Results of linear regression applied to assess the associations between ankle JSWs and right hip JSW.

Ankle JSW (mm) N=206	Right hip JSW (mm)							
	Model 1				Model 2			
	Coefficient	95% CI	P	R^2	Coefficient	95% CI	P	R^2
Tibial plafond	0.049	[0.005, 0.09]	0.027*	0.03	0.042	[0.002, 0.082]	0.032*	0.21
Medial malleolus	0.040	[-0.009, 0.09]	0.111	0.01	0.029	[-0.016, 0.076]	0.205	0.15
Talonavicular	0.09	[0.026, 0.15]	0.006*	0.04	0.077	[0.018, 0.13]	0. 011*	0.16
Tibiofibular	0.044	[0.001, 0.08]	0.041*	0.02	0.042	[0.004, 0.081]	0.030*	0.13
Subtalar posterior facet	0.090	[0.031, 0.14]	0.002*	0.05	0.080	[0.027, 0.13]	0.003*	0.18
Subtalar medial facet	-0.07	[-0.31, 0.17]	0.574	0.001	-0.11	[-0.34, 0.11]	0.335	0.09

Model 1 represents the univariable analysis and model 2 the multivariable analysis adjusted for sex and BMI. Regression models were applied to the log values of the JSWs for the tibial plafond, medial malleolus, tibiofibular and subtalar posterior facet.

Table 7-25. Results of linear regression applied to assess the associations between ankle JSWs and left hip JSW.

Ankle JSW (mm) N=206	Left hip JSW (mm)							
	Model 1				Model 2			
	Coefficient	95% CI	P	R^2	Coefficient	95% CI	P	R^2
Tibial plafond	0.013	[-0.029, 0.056]	0.532	0.001	0.013	[-0.022, 0.051]	0.468	0.12
Medial malleolus	0.016	[-0.035, 0.061]	0.588	0.001	0.008	[-0.036, 0.052]	0.716	0.10
Talonavicular	0.063	[0.002, 0.12]	0.042*	0.02	0.057	[-0.0005, 0.11]	0.052	0.13
Tibiofibular	0.018	[-0.022, 0.059]	0.375	0.003	0.022	[-0.016, 0.060]	0.261	0.11
Subtalar posterior facet	0.037	[-0.017, 0.091]	0.180	0.009	0.032	[-0.019, 0.083]	0.220	0.12
Subtalar medial facet	-0.019	[-0.25, 0.21]	0.871	0.0003	-0.025	[-0.25, 0.20]	0.824	0.08

Model 1 represents the univariate analysis and Model 2 the multivariable analysis adjusted for sex and BMI. Regression models were applied to the log values of the JSWs for the tibial plafond, medial malleolus, tibiofibular and subtalar posterior facet.

Table 7-26. Results of linear regression applied to assess the associations between ankle JSWs and left hip JSW.

Ankle JSW (mm) N=206	Ipsilateral hip JSW (mm)							
	Model 1				Model 2			
	Coefficient	95% CI	P	R^2	Coefficient	95% CI	P	R^2
Tibial plafond	0.05	[0.006, 0.09]	0.023*	0.04	0.041	[0.002, 0.079]	0.030*	0.21
Medial malleolus	0.043	[-0.004, 0.09]	0.074	0.02	0.033	[-0.011, 0.07]	0.141	0.15
Talonavicular	0.083	[0.022, 0.14]	0.008*	0.03	0.071	[0.014, 0.12]	0.015*	0.15
Tibiofibular	0.044	[0.003, 0.084]	0.033*	0.02	0.040	[0.002, 0.078]	0.038*	0.14
Subtalar posterior facet	0.086	[0.032, 0.14]	0.002*	0.05	0.077	[0.024, 0.12]	0.004*	0.17
Subtalar medial facet	-0.042	[-0.27, 0.19]	0.723	0.0007	-0.085	[-0.31, 0.14]	0.457	0.09

Model 1 represents the univariate analysis and Model 2 the multivariable analysis adjusted for sex and BMI. Regression models were applied to the log values of the JSWs for the tibial plafond, medial malleolus, tibiofibular and subtalar posterior facet.

To explore the potential interaction of sex with the relationship between hip JSW variables quantified from the right, left and ipsilateral hip and ankle JSWs, linear regression analysis was conducted which included an interaction term between hip JSW and sex. This approach allowed for the examination of the effect of hip JSW on ankle JSW while accounting for potential differences in this relationship between males and females. The results presented in tables 7-27, show that the interaction term only had a significant effect on JSWs of the tibial plafond and subtalar posterior facet for both the right and ipsilateral hip.

Table 7-27. Results of linear regression applied to assess the interaction between sex and hip JSW on ankle JSW : the P values presented are for the interaction term

Ankle JSWs (mm) N=206	Interaction term P value for sex with hip JSW on ankle JSW		
	Right hip JSW	Left hip JSW	Ipsilateral hip JSW
	P-value	P-value	P-value
Tibial plafond	p=0.007*	p=0.787	p=0.007*
Medial malleolus	p=0.503	p=0.760	p=0.512
Talonavicular	p=0.865	p=0.256	p=0.927
Tibiofibular	p=0.165	p=0.510	p=0.209
Subtalar posterior facet	p=0.014*	p=0.549	p=0.020*
Subtalar medial facet	p=0.203	p=0.179	p=0.167

As a result of the significant interaction noted in the above analysis, and to gain a more in-depth explanation of the effect of sex on the association between hip JSW and ankle JSW, the data was stratified according to the participants' sex. Subsequently, the regression models were run again on each sex group separately so as to assess the association between ankle JSWs and hip JSW quantified from the right, left, and ipsilateral hip to the scanned ankle. In both groups two models were produced: the univariable Model 1; and the multivariable Model 2 adjusted for BMI.

The results in table 7-28 show that the significant association between the right hip JSW and ankle JSWs noted above is mainly related to the male population. The JSW for the tibial plafond showed a significant positive association with right hip JSW in the final model adjusted for BMI (R^2 = 0.18, *b* = 0.23, P = 0.002), which suggests that an increase of 0.23mm in the tibial plafond JSW is associated with an increase of 1 mm in the right hip's JSW. Also, the talonavicular JSW was also significantly positively associated with the right hip JSW in the final adjusted model (R^2 = 0.11, *b* = 0.08, P = 0.029).

In addition, the tibiofibular showed a similar association with the right hip JSW with a p-value of 0.005, a coefficient of 0.20, and R^2 of 18%. The Subtalar posterior facet was also significantly associated with the right hip JSW (R^2 = 0.19, *b* = 0.14, P < 0.001). The log value for the subtalar posterior facet was used in this model, and so *b*= 0.14 can be interpreted as a 14% increase in the mean of the dependent variable for every one-unit increase in the independent one. The results also shows that the left hip's JSW was not significantly associated with any of the ankle JSWs in the male population.

Regarding the associations between ankle JSWs and the ipsilateral hip on the same side as the dominant ankle scanned, the results of the fitting of the regression models were consistent with those obtained from the right-side hip JSW, since most male participants had a right dominant ankle (N=73) and only 10 had a left dominant ankle. The results are presented in table 7-28 below.

On the other hand, two models were produced for the female participants: a univariable model and a multivariable model adjusted for BMI. In both, log values were obtained of

the JSWs for the tibial plafond and the subtalar posterior facet to satisfy the normality and homoscedasticity assumptions. The results in table 7-29 below show that none of the ankle JSWs had a significant association with hip JSWs in the female population. Overall, when comparing the magnitude and direction of the associations in male and females, differences are shown in some joints, and this indicates that these associations differ between the sexes. Furthermore, when comparing the outcomes of the stratified and combined analyses, it can be noted that the significant associations seen in the analyses which included both sexes are more influenced by the stronger association noted in the male population, further confirming the sex modification affect.

Table 7-28. Results of the linear regression models applied to assess the associations between right, left, and ipsilateral hip JSWs and ankle JSWs in the male population.

Male ankle JSWs (mm) N=83	Right hip JSW		Left hip JSW		Ipsilateral hip JSW	
	Model 1	Model 2	Model 1	Model 2	Model 1	Model 2
	Coefficient 95%CI	Coefficient 95%CI	Coefficient 95%CI	Coefficient 95%CI	Coefficient 95%CI	Coefficient 95%CI
Tibial plafond	0.19* (0.05, 0.34)	0.23* (0.09, 0.37)	0.04 (-0.09, 0.18)	0.07 (-0.07, 0.20)	0.19* (0.05, 0.33)	0.23* (0.08, 0.35)
Medial malleolus	0.05 (-0.017, 0.10)	0.04 (-0.019, 0.10)	0.016 (-0.04, 0.07)	0.012 (-0.05, 0.07)	0.05 (-0.012, 0.11)	0.04 (-0.014, 0.10)
Talonavicular	0.09* (0.011, 0.17)	0.08* (0.007, 0.16)	0.10 (-0.03, 0.18)	0.09 (-0.02, 0.17)	0.09* (0.013, 0.16)	0.08* (0.008, 0.16)
Tibiofibular	0.18* (0.03, 0.33)	0.20* (0.06, 0.34)	0.12 (-0.01, 0.25)	0.13 (-0.009, 0.26)	0.19* (0.03, 0.31)	0.20* (0.04, 0.32)
Subtalar posterior facet	0.15* (0.07, 0.23)	0.14* (0.06, 0.22)	0.05 (-0.03, 0.13)	0.04 (-0.04, 0.12)	0.14* (0.06, 0.22)	0.13* (0.07, 0.21)
Subtalar medial facet	0.02 (-0.23, 0.23)	0.01 (-0.22, 0.23)	-0.08 (-0.24 0.33)	-0.06 (-0.26, 0.31)	-0.05 (-0.29, 0.29)	-0.04 (-0.29, 0.28)

Log values were obtained of JSWs for the medial malleolus and subtalar posterior facet. Model 1 represents the univariable analysis, and Model 2 the multivariable analysis adjusted for BMI.

Table 7-29. Results of the linear regression models applied to assess the associations between right, left, and ipsilateral hip JSW and ankle JSWs in the female population.

Female ankle JSWs (mm) N=123	Right hip mJSW		Left hip mJSW		Ipsilateral hip mJSW	
	Model 1	Model 2	Model 1	Model 2	Model 1	Model 2
	Coefficient 95%CI	Coefficient 95%CI	Coefficient 95%CI	Coefficient 95%CI	Coefficient 95%CI	Coefficient 95%CI
Tibial plafond	0.013 (-0.05, 0.07)	0.016 (-0.04, 0.07)	-0.014 (-0.07, 0.04)	-0.012 (-0.07, 0.04)	0.02 (-0.04, 0.08)	-0.019 (-0.04, 0.08)
Medial malleolus	-0.028 (-0.21, 0.15)	-0.021 (-0.20, 0.16)	-0.017 (-0.20, 0.17)	-0.027 (-0.21, 0.15)	-0.028 (-0.21, 0.15)	-0.018 (-0.19, 0.16)
Talonavicular	0.061 (-0.02, 0.14)	0.066 (-0.018, 0.15)	0.016 (-0.07, 0.09)	0.015 (-0.07, 0.10)	0.04 (-0.04, 0.12)	0.05 (-0.03, 0.13)
Tibiofibular	0.041 (-0.10, 0.18)	0.044 (-0.10, 0.19)	0.013 (-0.04, 0.07)	0.018 (-0.04, 0.08)	0.01 (-0.05, 0.06)	0.02 (-0.04, 0.06)
Subtalar posterior facet	0.017 (-0.05, 0.08)	0.021 (-0.04, 0.09)	0.02 (-0.04, 0.10)	0.03 (-0.04, 0.09)	0.015 (-0.05, 0.08)	0.018 (-0.04, 0.08)
Subtalar medial facet	-0.17 (-0.49, 0.13)	-0.18 (-0.49, 0.12)	-0.14 (-0.46, 0.18)	-0.13 (-0.45, 0.18)	-0.18 (-0.49, 0.12)	-0.19 (-0.50, 0.11)

Model 1 represents the univariable analysis, and Model 2 the multivariable analysis adjusted for BMI. Log values were obtained of the JSWs for the tibial plafond and subtalar posterior facet.

7.6 Association of 3D MRI ankle JSWs with WOMAC scores.

Another aim of this study is to investigate the relationship between ankle JSWs and the functional WOMAC index grading scores for pain, stiffness, and physical dysfunction. In this analysis, participants were separated into four categories of severity for each symptom (none, mild, moderate, and severe). The one-way ANOVA was used for normally distributed data, while the Kruskal-Wallis test was performed for non-normally distributed data. Tables 7-30 to 7-32 present the results, which show no significant differences in ankle JSW associated with the severity levels of pain, stiffness, and physical activity experienced by the participants.

Table 7-30. Results from tests of the association between ankle JSWs and pain scores.

Pain score	None (0)	Mild (1-19)	Moderate (20-59)	Severe (60-170)	P value
N	80	62	30	34	
Tibial plafond (median, IQR)	3.37 (2.00-2.74)	2.59 (2.08-3.03)	2.35 (1.96-2.65)	2.31 (1.91-2.85)	0.391
Medial malleolus (median, IQR)	3.03 (2.47-3.43)	3.03 (2.35-3.55)	3.02 (2.61-3.36)	3.05 (2.71-3.56)	0.818
Talonavicular (mean ± SD)	(1.52 ±0.31)	(1.41 ±0.39)	(1.34 ±0.36)	(1.33 ±0.32)	0.088
Tibiofibular (median, IQR)	2.38 (2.18-3.03)	2.38 (2.03-2.84)	2.39 (2.02-2.78)	1.98 (2.43-2.88)	0.507
Subtalar posterior facet (median, IQR)	2.89 (2.22-3.17)	2.61 (2.21-3.26)	2.86 (2.38-3.62)	2.46 (2.25-3.33)	0.667
Subtalar medial facet (mean ± SD)	(4.04 ±1.26)	(4.04 ±1.31)	(4.19 ±1.36)	(4.08 ±1.16)	0.922

One-way ANOVA was used for the talonavicular and subtalar medial facet JWSs and the Kruskal-Wallis test was performed for the remaining joints.

Table 7-31. Results from tests of the association between ankle JSWs and stiffness scores.

Stiffness score	None (0)	Mild (1-19)	Moderate (20-59)	Severe (60-170)	P value
N	104	46	33	23	
Tibial plafond (median, IQR)	2.39 (2.00-2.74)	2.35 (2.00-2.70)	2.45 (1.85-2.89)	2.43 (2.06-2.86)	0.824
Medial malleolus (median, IQR)	3.03 (2.51-3.41)	3.05 (2.35-3.59)	3.06 (2.63-3.50)	2.90 (2.52-3.56)	0.968
Talonavicular (mean ± SD)	(1.51 ±0.32)	(1.35 ±0.31)	(1.35 ±0.36)	(1.36 ±0.37)	0.134
Tibiofibular (median, IQR)	2.54 (2.18-3.12)	2.37 (2.03-2.83)	2.41 (2.06-2.84)	2.36 (2.09-2.78)	0.283
Subtalar posterior facet (median, IQR)	2.65 (2.25-3.29)	2.65 (2.28-3.18)	2.68 (2.19-3.34)	3.6 (2.64-3.23)	0.671
Subtalar medial facet (mean ± SD)	(4.00 ±1.23)	(4.24 ±1.37)	(3.84 ±1.44)	(4.21 ±0.96)	0.485

One-way ANOVA was used for the talonavicular and subtalar medial facet JWSs and the Kruskal-Wallis test was performed for the remaining joints.

Table 7-32 Results from testing the association between JSWs and physical function scores.

Physical function	None (0)	Mild (1-19)	Moderate (20-59)	Severe (60-170)	P value
N	79	59	36	32	
Tibial plafond (median, IQR)	2.37 (1.95-2.65)	2.38 (2.00-2.74)	2.36 (1.87-2.87)	2.48 (2.04-2.90)	0.728
Medial malleolus (median, IQR)	3.09 (2.51-3.64)	2.98 (2.45-3.48)	2.97 (2.46-3.20)	3.10 (2.66-3.59)	0.313
Talonavicular (mean ± SD)	(1.54 ±0.33)	(1.37 ±0.32)	(1.54 ±0.37)	(1.33 ±0.33)	0.156
Tibiofibular (median, IQR)	2.43 (2.02-2.83)	2.35 (2.02-3.83)	2.41 (2.10-3.00)	2.38 (2.09-3.03)	0.600
Subtalar posterior facet (median, IQR)	2.05 (2.20-3.32)	2.69 (2.25-3.26)	2.78 (2.50-3.62)	2.89 (2.26-3.20)	0.686
Subtalar medial facet (mean ± SD)	(4.05 ±1.28)	(3.99 ±1.28)	(4.20 ±1.35)	(4.04 ±1.17)	0.873

One-way ANOVA was used for the talonavicular and subtalar medial facet JWSs and the Kruskal-Wallis test was performed for the remaining joints.

7.7 Association of ankle JSWs with BMD variables

The relationship among participants between BMD as measured from four anatomical areas and JSWs was examined. Linear regression models were fitted separately for each joint as a dependent variable regressed against BMD content (g/cm2) measured from each of four different anatomical areas of the participant's body: the lower limbs, spine, right femoral neck, and right femoral total. To satisfy the assumptions of normality and homoscedasticity, log values were obtained of the joint space widths for the tibial plafond, medial malleolus, tibiofibular and subtalar posterior facet in all models.

Two models were fitted for each BMD measurement, the first model being a univariable model while the second was a multivariable model adjusted for sex and BMI. It should be noted that the coefficients obtained for all areas were consistently higher in the univariable model than those obtained after adjustment for sex and BMI, as shown in tables 7-33 to 7-36. In particular, the tibial plafond JWS was significantly associated with BMD as measured from the four areas. After adjusting for sex and BMI, statistically significant associations remained in the right femur neck and the total right femur measurements. The medial malleolus JWS was significantly associated with all BMD measures in the univariable model, but the associations remained significant after adjustment only in BMD measured from the lower limbs and the total right femur.

Meanwhile, in the final adjusted model, the talonavicular JSW only showed a significant association with BMD as measured from the spine, and similar results were obtained for both the subtalar posterior facet and subtalar medial facet articulations which were still statistically significant after adjustment for sex and BMI in all BMD areas measured except that from the spine. Finally, the tibiofibular JSW was not significantly associated with any of the BMD measurements in the final adjusted model.

Table 7-33. Results from linear regression applied to assess the association between JSWs and BMD measured from the spine.

Ankle JSW (mm) N=206	BMD measured from spine (g/cm^2)							
	Model 1				Model 2			
	Coefficient	95% CI	P	R^2	Coefficient	95% CI	P	R^2
Tibial plafond	0.35	[0.15, 0.56]	0.001*	0.05	0.09	[-0.16, 0.33]	0.505	0.13
Medial malleolus	0.44	[0.22, 0.67]	<0.001*	0.07	0.14	[-0.12, 0.41]	0.281	0.14
Talonavicular	0.71	[0.41, 1.02]	<0.001*	0.10	0.42	[0.05 , 0.79]	0.024*	0.13
Tibiofibular	0.24	[0.04, 0.44]	0.019*	0.03	0.11	[-0.13, 0.35]	0.378	0.06
Subtalar posterior facet	0.49	[0.21, 0.77]	<0.001*	0.06	0.20	[-0.13, 0.53]	0.243	0.10
Subtalar medial facet	1.94	[0.82, 3.06]	<0.001*	0.06	1.54	[0.17, 2.90]	0.027*	0.09

Model 1 is for the univariate analysis, and Model 2 the multivariable analysis adjusted for sex and BMI. Regression models were applied on log values of the JSWs for the tibial plafond, medial malleolus, tibiofibular and subtalar posterior facet.

Table 7-34. Results from linear regression applied to assess the association between JSWs and BMD measured from the lower limbs.

Ankle JSW (mm) N=206	BMD measured from lower limbs (g/cm^2)							
	Model 1				Model 2			
	Coefficient	95% CI	P	R^2	Coefficient	95% CI	P	R^2
Tibial plafond	0.45	[0.25, 0.65]	<0.001*	0.09	0.19	[-0.07, 0.45]	0.156	0.14
Medial malleolus	0.58	[0.36, 0.79]	<0.001*	0.11	0.33	[0.04, 0.61]	0.021*	0.16
Talonavicular	0.76	[0.47, 1.06]	<0.001*	0.11	0.51	[0.12 , 0.91]	0.010*	0.14
Tibiofibular	0.52	[0.25, 0.79]	<0.001*	0.06	0.20	[-0.15, 0.56]	0.267	0.10
Subtalar posterior facet	0.41	[0.22, 0.60]	<0.001*	0.08	0.39	[0.13, 0.65]	0.003*	0.10
Subtalar medial facet	2.5	[1.5, 3.6]	<0.001*	0.09	2.4	[0.99, 3.82]	0.001*	0.12

Model 1 is for the univariate analysis, and Model 2 the multivariable analysis adjusted for sex and BMI. Regression models were applied to the log values of the JSWs for the tibial plafond, medial malleolus, tibiofibular and subtalar posterior facet.

Table 7-35. Results from linear regression applied to assess the association between JSWs and BMD measured from the neck of the right femur.

Ankle JSW (mm) N=206	BMD measured from right femur neck (g/cm^2)							
	Model 1				Model 2			
	Coefficient	95% CI	P	R^2	Coefficient	95% CI	P	R^2
Tibial plafond	0.29	[0.04, 0.50]	0.012*	0.03	0.23	[0.02, 0.41]	0.032*	0.13
Medial malleolus	0.33	[0.07, 0.60]	0.013*	0.03	0.23	[-0.01, 0.49]	0.070	0.15
Talonavicular	0.33	[-0.03, 0.70]	0.072	0.02	0.19	[-0.16 , 0.55]	0.289	0.11
Tibiofibular	0.21	[-0.12, 0.55]	0.206	0.009	0.09	[-0.23, 0.42]	0.575	0.09
Subtalar posterior facet	0.32	[0.09, 0.55]	0.006*	0.04	0.32	[0.08, 0.56]	0.008*	0.08
Subtalar medial facet	2.4	[1.08, 3.74]	<0.001*	0.05	0.12	2.21	0.001*	0.12

Model 1 is for the univariate analysis, and Model 2 the multivariable analysis adjusted for sex and BMI. Regression models were applied on the log values of the JSWs for the tibial plafond, medial malleolus, tibiofibular and subtalar posterior facet.

Table 7-36. Results from linear regression applied to assess the association between ankle JSWs and BMD measured from the total right femur.

Ankle JSW (mm) N=206	BMD measured from total right femur (g/cm^2)							
	Model 1				Model 2			
	Coefficient	95% CI	P	R^2	Coefficient	95% CI	P	R^2
Tibial plafond	0.34	[0.14, 0.54]	0.001*	0.05	0.20	[0.03, 0.40]	0.028*	0.14
Medial malleolus	0.40	[0.18, 0.62]	<0.001*	0.06	0.24	[0.02, 0.47]	0.029*	0.15
Talonavicular	0.49	[0.19, 0.80]	0.001*	0.05	0.30	[-0.007, 0.60]	0.055	0.13
Tibiofibular	0.33	[0.05, 0.60]	0.019*	0.02	0.16	[-0.11, 0.44]	0.260	0.10
Subtalar posterior facet	0.38	[0.19, 0.57]	<0.001*	0.07	0.32	[0.13, 0.53]	0.001*	0.10
Subtalar medial facet	2.09	[1.08, 3.24]	<0.001*	0.06	0.11	[0.73 2.96]	0.001*	0.11

Model 1 is for the univariate analysis, and Model 2 the multivariable analysis adjusted for sex and BMI. Regression models were applied on the log values of the JSWs for the tibial plafond, medial malleolus, tibiofibular and subtalar posterior facet.

To investigate the potential interaction between sex and regional BMD variables on ankle JSWs, linear regression analysis that included an interaction term between the BMD variables and sex was performed separately for each BMD measurement on each ankle JSW. This approach allowed the association between BMD and ankle JSWs to be explored while accounting for possible sex differences in this relationship. The results presented in table 7-37, indicate that the interaction term was not statistically significant in any of the analyses, this providing no evidence that the sex of participants modified the relationship between ankle JSWs and BMD measurements.

Table 7-37 Results of linear regression applied to assess the interaction between sex and BMD measurements on ankle JSW : the P values presented are for the interaction term

Ankle JSW (mm) N=206	**BMD (gm/cm^2) from Interaction term P value for sex with hip JSW on ankle JSW**			
	Spine P-value	**Lower limbs P-value**	**RF neck P-value**	**RF total P-value**
Tibial plafond	p=0.867	p=0.910	p=0.724	p=0.594
Medial malleolus	p=0.327	p=0.908	p=0.942	p=0.286
Talonavicular	p=0.592	p=0.955	p=0.738	p=0.962
Tibiofibular	p=0.699	p=0.930	p=0.274	p=0.463
Subtalar posterior facet	p=0.447	p=0.658	p=0.767	p=0.591
Subtalar medial facet	p=0.126	p=0.168	p=0.183	p=0.199

Although no significant interaction was observed, the data were then stratified by the sex of participants so as to gain a more in-depth understanding of any effect of sex on the association between ankle JSWs and BMD. Linear regression models were fitted separately for each joint as the outcome variable was regressed against BMD content measured from the four anatomical areas of lower limbs, spine, right femoral neck, and right femoral total. To satisfy normality and homoscedasticity assumptions, log values were obtained of joint space widths for the tibial plafond, medial malleolus, tibiofibular, and subtalar posterior facet in all models.

The results obtained for the BMD measured from the spine shown in table 7-38 indicate a significant association only between the subtalar medial facet JSW and spine BMD in the male population (R^2 = 0.09, *b* = 2.05, P = 0.03) in the final model adjusted for BMI. In the female population one joint also showed a significant positive association in the final adjusted model, but in this case it was the talonavicular (R^2 = 0.10, *b* = 0.35, P = 0.02).

The results also show that, in the male population, the tibial plafond, subtalar posterior and subtalar medial facet JSWs all showed a significant positive association with BMD as measured from the lower limbs which persisted after adjusting for BMI with (R^2 = 0.09, *b* = 0.42, P = 0.03) (R^2 = 0.17, *b* = 0.54, P = 0.004) (R^2 = 0.12, *b* = 3.60, P = 0.003) respectively. Additionally, in the female population, the results from the final model adjusted for BMI showed significant positive associations between lower limb BMD and both the talonavicular and subtalar posterior JSWs (R^2 = 0.12, *b* = 0.70, P = 0.007; and R^2 = 0.15, *b* = 0.47, P = 0.009 respectively). The results are presented in table 7-39.

Furthermore, regarding the association between ankle JSWs and BMD as measured from the right femur neck, the results show that in the male population significant associations were observed in the univariable model with the tibial plafond, subtalar posterior, and subtalar medial facet JSWs. These associations remained statistically significant after adjustment for the confounding effect of BMI (R^2 = 0.10, *b* = 0.40, P = 0.03; R^2 = 0.20, *b* = 0.57, P = 0.001; and R^2 = 0.08, *b* = 2.05, P = 0.02 respectively).

However, the results for the female participants indicate that only the JSW for the subtalar posterior showed a significant association with BMD as measured from the right femur neck. The results are presented in table 7-40.

Table 7-41 shows the result for associations between total right femur BMD measurements and ankle JSWs for both males and females. Two joints showed significant associations with total right femur BMD in the male participants. The results for the subtalar posterior and subtalar medial facet JSWs in the final adjusted model are $R^2 = 0.19$, $b = 0.39$, $P = 0.002$ and $R^2 = 0.09$, $b = 2.12$, $P = 0.009$ respectively. On the other hand, in the female participants, only the tibial plafond JSW showed a significant association after adjustment for BMI ($R^2 = 0.09$, $b = 0.35$, $P = 0.02$).

Overall, the associations between BMD measurements and ankle JSWs have been examined in males and females separately. The directions of the associations found are positive, which is consistent with the combined data. However, there are some differences in the magnitude of the association between males and females. Additionally, some significant associations observed in the combined data disappeared or were only evident in one sex group after adjustment for sex and BMI, suggesting possible disparities in the association between BMD measurements and ankle JSWs between males and females. As a result, a final backward regression analysis was conducted on the stratified data.

Table 7-38. Results from linear regression applied to assess the association between JSWs and BMD measured from the spine in males and females.

Ankle JSWs (mm)	BMD measured from spine (g/cm^2)											
	Male Model 1 (N=83)			Male Model 2 (N=83)			Female Model 1 (N=123)			Female Model 2 (N=123)		
	Coeff	95% CI	P	Coeff	95% CI	P	Coeff	95% CI	P	Coeff	95% CI	P
Tibial plafond	0.08	[-0.29, 0.45]	0.668	0.10	[-0.28, 0.48]	0.600	0.21	[-0.06, - 0.50]	0.137	0.15	[-0.15, -0.45]	0.336
Medial malleolus	0.07	[-0.35, 0.48]	0.753	0.04	[-0.40, 0.46]	0.829	0.32	[-0.006, 0.65]	0.053	0.20	[-0.15, 0.56]	0.262
Talonavicular	0.31	[-0.24, 0.86]	0.271	0.18	[-0.38, 0.74]	0.518	**0.61**	**[0.20, 1.02]**	**0.004***	**0.53**	**[0.08, 0.99]**	**0.022***
Tibiofibular	0.17	[-0.19, 0.55]	0.343	0.18	[-0.18, 0.56]	0.324	0.21	[-0.16, 0.41]	0.392	0.15	[-0.16, 0.46]	0.345
Subtalar posterior facet	0.07	[-0.50, 0.65]	0.802	0.08	[-0.50, 0.66]	0.798	0.30	[-0.03, 0.63]	0.076	0.24	[-0.12, 0.60]	0.187
Subtalar medial facet	**2.04**	**[0.2, 4.70]**	**0.033***	**2.05**	**[0.21, 4.84]**	**0.032***	0.50	[-1.01, 2.05]	0.506	0.92	[-0.78, 2.63]	0.285

Model 1 represents the univariable analysis, Model 2 the multivariable analysis adjusted for sex and BMI. Regression models were applied to the log values of the JSWs for the tibial plafond, medial malleolus, tibiofibular and subtalar posterior facet.

Table 7-39. Results from linear regression applied to assess the association between JSWs and BMD measured from the lower limbs in males and females.

Ankle JSWs (mm)	BMD measured from lower limbs (g/cm^2)											
	Male Model 1 (N=83)			Male Model 2 (N=83)			Female Model 1 (N=123)			Female Model 2 (N=123)		
	Coeff	95% CI	P	Coeff	95% CI	P	Coeff	95% CI	P	Coeff	95% CI	P
Tibial plafond	**0.44**	**[0.04, 0.85]**	**0.030***	**0.42**	**[0.02, 0.83]**	**0.039***	**0.37**	**[0.03, -0.70]**	**0.033***	0.30	[-0.04, 0.64]	0.090
Medial malleolus	0.39	[-0.04, 0.83]	0.075	0.36	[-0.08, 0.8]	0.109	**0.48**	**[0.10, 0.87]**	**0.014***	0.38	[-0.02, 0.78]	0.065
Talonavicular	0.57	[-0.006, 1.15]	0.053	.049	[-0.08, 1.07]	0.093	**0.80**	**[0.32, 1.29]**	**0.001***	**0.70**	**[0.19, 1.22]**	**0.007***
Tibiofibular	0.07	[0.54, 0.69]	0.804	0.02	[-0.59, 0.63]	0.956	0.31	[-0.08, 0.70]	0.128	0.22	[-0.18, 0.63]	0.280
Subtalar posterior facet	**0.58**	**[0.20, 0.96]**	**0.003***	**0.54**	**[0.19, 0.92]**	**0.004***	**0.45**	**[0.11, 0.70]**	**0.009***	**0.47**	**[0.12, 0.81]**	**0.009***
Subtalar medial facet	**3.07**	**[1.41, 6.06]**	**0.002***	**3.60**	**[1.26, 5.95]**	**0.003***	0.83	[-0.97, 2.60]	0.365	1.01	[-0.76, 3.06]	0.236

Model 1 is for the univariable analysis, Model 2 for the multivariable analysis adjusted for sex and BMI. Regression models were applied to the log values of the JSWs of the tibial plafond, medial malleolus, tibiofibular and subtalar posterior facet.

Table 7-40. Results from linear regression applied to assess the association between JSWs and BMD measured from the right femur neck in males and females.

Ankle JSWs (mm)	BMD measured from right femur neck (g/cm^2)											
	Male Model 1 (N=83)			Male Model 2 (N=83)			Female Model 1 (N=123)			Female Model 2 (N=123)		
	Coeff	95% CI	P	Coeff	95% CI	P	Coeff	95% CI	P	Coeff	95% CI	P
Tibial plafond	**0.41**	**[0.03, 0.78]**	**0.031***	**0.40**	**[0.02, 0.77]**	**0.036***	0.24	[-0.04, 0.54]	0.099	0.20	[-0.09, 0.49]	0.188
Medial malleolus	0.19	[-0.21, 0.60]	0.352	0.21	[-0.19, 0.62]	0.306	0.29	[-0.04, 0.63]	0.092	0.21	[-0.13, 0.55]	0.234
Talonavicular	0.01	[-0.54, 0.56]	0.967	0.02	[-0.51, 0.56]	0.928	0.31	[-0.12, 0.74]	0.161	0.21	[-0.23, 0.66]	0.348
Tibiofibular	0.12	[-0.44, 0.69]	0.665	0.02	[-0.56, 0.58]	0.956	0.16	[-0.13, 0.46]	0.266	0.17	[-0.12, 0.47]	0.263
Subtalar posterior facet	**0.53**	**[0.18, 0.88]**	**0.003***	**0.57**	**[0.24, 0.91]**	**0.001***	**0.30**	**[0.04, 0.65]**	**0.029***	**0.32**	**[0.02, 0.63]**	**0.035***
Subtalar medial facet	**2.29**	**[0.70, 4.52]**	**0.043***	**2.05**	**[0.32, 4.83]**	**0.025***	1.36	[-0.20, 2.93]	0.087	1.61	[-0.01, 3.23]	0.052

Model 1 is for the univariable analysis, Model 2 for the multivariable analysis adjusted for BMI. Regression models were applied to the log values of the JSWs for the tibial plafond, medial malleolus, tibiofibular and subtalar posterior facet.

Table 7-41. Results from linear regression applied to assess the association between JSWs and BMD measured from the total right femur in males and females.

Ankle JSWs (mm)	BMD measured from total right femur (g/cm^2)											
	Male Model 1 (N=83)			Male Model 2 (N=83)			Female Model 1 (N=123)			Female Model 2 (N=123)		
	Coeff	95% CI	P	Coeff	95% CI	P	Coeff	95% CI	P	Coeff	95% CI	P
Tibial plafond	**0.28**	**[0.009, 0.56]**	**0.043***	0.23	[-0.05, 0.51]	0.103	**0.39**	**[0.06, 0.72]**	**0.019***	**0.35**	**[0.07, 0.69]**	**0.022***
Medial malleolus	0.13	[-0.16, 0.43]	0.365	0.16	[-0.16, 0.45]	0.289	0.25	[-0.03, 0.54]	0.089	0.20	[-0.10, 0.50]	0.189
Talonavicular	0.17	[-0.22, 0.56]	0.390	0.21	[-0.17, 0.60]	0.268	0.35	[-0.07, 0.78]	0.102	0.24	[-0.20, 0.69]	0.288
Tibiofibular	0.09	[-0.32, 0.50]	0.668	0.19	[-0.23, 0.61]	0.367	0.22	[-0.06, 0.52]	0.124	0.25	[-0.04, 0.54]	0.102
Subtalar posterior facet	**0.38**	**[0.12, 0.63]**	**0.004***	**0.39**	**[0.15, 0.69]**	**0.002***	0.09	[-0.24, 0.43]	0.588	0.02	[-0.33, 0.36]	0.932
Subtalar medial facet	**2.02**	**[0.44, 3.60]**	**0.013***	**2.12**	**[0.53, 3.70]**	**0.009***	1.02	[-0.52, 2.57]	0.192	1.34	[-0.29, 2.97]	0.107

Model 1 is for the univariable analysis, Model 2 the multivariable analysis adjusted for BMI. Regression models were applied to the log values of the JSWs for the tibial plafond, medial malleolus, tibiofibular and subtalar posterior facet.

Following the stratified analysis exploring the associations between ankle JSWs and BMD measurements, the significantly associated BMD regions with each ankle JSW were fitted using backwards regression analyses for males and females separately. The aim of this was to determine which BMD region is most strongly associated with each ankle JSW. To address any multicollinearity, the correlations among independent variables (the BMD measurements) were tested using the variance inflation factor (VIF). Independent variables with a value of VIF greater than 10 were excluded from the regression models. Initially, all independent variables and body mass index (BMI) measures were included in the models, but the variable with the largest p-value was manually removed and the analysis then repeated until the final model only included statistically significant predictors. The results from the final models are presented next.

In males, the tibial plafond JSW showed a significant association with BMD from the right femur neck (R^2 = 0.12, b = 0.40, P = 0.03). This finding indicates that every increase of one unit in the BMD of the right femur neck is associated with a 40% increase in tibial plafond JSW. The subtalar posterior JSW was also significantly associated with BMD from the right femur neck (R^2 = 0.20, b = 0.57, P = 0.001). This coefficient can be interpreted as a 57% increase in JSW associated with a one-unit increase in BMD, since the regression models here were applied to the log values of the subtalar posterior JSW. Finally, the BMD for lower limbs showed a significant association with the subtalar medial facet (R^2 = 0.13, b = 3.60, P = 0.003).

In females, the tibial plafond JSW was significantly associated with BMD from the total right femur (R^2 = 0.08, *b* = 0.9, P = 0.04), which means that every one unit in g/cm^2 increase in the BMD of the right femur neck is associated with a 0.9mm increase in the tibial plafond JSW. In addition, the results of the backward regression showed that the talonavicular JSW was associated with BMD measured from the spine (R^2 = 0.08, *b* = 0.61, P = 0.004). Finally, regarding the subtalar posterior JSW, the backward regression showed a significant association with the right femur neck with (R^2 = 0.10, *b* = 0.32, P = 0.03).

Chapter 8: Discussion

The first objective of this study was to reconstruct SSMs of the ankle joint complex, which consists of five bones (the distal tibia, distal fibula, talus, calcaneus, and navicular), to evaluate its morphological variations. Models were constructed using MRI images from 206 participants in an original birth cohort of the same age (62 years). To train the models, 30 MRI scans were manually segmented, and an automatic segmentation approach (AAM) was used to segment the remaining images. Five SSMs were produced: a full ankle model, tibia-talus-navicular model, calcaneus model, full ankle female model, and full ankle male model. These models enabled the reconstruction of bone geometry using anatomically corresponding landmarks, and this facilitated the evaluation of variations in ankle complex bone shape, bone area, and joint space width (JSW) in the population studied.

The second objective of this research was to use the 3D SSMs of the ankle complex region to describe normal population variations in terms of sex differences, body anthropometry, and pain. Additionally, the study aimed to explore the relationship between the morphological variables extracted from the ankle 3D SSMs and several clinical measures, including OA radiographic features in the knee and hip joints, systematic BMD measurements, and WOMAC scores. This study is the first to use such a robust method to produce MRI 3D SSMs of the ankle complex region, allowing for the evaluation of morphological variations in the population and an examination of their association with several clinical musculoskeletal variables related to the lower limbs.

In this chapter, the key findings from the results presented in the previous two chapters are discussed in the context of previous work and in terms of clinical implications. Firstly, key findings in bone shape variations are discussed, followed by those from the analyses of JSW. After that, the strengths and limitations of the present research are considered, followed by the presentation of the study's overall conclusions and recommendations for future work.

8.1 Morphological variation in bone shape and area

The study used several SSMs to assess variation in bone shape and area. Initially, the full ankle model was used to evaluate variations in bone shape according to sex and body anthropometry. After examining the associations in the full model presented in tables 6-3 and 6-4 and figure 6-4, two models were produced to focus on the bones that showed the greatest variations between the sexes. Additionally, separate male and female models were used to examine the variations in ankle bones between participants with OA and those without in both the hip and knee joints, with the aim to establish any consistent sex differences. The next sections discuss the key findings for bone shape variation, including those related to sex differences, OA status, and body anthropometry.

8.1.1 Morphological variation in ankle complex bone shape and area between sexes

To explore bone shape variations between the sexes, the full ankle model was initially used. The independent t-test on the population bone shape vector showed significant differences ($p<0.0001$) between males and females (table 6-3). Further analysis of individual principal component (PC) modes revealed significant variations in bone shape between the sexes (table 6-4; figure 6-4). Also, associations between height and weight and the PC modes for which significant differences in bone shape between sexes were found were also examined, but no statistically significant results were found, indicating that variations in bone shape are more closely related to sex rather than body size (table 6-5).

The distal tibia-talus-navicular SSM showed significant sex-related differences between males and females in the distal tibia bone. Females showed a decrease in the width of the distal tibia, particularly in the anterior and posterior portions, and a thinner and more inferiorly projected medial malleolus bone when compared to males. These findings were presented in table 6-7 and figure 6-7.

In the same model, the talus bone exhibited significant differences between males and females, as evidenced by the t-test results (table 6-7), and PC3 revealed variations in bone shape, with males having a larger and wider talus (figure 6-8). Females, on the other hand, had a smaller talus dome that became more narrowed posteriorly and laterally shifted. Additionally, females had a relatively smaller talus head and neck compared to males. A posterior view of the talus bone in males also revealed a larger posterior calcaneal articulation surface compared to females.

Bone area measurements were consistent with the analysis of PC modes, showing that all six anatomical bone measures quantified from the SSM (talus dome, talus head, posterior articulation surface with the calcaneus, talus width, height, and length) were significantly larger in males (table 6-8).

Finally, in the same SSM, the navicular bone showed significant differences between the sexes in PC 7 (table 6-7). Overall, variations were seen in the anterior surface of the bone where males had a wider anterior bone area and a more concave surface for articulation with the head of the talus (figure 6-8).

The assessment of variations in the shape of the calcaneus bone was performed separately in a distinct model due to its size. The t-test results for the population bone shape vector indicate significant differences in calcaneus shape between males and females ($p=0.0003$, table 6-9). The analysis also revealed significant variations in the modes of PC1, PC4, and PC5 (as shown in table 6-10 and figure 6-11). Females had a more concave calcaneal body shape, thinner posterior facets, and a narrower bone width, while males had a longer calcaneum, a wider posterior calcaneus tuberosity, and larger sustentaculum tali.

Moreover, the position of the medial calcaneal tuberosity process was more inferiorly projected in females, while males exhibited slightly bigger Gissane and Bohler's angles. Additionally, the calcaneus bone measurements (table 6-11) were consistent with the PC mode analysis, revealing significant differences in calcaneal length, posterior tuberosity width, and bone area between males and females, with males exhibiting significantly larger morphological measurements.

To the best of the author's knowledge, no previous study has used MRI 3D SSM to explore morphological variations between the sexes in the shape of bones in the ankle complex region, limiting any direct comparison with other research findings. However, some recent studies found in the literature have used different imaging modalities and methods of SSM reconstruction. One study used CT images to build ankle joint complex SSMs (55) with the aim to explore side-to-side symmetry and sex differences in the tibia, talus, and calcaneum. As in the present study, they found significant differences between males and females in the distal tibia. Males had a larger and wider distal bone compared to females, as in our population, and they also reported significant sex differences in calcaneal bone shape with females having a

thinner and longer calcaneus than males. The present results agree in that females have a thinner calcaneum but disagree since this bone was found in this study to be shorter in females. The results of both the PC mode and bone area analysis show that males have a longer calcaneus bone when compared to females. Finally, contrary to the several significant differences between sexes found here in talus bone shape, Gabrielli, Gale (55) found no significant variations between sexes in this bone, but that was a much smaller study and likely to be underpowered.

A study conducted by Moore, Kindig (392) also used CT images to reconstruct morphometric shape models of the talus, calcaneus, and navicular bones with the aim to assess the relationships between bone shape and both foot type and sex. They reported some significant variations between the sexes which are consistent with the results of the present study, such as the navicular bone in males having a wider inferior notch with a more concave articulation surface with the talus. Moreover, they concluded that the female talus bone is thinner with a smaller talus dome than in males. However, contrary to the results presented in this study, they reported no evidence of significant differences between sexes regarding the shape of the calcaneus bone, and this is discussed further below.

Like the previous two studies, Tümer, Arbabi (57) used CT images to reconstruct SSMs and analyse sex-related morphological variations in the fibula, tibia, calcaneus and talus bones using principal component analysis. In accordance with the results found in the present study, they reported significant differences between the sexes regarding the distal tibia, where females tend to have smaller bones than males, and reported significant variations in the talus between sexes. Their results showed that male talus bones have a larger posterior facet, a wider talar dome and a wider talar head than in females. On the other hand, their calcaneus bone shape results suggest that females have a longer calcaneum, whereas this study found it to be shorter than that of males.

The previous three studies showed significant sex-related variations in the shapes of bones in the ankle complex region. However, in neither case is their full agreement with each other or with the findings of the present study. There are discrepancies between the four studies in specific bone variations between the sexes. For example, some studies noted significant differences in the calcaneus bone shape between males and females, but in the same or

opposite directions, while others did not. Also, some studies showed significant variations between the sexes in the shape of the talus bone and others reported no such variations.

One possible explanation for this inconsistency might be variations in the populations studied, such as in sample size and the age and ethnicity of participants included. Gabrielli, Gale (55) studied a sample of only 20 participants who were aged 31 ± 6 years on average and included equal numbers of men and women. The participants' ethnic background was not noted, as in Moore, Kindig (392) sample of 40 participants (23 males and 17 females) with a mean age of 53 ± 9 years. Meanwhile, the study conducted by Tümer, Arbabi (57) included a larger sample compared to the previous two studies, with 66 participants (55 male, mean age 61 ± 10 years; 11 female, mean age 53± 15 years) whose ethnic backgrounds were again not mentioned. All three studies had the additional limitation of relatively low sample sizes, where even the largest might be considered to be unsuitable for the analysis of sex differences given a heavily skewed sex ratio.

Such variations in the sampling frame could contribute to the discrepancies observed in the results. A smaller sample may not allow the detection of all morphological variations between sexes, potentially leading to both type I error (including false positive findings in the opposite direction) or type II false negative errors. Likewise, age and ethnicity are important factors which should be considered when determining morphological variations in bone shape. Several studies have reported that aspects of bone morphology such as size, shape, strength, and volume as well as mechanical functioning may change with increasing age (211, 212, 393, 394). Equally, various studies show that lower limb bones may differ in terms of size and shape between ethnic groups (395-398). Therefore, variations in samples in terms of size, age and ethnicity may account for inconsistencies in the findings in the studies cited but, in general, studies using the largest samples and the most effective imaging and analysis techniques should be given most weight.

Before the most recent studies using 3D SSM, morphological variations in the shape of bones in the ankle complex region were mainly assessed using 2D radiographs or by the analysis of predefined measurements from cadaveric specimens (229, 241, 399-406). Both methods are associated with limitations that may result in the underestimation of sex-related variations in bone morphology. For instance, the ankle complex region comprises several overlapping bones that present as a 3D object with a triplane motion (181). 2D methods such as

radiography are clinically relevant and widely available, but their use for the representation and assessment of 3D objects with overlapping bones can lead to difficulties not only in the evaluation of sex-related variation, but also in the examination and quantification of any morphological variations in a given population. Likewise, in order to assess variations in bone shape and size, this method is applied using single views from different directions resulting in increasing radiation exposer.

Furthermore, when using 2D conventional radiography, the apparent morphology of the bone is affected by any change in the source-to-image receptor distance (407). This results in images that vary in apparent bone position and size due to image-acquisition variations that can affect the accuracy of any measurements taken. Finally, the use of cadaveric specimens to examine sex-related morphological variations in ankle bones usually focuses on predefined measurements (406), in which case other important morphological aspects within the bone may potentially be ignored.

The present study offers important insights into sex-related variations in bone shape and overcomes the aforementioned limitations in the limited number of recent studies using SSM methods and those using radiography and cadaveric specimens. This is due to the use of MRI 3D SSM, which is a reliable method with the ability to fully represent the 3D bone geometry from an anatomically complex region (50).

The use of this method can contribute to a clearer understanding of the variations between sexes in ankle bone shape, thanks to a more comprehensive and robust analytic method when compared to studies using radiography and cadaveric specimens. Furthermore, this study's sample included 206 participants in a true population cohort that represents a specific age group (62 years) with a single ethnic background. This allows the assessment of ankle bone shape variations between sexes in a larger sample and without needing to control for the influence of race and age.

The findings of the analysis of data in this research support the hypothesis that sex-related variations in the bone shapes in the ankle complex region can be examined and summarised using 3D MRI SSM. The detailed knowledge of bone shape variations between males and females gained using 3D MRI SSM has several important implications for research and clinical practice. For example, the results presented here may help inform orthopaedic surgeons in

planning treatment and surgery. Many types of ankle and hindfoot surgery, such as ankle arthrodesis, total ankle replacement, and joint stabilisation surgery, require a comprehensive preoperative plan that focuses on detailed information on joint and bone morphology (408, 409).

Therefore, a clear understanding of sex-related variations in bone shapes from the use of MRI SSM can help in illustrating variations between sexes in normal and pathological bone shapes in the ankle region. This can lead to a better-informed preoperative planning strategy, potentially increasing the success rates of surgery. This approach has been successful in other areas of the anatomy, including the hip and knee (410, 411).

As discussed in chapter 3 the ankle complex region plays an important role in the gait cycle, which begins with the movement of the ankle and foot when interacting with the ground and mainly consists of interactions between skeletal, muscular, and neurological systems (412). However, the skeletal system is responsible for creating the overall functional framework of the human body (413). Several studies have confirmed the existence of sex-specific variations in gait between males and females and that such variations may be due to variations in muscle strength and ligamentous laxity (213, 414, 415). However, an alternative hypothesis is that, since the gait cycle mainly starts at the ankle complex region, variations in bone shape between the sexes may help explain some or all sex-specific variations in gait. Therefore, the results in this study showing variations in bone shape between sexes can contribute to providing clinicians and researchers with a better understanding of sex-specific variations in gait.

For example, a study by Ko, Tolea (213) exploring variations between older males and females over 60 years old in gait patterns. The results showed that females have a significantly greater sagittal plane ankle range of motion in plantarflexion and dorsiflexion compared to males. It seems possible that these results may be better understood by considering bone shape variations between sexes, especially those found here in the shape of the distal tibia and talus bone. The ankle's range of motion for plantarflexion/dorsiflexion is primarily associated with the main ankle joint, which involves the articulation of the talar dome fitted into a mortice formed by the medial and lateral malleolus (181). In this study, it has been found that males tend to have a wider talar dome and a wider distal tibia, and therefore a wider mortice socket,

but a shorter medial malleolus compared to females. This might limit the range of motion more in males, compared to females.

A study using X-ray fluoroscopy to assess foot bone kinematics by Fukano, Fukubayashi (416) showed that females have a significantly larger subtalar range of motions of eversion and inversion than in males. Many factors affect this range of joint motion, including the size and shape of the bone articular surface (417). Fukano et al.'s results could be explained with the help of the present study's identification of variations between the sexes in the calcaneus posterior facet, which is within the subtalar joint area. Females in this study have a smaller calcaneus articular surface with the talus, which orientates more medially compared to males. During the stance phase in the gait, the calcaneus bone undertakes eversion movement as a result of contact with the ground (181). At the same time, the talus bone adapts to the movement of the calcaneus bone by sliding more medially on the articular surface with the calcaneus. Therefore, if females have smaller and more medially orientated calcaneus posterior articular facets, they are likely to have a greater range of motion in the subtalar joint than males.

Additionally, the sex-related ankle bone shape variations presented here may provide a better understanding of the sex-specific aetiology and incidence of some foot and ankle disorders. Several studies conclude that the prevalence of foot, ankle, and knee disorders such as ankle sprains, flat feet, hallux valgus and knee OA is higher in elderly females than males (5, 418-420). For instance, the present study finds that calcaneal bone shape in females shows variations in the height of the medial and lateral processes (see figure 6-11, PC1 lateral view), where the lateral process is more inferiorly projected in females. On the other hand, in males these two processes are similar in height. This implies that, during gait, males could benefit from firmer contact with the ground, whereas a female's calcaneus with a medial process projected more inferiorly could lead to more unstable contact with the ground during. Such variations may indicate that males have a more stable and less-everted calcaneus, especially during ground contact. In contrast, females tend to have a more unstable and more everted calcaneus where the degree of eversion may depend on how much the medial process is projected inferiorly.

Some researchers point to a possible link between calcaneus bone movement (eversion) and the pathogenetic mechanisms of some foot, ankle, and knee musculoskeletal conditions and

particularly those that show higher prevalence in females such as flat feet (421), ankle sprains (422), and knee OA (423). The findings from the present study suggest that the morphological variations noted between sexes in the shapes of the lateral and medial processes of the calcaneus tuberosity and the calcaneus posterior facet in the subtalar joint area could explain observed sex differences in gait which may represent a risk factor for some foot, ankle, and knee musculoskeletal disorders. The assessment in this study of differences in ankle bone shape between participants with knee or hip OA and those without may have some bearing on these issues and are discussed next.

8.1.2 Morphological variations in bone shape in the ankle complex between participants with and without knee and hip OA

One of the aims of this study was to examine whether or not morphological variations in bone shape in the ankle complex differ between participants with knee/hip OA and those without. To achieve this, 3D SSMs were constructed separately for males and females. This approach was necessary due to differences in ankle bone shape between the sexes which may impact the detection of OA-related differences in a combined model. By constructing separate models for each sex, the bone morphology could be described, and principal components that show significant morphological variations between participants with and without knee or hip OA could be identified for each sex independently. The results of independent t-tests showed significant differences in PC modes between male participants with and without knee OA (table 6-12 and figure 6-13). Specifically, PC mode 3 was found to be significantly related to variations in bone alignment in the ankle complex region, indicating the role of foot posture or foot type. The OA group demonstrated a pes planus foot structure or pronated foot compared to the non-OA group. Likewise, significant differences were observed for PC mode 4 between male participants with and without hip OA (table 6-13 and figure 6-13). PC mode 4 also showed variation in terms of the articulation alignments of the ankle bones. The hip OA group exhibited a pes cavus foot type or supinated foot compared to the non-hip OA group.

In contrast, the results from the female SSM were consistent with those of the male participants, except with differences in the rankings of the statistically significant PC modes in the model. PC4 displayed significant differences between female participants with and without knee OA similar to male participants, indicating bone shape alignment representing a pes planus foot structure (pronated foot) in females with knee OA (table 6-14 and figure 6-

15). Additionally, PC5 exhibited significant differences between female participants with and without hip OA equivalent to that for PC4 in the male model, where variations in the articulation alignments of the ankle bones indicate a pes cavus foot type (supinated foot) in females with hip OA (table 6-15 and figure 6-15).

The proportions of participants with knee and hip OA in both sexes were similar, with a slightly higher proportion of females having OA. One might therefore expect that the differences between OA and non-OA groups would be stronger in females rather than males. However, the differences found in males tended to be more statistically significant and for lower-ranking PC modes in accounting for variance in the model, indicating stronger differences than those in the female model. For instance, PC3 explains approximately 9% of the variance in the male model, and significant differences in this mode were found between male participants with OA in the knee and those without. Meanwhile, PC4 in the female model gave similarly significant results but explained less variance in the model at approximately 5.5%.

This could be explained in terms of the differences in bone shape between males and females discussed in the previous section. Of particular significance is variation in the shape of the posterior facet of the calcaneus, in the subtalar joint area, where females, in general, had a smaller bone surface with more flexibility and mobility resulting in a wider range of pronation and supination motions compared to males. This means that the detection of differences in articulation alignment in the model between females with and without OA is weaker and describes less variations compared to between males who normally have a smaller range of motion in the joint. Other factors might also affect the range of motion of a joint, such as muscle strength and ligament flexibility, and females are known to have more greater ligamentous laxity in the ankle joint compared to males (191). This also might make the detection of differences in the subtalar joint range of motion between females in both the OA and non-OA groups weaker compared to males due to other variables affecting such an association.

To the best of my knowledge, this study represents the first attempt to evaluate morphological differences in bone shape within the ankle complex region between individuals who have or do not have OA affecting both the knee and hip joints via the use of 3D MRI SSM. As a result, it may not be straightforward to directly compare the findings with those of previous research.

However, some studies have used other methods that focus more on assessing the foot and ankle structure of OA and non-OA participants using clinical observation and palpation methods. These include the foot posture index, navicular height test and calcaneal angle (36, 38, 424), which are methods widely used to classify foot types. Therefore, comparing the observed bone variations in the present study with the results of studies examining the foot and ankle structure in OA and non-OA patients may be feasible to provide a better understanding of these morphological variations.

The results presented here are consistent with those of a study by Reilly, Barker (36) which examined differences in foot types between three groups of age-matched participants: 60 participants with end-stage knee OA waiting for surgery; another 60 participants with end-stage hip OA; and a control group of healthy participants. The methods of assessment used were measurements of navicular height and calcaneal angle, which are involved in the pronation and supination of the foot. Analysis of the results showed significant differences between the three groups, where the knee OA group had greater calcaneal eversion and lower navicular height, representing a pronated foot, and the hip OA group had more calcaneal inversion and an increased navicular height representing a supinated foot.

Furthermore, the foot posture index developed by Redmond, Crosbie (425) helped to fulfil the need for a clinical diagnostic tool for the measurement and categorisation of foot posture. That motivated Reilly et al.'s research team to conduct another study using only the foot posture index in assessing foot type (37). Their sample included 60 participants, 20 each with knee and hip OA (all at end-stage) and 20 healthy age-matched participants. The results showed significant differences in foot type between the three groups. Participants in the knee OA group had a more pronated foot and those with hip OA a more supinated foot. These results confirmed the significant association noted in their previous study (Reilly, Barker (36) which used different measurements to classify foot posture.

In another study, the association between foot type using the foot posture index and knee OA was examined in a Moroccan population (Abourazzak, Kadi (38). The sample included 100 participants in the knee OA group and 80 asymptomatic controls). A significant correlation was noted between the foot posture index scores and knee OA, indicating a pronated foot posture associated to the knee OA group. The result of the studies agrees with those of the studies mentioned above.

Using 3D SSM, the present study has identified differences ankle bone morphology between participants with and without knee and hip OA. Such results are consistent with the previously discussed studies. However, in studies that aimed to evaluate foot posture using 2D measurements, subjective components of assessment are involved that depend on clinical observation and palpation methods. This subjectivity can hinder accuracy and repeatability, as has been reported regarding the use of the foot posture index, navicular height and calcaneal angle (426, 427). In the present study a novel 3D SSM method was used to explore and visualise variations in bone shape and alignment using an automated method representing real ankle complex bone orientations in a sample from an actual population.

Previous studies aimed to assess differences in foot posture between OA and non-OA participants in a standing weight-bearing position where some degree of pronation or supination will occur. However, it is difficult to determine if that is due to structural variations in the alignment of the bones or simply the effect of the weight of the body. While, in this study the 3D SSMs were built from MRI images obtained from participants in a non-weight bearing supine position. This allowed a comparison of outcomes with those achieved using the weight-bearing position.

Previous studies also mainly focused on participants at the end stages of OA of the knee and hip. This prevented conclusions being drawn concerning participants graded at lower stages of OA. In the present study, many participants from the NTFS in both the knee and hip OA groups scored at K&L grade 2 for the knee and Croft grade 2 for the hip. Only 4 participants were graded with end-stage K&L grade 4 knee OA and 6 with Croft grade 5 hip OA. Despite fundamental differences between this study and other published research in the methods of assessment used and severity of OA in the populations compared, similar results were still noted. This suggests that the differences observed in ankle bone shape and alignment which represent foot posture between OA and non-OA cases in both the knee and hip are consistent and important.

This importance can be elucidated by addressing the differences observed in the shape of ankle bones between OA and non-OA groups and how such variations are linked to OA. Firstly, a brief explanation of the role played by ankle and foot bones during the gait cycle is necessary. Calcaneus eversion and inversion, navicular height and the plantarflexion and dorsiflexion movements of the talus are factors determining the degree of pronation and supination of

the foot and ankle in the gait cycle (181). During walking, some degree of pronation and supination occur and are considered to be natural and important aspects of the gait cycle (428).

Pronation of the foot occurs during initial contact with the floor in the first period of the stance phase of the gait cycle. The calcaneus everts at the subtalar joint, which leads the talus to adduct, the plantar to flex, and the navicular bone to drop (428). The combination of these movements leads the foot to roll inwards to absorb the shock during the initial period of the stance phase. In the midstance phase of the gait cycle, pronation stops, and the foot starts to supinate. The calcaneus inverts at the subtalar joint, leading the talus bone to abduct and dorsiflex and the navicular bone to move upwards (428). The combination of these movements leads the foot to roll outward, forming a rigid structure that allows propulsion. Therefore, the normal transition from pronation to supination during the stance phase is an important aspect in allowing the normal free flow of the gait cycle. Any interruption, or supination or pronation occurring at the wrong time, will result in a disturbance of the kinetic chain (206).

In this study, significant differences were found between participants with and without knee OA associated with the bone alignments in the ankle complex region in a natural non-weight-bearing supine position. Such differences in bone alignment may disrupt the normal gait cycle and lead to increased force applied to other lower limb joints such as the knee and hip (429). For instance, participants in the knee OA group exhibited a more everted calcaneus and dropped navicular, and greater plantar flexion movement of the talus, which indicate a more pronated foot (flat foot) type. Meanwhile, studies suggest that the degree of pronation of the subtalar joint (everted calcaneus) in a weight-bearing standing position is 37% higher than that seen in a non-weight-bearing supine position (430). Thus, the present study's participants in the knee OA group would have had even more pronated feet when in a weight-bearing standing position than when assessed while supine.

Therefore, in the gait cycle, people with a more pronated foot type are likely to have a subtalar joint that continues to pronate throughout the midstance phase. This is because the joint will need more time to move from over-pronation to supination, which is the normal movement of the subtalar joint at this phase, thereby causing the knee to be subjected to high axial force due to the external rotation moment on the femur caused by the advanced movement of the

contralateral pelvis during the midstance phase (206). In people with more pronated feet, such as those in the knee OA group, this force on the knee is repeated during everyday activities such as walking. Such force is applied more to the medial compartment of the knee during the midstance phase of gait, which coincides with the perriod when the subtalar joint is still pronated (431). The medial compartment of the knee is known to be most often affected by OA (106), probably because it is mechanically driven. Approximately 60% of the load goes through the medial part of the knee in the midstance phase of gait (432). Therefore, having a more pronated foot type could be an important risk factor for knee OA in both males and females with overpronation, resulting in an increased load on the medial part of the knee where OA is most common.

During normal walking, and especially during the heel strike, the lower limbs are subjected to repetitive impulsive forces that pass through the lower components of the musculoskeletal system to the upper components, possibly causing joint damage (433). Some of this force is absorbed when the foot pronates during the heel strike; however, people that have bone components that indicate a supinated foot will have a lower range of dorsiflexion and a more inverted calcaneus. This hinders foot pronation by shortening the duration of its occurrence, thus reducing shock absorption (201). This is the same phenomenon as that noted in the ankle bones of the hip OA group. However, it is important to note that in this study participants were examined in the non-weight-bearing position and that when bearing weight, for example during walking, it is expected that the amount of supination will increase. This will result in more force being applied to the hip and knee joints. The knee has features which allow the menisci to act as a protective shock absorbers, but the hip does not, which exposes it to more force than the knee (133).

In addition, after the heel strike and throughout the midstance to toe-off phases, the body passes over the foot with the knee joint fully extended (206). If a person has a limited dorsiflexion range of motion, as seen in people with supinated feet, this will result in having more body weight sustained over the extending hip joint (133). This might explain the wear of the acetabulum in the superolateral part noted in hip OA as a local mechanical factor (434).

The present study aimed to explore the morphological variations between participants with and without OA in both the knee and hip joints. It was hypothesised that participants with OA would exhibit differences in the structure of the ankle complex region when compared to

those in the non-OA group. The results presented in this study support this hypothesis with evidence of significant differences in ankle bone shape between OA and non-OA participants. The relationships between the JSWs in the ankle complex region and those in the hip and knee are discussed in the next section. The JSW is the only imaging biomarker currently recommended by the US Food and Drug Administration (FDA) as a structural outcome in clinical studies focusing on OA (435) and it provides an indirect assessment of cartilage thickness and width. Therefore, comparisons of cartilage width results with those obtained from bone shape data may provide a better understanding of those relationships.

8.2 3D Morphological variations in ankle complex JSWs

This study employed a full ankle complex 3D SSM to measure joint space widths (JSW) in the 206 participants across six main joints in the ankle complex region: the tibial plafond, medial malleolus, talonavicular, talofibular, subtalar posterior facet, and subtalar medial facet. A novel semi-automatic quantification method was used to obtain JSW measurements, which were recorded as mean (± SD) JSW values for each joint. The JSW data were then used to test hypotheses concerning the relationships with other relevant clinical measures, as discussed next.

8.2.1 Association between sex and body anthropometry variables with ankle complex JSWs

It was hypothesised that ankle complex JSWs measurements quantified using the 3D SSM would be different between male and female NTFS participants and that male participants would exhibit bigger JSWs compared to females. To test this hypothesis, differences between males and females in the JSWs of all six joints in the ankle complex region were assessed separately using an independent t-tests. The results showed significant differences in JSW between sexes in all six joints. Males in the sample tended to have highly significantly bigger joint spaces when compared to females in the six ankle joints, as seen in table 7-4.

Additionally, the relationships between ankle complex JSWs and body anthropometric variables of height, weight, and BMI were evaluated using linear regression models. The univariable models indicated significant associations between certain JSWs and body anthropometry variables as shown in tables 7-5 to 7-7. However, after adjusting for sex in the multivariable models, the statistical significance of the associations disappeared, indicating that sex may have been a confounding factor. Nonetheless, two JSWs, the medial malleolus

and talonavicular JSWs, remained significantly associated with BMI even after adjustment for sex.

Furthermore, tests were conducted to identify possible interactions between body anthropometry variables and sex, but no significant interactions were noted (see table 7-8). To explore the effect of the associations for each sex, the data were first stratified by sex and the analysis was then repeated. The results showed no significant association between any of the body anthropometry variables and JSWs, except for the medial malleolus and talonavicular JSWs in females, which showed a weak association with BMI (see tables 7-9 to 7-11).

It is important to note that, in reporting the p-values in the results section, no adjustments for multiple testing were applied, taking into consideration the fact that, if Bonferroni correction was applied, some borderline significant results might still be questioned. For example, in this study, the results show a significant association between the medial malleolus and the talonavicular JSWs with BMI in the adjusted and stratified regression models. In the adjusted-for-sex model, the respective values of p for those joints were 0.045 and 0.017, while in the stratified model they were 0.018 and 0.025. If Bonferroni correction had been applied those associations would no longer be statistically significant. However, in both cases, the values of the coefficients were relatively small, indicating rather weak associations. Conversely, if the adjustment was applied to the results of the t-tests for differences in JSWs between the sexes, the conclusions would remain the same due to their much stronger levels of statistical significance.

To the best of the author's knowledge, this study is the first to analyse morphological JSW variations in main ankle joints using 3D MRI SSM, and then to examine their association with clinical variables obtained from a true population cohort. Joint space width is an indirect measurement that represents the amount of cartilage in the joint. Reduced JSW can represent structural joint damage, which is a key indicator of OA. Conventional radiography is the primary method used to assess ankle JSWs both in the clinic and for epidemiological purposes. However, the anatomy of the ankle is very complex as it includes bones which overlap, which makes it difficult to accurately assess JSW using conventional 2D measurements (279).

A few recent studies have aimed to quantify the JSWs of the ankle joints using 3D SSMs derived from CT images. One study used weight-bearing cone-beam CT to build the SSM and quantify anatomical talocrural joint variation including only 3 joints, two of which are analysed in this study: the tibial plafond and talofibular (47). The results of the two studies are comparable, with mean JSWs (±SD) for the tibial plafond of 2.15 (± 0.41) mm in the previous study compared to 2.41 (± 0.56) mm here and for the talofibular 2.13 (± 0.20) mm compared to 2.45 (± 0.55) mm respectively, with the differences possibly attributable to sex ratios in the samples and patient positioning during scanning. Additionally, Krähenbühl, Lenz (56) also used weight-bearing cone-beam CT to reconstruct SSMs and quantify the JSWs of the posterior and anteromedial subtalar joint. Direct comparison with their results is possible for the subtalar posterior facet but not for the anteromedial subtalar joint since different methods were used in defining the joint. In the previous study the anterior and the medial facets were combined and treated as a single joint, whereas in the present study only the medial facet was quantified. The results for the subtalar posterior facet were also comparable, with mean JSW (± SD) values of 2.07 (± 0.44) mm compared to 2.88 (± 0.97) mm in the present study, with the differences again likely attributable to sample sex ratios and patient positioning during scanning.

Both of those previous studies were conducted on the same population with a relatively small sample size of only 27 'healthy individuals' (7 males and 20 females) with no explicit sampling frame, which is the main limitation of such studies reducing the generalisability of their results. Moreover, their small samples might explain why no investigation was conducted in either study of relationships with sex or body anthropometry, possibly due to a lack of statistical power. Therefore, there is a need to establish normative ankle 3D JSW values which can overcome the limitations noted above in using 2D radiographic methods and so that the findings can be generalised. That will also help in exploring morphological variations and their association with other clinical variables within a true population.

Such limitations in previous studies were addressed in the present study, which included 206 (83 males and 123 females) participants within the same age group who are members of a birth cohort that represent a sample of a true population. That allowed the assessment of differences between sexes in ankle JSWs and an investigation of the association with body anthropometry in the population. No studies using the 3D measurements method have

previously explored sex differences in the JSWs of the joints in the ankle complex region or their association with body anthropometry. Therefore, a direct comparison of the present results with those of existing research for males and females is not possible. However, several radiographic studies have demonstrated sex-related differences in ankle JSWs, where males were found to have wider joint spaces than females (436-438). Such findings are in accordance with the results of the present study has also found significant differences between sexes with males having wider joint spaces.

Such variations might be predicted to be due to the clear sexual dimorphism between males and females in body size (439). Physical differences between males and females are clear, where males tend to have taller and bigger skeletons (439). This might suggest that body size may also affect JSWs in both sexes. However, results from multiple regression models exploring the association between body anthropometry and sex have shown no associations between the JSWs and height, weight, and BMI after adjustment for sex. This indicates that obese, tall, or short people all have similar ankle JSWs, representing a similar amount of cartilage, with significant differences mainly associated with sex and not with body anthropometry. Similar results have been shown for knee JSWs, where no association was found with body anthropometry (440).

The presentation of evidence of significant sex-related variations in the JSWs of the joints in the ankle complex region which are independent of body anthropometry has important clinical relevance. The overall prevalence of symptomatic ankle OA is reported to be 3.4%, which is lower than the prevalence of either hip or knee OA (441). However, one in five people in the UK seeking treatment for OA in other joints exhibits evidence of OA in the foot or ankle (279). Many radiographic classifications are used to grade OA severity, such as the Kellgren and Lawrence (K&L) scale and minimal joint space width (mJSW), although these are not specific to the ankle.

They have been widely used in epidemiological studies despite the limitations mainly associated with conventional radiography (262). Such classifications depend on general threshold values for JSW used to distinguish between normal and narrowed joints. The results of this study provide evidence that such thresholds for normal and narrowed JSWs should depend on specific patient factors such as sex. For example, when grading ankle OA, what is reported to be a narrowed JSW for males could be reported as narrowed or pathological for

females if the same threshold was used for both sexes. This could result in a risk of false positive diagnoses higher for females or lower for males.

A recent systematic review by Tschon, Contartese (442) considered studies of the association between OA features and sex/gender differences, and the authors concluded that gender/sex-oriented protocols should be implemented in the diagnosis and treatment of OA due to the significant differences between the sexes in OA characteristics. Therefore, for the diagnosis of ankle OA using JSWs or any of the grading systems, thresholds for normal JSWs should be established for males and females separately. Taking into account the sex-specific differences in JSWs of the six joints in the ankle complex region, the findings presented in this study provide a rational, sex-specific normative data set.

8.2.2 Association between systematic BMD measurements and ankle complex JSWs

The present study aimed to explore the association between systematic BMD from four anatomical areas and measurements of JSWs in the ankle complex region. Linear regression was used in the analysis of data, which was initially conducted on the full sample and sex interaction was assessed. The interaction analysis did not find any evidence that sex affected the association between JSW and BMD. However, when the male and female models were analysed separately and adjusted for BMI, some of the associations failed to meet the threshold for statistical significance. This loss of significance can be attributed to reduced sample size, resulting in decreased statistical power. The associations which maintained significance exhibited differences in the values of the regression coefficients, suggesting a modifying effect of sex on these associations.

All statistically significant associations with each ankle JSW from the analysis of stratified data were included in a backward regression model. The results for males showed that the tibial plafond JSW was significantly associated with the right femur neck BMD. Similarly, the subtalar posterior JSW was also associated with right femur neck BDM. Finally, the subtalar medial JSW was associated with the lower limb BMD.

Furthermore, the female data showed that the tibial plafond JSW was associated with the total right femur BMD, while the subtalar posterior JSW was associated with right femur neck BDM. Finally, the talonavicular JSW showed an association with BMD measured from the spine.

It has been hypothesised that, in general, both local and systematic BMD is associated with the pathogenesis of cartilage loss particularly in the hand, hip, and knee joints. Evidence supporting this hypothesis is far from conclusive and the subject is still a matter of debate in the literature. Some cross-sectional studies show a positive association between systematic BMD and knee cartilage volume as assessed by MRI (443-445). Another study using radiographic mJSW as a measure of cartilage thickness in 45 healthy women showed positive associations between high tibia BMD and increased knee mJSW and high femoral trochanter BMD and increased knee mJSW (130). In contrast, some studies suggest that higher systematic BMD is associated with cartilage loss and radiographic knee and hip OA (124, 126, 446). Such conflicting outcomes from studies of hand, hip and knee joints could be attributed to differences between the studies regarding the measures used, characteristics of the participants, or the health status of the joints studied.

However, no studies have investigated whether or not a similar association exists between systematic BMD measurements and ankle joints. This is probably because OA in the ankle is not as common as it is in other joints. The results of the present study complement and extend what has been found in other studies of association between high BMD and radiographic JSWs in the knee and hip. In particular, there is a positive linear association in the NTFS population between ankle JSWs and systematic BMD measurements taken from the right femur, lower limbs, and spine, which suggests that healthier (not narrowed) ankle joints are related to the greater robustness of bones in both males and females, but the magnitude of the association appears to be stronger in males. The reasons for these sex differences remain unclear and cannot be explained in this study. BMI was controlled for in the analysis and has been shown to be associated with BMD in previous studies of the same cohort (447, 448). However, information concerning other variables such as bone size and physical activity levels were not available, whereas these factors might vary between the sexes and could help explain the differences noted between sexes.

A possible explanation for this association could be due to biomechanical factors affecting the relationship between ankle JSWs and lower limb bones and joints. It has been found that bone health is directly influenced by mechanical loading, as demonstrated by Wolff's law (449), which states that both the external shape and internal structure of a bone change as a direct response to the mechanical forces that is subjected to (449). Many studies have tested the

effect of mechanical force on bone health. For instance, studies of BMD in stroke and spinal cord injury patients have concluded that reductions in weight-bearing activity result in the loss of mechanical force on the bones and thereby contribute to bone loss and lower BMD measurements (450-452). In addition, studies conducted of patients who are immobilised either due to long periods of hospitalisation, having total contact casts on one of the lower limbs, or using crutches and wheelchairs exhibit significant decreases in BMD measurements of the femoral neck and total hip, which is attributed to reductions in mobility and weight-bearing activity (453-455).

This could be due to those with healthy ankles and normal JSWs being more likely to take part in physical activities that increase the transmission of mechanical force from the ankle joints after contact with the ground to the other bones and joints of the lower limb. Conversely, participants with altered ankle joints or structural change are less likely to partake in many physical activities, thus decreasing the loads on other bones and joints and affecting systematic BMD measurements.

This study's findings show an association between systematic BMD measurements and ankle JSWs, which might indicate a biomechanical link between joints in the lower extremities and especially between the ankle and the hip joints, since a significant association was found with femoral neck BMD in both males and females. As mentioned previously, many studies have explored the relationship between BMD and OA of the hip and knee. Therefore, the relationship between BMD and ankle JSWs could have a biomechanical explanation, which would provide new insights into the role of ankle joint morphology and its biomechanical effects in influencing the development and progression of knee and hip OA. The next section discusses the association between ankle JSWs and hip and knee OA, focusing on both radiographic and clinical data.

8.2.3 Association between hip and knee OA data and ankle complex JSWs

It is generally thought that, when OA symptoms or structural changes occur in one of the lower extremity joints such as the knee, they can in turn have a direct effect on other kinematically related joints such as the hip and ankle (35). Despite this, most studies have mainly focused on the relationship between the knee and hip joints, while the association between ankle joints and OA-related symptoms or radiographic features in either the knee or hip joints have received less attention. Therefore, the final aim of this study was to explore

the association between ankle JSWs and the radiographic features of OA for both the hip and knee, including JSWs and the grading of OA severity. Also, the relationships between ankle JSWs and functional clinical variables from both the knee and hip joints would also be explored, such as reported pain in the joints and WOMAC gradings that assess pain, stiffness, and the physical function of both the hip and knee joints.

It was hypothesised that ankle joint JSWs measured using the 3D SSM technique are associated with the JSWs of other lower limb joints, including the hip and knee. Additionally, it was predicted that participants with hip or knee pain or higher WOMAC scores may have different JSW measurements compared to those without these conditions. This section summarises the findings and discusses the associations between ankle JSW and functional clinical variables and the structural radiographic features of OA.

8.2.3.1 Association between ankle JSWs and knee and hip functional assessments

In the NTFS population, no statistically significant differences in ankle JSWs were found between participants who reported pain in either the knee and hip joints and those who did not, as shown in tables 7-12 and 7-20. In addition, no significant differences in ankle JSWs were noted between severity groups in the WOMAC grading system which assesses pain, stiffness, and physical function in the knee and hip, as seen in tables 7-30 to 7-32.

No studies have previously specifically explored such an association with ankle JSWs, and therefore the outcomes of this study cannot be compared directly with others. However, some studies have investigated the association between ankle and foot symptoms of stiffness, pain, and itching and knee and hip OA symptoms of pain and WOMAC gradings.

Using data from the Framingham study, (32) found no association between self-reported hip pain and rear-foot varus alignment, as determined using digital photography in a non-weight bearing position and then the calculation of the angle of the calcaneus bone. Other results match those findings despite clear differences in the methodologies used. The rear-foot region contains the bones forming the ankle joint complex, and changes in the varus alignment of the rear foot results in variations in the JSWs of the ankle joint complex (456). This present study explored the relationship between all six joints forming the ankle joint complex and reported hip pain directly using a more robust method of assessment and found no such association.

Meanwhile, Paterson, Hinman (33) used WOMAC scoring to examine differences in knee pain, stiffness and physical function between participants reporting ankle pain and those without. They concluded that participants with ankle pain reported a 39% worse score on all WOMAC subscales, indicating a progression of symptomatic OA in the knee joint. Their further longitudinal study Paterson, Kasza (34) that used data from the Osteoarthritis Initiative study over the subsequent 4 years to explore the association between self-reported ankle and foot symptoms of stiffness, aching or pain and the risk of worsening knee pain and radiographic knee mJSW. The results showed that the reported ankle and foot symptoms were associated with worsening knee pain during the period of the study. However, no such association with OA radiographic knee mJSW was noted. Furthermore, a recent study by Perry, Segal (35) using data from the Multicentre Osteoarthritis Study investigated the association between baseline ankle and foot pain with frequent knee pain at more than one follow-up. The study showed a significant association between ankle pain and knee pain.

A limitation of all these studies was the dependence on self-reported symptoms, so that the causes of ankle and foot pain were not considered. It could occur due to a variety of factors, including ligament or tendon sprains, joint degeneration, tendinitis, or flat foot (457). The explanation provided by the authors for the association between ankle and knee pain involves the biomechanical links between the lower limb joints, and especially the way that the ankle joints compensate for the effect of structural changes happening in the knee; for example, the adoption of a more pronated foot pattern which has been noted in knee OA patients who report pain in the ankle and foot.

Although such a hypothesis is logically feasible, it has not so far been tested. Perry, Segal (35) concluded that future research should explore the association further by exploring the individual contributions of other foot and ankle characteristics, such as in the subtalar and talocrural ankle joints, to the symptomatic and radiographic features of knee OA. The present study contributes to and extends research on the association presented in prior studies by focusing on one possible cause of ankle pain, which is reduced JSWs in the ankle region. This study found no significant differences in ankle JSWs between participants who reported knee and hip pain and those who did not, or between the severity of symptoms measured by the WOMAC subscales. This contradicts the hypothesis that there would be significant differences in ankle JSWs between the two groups. However, the number of participants reporting pain

in either the knee or hip could be argued to be low (66 knee pain and 44 hip pain), as with the moderate and severe groups according to the WOMAC subscales. This might have affected the statistical power of this analysis. Investigations for bigger samples with more participants reporting pain in both the hip and knee would generate more valid findings that may agree with or contradict those presented here.

8.2.3.2 Association between ankle JSWs and knee/hip radiographic structural assessments

A further question this research aimed to answer is whether or not there are associations between the JSWs in the ankle complex region and radiographic features of knee and hip OA in terms of JSWs and OA severity grading. Participants with knee OA showed no significant differences in the ankle JSWs compared with participants without knee OA. However, a trend of a more narrowed JSW was noted in the knee OA group compared to the non-OA group. Especially in the subtalar posterior JSW which showed a near significant p value, as shown in table 7-13. Likewise, all ankle JSWs were narrower in participants with hip OA than those without hip as seen in table 7-23, and these differences were significant in three of the six ankle JSWs: the tibial plafond, tibiofibular, and subtalar posterior.

Linear regression models revealed that four of the six ankle joints showed a significant positive association with the radiographic JSW of the right knee in the univariable analysis reported in table 7-14. However, after adjustment for sex and BMI, the JSWs of only two ankle joints remained significantly associated with right knee mJSW: the tibial plafond and subtalar posterior, as shown in table 7-14. No significant associations were found between the radiographic mJSW of the left knee and ankle JSWs (table 7-15). In addition, the association between ankle JSW and the mJSW of the ipsilateral knee was similar, with only a slight change in the regression coefficient compared to the right knee analysis (table 7-16).

The interaction analysis produced no evidence that sex modified the association between ankle JSWs and radiographic knee mJSW, as shown in table 7-19. Stratification of the data according to sex and adjustment for BMI showed that only the subtalar posterior facet had a significant association with the right knee JSW in both males and females. With the association being stronger in males, while the tibial plafond did not show any significant association in both sexes possibly due to the smaller sample size (see tables 7-18 and 7-19).

Similar initial analyses were conducted to explore the association between radiographic hip JSW and 3D ankle JSWs. Evidence of the association between the two joints being modified by sex found when the interaction coefficient was added to the model, as seen in table 7-27. When the analysis was conducted on the stratified data, it was found that the magnitude and significance level of the associations was stronger in males than females, and in the latter no statistically significant association was noted between any of the ankle JSWs and the hip JSW measurements. However, in males there were significant positive associations between the right hip JSW and the JWS of the tibial plafond, talonavicular, tibiofibular, and subtalar posterior facet. There were similar outcomes from the ipsilateral analysis and no significant association was found between any of the ankle JSWs and the left hip JSW.

Scant research explored the direct structural association between ankle JSWs and either knee or hip JSW. This could be attributed to, for example, the significant limitations associated with the ability of 2D radiography, which is widely used in many studies, to evaluate the 3D morphology of the joints in the ankle complex region (458). Also, the prevalence of ankle OA is much lower than that of the hip and knee and likely has a different aetiology and leads to nowhere near the same volume of surgical interventions. All of these factors might lead research groups to direct more attention to the knee and hip joints (279) and, for such reasons, comparison of the outcomes of the present study with those of other research is necessarily limited.

Although published studies on the association between JSWs of the ankle and those of the knee and hip are sparse, Eckstein, Siedek (459) investigated the correlation between knee and ankle cartilage thickness assessed using MRI in a sample of 29 healthy adults. Their findings are similar to those of this present study, and they reported a moderate correlation between the thickness of cartilage in the knee and that of the tibial plafond and the subtalar joints. In the present study, the JSWs of both joints also showed a significant positive association with the knee JSW.

Furthermore, Kraus, Worrell (44) assessed abnormality in the ankle joint complex using nuclear medicine bone scans from 159 participants with radiographic knee OA during a 3-year follow-up. The baseline results showed a significant association between knee joint space narrowing and ankle bone scan abnormalities. Radiographs of the ankle were taken, and bone scans was repeated on 138 participants who returned for follow up. The results showed that

bone scan abnormalities were associated with the narrowing of the tibial plafond JSW measured using radiographic ankle images. Although they did not directly assess the association between the ankle and knee JSWs, their results indicate an association between the two joints like that found in this study.

Regarding the association between the JSWs of the ankle and hip, Goker, Gonen (438) used 2D radiography to quantify ankle JSWs for 95 participants using digital software and correlated the results with those of the ipsilateral hip joint. They focused only on the main ankle joint, the tibial Plafond, and reported significant correlations between the JSWs of the lateral and medial joint and that of the ipsilateral hip. The results from the present study are consistent with those findings. However, Goker et al. only explored the main ankle joint and did not mention any interaction or adjustment analysis performed to evaluate the confounding or mediating effect of sex. In the present study, all the joints in the ankle complex region were explored and a much deeper analysis was performed. Associations were found the JSWs of four of the six joints in the ankle complex and the hip, including the tibial plafond which showed a more significant association in males compared to females.

Other studies have explored the structural associations between the hip, knee, and ankle joints using lower limb alignment measurements. For instance, Xie, Jiang (43) investigated the relationship between ankle OA in adults with varus knee malalignment, which is common in end-stage knee OA. The authors reviewed 96 full-leg radiographic images of the participants who had undergone knee arthroplasty. The association between varus knee malalignment and incident radiographic ankle OA was determined by both the medial proximal tibial angle and the hip-knee-ankle angle measurements. While this indicated a structural association between the two joints, as in the previously mentioned study, the focus was again on the main ankle joint. No other joints were assessed, including the subtalar joint which showed a stronger association in the present study. A possible reason for the main or exclusive focus on the main ankle joint is its anatomical position, which hinders the ability to accurately assess the subtalar joint using conventional radiography (460). A novelty of the current study is the use of 3D-SSM to assess the ankle complex region, which allowed direct quantification of all joints and an exploration of their associations with lower limb joints.

This is the first study to directly look at the association between JSWs as a known measure of cartilage thickness in the ankle complex region and those of the knee and hip joints. No earlier

research has been located that has examined such an association on older adults who are member of a birth cohort more susceptible to OA, or in using 3D-SSM to quantify JSWs in the ankle complex region. The results of this study augment and expand upon those of earlier research regarding the interrelationships between foot and ankle characteristics and knee and hip OA.

The results confirm a significant linear association between the JSWs of the knee and both the tibial plafond and the subtalar joints. A one mm increase or decrease in the knee JSW is associated with a 4% (0.10 mm) and 8% (0.20 mm) increase/decrease in the JSWs of the tibial plafond and subtalar posterior joints respectively. Knee JSW narrowing is the only gold standard approved by the FDA as a surrogate for knee OA progression (15). The results from the linear regression models indicate a positive liner association. Similarly, both joints showed narrower JSW in the knee OA group when compared to the known OA group.

Although the magnitude of such associations might appear statistically weak, it should be noted that the average normal knee JSW ranges from 4.8-5.7 mm in healthy adults (461) which is approximately double that of the tibial plafond which has an average range of 2.4-2.7 mm (438) while the average JSW of the subtalar posterior facet is between 2.07-2.8mm (56). Therefore, when considering the differences in the normal mean values for the knee and the ankle joints, such percentages do have important clinical relevance.

In the hip JSW analysis, the results showed significant association with four of the six ankle joints in the male population only. The association was statistically stronger with both the tibial plafond and the subtalar posterior facet. The hip OA group had smaller ankle JSWs in both sexes; however, this difference was statistically significant only in the male population. A possible explanation for this is that men and women have distinct skeletal characteristics, which may have an impact on how the ankle and hip joints are aligned and connected.

For instance, women are more likely than males to have wider hips and a more pronounced quadriceps angle between the thigh and the ankle, which may have an impact on how the ankle and hip joints align (462). In addition, other relevant variables such as muscle mass and physical activity measurements were not available in this analysis and could have added further explanation of the sex differences found. Therefore, no explanation can be offered as

to why a significant relationship was demonstrated only in men. Further research into sex differences regarding this association is required.

In both the knee and hip analyses, the strength of the association between the ankle JSWs and those of the hip and knee varied depending on the joint examined. For example, in the knee analysis, the association is more significant for the subtalar posterior JSWs compared to the tibial plafond indicating that the subtalar joint is more important. However, the ankle complex region is an object connected in three dimensions encompassing several joints (456). Therefore, a variation in one joint may affect other joints, especially the ones that share the same plane of motion (456).

For instance, the motion of the subtalar joint is tri-planar which involves external and internal rotation and eversion and inversion motions, and thus any variation in the JSW of the subtalar joint would be expected to affect that of the tibial plafond since they work together as a combined joint and share similar motion planes (181, 463). This may explain the stronger association between the knee JSW and the subtalar JSW compared to that of the tibial plafond, in that the former joint is more important and the relationship with the main ankle joint is secondary. This would also apply to the hip analysis given that the strength and magnitude of the associations differ from one ankle joint to another.

As mentioned previously in this chapter, when discussing the association of ankle JSWs with sex and body anthropometry variables, the results of the ankle JSWs were presented without correction for multiple testing since the ankle is a complex 3D structure and each of the six joints may vary in the strength and the magnitude of their association with other variables. For example, if correction had been applied, the association between the tibial plafond and knee JSWs would be deemed not statistically significant and instead attributed to chance. But it does have a clinically meaningful association even though the subtalar posterior joint is more significant. It is narrower in the OA group, and therefore when the alignment of this joint is affected it will affect to some degree the alignment of the tibial plafond since these two joints share coupled motions (463).

In summary, the results indicate that there are associations between some JSWs of the joints in the ankle complex region and those of both the hip and knee. Such associations are stronger for the tibial plafond and subtalar posterior joints. In addition, participants with degenerating

joints in either the hip or knee due to OA had narrower ankle complex joint spaces which were more significant in the hip analysis. This indicates that lower JSWs in the ankle complex region are common in participants with both hip and knee OA.

These associations could have several possible explanations. Firstly, they could result from the structural changes occurring in the hip or the knee joints caused by OA which might affect the alignment of the lower limbs. For example, several studies have concluded that both varus and valgus deformity in the knee joint could have a severe impact on the alignment of the lower limb, depending on the degree of deformity, resulting in altered hip-knee-ankle alignment which would affect the lower extremity including the ankle (41-43). That could affect balance, causing the subtalar joint and the motion of the ankle complex region to adopt a different pattern in order to compensate in the balancing of the lower limb for by the misalignment occurring as a result of knee deformity (42). Such adaptations could result in corresponding changes in the alignment of the ankle complex joints, resulting in increased pressure on them leading to structural change developing over time (464).

In support of this, several studies show that the prevalence of ankle OA in knee OA patients is high. Tallroth, Harilainen (45) reported that 29% of their participants with knee OA also showed some form of ankle OA. Furthermore, Xie, Jiang (43) found the incidence of ankle OA at 37% among such patients to be higher than that in the general population. Finally, Kikuchi, Kanamori (46) recently reported the incidence of ankle OA to be 24% in their sample with knee OA.

Another hypothesis that would explain the narrowing of JSWs in the ankle complex region is that patients with knee and hip pain could alter their gait to lower the pressure on the hip or knee joints so as to avoid further pain. One study examined ankle biomechanics in patients with hip pain using 3D kinematic data (465). The results showed that the participants with hip pain exhibited altered ankle kinematics, such as reduced dorsiflexion in the ankle. If adopted for longer periods, this would affect the joints of the ankle complex region which would be subjected to increased stress leading to the development of some form of joint degeneration.

A further explanation for such an effect might be related to variations in foot type between participants with hip and knee OA compared to those without these conditions. In this study, the results of the ankle bone shape variations between participants with and without OA and

the results of other several studies, have noted that participants with hip OA have a foot type that is more supinated and that participants with knee OA have foot types that are more pronated (36-38, 424). Excessively supinated or pronated foot types could represent variations in how the bones in the ankle complex region are aligned with each other. Such variations could result in differences in the JSWs of the joints connecting the bones. These would be expected to have a greater effect the subtalar and tibial plafond joints which are mainly associated with supination and pronation movements in the ankle complex region (456). Excessive or prolonged pronation or supination can result in flat feet or foot types with a higher arch as well as issues such as overuse injuries, which can in turn contribute to subtalar joint degeneration (181).

The principal purpose of the subtalar joint, which is located between the talus and calcaneus bones of the foot, is to permit the inversion and eversion of the foot. The cartilage that cushions the joint might become increasingly worn and torn as a result of prolonged or severe pronation and/or supination, causing the bones in the joint to brush against one another more frequently than they should (181). In addition, those bones may also move out of position as a result of excessive pronation or supination, which can contribute to the degeneration of the subtalar joint (36).

Previously in this chapter, variations in the shapes of bones in the ankle complex region between participants with and without hip and knee OA were discussed. Knee OA participants showed ankle complex bone shape which indicate a pes planus foot structure (pronated foot) with a more everted calcaneus and a dropped navicular bone, whereas the hip OA participants presented a more pes cavus foot structure (supinated foot) with a more inverted calcaneus and an increase in navicular bone height. These findings support the results noted in this analysis. Where such associations between both the tibial plafond and the subtalar JSWs with both the hip and knee JSW are consistent. Variations in the alignment and structure of the ankle joint complex could have a biomechanical effect on both the knee and hip joints since they share the same kinetic chain. Such effects are mainly initiated during the gait cycle and are linked to how force applied passes from the ground through the lower limb. Studies discussed in section 8.1.2 explained how alterations in the ankle complex region caused by variations in foot type affect the distribution of mechanical force throughout the lower limb.

This raises an important question regarding cause and effect. Are the morphological variations found in the bone of the ankle complex region and their association with the JSWs of the hip and knee joints promoting the incidence or progression of OA in the joints of the kinetic chain in the lower limb such as the knee and hip joint? Alternatively, are morphological variations in bone shape and ankle joint JSWs a result of a compensatory mechanism secondary to the development of OA in other joints sharing the same kinetic chain? This important question cannot be definitively answered in this study since a cross-sectional analysis cannot determine causation.

However, it should be noted that the theory that such relationships are driven by the ankle joint's ability to compensate for the imbalance caused by malignment in the lower limb might be supported by the findings from studies which evaluate the ankle joints in the upright weight-bearing position, where some form of adaptation to the surface will occur. In the present study, the ankle complex region was examined using MRI while participants were in a non-weight bearing position, but similar associations were nonetheless found. This supports an explanation in terms of morphological variations in the ankle complex region affecting how the bones are aligned together. In addition, the presence of these associations even in the early stages of knee and hip OA as well as plausible direct mechanisms related to mechanical force and gait suggest that ankle morphology drives knee and hip OA and not *vice versa*. This analysis and further research with the NTFS cohort present a unique opportunity to test such hypotheses using data from subsequent reviews in order to determine how much baseline morphology at age 62 predicts incident and progressive knee and hip OA.

8.3 Strengths of the study

This study has several strengths as listed below:

- It is possible to generalise the findings to a larger population, since the participants studied are members of a birth cohort representative of the general population at the time of their birth.
- The use of statistical shape modelling which applies novel machine learning algorithms to construct detailed models of a structurally complex joint such as the ankle joint using MRI images facilitates the accurate quantification of various measurements such as bone shape, bone area, and joint space width.
- In comparison to other studies of ankle morphology using SSM, a larger sample of 206 participants were examined within the specific age group of those aged 62 years old who share the same ethnicity and are more susceptible to OA. This helped in minimising bias related to different age, genetic and lifestyle factors that may vary between ethnic groups and which could affect the morphology of the ankle.
- A quantitative assessment is provided of variations in ankle morphology which can be used as a reference for future research and clinical practice.
- Several variables are considered for which data had been collected previously, such as assessments of pain and function related to OA, body anthropometry, OA radiographical features and systematic bone density measurements.
- The associations between ankle morphology and OA in multiple joints of the lower limb are examined, which allows for a more comprehensive understanding of the relationships between joints sharing the same kinematic chain and could potentially lead to improved diagnostic and treatment options for patients with OA.

8.4 Potential weaknesses of the study

To correctly evaluate and utilise the findings of this study, it is crucial to recognise and comprehend its limitations. The major limitations of this study are described below:

- The utilisation of a low-field (0.2T) Esaote C-Scan MRI scanner for the imaging of the ankle joint is limited by its low resolution. The decision to use this scanner was made to reduce the risk of claustrophobia among participants and to increase study participation, and the scanning was accomplished in the Clinical Research Facility where a range of other measurements were also completed. Since the SSM reconstruction was based on manual bone segmentation from a trained sample, the quality of the images was deemed to be acceptable, and it is unlikely that major morphological bone features were missed during the process.
- The sample size still carries some risk of both type 1 (false positive) type 2 (false negative) errors, which may have therefore affected some estimates. Although the sample of participants in this study was three times larger than those in the most relevant previous studies, an even larger sample size might produce more robust results and further reduce the likelihood of type 1 & 2 errors.
- The morphological variations and associations presented in this study are for participants who were 62 years of age, and therefore the results may not be generalisable to other age groups. It is important to consider this when interpreting the results of the study.
- The 3D-SSMs were constructed based on the segmentation of bone surfaces from MRI images with no direct segmentation of the cartilage, and therefore, all JSW results should be interpreted accordingly.
- This study is cross-sectional in nature, which limits the ability to establish causality or track changes over time. Future musculoskeletal assessments planned by the NTFS could enable the longitudinal examination of the findings of this study. Also, further data could be included such as from gait analysis, muscle mass evaluation, foot and ankle and ligament assessments that can help in determining the impact of the morphological variations found in the ankle complex region on gait kinematics and

kinetics. This to lead to more categorical explanations of the relationships between the associations presented in this study and other joints in the lower limb.

- Another issue relates to the use of radiographic images to evaluate the JSWs of the knee and hip. Several limitations have been associated with such methods which may increase the variability in the data and could affect the estimate of the R-squared in regression analysis. Further research quantifying JSW from knee and hip 3D-MRI SSMs has shown better accuracy and including those models rather than radiographic knee and hip data may provide better estimates.

8.5 Recommendations

This study has shown that the association between the JSWs of joints in the ankle complex region and the differences in bone shape between knee/hip OA and non-OA groups is of clinical importance. Clinicians should consider evaluating ankle structure, especially in patients with lower limb OA. The clinical assessment of foot posture would also be valuable, as would the consideration of radiographic assessments in selected patients. The correction of foot posture with orthoses may have a role in preventing the onset and/or progression of knee and hip OA, which would be particularly important if prospective studies showed subsequent delays in or avoidance of joint replacement surgery. In any case, surgeons should evaluate the ankle complex region in preoperative planning for both total knee and hip surgeries. In addition, further research exploring variation in ankle morphology and gait would add value. Also, repeating such analysis on a younger cohort to assess if such associations noted in this research are already apparent earlier would add more insight to such relationships. In a forthcoming review of the NTFS, further data such as gait and foot and ankle assessments along with higher resolution MRI images of the hip, knee, and ankle are warranted. The use of 3D-SSM to reconstruct shape models for all three joints and investigations of their interrelation would deepen our understanding of the relationships between joints in the lower limb in addition to giving insights into the temporal relationships involved in structural changes in the ankle, knee, and hip.

8.6 Conclusion

This is the first population-based study which has used MRI images of the ankle complex region to reconstruct 3D SSMs using machine learning algorithms. Through this approach, the anatomical complexity of the ankle joint was simplified, enabling the analysis of morphological variation in the studied population. Several significant morphological variations in bone shape, bone area, and JSW were found between the sexes. Males in the population showed wider and larger bone shapes when compared to females, independent of body anthropometry. Furthermore, bone area and JSW measurements further confirmed the variations noted in the PC bone shape modes between the sexes. The PC modes of variation also showed significant differences between participants with hip/knee OA and those without in both sexes. Participants with knee OA were found to have bone shapes and alignments representing a *pes planus* foot type, while those with hip OA participants had bone shapes and alignments representing the *pes cavus* foot type. Given these variations in the ankle complex region even at the early stages of OA, strategies of correction could be promising methods for the prevention of progressive knee and hip OA and delaying or avoiding joint replacement surgery.

The joint space widths of the six ankle joints comprising the ankle complex region were quantitatively evaluated from 3D-SSM. The results revealed that all joints demonstrated significant differences between males and females, with females exhibiting narrower JSWs compared to males regardless of body anthropometry. A backward regression analysis found a positive correlation between systematic BMD measurements and certain JSWs in the ankle complex. Additionally, the relationships between the JSWs of the hip and knee joints and those of six joints in the ankle were examined. Both males and females displayed a significant positive association between the JSWs of the right and ipsilateral knee and those of the tibial plafond and subtalar posterior. In males only, a significant positive association was also observed between the right and ipsilateral hip JSWs and four of the ankle JSWs. Participants with hip OA also exhibited narrower ankle JSWs compared to those without, and this difference was statistically significant in males although a similar but weaker trend was observed in females. Plausible explanations were offered for the associations discussed in this study, suggesting a direct mechanism related to mechanical force and gait.

This study shows a significant difference in the way that the ankle complex region is constructed between sexes. Such differences are attributable to the variations between the sexes associated with bone size and the way bones are connected which also result in females having smaller JSWs compared to males. It is well established that OA is more common in females compared to males. In addition, the results show that both males and females with OA in the hip and knee have narrower ankle JSWs, which could be attributed to morphological variations in the way that the bones align in the ankle complex region. Alterations in the structure of the ankle complex region have previously been linked to altered gait patterns, which may then alter the distribution of the mechanical load throughout the lower limb. We know that progressive OA is biochemically mediated, but mechanically driven. All indications suggest that ankle morphology may directly influence knee and hip OA through the effects of gait and the distribution of mechanical force. However, further studies including 3D SSM of ankle morphology, and preferably of knee and hip morphology too; and perhaps including additional methods of gait assessment are needed to confirm this hypothesis. This could be tested in subsequent reviews of this cohort or by research on other populations.

References

1. Kraus VB, Blanco FJ, Englund M, Karsdal MA, Lohmander LS. Call for standardized definitions of osteoarthritis and risk stratification for clinical trials and clinical use. Osteoarthritis Cartilage. 2015;23(8):1233-41.
2. Dobson G, Letson H, Grant A, McEwen P, Hazratwala K, Wilkinson M, et al. Defining the osteoarthritis patient: back to the future. Osteoarthritis Cartilage. 2018;26(8):1003-7.
3. Birrell F, Howells N, Porcheret M. Osteoarthritis: pathogenesis and prospects for treatment. Rep Rheumatic Dis. 2011;10:1-2.
4. Allen KD, Golightly YM. Epidemiology of osteoarthritis: state of the evidence. Curr Opin Rheumatol. 2015;27(3):276.
5. Heidari B. Knee osteoarthritis prevalence, risk factors, pathogenesis and features: Part I. Caspian journal of internal medicine. 2011;2(2):205.
6. Osteoarthritis how common is it? [Internet]. National Institute for Health and Care Excellence. 2020 [cited 08/02/2023].
7. Lawrence JS. Rheumatism in populations chapter 5 ostioarthrites Elsevier; 2016.
8. OA Nation 2012 [Internet]. arthritiscare. 2012 [cited 08/02/2023].
9. Hootman JM, Helmick CG, Barbour KE, Theis KA, Boring MA. Updated projected prevalence of self-reported doctor-diagnosed arthritis and arthritis-attributable activity limitation among US adults, 2015–2040. Arthritis & rheumatology. 2016;68(7):1582-7.
10. Sinusas K. Osteoarthritis: diagnosis and treatment. Am Fam Physician. 2012;85(1).
11. Hayashi D, Roemer FW, Guermazi A. Imaging for osteoarthritis. Ann Phys Rehabil Med. 2016;59(3):161-9.
12. Kohn MD, Sassoon AA, Fernando ND. Classifications in brief: Kellgren-Lawrence classification of osteoarthritis. Springer; 2016.
13. Kellgren J, Lawrence J. Radiological assessment of osteo-arthrosis. Ann Rheum Dis. 1957;16(4):494.
14. Croft P, Cooper C, Wickham C, Coggon D. Defining osteoarthritis of the hip for epidemiologic studies. Am J Epidemiol. 1990;132(3):514-22.
15. Conaghan PG, Hunter DJ, Maillefert JF, Reichmann WM, Losina E. Summary and recommendations of the OARSI FDA osteoarthritis Assessment of Structural Change Working Group. Osteoarthritis Cartilage. 2011;19(5):606-10.
16. Rychel JK. Diagnosis and treatment of osteoarthritis. Top Companion Anim Med. 2010;25(1):20-5.
17. Bellamy N, Buchanan WW, Goldsmith CH, Campbell J, Stitt LW. Validation study of WOMAC: a health status instrument for measuring clinically important patient relevant outcomes to antirheumatic drug therapy in patients with osteoarthritis of the hip or knee. The Journal of rheumatology. 1988;15(12):1833-40.
18. Hunter DJ, Bierma-Zeinstra S. Osteoarthritis. The Lancet. 2019;393(10182):1745-59.
19. Peat G, Thomas M. Osteoarthritis year in review 2020: epidemiology & therapy. Osteoarthritis Cartilage. 2021;29(2):180-9.
20. Filardo G, Kon E, Longo UG, Madry H, Marchettini P, Marmotti A, et al. Non-surgical treatments for the management of early osteoarthritis. Knee Surg Sports Traumatol Arthrosc. 2016;24:1775-85.
21. Silverwood V, Blagojevic-Bucknall M, Jinks C, Jordan J, Protheroe J, Jordan K. Current evidence on risk factors for knee osteoarthritis in older adults: a systematic review and meta-analysis. Osteoarthritis Cartilage. 2015;23(4):507-15.
22. Zheng H, Chen C. Body mass index and risk of knee osteoarthritis: systematic review and meta-analysis of prospective studies. BMJ Open. 2015;5(12):e007568-e.

23. Anderson AS, Loeser RF. Why is osteoarthritis an age-related disease? Best practice & research Clinical rheumatology. 2010;24(1):15-26.
24. Johnson VL, Hunter DJ. The epidemiology of osteoarthritis. Best practice & research Clinical rheumatology. 2014;28(1):5-15.
25. Guilak F. Biomechanical factors in osteoarthritis. Best practice & research Clinical rheumatology. 2011;25(6):815-23.
26. Dawe EJ, Davis J. (vi) Anatomy and biomechanics of the foot and ankle. Orthopaedics and Trauma. 2011;25(4):279-86.
27. Richards J. The Comprehensive Textbook of Clinical Biomechanics. Elsevier Health Sciences; 2018.
28. Yamaguchi S, Sasho T, Kato H, Kuroyanagi Y, Banks SA. Ankle and subtalar kinematics during dorsiflexion-plantarflexion activities. Foot Ankle Int. 2009;30(4):361-6.
29. Harrold F, Abboud RJ. Biomechanics of the Foot and Ankle. Core Topics in Foot and Ankle Surgery. 2018:22-43.
30. Hazari A, Maiya AG, Nagda TV, Hazari A, Maiya AG, Nagda TV. Lever Systems at Human Joints and Muscles. Conceptual Biomechanics and Kinesiology. 2021:53-7.
31. Almeheyawi RN, Bricca A, Riskowski JL, Barn R, Steultjens M. Foot characteristics and mechanics in individuals with knee osteoarthritis: systematic review and meta-analysis. J Foot Ankle Res. 2021;14(1):24.
32. Gross KD, Niu J, Zhang YQ, Felson DT, McLennan C, Hannan MT, et al. Varus foot alignment and hip conditions in older adults. Arthritis & Rheumatism: Official Journal of the American College of Rheumatology. 2007;56(9):2993-8.
33. Paterson KL, Hinman RS, Hunter DJ, Wrigley TV, Bennell KL. Impact of concurrent foot pain on health and functional status in people with knee osteoarthritis: data from the osteoarthritis initiative. Arthritis Care Res (Hoboken). 2015;67(7):989-95.
34. Paterson KL, Kasza J, Hunter DJ, Hinman RS, Menz HB, Peat G, et al. Longitudinal association between foot and ankle symptoms and worsening of symptomatic radiographic knee osteoarthritis: data from the osteoarthritis initiative. Osteoarthritis Cartilage. 2017;25(9):1407-13.
35. Perry TA, Segal NA, Bowen C, Gates L, Arden N, Nevitt MC. Foot and ankle pain and risk of incident knee osteoarthritis and knee pain: Data from the Multicentre Osteoarthritis Study. Osteoarthritis and cartilage open. 2021;3(4):100210.
36. Reilly KA, Barker KL, Shamley D, Sandall S. Influence of foot characteristics on the site of lower limb osteoarthritis. Foot Ankle Int. 2006;27(3):206-11.
37. Reilly K, Barker K, Shamley D, Newman M, Oskrochi G, Sandall S. The role of foot and ankle assessment of patients with lower limb osteoarthritis. Physiotherapy. 2009;95(3):164-9.
38. Abourazzak F, Kadi N, Azzouzi H, Lazrak F, Najdi A, Nejjari C, et al. A positive association between foot posture index and medial compartment knee osteoarthritis in moroccan people. The open rheumatology journal. 2014;8:96.
39. Gross KD, Felson DT, Niu J, Hunter DJ, Guermazi A, Roemer FW, et al. Association of flat feet with knee pain and cartilage damage in older adults. Arthritis Care Res (Hoboken). 2011;63(7):937-44.
40. Zhang M, Nie MD, Qi XZ, Ke S, Li JW, Shui YY, et al. A Strong Correlation Between the Severity of Flatfoot and Symptoms of Knee Osteoarthritis in 95 Patients. Front Surg. 2022;9:936720.
41. McKellop HA, Llinás A, Sarmiento A. Effects of tibial malalignment on the knee and ankle. The Orthopedic Clinics of North America. 1994;25(3):415-23.
42. Norton AA, Callaghan JJ, Amendola A, Phisitkul P, Wongsak S, Liu SS, et al. Correlation of knee and hindfoot deformities in advanced knee OA: compensatory hindfoot alignment and where it occurs. Clinical Orthopaedics and Related Research®. 2015;473(1):166-74.
43. Xie K, Jiang X, Han X, Ai S, Qu X, Yan M. Association between knee malalignment and ankle degeneration in patients with end-stage knee osteoarthritis. The Journal of Arthroplasty. 2018;33(12):3694-8. e1.

44. Kraus VB, Worrell TW, Renner JB, Coleman RE, Pieper CF. High prevalence of contralateral ankle abnormalities in association with knee osteoarthritis and malalignment. Osteoarthritis Cartilage. 2013;21(11):1693-9.
45. Tallroth K, Harilainen A, Kerttula L, Sayed R. Ankle osteoarthritis is associated with knee osteoarthritis. Conclusions based on mechanical axis radiographs. Arch Orthop Trauma Surg. 2008;128(6):555-60.
46. Kikuchi N, Kanamori A, Kadone H, Okuno K, Hyodo K, Yamazaki M. Radiographic analysis using the hip-to-calcaneus line and its association with lower limb joint kinetics in varus knee osteoarthritis. The Knee. 2022;35:142-8.
47. Lenz AL, Krähenbühl N, Peterson AC, Lisonbee RJ, Hintermann B, Saltzman CL, et al. Statistical shape modeling of the talocrural joint using a hybrid multi-articulation joint approach. Sci Rep. 2021;11(1):1-14.
48. Baverel L, Brilhault J, Odri G, Boissard M, Lintz F. Influence of lower limb rotation on hindfoot alignment using a conventional two-dimensional radiographic technique. Foot Ankle Surg. 2017;23(1):44-9.
49. Lintz F, de Cesar Netto C, Barg A, Burssens A, Richter M, Group WBCIS. Weight-bearing cone beam CT scans in the foot and ankle. EFORT open reviews. 2018;3(5):278.
50. Bowes MA, Kacena K, Alabas OA, Brett AD, Dube B, Bodick N, et al. Machine-learning, MRI bone shape and important clinical outcomes in osteoarthritis: data from the Osteoarthritis Initiative. Ann Rheum Dis. 2021;80(4):502-8.
51. Ambellan F, Lamecker H, von Tycowicz C, Zachow S. Statistical shape models: understanding and mastering variation in anatomy. Biomedical Visualisation: Springer; 2019. p. 67-84.
52. Barr AJ, Dube B, Hensor EM, Kingsbury SR, Peat G, Bowes MA, et al. The relationship between three-dimensional knee MRI bone shape and total knee replacement—a case control study: data from the Osteoarthritis Initiative. Rheumatology. 2016;55(9):1585-93.
53. Bowes MA, Vincent GR, Wolstenholme CB, Conaghan PG. A novel method for bone area measurement provides new insights into osteoarthritis and its progression. Ann Rheum Dis. 2015;74(3):519-25.
54. Van Buuren M, Arden NK, Bierma-Zeinstra S, Bramer WM, Casartelli NC, Felson D, et al. Statistical shape modeling of the hip and the association with hip osteoarthritis: a systematic review. Osteoarthritis Cartilage. 2021;29(5):607-18.
55. Gabrielli AS, Gale T, Hogan M, Anderst W. Bilateral symmetry, sex differences, and primary shape factors in ankle and hindfoot bone morphology. Foot & ankle orthopaedics. 2020;5(1):2473011420908796.
56. Krähenbühl N, Lenz AL, Lisonbee RJ, Peterson AC, Atkins PR, Hintermann B, et al. Morphologic analysis of the subtalar joint using statistical shape modeling. Journal of Orthopaedic Research®. 2020;38(12):2625-33.
57. Tümer N, Arbabi V, Gielis WP, de Jong PA, Weinans H, Tuijthof GJ, et al. Three-dimensional analysis of shape variations and symmetry of the fibula, tibia, calcaneus and talus. J Anat. 2019;234(1):132-44.
58. Pearce MS, Unwin NC, Parker L, Craft AW. Cohort profile: the Newcastle Thousand Families 1947 birth cohort. Int J Epidemiol. 2009;38(4):932-7.
59. Scally G, Womack J. The importance of the past in public health. J Epidemiol Community Health. 2004;58(9):751.
60. Nuki G, Simkin PA. A concise history of gout and hyperuricemia and their treatment. Arthritis Res Ther. 2006;8(1):S1.
61. Dequeker J, Luyten F. The history of osteoarthritis-osteoarthrosis. Ann Rheum Dis. 2008;67(1):5-10.
62. Landre-Beauvais A. The first description of rheumatoid arthritis. Unabridged text of the doctoral dissertation presented in 1800. 2001.

63. Altman R, Asch E, Bloch D, Bole G, Borenstein D, Brandt K, et al. Development of criteria for the classification and reporting of osteoarthritis: classification of osteoarthritis of the knee. Arthritis & Rheumatism: Official Journal of the American College of Rheumatology. 1986;29(8):1039-49.
64. Blackburn S, Rhodes C, Higginbottom A, Dziedzic K. The OARSI standardised definition of osteoarthritis: A lay version. Osteoarthritis Cartilage. 2016;24:S192.
65. Goldring MB, Culley KL, Otero M. Pathogenesis of osteoarthritis in General. Cartilage: Springer; 2017. p. 1-25.
66. Felson DT, Zhang Y. An update on the epidemiology of knee and hip osteoarthritis with a view to prevention. Arthritis & Rheumatism: Official Journal of the American College of Rheumatology. 1998;41(8):1343-55.
67. Prieto-Alhambra D, Arden N, Hunter DJ. Osteoarthritis: The Facts: OUP Oxford; 2014.
68. Conaghan PG, Nelson AE. Fast facts: osteoarthritis: Karger Medical and Scientific Publishers; 2017.
69. Hayashi D, Roemer FW, Guermazi A. Clinical features and diagnosis of osteoarthritis. Atlas of Osteoarthritis: Springer; 2014. p. 55-68.
70. Kean W, Kean R, Buchanan W. Osteoarthritis: symptoms, signs and source of pain. Inflammopharmacology. 2004;12(1):3-31.
71. Hunter DJ, McDougall JJ, Keefe FJ. The symptoms of osteoarthritis and the genesis of pain. Rheumatic Disease Clinics of North America. 2008;34(3):623-43.
72. Hunter DJ, Guermazi A, Roemer F, Zhang Y, Neogi T. Structural correlates of pain in joints with osteoarthritis. Osteoarthritis Cartilage. 2013;21(9):1170-8.
73. Jordan K, Arden N, Doherty M, Bannwarth B, Bijlsma J, Dieppe P, et al. EULAR Recommendations 2003: an evidence based approach to the management of knee osteoarthritis: Report of a Task Force of the Standing Committee for International Clinical Studies Including Therapeutic Trials (ESCISIT). Ann Rheum Dis. 2003;62(12):1145-55.
74. McDougall JJ. Arthritis and pain. Neurogenic origin of joint pain. Arthritis Res Ther. 2006;8(6):220.
75. Kjeken I, Dagfinrud H, Slatkowsky-Christensen B, Mowinckel P, Uhlig T, Kvien TK, et al. Activity limitations and participation restrictions in women with hand osteoarthritis: patients' descriptions and associations between dimensions of functioning. Ann Rheum Dis. 2005;64(11):1633-8.
76. Pereira D, Peleteiro B, Araujo J, Branco J, Santos R, Ramos E. The effect of osteoarthritis definition on prevalence and incidence estimates: a systematic review. Osteoarthritis Cartilage. 2011;19(11):1270-85.
77. Eaton CB, Schaefer LF, Duryea J, Driban JB, Lo GH, Roberts MB, et al. Prevalence, Incidence, and Progression of Radiographic and Symptomatic Hand Osteoarthritis: The Osteoarthritis Initiative. Arthritis Rheumatol. 2022;74(6):992-1000.
78. Jordan JM, Helmick CG, Renner JB, Luta G, Dragomir AD, Woodard J, et al. Prevalence of knee symptoms and radiographic and symptomatic knee osteoarthritis in African Americans and Caucasians: the Johnston County Osteoarthritis Project. The Journal of rheumatology. 2007;34(1):172-80.
79. Lawrence RC, Felson DT, Helmick CG, Arnold LM, Choi H, Deyo RA, et al. Estimates of the prevalence of arthritis and other rheumatic conditions in the United States: Part II. Arthritis Rheum. 2008;58(1):26-35.
80. Murray C, Marshall M, Rathod T, Bowen CJ, Menz HB, Roddy E. Population prevalence and distribution of ankle pain and symptomatic radiographic ankle osteoarthritis in community dwelling older adults: a systematic review and cross-sectional study. PLoS One. 2018;13(4):e0193662.
81. Swain S, Sarmanova A, Mallen C, Kuo CF, Coupland C, Doherty M, et al. Trends in incidence and prevalence of osteoarthritis in the United Kingdom: findings from the Clinical Practice Research Datalink (CPRD). Osteoarthritis Cartilage. 2020;28(6):792-801.

82. Paget LD, Aoki H, Kemp S, Lambert M, Readhead C, Stokes KA, et al. Ankle osteoarthritis and its association with severe ankle injuries, ankle surgeries and health-related quality of life in recently retired professional male football and rugby players: a cross-sectional observational study. BMJ Open. 2020;10(6):e036775.
83. Felson DT, Zhang Y, Hannan MT, Naimark A, Weissman BN, Aliabadi P, et al. The incidence and natural history of knee osteoarthritis in the elderly, the framingham osteoarthritis study. Arthritis Rheum. 1995;38(10):1500-5.
84. Oliveria SA, Felson DT, Reed JI, Cirillo PA, Walker AM. Incidence of symptomatic hand, hip, and knee osteoarthritis among patients in a health maintenance organization. Arthritis & Rheumatism: Official Journal of the American College of Rheumatology. 1995;38(8):1134-41.
85. Prieto-Alhambra D, Judge A, Javaid MK, Cooper C, Diez-Perez A, Arden NK. Incidence and risk factors for clinically diagnosed knee, hip and hand osteoarthritis: influences of age, gender and osteoarthritis affecting other joints. Ann Rheum Dis. 2014;73(9):1659-64.
86. Rahman MM, Cibere J, Goldsmith CH, Anis AH, Kopec JA. Osteoarthritis incidence and trends in administrative health records from British Columbia, Canada. The Journal of rheumatology. 2014;41(6):1147-54.
87. Murray CJ, Lopez AD, Organization WH. The global burden of disease: a comprehensive assessment of mortality and disability from diseases, injuries, and risk factors in 1990 and projected to 2020: summary. 1996.
88. Vos T, Flaxman AD, Naghavi M, Lozano R, Michaud C, Ezzati M, et al. Years lived with disability (YLDs) for 1160 sequelae of 289 diseases and injuries 1990–2010: a systematic analysis for the Global Burden of Disease Study 2010. The lancet. 2012;380(9859):2163-96.
89. Brooks PM. Impact of osteoarthritis on individuals and society: how much disability? Social consequences and health economic implications. Curr Opin Rheumatol. 2002;14(5):573-7.
90. McDonough CM, Jette AM. The contribution of osteoarthritis to functional limitations and disability. Clin Geriatr Med. 2010;26(3):387-99.
91. Kauppila A-M, Kyllönen E, Mikkonen P, Ohtonen P, Laine V, Siira P, et al. Disability in end-stage knee osteoarthritis. Disabil Rehabil. 2009;31(5):370-80.
92. Palazzo C, Ravaud J-F, Papelard A, Ravaud P, Poiraudeau S. The burden of musculoskeletal conditions. PLoS One. 2014;9(3):e90633.
93. Control CfD, Prevention. Prevalence and most common causes of disability among adults--United States, 2005. MMWR Morb Mortal Wkly Rep. 2009;58(16):421-6.
94. Xing D, Xu Y, Liu Q, Ke Y, Wang B, Li Z, et al. Osteoarthritis and all-cause mortality in worldwide populations: grading the evidence from a meta-analysis. Sci Rep. 2016;6(1):24393.
95. Suri P, Morgenroth DC, Hunter DJ. Epidemiology of osteoarthritis and associated comorbidities. PM&R. 2012;4:S10-S9.
96. Nüesch E, Dieppe P, Reichenbach S, Williams S, Iff S, Jüni P. All cause and disease specific mortality in patients with knee or hip osteoarthritis: population based cohort study. BMJ. 2011;342:d1165.
97. Hawker GA, Croxford R, Bierman AS, Harvey PJ, Ravi B, Stanaitis I, et al. All-cause mortality and serious cardiovascular events in people with hip and knee osteoarthritis: a population based cohort study. PLoS One. 2014;9(3):e91286.
98. Liu R, Kwok W, Vliet Vlieland T, Kroon H, Meulenbelt I, Houwing-Duistermaat J, et al. Mortality in osteoarthritis patients. Scand J Rheumatol. 2015;44(1):70-3.
99. Le Pen C, Reygrobellet C, Gérentes I. Financial cost of osteoarthritis in France: the “COART” France study. Joint Bone Spine. 2005;72(6):567-70.
100. Leifer V, Katz J, Losina E. The burden of OA-health services and economics. Osteoarthritis Cartilage. 2022;30(1):10-6.
101. Kamaruzaman H, Kinghorn P, Oppong R. Cost-effectiveness of surgical interventions for the management of osteoarthritis: a systematic review of the literature. BMC Musculoskelet Disord. 2017;18(1):183.

102. Chen A, Gupte C, Akhtar K, Smith P, Cobb J. The global economic cost of osteoarthritis: how the UK compares. Arthritis. 2012;2012.
103. Salmon J, Rat A, Sellam J, Michel M, Eschard J, Guillemin F, et al. Economic impact of lower-limb osteoarthritis worldwide: a systematic review of cost-of-illness studies. Osteoarthritis Cartilage. 2016;24(9):1500-8.
104. Loeser RF. Age-related changes in the musculoskeletal system and the development of osteoarthritis. Clin Geriatr Med. 2010;26(3):371-86.
105. Cui A, Li H, Wang D, Zhong J, Chen Y, Lu H. Global, regional prevalence, incidence and risk factors of knee osteoarthritis in population-based studies. EClinicalMedicine. 2020;29:100587.
106. Ling SM, Ju YL. Chapter 116. Osteoarthritis. In: Halter JB, Ouslander JG, Tinetti ME, Studenski S, High KP, Asthana S, editors. Hazzard's Geriatric Medicine and Gerontology, 6e. New York, NY: The McGraw-Hill Companies; 2009.
107. Srikanth VK, Fryer JL, Zhai G, Winzenberg TM, Hosmer D, Jones G. A meta-analysis of sex differences prevalence, incidence and severity of osteoarthritis. Osteoarthritis Cartilage. 2005;13(9):769-81.
108. Grelsamer R, Dubey A, Weinstein C. Men and women have similar Q angles: a clinical and trigonometric evaluation. The Journal of bone and joint surgery British volume. 2005;87(11):1498-501.
109. Lu Y, Zheng Zl, Lv J, Hao Rz, Yang Yp, Zhang Yz. Relationships between morphological changes of lower limbs and gender during medial compartment knee osteoarthritis. Orthop Surg. 2019;11(5):835-44.
110. Hardcastle SA, Dieppe P, Gregson CL, Smith GD, Tobias JH. Osteoarthritis and bone mineral density: are strong bones bad for joints? BoneKEy reports. 2015;4.
111. Koh J, Suh Y. Female reproductive and hormonal factor and incidence of radiographic knee osteoarthritis. Osteoarthritis Cartilage. 2020;28:S427.
112. Hubley-Kozey C, Deluzio K, Landry S, McNutt J, Stanish W. Neuromuscular alterations during walking in persons with moderate knee osteoarthritis. J Electromyogr Kinesiol. 2006;16(4):365-78.
113. Gray GA. An approach to the classification and evaluation of obesity. obesity. 1992;294.
114. Coggon D, Reading I, Croft P, McLaren M, Barrett D, Cooper C. Knee osteoarthritis and obesity. Int J Obes. 2001;25(5):622.
115. Stürmer T, Günther K-P, Brenner H. Obesity, overweight and patterns of osteoarthritis: the Ulm Osteoarthritis Study. J Clin Epidemiol. 2000;53(3):307-13.
116. Lohmander LS, De Verdier MG, Rollof J, Nilsson PM, Engström G. Incidence of severe knee and hip osteoarthritis in relation to different measures of body mass: a population-based prospective cohort study. Ann Rheum Dis. 2009;68(4):490-6.
117. Felson DT, Zhang Y, Anthony JM, Naimark A, Anderson JJ. Weight loss reduces the risk for symptomatic knee osteoarthritis in women: the Framingham Study. Ann Intern Med. 1992;116(7):535-9.
118. Solanki P, Hussain SM, Abidi J, Cheng J, Fairley JL, Page MJ, et al. Association between weight gain and knee osteoarthritis: a systematic review. Osteoarthritis Cartilage. 2023;31(3):300-16.
119. Obesity and overweight [Internet]. The World Health Organization. 2021. Available from: https://www.who.int/news-room/fact-sheets/detail/obesity-and-overweight.
120. Almeida Paz I, Bruno L. Bone mineral density. Brazilian Journal of Poultry Science. 2006;8:69-73.
121. Berger A. How does it work?: bone mineral density scans. BMJ: British Medical Journal. 2002;325(7362):484.
122. Blake GM, Fogelman I, editors. An update on dual-energy x-ray absorptiometry. Semin Nucl Med; 2010: Elsevier.
123. Nevitt M, Felson D. High bone density and radiographic osteoarthritis: questions answered and unanswered. Osteoarthritis Cartilage. 2020;28(9):1151-3.

124. Bergink AP, Rivadeneira F, Bierma-Zeinstra SM, Zillikens MC, Ikram MA, Uitterlinden AG, et al. Are bone mineral density and fractures related to the incidence and progression of radiographic osteoarthritis of the knee, hip, and hand in elderly men and women? The Rotterdam Study. Arthritis & Rheumatology. 2019;71(3):361-9.
125. Zhang Y, Hannan M, Chaisson C, McAlindon T, Evans S, Aliabadi P, et al. Bone mineral density and risk of incident and progressive radiographic knee osteoarthritis in women: the Framingham Study. The Journal of rheumatology. 2000;27(4):1032-7.
126. Nevitt MC, Zhang Y, Javaid MK, Neogi T, Curtis JR, Niu J, et al. High systemic bone mineral density increases the risk of incident knee OA and joint space narrowing, but not radiographic progression of existing knee OA: the MOST study. Ann Rheum Dis. 2010;69(01):163-8.
127. Atalar H, Yanik B, Ozcakar B, Atalar E, Koktener A. Bone mineral density is not related to severity of osteoarthritis in the knee in postmenopausal women. Rheumatol Int. 2008;28:233-6.
128. Stamenkovic BN, Rancic NK, Bojanovic MR, Stojanovic SK, Zivkovic VG, Djordjevic DB, et al. Is Osteoarthritis Always Associated with Low Bone Mineral Density in Elderly Patients? Medicina. 2022;58(9):1207.
129. Anand V, Gupta A, Sethi S, Kumar S. Study of Relationship between Bone Mineral Density in Ipsilateral Proximal Femur and Severity of Osteoarthritis of Knee. Journal of Family Medicine and Primary Care. 2022;11(2):599.
130. Beattie K, Boulos P, Duryea J, O'Neill J, Pui M, Gordon C, et al. The relationships between bone mineral density in the spine, hip, distal femur and proximal tibia and medial minimum joint space width in the knees of healthy females. Osteoarthritis Cartilage. 2005;13(10):872-8.
131. Hart DJ, Cronin C, Daniels M, Worthy T, Doyle DV, Spector TD. The relationship of bone density and fracture to incident and progressive radiographic osteoarthritis of the knee: the Chingford Study. Arthritis Rheum. 2002;46(1):92-9.
132. Spector TD, Cooper C. Radiographic assessment of osteoarthritis in population studies: whither Kellgren and Lawrence? Osteoarthritis Cartilage. 1993;1(4):203-6.
133. Griffin TM, Guilak F. The role of mechanical loading in the onset and progression of osteoarthritis. Exerc Sport Sci Rev. 2005;33(4):195-200.
134. Hunt M, Charlton J, Esculier J-F. Osteoarthritis year in review 2019: mechanics. Osteoarthritis Cartilage. 2020;28(3):267-74.
135. DeFrate LE, Kim-Wang SY, Englander ZA, McNulty AL. Osteoarthritis year in review 2018: mechanics. Osteoarthritis Cartilage. 2019;27(3):392-400.
136. Webster KE, Hewett TE. Anterior cruciate ligament injury and knee osteoarthritis: an umbrella systematic review and meta-analysis. Clin J Sport Med. 2022;32(2):145-52.
137. Øiestad BE, Engebretsen L, Storheim K, Risberg MA. Winner of the 2008 systematic review competition: knee osteoarthritis after anterior cruciate ligament injury. The American journal of sports medicine. 2009;37(7):1434-43.
138. Gelber AC, Hochberg MC, Mead LA, Wang N-Y, Wigley FM, Klag MJ. Joint injury in young adults and risk for subsequent knee and hip osteoarthritis. Ann Intern Med. 2000;133(5):321-8.
139. Poulsen E, Goncalves GH, Bricca A, Roos EM, Thorlund JB, Juhl CB. Knee osteoarthritis risk is increased 4-6 fold after knee injury–a systematic review and meta-analysis. Br J Sports Med. 2019;53(23):1454-63.
140. Lieberthal J, Sambamurthy N, Scanzello CR. Inflammation in joint injury and post-traumatic osteoarthritis. Osteoarthritis Cartilage. 2015;23(11):1825-34.
141. Carbone A, Rodeo S. Review of current understanding of post-traumatic osteoarthritis resulting from sports injuries. J Orthop Res. 2017;35(3):397-405.
142. Andriacchi TP, Mündermann A. The role of ambulatory mechanics in the initiation and progression of knee osteoarthritis. Curr Opin Rheumatol. 2006;18(5):514-8.
143. Aaboe J, Bliddal H, Messier S, Alkjaer T, Henriksen M. Effects of an intensive weight loss program on knee joint loading in obese adults with knee osteoarthritis. Osteoarthritis Cartilage. 2011;19(7):822-8.

144. Messier SP, Resnik AE, Beavers DP, Mihalko SL, Miller GD, Nicklas BJ, et al. Intentional weight loss in overweight and obese patients with knee osteoarthritis: is more better? Arthritis Care Res (Hoboken). 2018;70(11):1569-75.
145. Messier SP, Legault C, Loeser RF, Van Arsdale SJ, Davis C, Ettinger WH, et al. Does high weight loss in older adults with knee osteoarthritis affect bone-on-bone joint loads and muscle forces during walking? Osteoarthritis Cartilage. 2011;19(3):272-80.
146. Runhaar J, Koes B, Clockaerts S, Bierma-Zeinstra S. A systematic review on changed biomechanics of lower extremities in obese individuals: a possible role in development of osteoarthritis. Obes Rev. 2011;12(12):1071-82.
147. McWilliams D, Leeb B, Muthuri S, Doherty M, Zhang W. Occupational risk factors for osteoarthritis of the knee: a meta-analysis. Osteoarthritis Cartilage. 2011;19(7):829-39.
148. Lo GH, Richard MJ, McAlindon TE, Park C, Strayhorn MT, Harkey MS, et al. Increased risk of incident knee osteoarthritis in those with greater work-related physical activity. Occup Environ Med. 2022;79(8):543-9.
149. Wang X, Perry TA, Arden N, Chen L, Parsons CM, Cooper C, et al. Occupational risk in knee osteoarthritis: a systematic review and meta-analysis of observational studies. Arthritis Care Res (Hoboken). 2020;72(9):1213-23.
150. Canetti EF, Schram B, Orr RM, Knapik J, Pope R. Risk factors for development of lower limb osteoarthritis in physically demanding occupations: A systematic review and meta-analysis. Appl Ergon. 2020;86:103097.
151. Lane NE, Buckwalter JA. Exercise: a cause of osteoarthritis? Rheumatic Disease Clinics of North America. 1993;19(3):617-33.
152. VillafaÑe JH, Bishop MD, Pedersini P, Berjano P. Physical activity and osteoarthritis: update and perspectives. Pain Med. 2019;20(8):1461-3.
153. Hunter DJ, Eckstein F. Exercise and osteoarthritis. J Anat. 2009;214(2):197-207.
154. Wolf BR, Amendola A. Impact of osteoarthritis on sports careers. Clin Sports Med. 2005;24(1):187-98.
155. Kuijt M-TK, Inklaar H, Gouttebarge V, Frings-Dresen MHW. Knee and ankle osteoarthritis in former elite soccer players: A systematic review of the recent literature. J Sci Med Sport. 2012;15(6):480-7.
156. Vigdorchik JM, Nepple JJ, Eftekhary N, Leunig M, Clohisy JC. What is the association of elite sporting activities with the development of hip osteoarthritis? The American journal of sports medicine. 2017;45(4):961-4.
157. Hirschmann MT, Becker R, Tandogan R, Vendittoli P-A, Howell S. Alignment in TKA: what has been clear is not anymore! Knee Surg Sports Traumatol Arthrosc. 2019;27(7):2037-9.
158. Rivière C, Villet L, Jeremic D, Vendittoli P-A. What you need to know about kinematic alignment for total knee arthroplasty. Orthopaedics & Traumatology: Surgery & Research. 2021;107(1):102773.
159. Vina ER, Kwoh CK. Epidemiology of osteoarthritis: literature update. Curr Opin Rheumatol. 2018;30(2):160.
160. Wang B, Liu Q, Wise BL, Ke Y, Xing D, Xu Y, et al. Valgus malalignment and prevalence of lateral compartmental radiographic knee osteoarthritis (OA): The Wuchuan OA study. Int J Rheum Dis. 2018;21(7):1385-90.
161. Van Tunen JA, Dell'Isola A, Juhl C, Dekker J, Steultjens M, Thorlund JB, et al. Association of malalignment, muscular dysfunction, proprioception, laxity and abnormal joint loading with tibiofemoral knee osteoarthritis-a systematic review and meta-analysis. BMC Musculoskelet Disord. 2018;19(1):1-15.
162. Eitzen I, Fernandes L, Kallerud H, Nordsletten L, Knarr B, Risberg MA. Gait characteristics, symptoms, and function in persons with hip osteoarthritis: a longitudinal study with 6 to 7 years of follow-up. J Orthop Sports Phys Ther. 2015;45(7):539-49.

163. Tateuchi H, Koyama Y, Akiyama H, Goto K, So K, Kuroda Y, et al. Daily cumulative hip moment is associated with radiographic progression of secondary hip osteoarthritis. Osteoarthritis Cartilage. 2017;25(8):1291-8.
164. Cavanagh PR, Lafortune MA. Ground reaction forces in distance running. J Biomech. 1980;13(5):397-406.
165. Riegger CL. Anatomy of the ankle and foot. Phys Ther. 1988;68(12):1802-14.
166. Bourne M, Sinkler MA, Murphy PB. Anatomy, Bony Pelvis and Lower Limb, Tibia. 2018.
167. Ray R, Gusman D, Christensen J. Anatomical variation of the tibial plafond: the anteromedial tibial notch. The Journal of foot and ankle surgery: official publication of the American College of Foot and Ankle Surgeons. 1994;33(4):419-26.
168. Gupton M, Munjal A, Kang M. Anatomy, Bony Pelvis and Lower Limb, Fibula. StatPearls. Treasure Island (FL): StatPearls Publishing

169. AnatomyStandard. Tarsus bones anatomy online Anatomy Standard; 2021 [updated 08/11/2021. Available from: https://www.anatomystandard.com/Lower_Limb/Foot_Bones/Tarsal_Bones.html.
170. Khan IA, Varacallo M. Anatomy, Bony Pelvis and Lower Limb, Foot Talus. 2019.
171. Singh V. Textbook of Anatomy Abdomen and Lower Limb; Volume II: Elsevier Health Sciences; 2018.
172. Mostafa E, Graefe S, Varacallo M. Anatomy, Bony Pelvis and Lower Limb, Leg Posterior Compartment. StatPearls [Internet]: StatPearls Publishing; 2021.
173. Hegazy AAM, Hegazy MA. Talus Bone: Unique Anatomy. International Journal of Cadaveric Studies and Anatomical Variations. 2022;3(2):52-5.
174. Hall RL, Shereff MJ. Anatomy of the calcaneus. Clinical Orthopaedics and Related Research (1976-2007). 1993;290:27-35.
175. Keener BJ, Sizensky JA. The anatomy of the calcaneus and surrounding structures. Foot and ankle clinics. 2005;10(3):413-24.
176. Gupton M, Özdemir M, Terreberry RR. Anatomy, Bony Pelvis and Lower Limb, Calcaneus. StatPearls [Internet]: StatPearls Publishing; 2022.
177. Bilodi A. Study of calcaneal articular facets in human tali. Kathmandu university medical journal. 2006;4(1):13-75.
178. Golano P, Fariñas O, Sáenz I. The anatomy of the navicular and periarticular structures. Foot and ankle clinics. 2004;9(1):1-23.
179. Prapto D, Dreyer MA. Anatomy, bony pelvis and lower limb, navicular bone. StatPearls [Internet]: StatPearls Publishing; 2022.
180. Renner K, McAlister JE, Galli MM, Hyer CF. Anatomic description of the naviculocuneiform articulation. The Journal of Foot and Ankle Surgery. 2017;56(1):19-21.
181. Brockett CL, Chapman GJ. Biomechanics of the ankle. Orthopaedics and trauma. 2016;30(3):232-8.
182. Golanó P, Vega J, De Leeuw PA, Malagelada F, Manzanares MC, Götzens V, et al. Anatomy of the ankle ligaments: a pictorial essay. Knee Surg Sports Traumatol Arthrosc. 2010;18:557-69.
183. Rockar Jr PA. The subtalar joint: anatomy and joint motion. J Orthop Sports Phys Ther. 1995;21(6):361-72.
184. Jastifer JR, Gustafson PA. The subtalar joint: biomechanics and functional representations in the literature. The foot. 2014;24(4):203-9.
185. Bartoníček J, Rammelt S, Naňka O. Anatomy of the subtalar joint. Foot and ankle clinics. 2018;23(3):315-40.
186. Krähenbühl N, Horn-Lang T, Hintermann B, Knupp M. The subtalar joint: a complex mechanism. EFORT open reviews. 2017;2(7):309.
187. Sammarco VJ. The talonavicular and calcaneocuboid joints: anatomy, biomechanics, and clinical management of the transverse tarsal joint. Foot and ankle clinics. 2004;9(1):127-45.

188. Kitaoka HB, Luo ZP. Contact features of the talonavicular joint of the foot. Clinical Orthopaedics and Related Research®. 1996;325:290-5.
189. Innocenti B. Biomechanics: a fundamental tool with a long history (and even longer future!). Muscles, ligaments and tendons journal. 2017;7(4):491.
190. Donatelli R. Normal biomechanics of the foot and ankle. J Orthop Sports Phys Ther. 1985;7(3):91-5.
191. Wilkerson RD, Mason MA. Differences in men's and women's mean ankle ligamentous laxity. Iowa Orthop J. 2000;20:46-8.
192. Normal Joint Range of Motion Study [Internet]. the Centers for Disease Control and Prevention (CDC) 2022 [cited 02/2023].
193. Lundberg A, Goldie I, Kalin B, Selvik G. Kinematics of the ankle/foot complex: plantarflexion and dorsiflexion. Foot Ankle. 1989;9(4):194-200.
194. Valderrabano V, Hintermann B, Nigg BM, Stefanyshyn D, Stergiou P. Kinematic changes after fusion and total replacement of the ankle part 1: range of motion. Foot Ankle Int. 2003;24(12):881-7.
195. Vandervoort AA, Chesworth BM, Cunningham DA, Paterson DH, Rechnitzer PA, Koval JJ. Age and sex effects on mobility of the human ankle. J Gerontol. 1992;47(1):M17-M21.
196. Sepic SB, Murray MP, Mollinger LA, Spurr G, Gardner GM. Strength and range of motion in the ankle in two age groups of men and women. Am J Phys Med Rehabil. 1986;65(2):75-84.
197. Grimston SK, Nigg BM, Hanley DA, Engsberg JR. Differences in ankle joint complex range of motion as a function of age. Foot Ankle. 1993;14(4):215-22.
198. Yang N, Waddington G, Adams R, Han J. Age-related changes in proprioception of the ankle complex across the lifespan. Journal of Sport and Health Science. 2019;8(6):548-54.
199. Kaufman KR, Brodine SK, Shaffer RA, Johnson CW, Cullison TR. The effect of foot structure and range of motion on musculoskeletal overuse injuries. The American journal of sports medicine. 1999;27(5):585-93.
200. Denegar CR, Hertel J, Fonseca J. The effect of lateral ankle sprain on dorsiflexion range of motion, posterior talar glide, and joint laxity. J Orthop Sports Phys Ther. 2002;32(4):166-73.
201. Astephen JL, Deluzio KJ, Caldwell GE, Dunbar MJ. Biomechanical changes at the hip, knee, and ankle joints during gait are associated with knee osteoarthritis severity. J Orthop Res. 2008;26(3):332-41.
202. Hoch MC, Staton GS, McKeon PO. Dorsiflexion range of motion significantly influences dynamic balance. J Sci Med Sport. 2011;14(1):90-2.
203. Kharb A, Saini V, Jain Y, Dhiman S. A review of gait cycle and its parameters. IJCEM International Journal of Computational Engineering & Management. 2011;13:78-83.
204. Shetty N, Bendall S. (i) Understanding the gait cycle, as it relates to the foot. Orthopaedics and trauma. 2011;25(4):236-40.
205. Shah K, Solan M, Dawe E. The gait cycle and its variations with disease and injury. Orthopaedics and Trauma. 2020;34(3):153-60.
206. Dubin A. Gait: the role of the ankle and foot in walking. Medical Clinics. 2014;98(2):205-11.
207. Mündermann A, Dyrby CO, Andriacchi TP. Secondary gait changes in patients with medial compartment knee osteoarthritis: increased load at the ankle, knee, and hip during walking. Arthritis Rheum. 2005;52(9):2835-44.
208. Pirker W, Katzenschlager R. Gait disorders in adults and the elderly: A clinical guide. Wien Klin Wochenschr. 2017;129(3-4):81-95.
209. Martin E, Hine R. morphology. Oxford University Press; 2008.
210. Neogi T. Clinical significance of bone changes in osteoarthritis. Arthritis Res Ther. 2012;14(2):1-8.
211. Szulc P. Changes in bone size and geometry with aging. Osteoporosis in men: Elsevier; 2010. p. 193-206.
212. Allen MD, McMillan SJ, Klein CS, Rice CL, Marsh GD. Differential age-related changes in bone geometry between the humerus and the femur in healthy men. Aging Dis. 2012;3(2):156.

213. Ko S-u, Tolea MI, Hausdorff JM, Ferrucci L. Sex-specific differences in gait patterns of healthy older adults: results from the Baltimore Longitudinal Study of Aging. J Biomech. 2011;44(10):1974-9.
214. Christensen AM, Passalacqua NV, Bartelink EJ. Chapter 12 - Individual Skeletal Variation. In: Christensen AM, Passalacqua NV, Bartelink EJ, editors. Forensic Anthropology. San Diego: Academic Press; 2014. p. 301-39.
215. Wohl GR, Boyd SK, Judex S, Zernicke RF. Functional adaptation of bone to exercise and injury. J Sci Med Sport. 2000;3(3):313-24.
216. Kim J, Lee G, Chang W, Ki Sh, Park J-C. Comparison and Contrast of Bone and Dentin in Genetic Disorder, Morphology and Regeneration: A Review. Journal of Bone Metabolism. 2021;28:1 - 10.
217. Wallace IJ, Winchester JM, Su A, Boyer DM, Konow N. Physical activity alters limb bone structure but not entheseal morphology. J Hum Evol. 2017;107:14-8.
218. Lenz AL, Lisonbee RJ. Biomechanical Insights Afforded by Shape Modeling in the Foot and Ankle. Foot and Ankle Clinics. 2023;28(1):63-76.
219. Muehleman C, Williams J, Bareither M. A radiologic and histologic study of the os peroneum: prevalence, morphology, and relationship to degenerative joint disease of the foot and ankle in a cadaveric sample. Clin Anat. 2009;22(6):747-54.
220. Gupta SC, Gupta CD, Arora AK. Pattern of talar articular facets in Indian calcanei. J Anat. 1977;124(Pt 3):651-5.
221. Ukoha UU, Obazie IF, Chioma O. Study of the morphologic and morphometric patterns of talar articular facets on dry adult calcaneal bones in South-Eastern Nigerian population. Revista Argentina de Anatomía Online. 2017;8(1):29-39.
222. Uygur M, Atamaz F, Celik S, Pinar Y. The types of talar articular facets and morphometric measurements of the human calcaneus bone on Turkish race. Arch Orthop Trauma Surg. 2009;129(7):909-14.
223. Badalahu, Qin B, Luo J, Zeng Y, Fu S, Zhang L. Classification of the subtalar articular surface and its matching situation: an anatomical study on Chinese subtalar joint. Surg Radiol Anat. 2020;42(10):1133-9.
224. Xia Z-r, Liu X-y, Zhang L, Li B-k, Tang X-g, Chen J-y, et al. Percutaneous and Arthroscopically Assisted Osteosynthesis for Calcaneal Fractures with Displacement of Different Calcaneal Talar Facet: A Retrospective Study. 2022.
225. Kim JS, Lim SH, Hong BY, Park SY. Ruptured popliteal cyst diagnosed by ultrasound before evaluation for deep vein thrombosis. Ann Rehabil Med. 2014;38(6):843-6.
226. Amuti T, Muuthuri N, Nichome L, Ouko I, Misiani M, Olabu B, et al. Morphometric dimensions of the calcaneus. The Journal of Foot and Ankle Surgery. 2020;59(5):949-52.
227. İlhan O, TETİKER H, TAŞTEMUR Y, SABANCIOĞULLARI V, KOŞAR Mİ, ÇİMEN M. Morphometric Measurements of Calcaneus; Boehler'sangle and bone length estimation. Cumhuriyet Üniversitesi Fen Edebiyat Fakültesi Fen Bilimleri Dergisi. 2017;38(2):256-63.
228. Mordecai SC, Ray PS. Management of calcaneal fractures: an evidence-based approach. Orthopaedics and Trauma. 2018;32(6):388-93.
229. Riepert T, Drechsler T, Schild H, Nafe B, Mattern R. Estimation of sex on the basis of radiographs of the calcaneus. Forensic Sci Int. 1996;77(3):133-40.
230. Zhang Z-H, Chen X-G, Li W-K, Yang S-Q, Deng Z-H, Yu J-Q, et al. Sex determination by discriminant analysis of calcaneal measurements on the lateral digital radiography. Fa yi xue za zhi. 2008;24(2):122-5.
231. Uzuner MB, Geneci F, Mert O, Bayram P, Sancak İT, Dolgun A, et al. Sex determination from the radiographic measurements of calcaneus. Anatomy. 2016;10(3):200-4.
232. Qiang M, Chen Y, Zhang K, Li H, Dai H. Measurement of three-dimensional morphological characteristics of the calcaneus using CT image post-processing. Journal of Foot and Ankle Research. 2014;7(1):19.

233. Garg R, Babuta S, Mogra K, Parashar R, Shekhawat S. Study of variations in pattern of calcaneal articular facets in human tali in the population of rajasthan (India). PJSR. 2013;6(2):19-23.
234. Lee JY, Jung M-H, Lee JS, Choi BY, Cho BP. Types of calcaneal articular facets of the talus in Korean. Korean journal of physical anthropology. 2012;25(4):185-92.
235. Phunchago N, Uabundit N, Chaisiwamongkol K, Chaichun A, Iamsaard S, PHUNCHAGO N, et al. Types and morphometric study of calcaneal articular facets on human tali of Thai population. Int j morphol. 2018;36(3):975-8.
236. Namburu BSP, Kaavya H, Reddy SM. A study of morphology of talus and its calcaneal facets. International journal of anatomy and research. 2017;5(4.2):4570-4.
237. Biswas A, Roy H, Bhar A, Pal A, Datta I. Talar Morphometry–A Study in West Bengal Population with. 2022.
238. Kasar H, Fazlıoğulları Z, Dursun FN, Ünver Doğan N, Karabulut AK, editors. Talus morphometry and morphological features2018: 1. INTERNATIONAL MEDITERRANEAN ANATOMY CONGRESS, 19. ULUSAL ANATOMİ KONGRESİ.
239. Siegler S, Toy J, Seale D, Pedowitz D. The Clinical Biomechanics Award 2013--presented by the International Society of Biomechanics: new observations on the morphology of the talar dome and its relationship to ankle kinematics. Clinical biomechanics. 2014;29(1):1-6.
240. Han Q, Liu Y, Chang F, Chen B, Zhong L, Wang J. Measurement of talar morphology in northeast Chinese population based on three-dimensional computed tomography. Medicine. 2019;98(37).
241. Magerkurth O, Knupp M, Ledermann H, Hintermann B. Evaluation of hindfoot dimensions: a radiological study. Foot Ankle Int. 2006;27(8):612-6.
242. Carrara C, Caravaggi P, Belvedere C, Leardini A. Radiographic angular measurements of the foot and ankle in weight-bearing: a literature review. Foot Ankle Surg. 2020;26(5):509-17.
243. Stevens PM. Radiographic distortion of bones: a marker study. SLACK Incorporated Thorofare, NJ; 1989. p. 1457-63.
244. Cadden AR, editor Imaging in total ankle replacement. Seminars in musculoskeletal radiology; 2012: Thieme Medical Publishers.
245. Braun HJ, Gold GE. Diagnosis of osteoarthritis: imaging. Bone. 2012;51(2):278-88.
246. Swinton A. Professor Röntgen's discovery. Nature Publishing Group; 1896.
247. Chodorow M, Symons R, Abe D, Abrams R, Danly B, Freund H, et al. 16 - Electron Tubes. In: Middleton WM, Van Valkenburg ME, editors. Reference Data for Engineers (Ninth Edition). Woburn: Newnes; 2002. p. 16-1--59.
248. Rosenbusch G, VAN EEKELEN ADK. Wilhelm Conrad Röntgen: Springer; 2019.
249. Posner E. Reception of Röntgen's discovery in Britain and USA. Br Med J. 1970;4(5731):357.
250. Glasser O. WC Roentgen and the Discovery of the Roentgen Rays. Cleve Clin Q. 1932;1.
251. Röntgen W. Upon a New Kind of Rays. 1895.
252. Glasser O. Wilhelm Conrad Röntgen and the early history of the Roentgen rays: Norman Publishing; 1993.
253. Goodman PC. The new light: discovery and introduction of the X-ray. AJR American journal of roentgenology. 1995;165(5):1041-5.
254. Thomas AM, Banerjee AK. The history of radiology: OUP Oxford; 2013.
255. Sansare K, Khanna V, Karjodkar F. Early victims of X-rays: a tribute and current perception. Dentomaxillofac Radiol. 2011;40(2):123-5.
256. Kang KW. History and Organizations for Radiological Protection. J Korean Med Sci. 2016;31 Suppl 1(Suppl 1):S4-5.
257. Lin EC, editor Radiation risk from medical imaging. Mayo Clin Proc; 2010: Elsevier.
258. Pearce MS, Salotti JA, Little MP, McHugh K, Lee C, Kim KP, et al. Radiation exposure from CT scans in childhood and subsequent risk of leukaemia and brain tumours: a retrospective cohort study. The Lancet. 2012;380(9840):499-505.

259. Kamiya K, Ozasa K, Akiba S, Niwa O, Kodama K, Takamura N, et al. Long-term effects of radiation exposure on health. The lancet. 2015;386(9992):469-78.
260. Hricak H, Brenner DJ, Adelstein SJ, Frush DP, Hall EJ, Howell RW, et al. Managing radiation use in medical imaging: a multifaceted challenge. Radiology. 2011;258(3):889-905.
261. Lee LS, Chan PK, Fung WC, Chan VWK, Yan CH, Chiu KY. Imaging of knee osteoarthritis: A review of current evidence and clinical guidelines. Musculoskeletal Care. 2021;19(3):363-74.
262. Hayashi D, Roemer FW, Guermazi A. Imaging of osteoarthritis-recent research developments and future perspective. Br J Radiol. 2018;91(1085):20170349.
263. Buckland-Wright C. Protocols for precise radio-anatomical positioning of the tibiofemoral and patellofemoral compartments of the knee. Osteoarthritis Cartilage. 1995;3:71-80.
264. Peterfy C, Li J, Zaim S, Duryea J, Lynch J, Miaux Y, et al. Comparison of fixed-flexion positioning with fluoroscopic semi-flexed positioning for quantifying radiographic joint-space width in the knee: test-retest reproducibility. Skeletal Radiol. 2003;32:128-32.
265. Duddy J, Kirwan J, Szebenyi B, Clarke S, Granell R, Volkov S. A comparison of the semiflexed (MTP) view with the standing extended view (SEV) in the radiographic assessment of knee osteoarthritis in a busy routine X-ray department. Rheumatology. 2005;44(3):349-51.
266. Duncan ST, Khazzam MS, Burnham JM, Spindler KP, Dunn WR, Wright RW. Sensitivity of standing radiographs to detect knee arthritis: a systematic review of level I studies. Arthroscopy: The Journal of Arthroscopic & Related Surgery. 2015;31(2):321-8.
267. Bliddal H, Boesen M, Christensen R, Kubassova O, Torp-Pedersen S. Imaging as a follow-up tool in clinical trials and clinical practice. Best Practice & Research Clinical Rheumatology. 2008;22(6):1109-26.
268. Buckland-Wright JC, Wolfe F, Ward RJ, Flowers N, Hayne C. Substantial superiority of semiflexed (MTP) views in knee osteoarthritis: A comparative radiographic study, without fluoroscopy, of standing extended, semiflexed (MTP), and schuss views. J Rheumatol. 1999;26(12):2664-74.
269. Hunter D, Zhang Y, Tu X, Lavalley M, Niu J, Amin S, et al. Change in joint space width: hyaline articular cartilage loss or alteration in meniscus? Arthritis & Rheumatism: Official Journal of the American College of Rheumatology. 2006;54(8):2488-95.
270. Mazzuca S, Le Graverand M-PH, Vignon E, Hunter D, Jackson C, Kraus V, et al. Performance of a non-fluoroscopically assisted substitute for the Lyon schuss knee radiograph: quality and reproducibility of positioning and sensitivity to joint space narrowing in osteoarthritic knees. Osteoarthritis Cartilage. 2008;16(12):1555-9.
271. Hayashi D, Roemer FW, Jarraya M, Guermazi A. Imaging of Osteoarthritis. Geriatric Imaging: Springer; 2013. p. 93-121.
272. Roemer FW, Eckstein F, Hayashi D, Guermazi A. The role of imaging in osteoarthritis. Best practice & research Clinical rheumatology. 2014;28(1):31-60.
273. Auleley GR, Duche A, Drape JL, Dougados M, Ravaud P. Measurement of joint space width in hip osteoarthritis: influence of joint positioning and radiographic procedure. Rheumatology. 2001;40(4):414-9.
274. Mourad C, Vande Berg B. Osteoarthritis of the hip: is radiography still needed? Skeletal Radiol. 2022.
275. Gold GE, Cicuttini F, Crema MD, Eckstein F, Guermazi A, Kijowski R, et al. OARSI clinical trials recommendations: hip imaging in clinical trials in osteoarthritis. Osteoarthritis Cartilage. 2015;23(5):716-31.
276. Yoshida et al JG, S. Galeasoler, R Barr, F. Gilbert1, R.Aspden, D M Reid,. Use of imaging DXA to grade osteoarthritis at the hip and knee: comparison with standard radiographs. Ann Rheum Diss. 2008;67(397).
277. Birrell F, Ottewell L, Rawlings D, Farley A, Francis R, editors. Is it feasible & valid to score IDXA hip images for osteoarthritis? Ann Rheum Dis; 2007: BMJ PUBLISHING GROUP BRITISH MED ASSOC HOUSE, TAVISTOCK SQUARE, LONDON WC1H ….

278. Yoshida K, Barr RJ, Galea-Soler S, Aspden RM, Reid DM, Gregory JS. Reproducibility and diagnostic accuracy of Kellgren-Lawrence grading for osteoarthritis using radiographs and dual-energy X-ray absorptiometry images. J Clin Densitom. 2015;18(2):239-44.
279. Barg A, Pagenstert GI, Hügle T, Gloyer M, Wiewiorski M, Henninger HB, et al. Ankle osteoarthritis: etiology, diagnostics, and classification. Foot and ankle clinics. 2013;18(3):411-26.
280. Weber M-A, Wünnemann F, Jungmann PM, Kuni B, Rehnitz C, editors. Modern cartilage imaging of the ankle. RöFo-Fortschritte auf dem Gebiet der Röntgenstrahlen und der bildgebenden Verfahren; 2017: © Georg Thieme Verlag KG.
281. Ostlere S. Imaging the ankle and foot. Imaging. 2003;15(4):242-69.
282. Whitley AS, Jefferson G, Holmes K, Sloane C, Anderson C, Hoadley G. Clark's Positioning in Radiography 13E: crc Press; 2015.
283. Gorbachova T, Melenevsky YV, Latt LD, Weaver JS, Taljanovic MS. Imaging and treatment of posttraumatic ankle and hindfoot osteoarthritis. Journal of Clinical Medicine. 2021;10(24):5848.
284. Benevides PC, de Souza Nery CA, Godoy-Santos AL, Alloza JFM, Prado MP. Study of the radiographic parameters of normal ankles: literature review and technical recommendations. Journal of the Foot & Ankle. 2020;14(1):84-8.
285. Smithuis R. Fracture mechanism and Radiography Radiology Assistant.2010 [Available from: https://radiologyassistant.nl/musculoskeletal/ankle/fracture-mechanism-and-radiography.
286. Altman RD, Gold GE. Atlas of individual radiographic features in osteoarthritis, revised. Osteoarthritis Cartilage. 2007;15:A1-A56.
287. Carr AJ, Robertsson O, Graves S, Price AJ, Arden NK, Judge A, et al. Knee replacement. The Lancet. 2012;379(9823):1331-40.
288. Wick MC, Kastlunger M, Weiss RJ. Clinical imaging assessments of knee osteoarthritis in the elderly: a mini-review. Gerontology. 2014;60(5):386-94.
289. Reichmann WM, Maillefert JF, Hunter DJ, Katz JN, Conaghan PG, Losina E. Responsiveness to change and reliability of measurement of radiographic joint space width in osteoarthritis of the knee: a systematic review. Osteoarthritis Cartilage. 2011;19(5):550-6.
290. Holzer N, Salvo D, Marijnissen A, Vincken K, Ahmad A, Serra E, et al. Radiographic evaluation of posttraumatic osteoarthritis of the ankle: the Kellgren–Lawrence scale is reliable and correlates with clinical symptoms. Osteoarthritis Cartilage. 2015;23(3):363-9.
291. Chen P, Gao L, Shi X, Allen K, Yang L. Fully automatic knee osteoarthritis severity grading using deep neural networks with a novel ordinal loss. Comput Med Imaging Graph. 2019;75:84-92.
292. Kumar H, Pal CP, Sharma YK, Kumar S, Uppal A. Epidemiology of knee osteoarthritis using Kellgren and Lawrence scale in Indian population. Journal of Clinical Orthopaedics and Trauma. 2020;11:S125-S9.
293. Felson DT, Naimark A, Anderson J, Kazis L, Castelli W, Meenan RF. The prevalence of knee osteoarthritis in the elderly. The Framingham Osteoarthritis Study. Arthritis & Rheumatism: Official Journal of the American College of Rheumatology. 1987;30(8):914-8.
294. Bagge E, Bjelle A, Valkenburg H, Svanborg A. Prevalence of radiographic osteoarthritis in two elderly European populations. Rheumatol Int. 1992;12:33-8.
295. SCOTT JR WW, Lethbridge-Cejku M, Reichle R, Wigley FM, Tobin JD, Hochberg MC. Reliability of grading scales for individual radiographic features of osteoarthritis of the knee: the Baltimore longitudinal study of aging atlas of knee osteoarthritis. Invest Radiol. 1993;28(6):501.
296. Wright RW, Ross JR, Haas AK, Huston LJ, Garofoli EA, Harris D, et al. Osteoarthritis classification scales: interobserver reliability and arthroscopic correlation. The Journal of bone and joint surgery American volume. 2014;96(14):1145.
297. Damen J, Schiphof D, Ten Wolde S, Cats H, Bierma-Zeinstra S, Oei E. Inter-observer reliability for radiographic assessment of early osteoarthritis features: the CHECK (cohort hip and cohort knee) study. Osteoarthritis Cartilage. 2014;22(7):969-74.
298. Salat P, Salonen D, Veljkovic AN. Imaging in osteoarthritis. Osteoarthritis: Springer; 2015. p. 131-54.

299. Javaid MK, Lynch J, Tolstykh I, Guermazi A, Roemer F, Aliabadi P, et al. Pre-radiographic MRI findings are associated with onset of knee symptoms: the most study. Osteoarthritis Cartilage. 2010;18(3):323-8.
300. DiMasi JA, Grabowski HG, Hansen RW. Innovation in the pharmaceutical industry: new estimates of R&D costs. J Health Econ. 2016;47:20-33.
301. Le Graverand M-PH, Clemmer RS, Brunell RM, Hayes CW, Miller CG, Vignon E, editors. Considerations when designing a disease-modifying osteoarthritis drug (DMOAD) trial using radiography. Semin Arthritis Rheum; 2013: Elsevier.
302. Guermazi A, Niu J, Hayashi D, Roemer FW, Englund M, Neogi T, et al. Prevalence of abnormalities in knees detected by MRI in adults without knee osteoarthritis: population based observational study (Framingham Osteoarthritis Study). BMJ. 2012;345:e5339.
303. Hayashi D, Felson D, Niu J, Hunter D, Roemer F, Aliabadi P, et al. Pre-radiographic osteoarthritic changes are highly prevalent in the medial patella and medial posterior femur in older persons: Framingham OA study. Osteoarthritis Cartilage. 2014;22(1):76-83.
304. Kinds M, Vincken K, Hoppinga T, Bleys R, Viergever M, Marijnissen A, et al. Influence of variation in semiflexed knee positioning during image acquisition on separate quantitative radiographic parameters of osteoarthritis, measured by Knee Images Digital Analysis. Osteoarthritis Cartilage. 2012;20(9):997-1003.
305. Kauffman G. Nobel prize for MRI imaging denied to Raymond V. Damadian a decade ago. Chem Educator. 2014;19:73-90.
306. Shampo MA, Kyle RA, Steensma DP. Isidor Rabi-1944 Nobel laureate in physics. Mayo Clin Proc. 2012;87(2):e11.
307. Kumar A. History of MRI. Journal of the Indian Institute of Science. 2014;94(4):363-70.
308. Geva T. Magnetic resonance imaging: historical perspective. J Cardiovasc Magn Reson. 2006;8(4):573-80.
309. Damadian R. Tumor detection by nuclear magnetic resonance. Science. 1971;171(3976):1151-3.
310. Lauterbur PC. Image formation by induced local interactions: examples employing nuclear magnetic resonance. Nature. 1973;242(5394):190-1.
311. Mansfield P. Multi-planar image formation using NMR spin echoes. Journal of Physics C: Solid State Physics. 1977;10(3):L55.
312. Mansfield P. Snapshot magnetic resonance imaging (Nobel lecture). Angewandte Chemie International Edition. 2004;43(41):5456-64.
313. Turner R. Peter Mansfield (1933–2017). Nature. 2017;543(7644):180-.
314. Evens R. Nuclear magnetic resonance: another new frontier for radiology? Radiology. 1980;136(3):795-6.
315. Edelman RR. The history of MR imaging as seen through the pages of radiology. Radiology. 2014;273(2S):S181-S200.
316. Conaghan PG, McQueen FM, Peterfy CG, Lassere MN, Ejbjerg B, Bird P, et al. The evidence for magnetic resonance imaging as an outcome measure in proof-of-concept rheumatoid arthritis studies. The Journal of rheumatology. 2005;32(12):2465-9.
317. Peterfy C, Kothari M. Imaging osteoarthritis: magnetic resonance imaging versus x-ray. Curr Rheumatol Rep. 2006;8(1):16.
318. Emery DJ, Forster AJ, Shojania KG, Magnan S, Tubman M, Feasby TE. Management of MRI wait lists in Canada. Healthcare Policy. 2009;4(3):76.
319. Menashe L, Hirko K, Losina E, Kloppenburg M, Zhang W, Li L, et al. The diagnostic performance of MRI in osteoarthritis: a systematic review and meta-analysis. Osteoarthritis Cartilage. 2012;20(1):13-21.
320. Fazel R, Krumholz HM, Wang Y, Ross JS, Chen J, Ting HH, et al. Exposure to low-dose ionizing radiation from medical imaging procedures. N Engl J Med. 2009;361(9):849-57.

321. Radiology ACo. Radiation dose to adults from common imaging examinations. ACR Reston, VA; 2017.
322. Walter SS, Fritz B, Kijowski R, Fritz J. 2D versus 3D MRI of osteoarthritis in clinical practice and research. Skeletal Radiol. 2023:1-14.
323. Hayashi D, Roemer FW, Guermazi A. Magnetic resonance imaging assessment of knee osteoarthritis: current and developing new concepts and techniques. Clin Exp Rheumatol. 2019;37(Suppl 1):88-95.
324. Caliva F, Namiri NK, Dubreuil M, Pedoia V, Ozhinsky E, Majumdar S. Studying osteoarthritis with artificial intelligence applied to magnetic resonance imaging. Nature Reviews Rheumatology. 2022;18(2):112-21.
325. Peterfy C, Guermazi A, Zaim S, Tirman P, Miaux Y, White D, et al. Whole-organ magnetic resonance imaging score (WORMS) of the knee in osteoarthritis. Osteoarthritis Cartilage. 2004;12(3):177-90.
326. Guermazi A, Roemer FW, Haugen IK, Crema MD, Hayashi D. MRI-based semiquantitative scoring of joint pathology in osteoarthritis. Nature Reviews Rheumatology. 2013;9(4):236-51.
327. Roemer FW, Guermazi A, Demehri S, Wirth W, Kijowski R. Imaging in osteoarthritis. Osteoarthritis Cartilage. 2022;30(7):913-34.
328. Hunter DJ, Lo GH, Gale D, Grainger AJ, Guermazi A, Conaghan PG. The reliability of a new scoring system for knee osteoarthritis MRI and the validity of bone marrow lesion assessment: BLOKS (Boston–Leeds Osteoarthritis Knee Score). Ann Rheum Dis. 2008;67(2):206-11.
329. Kornaat PR, Ceulemans RY, Kroon HM, Riyazi N, Kloppenburg M, Carter WO, et al. MRI assessment of knee osteoarthritis: Knee Osteoarthritis Scoring System (KOSS)—inter-observer and intra-observer reproducibility of a compartment-based scoring system. Skeletal Radiol. 2005;34:95-102.
330. Hunter DJ, Guermazi A, Lo GH, Grainger AJ, Conaghan PG, Boudreau RM, et al. Evolution of semi-quantitative whole joint assessment of knee OA: MOAKS (MRI Osteoarthritis Knee Score). Osteoarthritis Cartilage. 2011;19(8):990-1002.
331. Hunter DJ, Li J, LaValley M, Bauer DC, Nevitt M, DeGroot J, et al. Cartilage markers and their association with cartilage loss on magnetic resonance imaging in knee osteoarthritis: the Boston Osteoarthritis Knee Study. Arthritis Res Ther. 2007;9(5):1-8.
332. Roemer FW, Neogi T, Nevitt MC, Felson DT, Zhu Y, Zhang Y, et al. Subchondral bone marrow lesions are highly associated with, and predict subchondral bone attrition longitudinally: the MOST study. Osteoarthritis Cartilage. 2010;18(1):47-53.
333. Eckstein F, Wirth W, Nevitt MC. Recent advances in osteoarthritis imaging—the osteoarthritis initiative. Nature Reviews Rheumatology. 2012;8(10):622-30.
334. Felson DT, Lynch J, Guermazi A, Roemer FW, Niu J, McAlindon T, et al. Comparison of BLOKS and WORMS scoring systems part II. Longitudinal assessment of knee MRIs for osteoarthritis and suggested approach based on their performance: data from the Osteoarthritis Initiative. Osteoarthritis Cartilage. 2010;18(11):1402-7.
335. Lynch JA, Roemer FW, Nevitt MC, Felson DT, Niu J, Eaton CB, et al. Comparison of BLOKS and WORMS scoring systems part I. Cross sectional comparison of methods to assess cartilage morphology, meniscal damage and bone marrow lesions on knee MRI: data from the osteoarthritis initiative. Osteoarthritis Cartilage. 2010;18(11):1393-401.
336. Hunter D, Zhang W, Conaghan P, Hirko K, Menashe L, Reichmann W, et al. Responsiveness and reliability of MRI in knee osteoarthritis: a meta-analysis of published evidence. Osteoarthritis Cartilage. 2011;19(5):589-605.
337. Roemer FW, Hunter DJ, Crema MD, Kwoh CK, Ochoa-Albiztegui E, Guermazi A. An illustrative overview of semi-quantitative MRI scoring of knee osteoarthritis: lessons learned from longitudinal observational studies. Osteoarthritis Cartilage. 2016;24(2):274-89.

338. Crema MD, Roemer FW, Nevitt MC, Felson DT, Marra MD, Lynch JA, et al. Cross-sectional and longitudinal reliability of semiquantitative osteoarthritis assessment at 1.0T extremity MRI: Multi-reader data from the MOST study. Osteoarthr Cartil Open. 2021;3(4):100214.
339. Eckstein F, Peterfy C. A 20 years of progress and future of quantitative magnetic resonance imaging (qMRI) of cartilage and articular tissues—personal perspective. Semin Arthritis Rheum. 2016;45(6):639-47.
340. Erickson BJ, Korfiatis P, Akkus Z, Kline TL. Machine learning for medical imaging. Radiographics. 2017;37(2):505-15.
341. Singh SP, Wang L, Gupta S, Goli H, Padmanabhan P, Gulyás B. 3D deep learning on medical images: a review. Sensors. 2020;20(18):5097.
342. Wang S, Summers RM. Machine learning and radiology. Med Image Anal. 2012;16(5):933-51.
343. Zhang Z, Sejdić E. Radiological images and machine learning: Trends, perspectives, and prospects. Comput Biol Med. 2019;108:354-70.
344. Chan VC, Ross GB, Clouthier AL, Fischer SL, Graham RB. The role of machine learning in the primary prevention of work-related musculoskeletal disorders: A scoping review. Appl Ergon. 2022;98:103574.
345. Cootes TF, Taylor CJ, Cooper DH, Graham J. Active shape models-their training and application. Computer vision and image understanding. 1995;61(1):38-59.
346. Sarkalkan N, Weinans H, Zadpoor AA. Statistical shape and appearance models of bones. Bone. 2014;60:129-40.
347. Lamecker H, Zachow S. Statistical shape modeling of musculoskeletal structures and its applications. Computational radiology for orthopaedic interventions: Springer; 2015. p. 1-23.
348. Dieppe P. Subchondral bone should be the main target for the treatment of pain and disease progression in osteoarthritis. Osteoarthritis Cartilage. 1999;7(3):325-6.
349. Eckstein F, Hudelmaier M, Cahue S, Marshall M, Sharma L. Medial-to-lateral ratio of tibiofemoral subchondral bone area is adapted to alignment and mechanical load. Calcif Tissue Int. 2009;84(3):186-94.
350. Frobell RB, Nevitt MC, Hudelmaier M, Wirth W, Wyman BT, Benichou O, et al. Femorotibial subchondral bone area and regional cartilage thickness: A cross-sectional description in healthy reference cases and various radiographic stages of osteoarthritis in 1,003 knees from the Osteoarthritis Initiative. Arthritis Care Res (Hoboken). 2010;62(11):1612-23.
351. Barr A, Dube B, Hensor E, Kingsbury S, Peat G, Bowes M, et al. The relationship between clinical characteristics, radiographic osteoarthritis and 3D bone area: data from the Osteoarthritis Initiative. Osteoarthritis Cartilage. 2014;22(10):1703-9.
352. Bowes MA, Maciewicz RA, Waterton JC, Hunter DJ, Conaghan PG. Bone area provides a responsive outcome measure for bone changes in short-term knee osteoarthritis studies. The Journal of rheumatology. 2016;43(12):2179-82.
353. Chen J-H, Liu C, You L, Simmons CA. Boning up on Wolff's Law: mechanical regulation of the cells that make and maintain bone. J Biomech. 2010;43(1):108-18.
354. Bredbenner TL, Eliason TD, Potter RS, Mason RL, Havill LM, Nicolella DP. Statistical shape modeling describes variation in tibia and femur surface geometry between Control and Incidence groups from the osteoarthritis initiative database. J Biomech. 2010;43(9):1780-6.
355. Neogi T, Bowes M, Niu J, De Souza K, Vincent G, Goggins J, et al. MRI-based three-dimensional bone shape of the knee predicts onset of knee osteoarthritis: Data from the Osteoarthritis Initiative. Arthritis Rheum. 2013;65(8):2048.
356. Grant TM, Diamond LE, Pizzolato C, Killen BA, Devaprakash D, Kelly L, et al. Development and validation of statistical shape models of the primary functional bone segments of the foot. PeerJ. 2020;8:e8397.
357. Peterson AC, Lisonbee RJ, Krähenbühl N, Saltzman CL, Barg A, Khan N, et al. Multi-level multi-domain statistical shape model of the subtalar, talonavicular, and calcaneocuboid joints. Frontiers in Bioengineering and Biotechnology. 2022;10.

358. Tümer N, Blankevoort L, van de Giessen M, Terra MP, de Jong PA, Weinans H, et al. Bone shape difference between control and osteochondral defect groups of the ankle joint. Osteoarthritis Cartilage. 2016;24(12):2108-15.
359. Tümer N, Vuurberg G, Blankevoort L, Kerkhoffs GMMJ, Tuijthof GJM, Zadpoor AA. Typical Shape Differences in the Subtalar Joint Bones Between Subjects with Chronic Ankle Instability and Controls. J Orthop Res. 2019;37(9):1892-902.
360. Spence J, Miller F. Report of an Investigation into the Causes of Infant Mortality in Newcastle upon Tyne, 1939. Christie, Malcolm: Newcastle upon Tyne. 1941.
361. Spence J, Walton W, Miller F. A thousand families in Newcastle upon Tyne. A Thousand Families in Newcastle upon Tyne. 1954.
362. Miller FJW. The School Years in Newcastle-upon-Tyne, 1952-62: Being a Further Contribution to the Study of a Thousand Families: Oxford University Press; 1974.
363. Miller F, Court R, Walton W, Knox E. Growing Up in Newcastle-upon-Tyne. London. 1960.
364. Lamont D, Parker L, White M, Unwin N, Bennett SM, Cohen M, et al. Risk of cardiovascular disease measured by carotid intima-media thickness at age 49-51: lifecourse study. BMJ. 2000;320(7230):273-8.
365. van Melick N, Meddeler BM, Hoogeboom TJ, Nijhuis-van der Sanden MW, van Cingel RE. How to determine leg dominance: The agreement between self-reported and observed performance in healthy adults. PLoS One. 2017;12(12):e0189876.
366. Hassum A. Prevalence of structural changes of osteoarthritis in the Newcastle Thousand Families 1947 birth cohort. online: Newcastle University; 2015.
367. Vincent G, Wolstenholme C, Scott I, Bowes M. Fully automatic segmentation of the knee joint using active appearance models. Medical Image Analysis for the Clinic: A Grand Challenge. 2010;1:224.
368. Neogi T, Bowes MA, Niu J, De Souza KM, Vincent GR, Goggins J, et al. Magnetic resonance imaging–based three-dimensional bone shape of the knee predicts onset of knee osteoarthritis: data from the Osteoarthritis Initiative. Arthritis Rheum. 2013;65(8):2048-58.
369. Cootes TF, Edwards GJ, Taylor CJ. Active appearance models. IEEE Transactions on Pattern Analysis & Machine Intelligence. 2001(6):681-5.
370. Lorensen WE, Cline HE. Marching cubes: A high resolution 3D surface construction algorithm. ACM siggraph computer graphics. 1987;21(4):163-9.
371. Polfliet M, Klein S, Huizinga W, Paulides MM, Niessen WJ, Vandemeulebroucke J. Intrasubject multimodal groupwise registration with the conditional template entropy. Med Image Anal. 2018;46:15-25.
372. Alam F, Rahman SU. Medical image registration: Classification, applications and issues. JPMI. 2018;32(4):300.
373. Cootes TF, Twining CJ, Petrovic VS, Schestowitz R, Taylor CJ, editors. Groupwise Construction of Appearance Models using Piece-wise Affine Deformations. BMVC; 2005.
374. Pearson K. LIII. On lines and planes of closest fit to systems of points in space. The London, Edinburgh, and Dublin philosophical magazine and journal of science. 1901;2(11):559-72.
375. Hotelling H. Analysis of a complex of statistical variables into principal components. J Educ Psychol. 1933;24(6):417.
376. Jolliffe IT, Cadima J. Principal component analysis: a review and recent developments. Philosophical Transactions of the Royal Society A: Mathematical, Physical and Engineering Sciences. 2016;374(2065):20150202.
377. Williams TG, Vincent G, Bowes M, Cootes T, Balamoody S, Hutchinson C, et al., editors. Automatic segmentation of bones and inter-image anatomical correspondence by volumetric statistical modelling of knee MRI. 2010 IEEE International Symposium on Biomedical Imaging: From Nano to Macro; 2010: IEEE.

378. Hunter D, Nevitt M, Lynch J, Kraus VB, Katz JN, Collins JE, et al. Longitudinal validation of periarticular bone area and 3D shape as biomarkers for knee OA progression? Data from the FNIH OA Biomarkers Consortium. Ann Rheum Dis. 2016;75(9):1607-14.
379. Mostafa E, Graefe SB, Varacallo M. Anatomy, Bony Pelvis and Lower Limb, Leg Posterior Compartment. StatPearls. Treasure Island (FL): StatPearls Publishing

380. Hunter D, Bowes M, Eaton C, Holmes A, Mann H, Kwoh C, et al. Can cartilage loss be detected in knee osteoarthritis (OA) patients with 3–6 months' observation using advanced image analysis of 3 T MRI? Osteoarthritis Cartilage. 2010;18(5):677-83.
381. Suttorp MM, Siegerink B, Jager KJ, Zoccali C, Dekker FW. Graphical presentation of confounding in directed acyclic graphs. Nephrology Dialysis Transplantation. 2015;30(9):1418-23.
382. Wason J, Stecher L, Mander AP. Correcting for multiple-testing in multi-arm trials: is it necessary and is it done? Trials. 2014;15(1):1-7.
383. Dunn OJ. Multiple comparisons among means. Journal of the American statistical association. 1961;56(293):52-64.
384. VanderWeele TJ, Mathur MB. Some desirable properties of the Bonferroni correction: is the Bonferroni correction really so bad? Am J Epidemiol. 2019;188(3):617-8.
385. Rothman KJ. No adjustments are needed for multiple comparisons. Epidemiology. 1990:43-6.
386. Savitz DA, Olshan AF. Multiple comparisons and related issues in the interpretation of epidemiologic data. Am J Epidemiol. 1995;142(9):904-8.
387. Perneger TV. What's wrong with Bonferroni adjustments. BMJ. 1998;316(7139):1236-8.
388. Rubin M. When to adjust alpha during multiple testing: A consideration of disjunction, conjunction, and individual testing. Synthese. 2021;199(3):10969-1000.
389. Greenland S, Morgenstern H. Confounding in health research. Annu Rev Public Health. 2001;22(1):189-212.
390. Lievense A, Bierma-Zeinstra S, Verhagen A, Van Baar M, Verhaar J, Koes B. Influence of obesity on the development of osteoarthritis of the hip: a systematic review. Rheumatology. 2002;41(10):1155-62.
391. Holmberg S, Thelin A, Thelin N. Knee osteoarthritis and body mass index: a population-based case–control study. Scand J Rheumatol. 2005;34(1):59-64.
392. Moore ES, Kindig MW, McKearney DA, Telfer S, Sangeorzan BJ, Ledoux WR. Hind-and midfoot bone morphology varies with foot type and sex. Journal of Orthopaedic Research®. 2019;37(3):744-59.
393. Boskey AL, Coleman R. Aging and bone. J Dent Res. 2010;89(12):1333-48.
394. Goltzman D. The aging skeleton. Human Cell Transformation. 2019:153-60.
395. Mahfouz M, Abdel Fatah EE, Bowers LS, Scuderi G. Three-dimensional morphology of the knee reveals ethnic differences. Clinical Orthopaedics and Related Research®. 2012;470(1):172-85.
396. Castro-Aragon O, Vallurupalli S, Warner M, Panchbhavi V, Trevino S. Ethnic radiographic foot differences. Foot Ankle Int. 2009;30(1):57-61.
397. Nelson AE, Golightly YM, Lateef S, Renner JB, Jordan JM, Aspden RM, et al. Cross-sectional associations between variations in ankle shape by statistical shape modeling, injury history, and race: the Johnston County Osteoarthritis Project. Journal of Foot and Ankle Research. 2017;10(1):1-7.
398. Golightly YM, Hannan MT, Dufour AB, Jordan JM. Racial differences in foot disorders and foot type. Arthritis Care Res (Hoboken). 2012;64(11):1756-9.
399. Kuo C-C, Lu H-L, Lu T-W, Lin C-C, Leardini A, Kuo M-Y, et al. Effects of positioning on radiographic measurements of ankle morphology: a computerized tomography-based simulation study. Biomed Eng Online. 2013;12(1):1-16.
400. Fessy M, Carret J, Bejui J. Morphometry of the talocrural joint. Surg Radiol Anat. 1997;19(5):299-302.

401. Stagni R, Leardini A, Ensini A, Cappello A. Ankle morphometry evaluated using a new semi-automated technique based on X-ray pictures. Clinical biomechanics. 2005;20(3):307-11.
402. Stagni R, Leardini A, Catani F, Cappello A. A new semi-automated measurement technique based on X-ray pictures for ankle morphometry. J Biomech. 2004;37(7):1113-8.
403. Zakaria MS, Mohammed AH, Habib SR, Hanna MM, Fahiem AL. Calcaneus radiograph as a diagnostic tool for sexual dimorphism in Egyptians. J Forensic Leg Med. 2010;17(7):378-82.
404. Otong ES, Amaza DS, Bello SA, Rufai AA, Mustapha Z, Jacks TW. RADIOLOGICAL ESTIMATION OF SEX USING TROCHLEAR SURFACE OF TALUS IN ADULT NORTH EASTERN NIGERIANS.
405. Lee UY, Han SH, Park DK, Kim YS, Kim DI, Chung IH, et al. Sex determination from the talus of Koreans by discriminant function analysis. J Forensic Sci. 2012;57(1):166-71.
406. Zhao D-H, Huang D-C, Zhang G-H, Shi J-Q, Wang C, Geng X, et al. Gender variation in the shape of superior talar dome: a cadaver measurement based on Chinese population. BioMed research international. 2018;2018.
407. Tompe A, Sargar K. X-Ray Image Quality Assurance. StatPearls [Internet]: StatPearls Publishing; 2020.
408. Bonasia DE, Dettoni F, Femino JE, Phisitkul P, Germano M, Amendola A. Total ankle replacement: why, when and how? The Iowa orthopaedic journal. 2010;30:119.
409. Leung KH, Fang CXS, Lau TW, Li Leung FK. Preoperative radiography versus computed tomography for surgical planning for ankle fractures. Journal of Orthopaedic Surgery. 2016;24(2):158-62.
410. Joskowicz L. Future perspectives on statistical shape models in computer-aided orthopedic surgery: Beyond statistical shape models and on to big data. Computer Assisted Orthopaedic Surgery for Hip and Knee: Springer; 2018. p. 199-206.
411. Wilson DA, Anglin C, Ambellan F, Grewe CM, Tack A, Lamecker H, et al. Validation of three-dimensional models of the distal femur created from surgical navigation point cloud data for intraoperative and postoperative analysis of total knee arthroplasty. Int J Comput Assist Radiol Surg. 2017;12(12):2097-105.
412. Nishikawa K, Biewener AA, Aerts P, Ahn AN, Chiel HJ, Daley MA, et al. Neuromechanics: an integrative approach for understanding motor control. Integr Comp Biol. 2007;47(1):16-54.
413. Sheehan FT, Brainerd EL, Troy KL, Shefelbine SJ, Ronsky JL. Advancing quantitative techniques to improve understanding of the skeletal structure-function relationship. J Neuroeng Rehabil. 2018;15(1):1-7.
414. Phinyomark A, Osis ST, Hettinga BA, Kobsar D, Ferber R. Gender differences in gait kinematics for patients with knee osteoarthritis. BMC Musculoskelet Disord. 2016;17(1):1-12.
415. Bruening DA, Baird AR, Weaver KJ, Rasmussen AT. Whole body kinematic sex differences persist across non-dimensional gait speeds. PLoS One. 2020;15(8):e0237449.
416. Fukano M, Fukubayashi T, Banks SA. Sex differences in three-dimensional talocrural and subtalar joint kinematics during stance phase in healthy young adults. Human movement science. 2018;61:117-25.
417. Agarwal S, Garg S, Vasudeva N. Subtalar joint instability and calcaneal spurs associated with the configuration of the articular facets of adult human calcaneum in Indian population. Journal of Clinical and Diagnostic Research: JCDR. 2016;10(9):AC05.
418. Doherty C, Delahunt E, Caulfield B, Hertel J, Ryan J, Bleakley C. The incidence and prevalence of ankle sprain injury: a systematic review and meta-analysis of prospective epidemiological studies. Sports Med. 2014;44(1):123-40.
419. Aenumulapalli A, Kulkarni MM, Gandotra AR. Prevalence of flexible flat foot in adults: a cross-sectional study. Journal of clinical and diagnostic research: JCDR. 2017;11(6):AC17.
420. Nix S, Smith M, Vicenzino B. Prevalence of hallux valgus in the general population: a systematic review and meta-analysis. Journal of foot and ankle research. 2010;3(1):1-9.

421. Cody EA, Williamson ER, Burket JC, Deland JT, Ellis SJ. Correlation of talar anatomy and subtalar joint alignment on weightbearing computed tomography with radiographic flatfoot parameters. Foot Ankle Int. 2016;37(8):874-81.
422. Tümer N, Vuurberg G, Blankevoort L, Kerkhoffs GMM, Tuijthof GJ, Zadpoor AA. Typical shape differences in the subtalar joint bones between subjects with chronic ankle instability and controls. Journal of Orthopaedic Research®. 2019;37(9):1892-902.
423. Mani E, Tüzün EH, Angın E, Eker L. Lower extremity proprioceptive sensation in patients with early stage knee osteoarthritis: a comparative study. The Knee. 2020;27(2):356-62.
424. Levinger P, Menz HB, Fotoohabadi MR, Feller JA, Bartlett JR, Bergman NR. Foot posture in people with medial compartment knee osteoarthritis. Journal of foot and ankle research. 2010;3(1):1-8.
425. Redmond AC, Crosbie J, Ouvrier RA. Development and validation of a novel rating system for scoring standing foot posture: the Foot Posture Index. Clinical biomechanics. 2006;21(1):89-98.
426. Wrobel JS, Armstrong DG. Reliability and validity of current physical examination techniques of the foot and ankle. J Am Podiatr Med Assoc. 2008;98(3):197-206.
427. Barton CJ, Bonanno D, Levinger P, Menz HB. Foot and ankle characteristics in patellofemoral pain syndrome: a case control and reliability study. J Orthop Sports Phys Ther. 2010;40(5):286-96.
428. Czerniecki JM. Foot and ankle biomechanics in walking and running. A review. Am J Phys Med Rehabil. 1988;67(6):246-52.
429. Shakoor N, Lidtke RH, Sengupta M, Fogg LF, Block JA. Effects of specialized footwear on joint loads in osteoarthritis of the knee. Arthritis Care & Research: Official Journal of the American College of Rheumatology. 2008;59(9):1214-20.
430. Lattanza L, Gray GW, Kantner RM. Closed versus open kinematic chain measurements of subtalar joint eversion: implications for clinical practice. J Orthop Sports Phys Ther. 1988;9(9):310-4.
431. Tiberio D. The effect of excessive subtalar joint pronation on patellofemoral mechanics: a theoretical model. J Orthop Sports Phys Ther. 1987;9(4):160-5.
432. Jones RK, Chapman GJ, Findlow AH, Forsythe L, Parkes MJ, Sultan J, et al. A new approach to prevention of knee osteoarthritis: reducing medial load in the contralateral knee. The Journal of rheumatology. 2013;40(3):309-15.
433. Schipplein O, Andriacchi T. Interaction between active and passive knee stabilizers during level walking. J Orthop Res. 1991;9(1):113-9.
434. Murray D, O'Connor J. Superolateral wear of the acetabulum. The Journal of bone and joint surgery British volume. 1998;80(2):197-200.
435. Paixao T, DiFranco MD, Ljuhar R, Ljuhar D, Goetz C, Bertalan Z, et al. A novel quantitative metric for joint space width: data from the Osteoarthritis Initiative (OAI). Osteoarthritis Cartilage. 2020;28(8):1055-61.
436. Murphy JM, Kadakia AR, Schilling PL, Irwin TA. Relationship among radiographic ankle medial clear space, sex, and height. Orthopedics. 2014;37(5):e449-e54.
437. Jonsson K, Fredin H, Cederlund C, Bauer M. Width of the normal ankle joint. Acta Radiologica Diagnosis. 1984;25(2):147-9.
438. Goker B, Gonen E, Demirag MD, Block JA. Quantification of the radiographic joint space width of the ankle. Clinical Orthopaedics and Related Research®. 2009;467(8):2083-9.
439. Arak A. Sexual dimorphism in body size: a model and a test. Evolution. 1988;42(4):820-5.
440. Maleki-Fischbach M, Jordan JM. New developments in osteoarthritis. Sex differences in magnetic resonance imaging-based biomarkers and in those of joint metabolism. Arthritis Res Ther. 2010;12(4):212.
441. Murray CL, Marshall M, Rathod-Mistry T, Menz H, Roddy E. Population prevalence and distribution of ankle pain and symptomatic radiographic ankle osteoarthritis in community-dwelling older adults. Rheumatology. 2016;55:79-.

442. Tschon M, Contartese D, Pagani S, Borsari V, Fini M. Gender and sex are key determinants in osteoarthritis not only confounding variables. A systematic review of clinical data. Journal of Clinical Medicine. 2021;10(14):3178.
443. Brennan S, Pasco JA, Cicuttini FM, Henry M, Kotowicz M, Nicholson G, et al. Bone mineral density is cross sectionally associated with cartilage volume in healthy, asymptomatic adult females: Geelong Osteoporosis Study. Bone. 2011;49(4):839-44.
444. Berry PA, Wluka AE, Davies-Tuck ML, Wang Y, Strauss BJ, Dixon JB, et al. Sex differences in the relationship between bone mineral density and tibial cartilage volume. Rheumatology. 2011;50(3):563-8.
445. Cao Y, Stannus OP, Aitken D, Cicuttini F, Antony B, Jones G, et al. Cross-sectional and longitudinal associations between systemic, subchondral bone mineral density and knee cartilage thickness in older adults with or without radiographic osteoarthritis. Ann Rheum Dis. 2014;73(11):2003-9.
446. Teichtahl AJ, Wang Y, Wluka AE, Strauss BJ, Proietto J, Dixon JB, et al. Associations between systemic bone mineral density and early knee cartilage changes in middle-aged adults without clinical knee disease: a prospective cohort study. Arthritis Res Ther. 2017;19(1):1-11.
447. Pearce MS, Birrell FN, Francis RM, Rawlings DJ, Tuck SP, Parker L. Lifecourse study of bone health at age 49–51 years: the Newcastle thousand families cohort study. J Epidemiol Community Health. 2005;59(6):475-80.
448. Tuck S, Pearce M, Rawlings D, Birrell F, Parker L, Francis R. Differences in bone mineral density and geometry in men and women: the Newcastle Thousand Families Study at 50 years old. The British journal of radiology. 2005;78(930):493-8.
449. Wolff J. The law of bone remodelling. Translated by P. Maquet and R. Furlong. New York, S pringer. 1986;1(9):8.
450. Jiang S-D, Dai L-Y, Jiang L-S. Osteoporosis after spinal cord injury. Osteoporos Int. 2006;17(2):180-92.
451. Alekna V, Tamulaitiene M, Sinevicius T, Juocevicius A. Effect of weight-bearing activities on bone mineral density in spinal cord injured patients during the period of the first two years. Spinal Cord. 2008;46(11):727-32.
452. Lee S-H, Park SY, Jang MU, Kim Y, Lee J, Kim C, et al. Association between osteoporosis and cognitive impairment during the acute and recovery phases of ischemic stroke. Medicina. 2020;56(6):307.
453. Nejatian MM, Sobhi S, Sanchez BN, Linn K, Manning L, Soh S-C, et al. Reduction in femoral neck and total hip bone mineral density following hospitalisation for diabetes-related foot ulceration. Sci Rep. 2021;11(1):1-9.
454. van der Poest Clement Ev, Van der Wiel H, Patka P, Roos J, Lips P. Long-term consequences of fracture of the lower leg: cross-sectional study and long-term longitudinal follow-up of bone mineral density in the hip after fracture of lower leg. Bone. 1999;24(2):131-4.
455. Therbo M, Petersen M, Nielsen P, Lund B. Loss of bone mineral of the hip and proximal tibia following rupture of the Achilles tendon. Scand J Med Sci Sports. 2003;13(3):194-9.
456. Apostle KL, Sangeorzan BJ. Anatomy of the varus foot and ankle. Foot and Ankle Clinics. 2012;17(1):1-11.
457. Bálint GP, Korda J, Hangody L, Bálint PV. Foot and ankle disorders. Best practice & research Clinical rheumatology. 2003;17(1):87-111.
458. Low KT, Peh WC. Radiography limitations and pitfalls. Pitfalls in Musculoskeletal Radiology. 2017:3-32.
459. Eckstein F, Siedek V, Glaser C, Al-Ali D, Englmeier K, Reiser M, et al. Correlation and sex differences between ankle and knee cartilage morphology determined by quantitative magnetic resonance imaging. Ann Rheum Dis. 2004;63(11):1490-5.
460. Krähenbühl N, Lenz AL, Lisonbee R, Deforth M, Zwicky L, Hintermann B, et al. Imaging of the subtalar joint: A novel approach to an old problem. J Orthop Res. 2019;37(4):921-6.

461. Beattie KA, Duryea J, Pui M, O'Neill J, Boulos P, Webber CE, et al. Minimum joint space width and tibial cartilage morphology in the knees of healthy individuals: a cross-sectional study. BMC Musculoskelet Disord. 2008;9(1):1-9.
462. Nguyen A-D, Shultz SJ. Sex differences in clinical measures of lower extremity alignment. J Orthop Sports Phys Ther. 2007;37(7):389-98.
463. Yang S, Canton SP, Hogan MV, Anderst W. Healthy ankle and hindfoot kinematics during gait: Sex differences, asymmetry and coupled motion revealed through dynamic biplane radiography. J Biomech. 2021;116:110220.
464. Reilingh ML, Beimers L, Tuijthof GJ, Stufkens SA, Maas M, van Dijk CN. Measuring hindfoot alignment radiographically: the long axial view is more reliable than the hindfoot alignment view. Skeletal Radiol. 2010;39(11):1103-8.
465. Foster SN, Harris MD, Hastings MK, Mueller MJ, Salsich GB, Harris-Hayes M. Static ankle dorsiflexion and hip and pelvis kinematics during forward step-down in patients with hip-related groin pain. Journal of sport rehabilitation. 2020;30(4):638-45.